The nature of the interstellar medium in the starburst of NGC 253

Andrew Paul Harrison

Doctor of Philosophy
University of Edinburgh
1996

This thesis is my own composition and consists entirely of my own work except where specifically indicated in the text.

Andrew Paul Harrison

September 1996

Abstract

This thesis contains several complementary sets of observations of the starburst in the nucleus of NGC 253. The observations probe the interface between ionised and molecular gas, where UV photons from young stars dominate the heating and chemistry of the gas. The thesis describes how observations of the emission from these photon-dominated regions (PDRs), particularly in the near-IR to millimetre range of the electromagnetic spectrum, can be used to constrain the dominant energy inputs, chemistry and geometry of the star-formation process in a starburst.

The near-IR shows several lines of H_2. Observations of excited H_2 in Galactic PDRs indicates that the ortho to para (o/p) ratio of H_2 is $\sim$2 whereas in shocked regions the o/p ratio is observed to be 3. Towards NGC 253, the o/p ratio of H_2 is observed to be $\sim$2 across the entire starburst and so this is direct evidence that PDRs produce the bulk of the H_2 emission in the starburst region. Furthermore, the ratio of Brγ/1-0S(1) shows a maximum on the nucleus. With the knowledge that the H_2 emission arises in PDRs, the most plausible way to explain the observed Brγ/1-0S(1) ratio is for a large fraction of the O & B stars to be clustered into groups. Away from the nucleus, it appears that the H_2 emission is arising from PDRs that are bathed by a relatively diffuse FUV radiation field. There seems to be a clear difference between the geometry of OB stars and PDRs in the starburst to that of the geometry away from the starburst.

Observations of isotopic CO show that the bulk of ^{13}CO emission arises from warm gas whereas the bulk of C^{18}O emission appears to arise from cold gas. It thus appears that some process is at work in NGC 253 that removes C^{18}O from the warm gas associated with PDRs. A proposed mechanism is selective photodissociation of CO and it's isotopomers.

Observations of the fine-structure transitions of atomic carbon show a significant overabundance, a factor of 10 or more, with theoretical models of PDRs. Considerations of the size of the compact starburst, traced by the mid to far IR radiation from dust, indicates that the starburst is centrally concentrated within the central 100 pc of NGC 253. The luminosity coming from such a region, $\sim 10^{10}$ L$_\odot$, indicates that the UV field is very high within the starburst, possibly greater than 10^5 times the local value. If all the C$^+$ flux is generated within this region, as is likely, then the ionised carbon emission is also a factor of 10 or more brighter than is predicted by PDR models. The most likely explanation for the discrepancy between the brightness of C^0 and C$^+$ and the models is that the elemental abundance of carbon is higher in NGC 253 than it is in the PDR models with which we compare our observations. There is no obvious reason why carbon is over-abundant in the gas-phase of NGC 253.

ACKNOWLEDGEMENTS

During my time in Edinburgh I have been lucky enough to have my work supervised by three intelligent and caring friends, Peter Brand, Phil Puxley and Adrian Russell. From each of them I have learnt many, many things and to them each I give a big **Thank You**. If anything in this thesis turns out to be true, the reader should thank these people.

My life at Edinburgh, in and outside the Observatory, has been fun because of my office mates. I am indebted to, and I thank, Drs (pending) Steve McNally, Andrew Thackrah & Jonny Tedds. To them R8 was an office, to me it was a place to let off steam and kick off about various issues and people. I thank them for their patience and laughs and I look forward to watching us grow old together. Predictions: SM - Cambridge Professor and stuck in revolving doors; AT - Missionary; JT - Late Show presenter.

I have enjoyed the good life in Edinburgh and I take this opportunity to thank Steve Bond (for laughs, deep philosophical discussions and quotes), Stephen Dodds (for laughs, deep philosophical discussions and quotes) and Henry Buckley (for explaining lots of physics to me and being a very nice chap). I also look forward to watching these people grow old. Predictions: SB - Writer (about agricultural issues); SD - Barley Farmer in Bali; HB - see predictions for SM.

Amongst the many people who have watched me play football in awe, I particularly thank Alistair Glasse (for listening to my views on dust and not getting too depressed about Newcastle), Rob Ivison (for doing all the work for a paper and then putting my name on it—Cheers, and also for keeping me up with his life, the running soap opera), The Cat Casali (for being a fashion role model and not getting too depressed about d(Grey)/dt>0), Eelco van Kampen (for always smiling and not getting too depressed about the state of Britain) and Alan Heavens (for being an easy person to talk with and not getting too depressed about Leeds).

My life as a student in the Observatory has been easy because of the hard work of many people. Angus Macdonald, Shona McEachern, Sally MacIntosh and Sarah Graham run a wonderful library and I thank them for all the times they have listened to my confused babblings over articles and then led me straight to what I wanted. Liz Gibson told me how and what forms I needed to fill in which meant that I missed no planes and I didn't have to pay for any damaged cars, and I thank her for her mastery of my administration matters. Horst Meyerdicks, who has to be the 2nd most patient person in the world, John Barrow and Ewan Brown have made all my computer problems disappear for which I am eternally grateful. I am also very grateful to Jason Cowan who was always willing to scan images, whenever I needed them.

Between them, Mike McCartney, Suzie Ramsay and Karen Willacy answered all my questions about H_2 and I thank each of them for their patience, especially Karen who is the 3rd most patient person. I would also like to thank Christian Henkel, Jocelyn Keene, Padeli Papadopoulos and Ewine van Dishoeck for discussions on CO, CI and PDRs.

As well as knowing all the wonderful people mentioned above, I have been blessed with my parents. I hope they are as proud as me as I am of them. I thank them for so many things, particularly the support they have given me that has allowed me to do something as interesting, but *potentially* useless, as Astronomy. It is with great love and pride that I can finally dedicate this bloody thesis to them.

Finally, I thank my *enana mata*, Milagros del Carmen Ruiz Nishiky. Milagros is the most patient person in the world and I owe her so much. I thank her for spending part of her life with me and I hope she to continues to suffer from complete, and absolute, 100%, deludisation.

Dedicated to my Mother and Father

Contents

Chapter 1

Introduction

1.1 An introduction to star formation

1.1.1 Where do stars form?

Optical photographs of rich star fields in our Milky Way Galaxy show dark regions present where stars do not shine. Closer examination shows that stars are present but that their light is heavily extinguished, that is the brightness of the light reaching the ground from the extinguished stars is weaker than unextinguished stars. In the visible, the extinction is approximately proportional to $1/\lambda$; this portion of the curve shows that the origin of the extinction as being due to particles which have a diameter comparable with the wavelength of visible light ($\sim 5{\times}10^{-7}$ μm) (further details can be found in Dyson & Williams 1980). These small particles have been termed dust grains. The dust grains are very efficient at absorbing light (optical and ultra-violet), and hence they are efficient at absorbing energy from the impinging photons. This means that the dust quickly reaches thermodynamic equilibrium with the radiation field in which it finds itself. As well as absorbing radiation the grains also radiate and a thermal equilibrium is reached when

$$\int F(\lambda) Q_{abs}(a,\lambda) d\lambda \; = \; \int Q_{abs}(a,\lambda) B(\lambda, T_g) d\lambda \qquad (1.1)$$

where F(λ) is the energy flux of the impinging UV field, B is the Planck function, Q_{abs} is the efficiency for absorption of radiation by the grain, a is the size of the grain and T_g is the equilibrium dust temperature.[1] The two integrals contribute over different wavelength ranges. The left-hand side calculates the energy input into the grain from the radiation field in the visible and UV. The right-hand side calculates the energy emitted, and this wavelength is generally in the infrared. Were the grain a perfect radiator, its temperature would reflect the energy content of space and be equal to the black-body temperature $T_{BB} \approx 3$ K (Dyson & Williams 1980). At this temperature, however, the peak of the Planck function occurs in the millimetre range, and grains of approximately 10^{-7} m radius cannot readily radiate at these wavelengths. Consequently T_g is higher than T_{BB}.

Within the last 25 yrs there has been the realisation that the dark clouds are the birthplace and nursery of the youngest stars within our galaxy (Shu *et al.* 1987). There were previous clues to the interplay between the dark clouds and young stars from optical studies because in some cases the optical radiation from the embedded young stars can escape through holes in the cloud and reflect off nearby material, giving rise to extended nebulae, a good example being the

[1] As we discuss later, strictly speaking equation 1.1 should also have terms due to the energy transfer by particles that are ejected by the dust, such as fast moving electrons, and by particles that collide with and heat the dust

Orion Nebula. But it is only through the realisation of the promise of infra-red, sub-millimetre and millimetre detectors that astronomers have been able to study and quantify the process by which stars are formed through the gravitational collapse of the dark clouds.

For the same reason that optical and ultra-violet gets absorbed from stars behind the layer of dust, a cloud of dust can shield its interior from optical and UV radiation. This shielding from the heating effect of the radiation results in the centres of these clouds becoming cold ($\sim$ 20 K). Grains at this temperature emit strongly in the far-infrared. The InfraRed Astronomical Satellite (IRAS) discovered that, as expected, the bulk of the dark clouds bolometric luminosity is indeed emitted at wavelengths that are undetectable by the eye.

The shielding from the radiation, and the low temperatures and increased densities within the clouds, allows molecules to form. Outside these clouds, molecules are readily dissociated by the radiation field. The shielding and formation of molecules is efficient and $\approx$ 99% of the mass of non-stellar gas within the clouds is in the form of molecules (such as H_2 and CO). For some molecules, such as H_2, the dust plays a further parental role in the molecules' evolution as the grain's surface provides the site of formation of the molecule.

The typical temperatures found in the molecular clouds (5-300 K) mean that molecular rotational energy levels, and in some cases vibrational levels, are readily excited. Lines are emitted by the molecules as they switch from one excited state to another. The wavelength of these lines is far larger than the size of the dust grains within the cloud and so the radiation is not absorbed by the grains. The clouds are so large, though, and are so abundant in many molecular species that there becomes a high chance for certain lines that radiation emitted by an excited molecule will be absorbed by the same molecular species before the radiation has reached the edge of the cloud. The opacity of the clouds' molecules to their own radiation provides a diagnostic, as well as a constraint, over what we can know about the region. If the cloud is transparent in a molecule's line then it is known as "optically thin" whereas if the cloud is opaque for a molecular line then it is known as "optically thick". The typical wavelengths of the rotational lines are of order a millimetre and that is why it is only with the availability of telescopes dedicated to work at these wavelengths that we have been able to "literally scratch" below the surface of these dark clouds. The dark clouds, because of the vast quantities of molecular gas which they contain, are now more commonly known as molecular clouds.

Observation at IR wavelengths showed that there were many individual objects embedded within the clouds. Many of these objects are invisible at optical wavelengths. The objects are believed to be stars in the earliest stages of their evolution because of the characteristics of their infrared spectral energy distributions (Shu *et al.* 1987). Some of these young stars are so deeply embedded that even observations in the IR are affected by the thick layers of dust between us and the young stars and so to study these objets we need to go to longer wavelengths, such as the sub-mm. These most embedded of objects are now believed to true "proto-stars" (André *et al.* 1993). The formation of stars tends to be associated with the densest cores of these clouds. Further evidence for the direct association of molecular clouds with the formation of stars has come from Galactic studies of the locations of molecular clouds, *e.g.* Combes (1991). These studies show that the clouds lie predominantly along the disk of the Milky Way, distributed in a similar way to the bright gaseous nebulae ionised by hot young stars.

In our Galaxy, about half of the total luminosity emerges at infrared wavelengths, and most of that is from regions of recent star formation; this fraction seems to be fairly typical of normal spiral galaxies. There are some galaxies, however, which have much greater fractions of their total output emerging in the infrared. In some cases, over 90% of the galaxy's bolometric

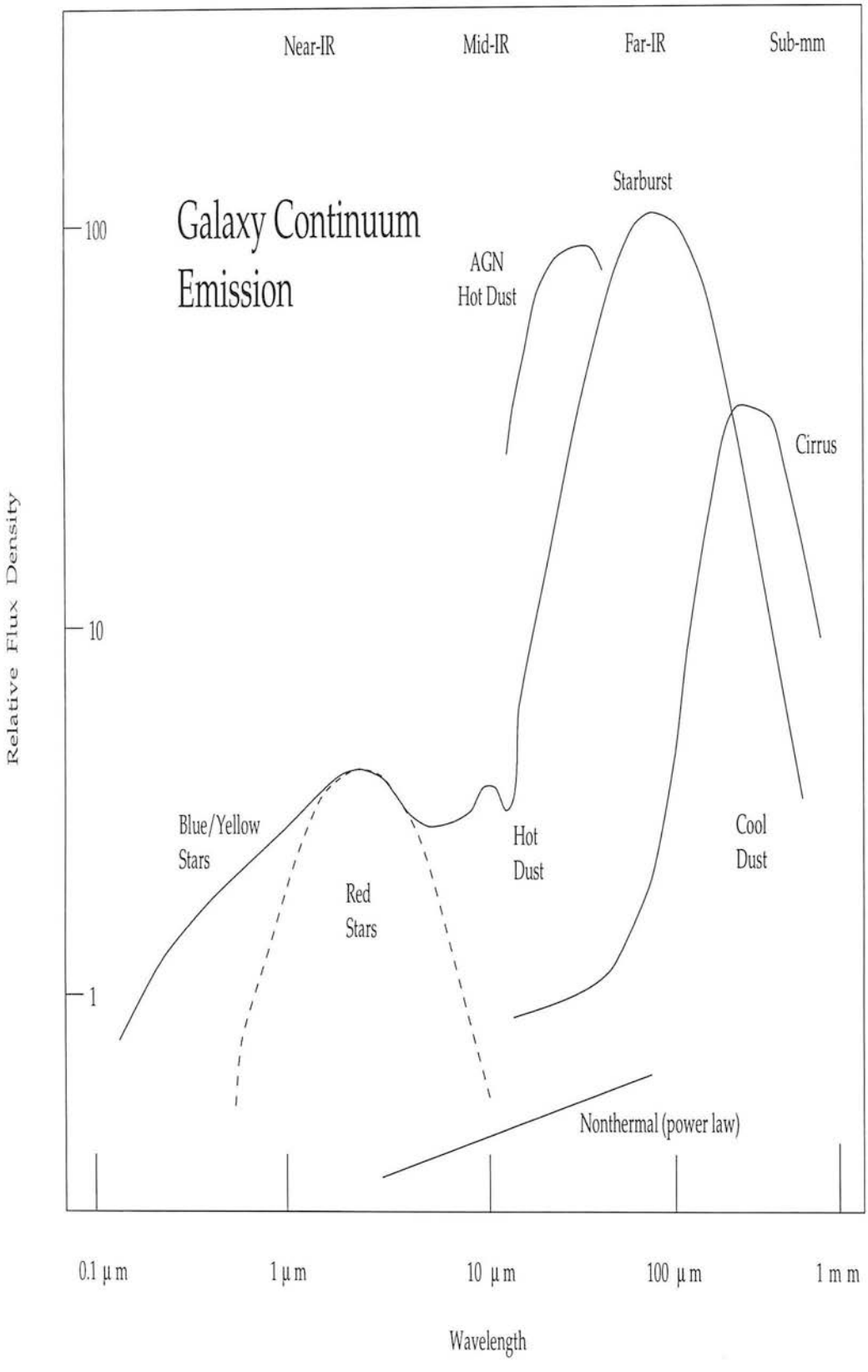

Figure 1.1: Various components that make up the spectral energy distribution that is typically observed from a galaxy with an enhanced rate of star formation. The figure is adapted from Telesco (1993).

luminosity is emitted at IR wavelengths, (Telesco 1988). As infrared radiation is generated in star forming regions and many of these IR-luminous galaxies are also rich in molecular gas, (Henkel *et al.* 1991), it is reasonable to suspect that these galaxies are currently forming stars much more vigorously than the Milky Way. Many of these galaxies have so much dust and gas associated with them that the UV radiation from young stars that are no longer embedded within the clouds still gets absorbed by nearby gas. This absorbing dust then reprocesses the radiation to longer wavelengths. Figure 1.1 shows a schematical spectral energy distribution that is typically observed from such a gas-rich galaxy nucleus.

There are, of course, physical reasons why one galaxy should be richer in molecular gas than other galaxies and why one galaxy should be forming stars at a much faster rate than another. The IR activity often appears to occur near the centres of galaxies so this must mean that some large-scale disturbance must cause the gas in a galaxy to lose angular momentum and fall rapidly towards the centre. Alternatively, gas with little angular momentum must fall in from outside the galaxy. Combes (1988) discussed two possible effects that act to transfer angular momentum and allow gas to fall towards the centre:

- a bar-like distortion in the mass distribution
- a tidal interaction or merger with a companion galaxy

The non-axisymmetric potential exerts a torque and the consequent transfer of angular momentum can drive large gas flows towards the centre. Simulations show that the time-scale of inflow can be as short as few $\times$ 10^7 yrs if the tidal perturbation is strong enough—grazing direct passage of an equal-mass distribution (Combes 1988). These ideas are supported by the observations. Infrared activity is associated with three main types of object. There are nearby, usually isolated galaxies with infrared luminosities of few $\times$ 10^{9-10} $L_\odot$ coming from the central kiloparsec. The majority of these objects appear to have a bar running across the centre. Further up the scale, $L_{IR} = 10^{10-12}$ $L_\odot$, are interacting galaxies, in which it seems that a close tidal encounter between two gas-rich spirals has triggered an extensive episode of prolific star formation (Joseph & Wright 1985). Most extreme of all are the so-called ultra-luminous galaxies, $L_{IR} > 10^{12}$ $L_\odot$, which are, almost without exception, merger systems (Sanders *et al.* 1988).

The sudden increase in the number density of massive stars and the evolution of these massive stars into supernovae will have a significant effect on the IR-galaxy's evolution. If we are to understand the differences between the Milky Way and these IR-luminous galaxies and what effects the population of massive stars have had, and will have, on galactic evolution we need to be able to quantify the scale of star formation, the time-scale of the star formation and the impact of a new population of stars upon the contents of a galaxy. In the next section there is an overview of the interstellar medium and large scale star formation.

1.2 The "stuff" from which stars form

1.2.1 The nature of the interstellar medium

Rather than the ISM being a fairly homogeneous soup, it is a mixture of distinct phases.[2] The physical processes behind the various phases have been reviewed before, *e.g.* in the book Interstellar Processes (Hollenbach & Thronson 1987). The nature of these phases and why these individual phases have a certain range of temperatures and densities is due to a balance between

[2] Much of this section has been taken from Begelman (1989)

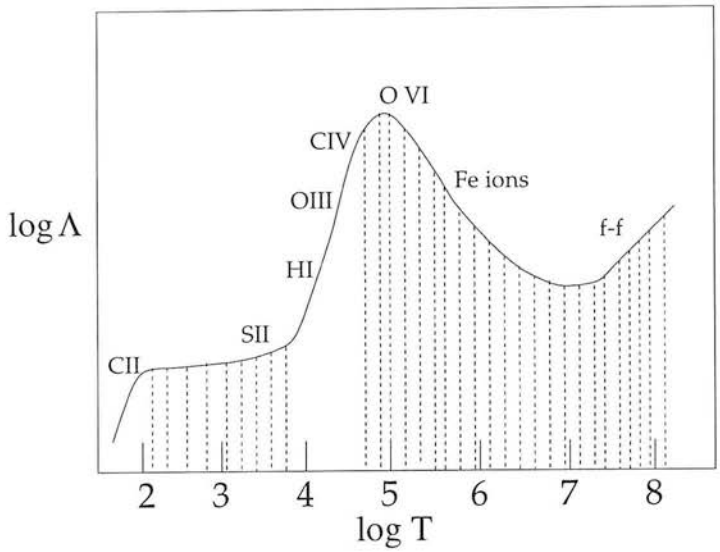

Figure 1.2: Radiative cooling of optically thin, low density interstellar gas. Regions which are thermally unstable are shaded. The dominant coolants are shown. The figure is adapted from Shull (1987).

various heating and cooling processes. If $\Gamma(n,T,x_j)$ is the heating rate per particle and $\Lambda(n,T,x_j)$ is the cooling function, then the equation of thermal equilibrium is written

$$n\Gamma - n^2\Lambda \stackrel{\text{def}}{\equiv} n^2\mathcal{L} = 0 \tag{1.2}$$

where n is the density of the hydrogen nuclei, T is the temperature, and x_j represents the fractional concentrations of various species, $x_j \equiv n_j/n$. The pressure is given by $p = x_t\ n\ K\ T$, where $x_t = \Sigma\ x_j$ is the number of particles per hydrogen nucleus. Γ, and sometimes Λ (*e.g.* in the case of inverse Compton cooling), may also depend on the magnitude of some external heating or ionisation agent, which has an energy density u_Γ. Figure 1.2 shows a schematic radiative cooling curve for interstellar gas of cosmic abundances, adapted from Shull (1987). The salient features of the cooling function $\Lambda(T)$ are: 1) steeply rising portions below 100 K and between about 10^4 and 10^5 K; 2) a relatively flat portion from 10^2 to 10^4 K; 3) a falling portion for $5.3 < \log T < 7.0$; and 4) a high temperature portion, with $\Lambda \propto T^{1/2}$, due to thermal bremsstrahlung. The shape of $\Lambda(T)$ results from the efficiency of radiative cooling of the dominant species at each temperature: excitation of the CII infrared fine structure line at low temperature; excitation of CII and optical forbidden lines at moderate temperatures; HI (Ly α) excitation above about 7000 K; and excitation of permitted and semi-forbidden lines of ions of C, O and Fe above 20,000 K. For temperatures between about 10^6 and 10^7 K, the cooling is dominated by iron ions, which are the only abundant species which retain their bound electrons at such temperatures.

If the heating rate, Γ, is held fixed then the solution of the equilibrium equation generates a curve in the Γ - T plane which separates the heating region ($\Gamma > n\Lambda$) from the cooling region ($\Gamma < n\Lambda$). In general the curve has a complex shape and is multivalued. Figure 1.3 shows the equilibria for a constant heating rate Γ and the standard interstellar cooling function $\Lambda(T)$. The function $\Lambda(T)/T$, which equals (Γ/nT), plotted versus T represents the locus of equilibria for which heating equals cooling ($\mathcal{L} = 0$). Above the curve, the gas is being heated ($\mathcal{L} > 0$); below the curve, the gas is cooling ($\mathcal{L} < 0$). Equilibrium solutions are found when the curve $\Lambda(T)/T$

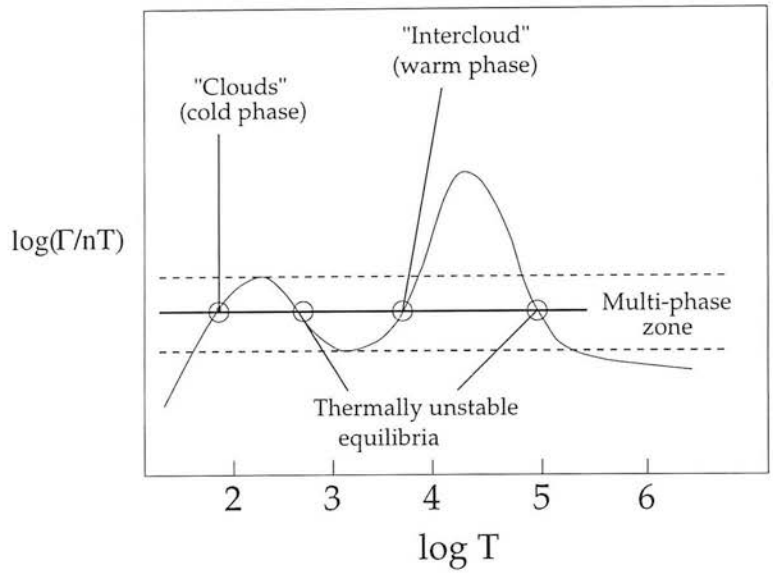

Figure 1.3: Locus of equilibria for interstellar gas with constant heating rate H and constant pressure nT.

is intersected by a horizontal line corresponding to the ratio (Γ/nT).

In figure 1.3 there are 4 possible solutions, two are thermally stable and the other two, which are on the downward sloping portions of the curve are thermally unstable, *i.e.* when the gas is thermally unstable a slight increase/decrease in the gas heating rate is not balanced by an equivalent increase/decrease in the gas cooling rate and so there is an increase/decrease in the gas temperature until another balance between heating and cooling is reached at a new temperature in the regions of thermal stability.

Because there are two or more phases of differing n (or, equivalently, of T) which can reach an equilibrium between heating and cooling for a given heating rate, then a multiphase medium results: a relatively cool, dense region can coexist with one or more warmer, less dense regions in pressure equilibrium. There is an intimate connection between the existence of thermal phases and the thermal stability of a system: any system exhibiting multiphase equilibria must be thermally unstable over a range of thermodynamic parameters. If the gas is in equilibrium ($\mathcal{L} = 0$) then the instability criterion is

$$\left(\frac{\partial \mathcal{L}}{\partial T}\right)_A < 0 \quad (\mathcal{L} = 0) \tag{1.3}$$

A characteristic feature of multi-phase systems is that the coldest phase cannot exist below some minimum pressure p_{min}, while the hottest phase cannot exist above some maximum pressure p_{max}. The condition that there be multiple stable phases implies that $p_{max} > p_{min}$. A homogeneous system with a density $n_1 < \bar{n} < n_2$ is clearly unstable in this homogeneous state. However, it is possible to stabilise the system by making it inhomogeneous, while keeping the mean density constant. The trick is to put most of the mass in the cold phase, with density $n_c > n_2$, while a small fraction of the matter forms a hot intercloud medium, with density $n_h < n_1$ and temperature T_h. Pressure balance requires $n_c/n_h = \mathrm{T}_h/\mathrm{T}_{cl}$. If f is the filling factor in cold gas, then the mean density constraint is $\bar{n} = (1-f)n_h + fn_c$, and f satisfies $T_{cl}/T_h \ll f \ll 1$ if $n_1 \ll \bar{n} \ll n_2$.

The physical properties of the local interstellar medium are summarised in Table 1.1; the table is adapted from Knapp (1989). As can be seen, most of the volume is filled by the hottest

Table 1.1: The local interstellar medium

Component	f_v	$< n_H >$ cm^{-3}	T_e K	f_M	Probes
Hot ICM	0.5	0.005	5×10^5	0.001	Xrays
Warm ICM	0.5	0.3	8000	0.1	HI,Hα
HI Clouds	0.05	5-20	10-100	0.4	HI,etc
H_2	0.005	300	5-30	0.5	CO
HII	0.001	10-10^4	10^4	0.02	Hα
SNR					radio, Xrays
Dust	1.0		5-50	0.01	IR, extinction

phases of the ISM but most of the mass is contained within the coolest phases of the ISM. There is an approximate thermal pressure equilibrium between many of the phases. The phase that has the highest derived thermal pressure is that of molecular clouds. The reason why this phase is not rapidly expanding is because of gravity. This overpressure of the long lasting molecular clouds thus indicates that these are bound objects, unlike the other phases. When it was first realised that the molecular clouds were bound it was also realised that the derived thermal pressures were not high enough to support the clouds against gravitational collapse. If the molecular clouds were collapsing then the large number of such clouds suggested that the current rate of star formation was far higher than was measured from estimations of the Milky Way's IR luminosity and from the number of O and B stars. Therefore, other supports of molecular clouds, other than just thermal pressure, were needed to slow down the rate of cloud collapse. The two most likely non-thermal pressure supports are magnetic fields and turbulence, (Shu *et al.* 1987).

The interface between the phases of HI and H_2 is the vital transition in the ISM as these two components comprise most of the mass of the ISM. Understanding any evolutionary links between the two phases will highlight what environmental conditions control the relative fraction of the two phases. The material from which stars form will be molecular but will have been, at some point in its history, atomic. The cycling between the two dominant phases will control the amount of material available to form the stars and so must, to some degree, control the rate at which stars are forming. In the following section there is an overview of other factors which control the rate of star formation in a galaxy.

1.2.2 Factors controlling the rate of star formation

In normal spiral galaxies the formation of stars is a slow and well-regulated process.[3] The regulation of star formation occurs through a negative feedback effect. Unlike the uncertain effects of supernovae and stellar winds, where both negative and positive feedback effects on the rate of star formation can occur, the feedback effect of ionisation on star formation is unambiguously negative, since dense cool gas that might otherwise have formed stars is converted into hot ionised gas that cannot form stars.

A newly formed group of stars, containing only a few O stars, readily ionises many times its own mass of gas—Whitworth (1979) estimates that if only 4% of the mass of a molecular cloud

[3] Much of this section has been taken from Larson 1987

condenses into stars with a standard Initial Mass Function (IMF), enough ionising photons are emitted by these stars to completely ionise the rest of the cloud. This means that the efficiency of star formation is predicted to be small, at least when averaged over a region large enough to contain significant numbers of O stars. Defining the efficiency of star formation as the ratio of "output", taken as the mass of stars formed, to "input", taken as the mass going into star-forming clouds, we obtain

$$efficiency\ \epsilon = stellar\,mass/cloud\,mass \approx 0.05 \tag{1.4}$$

If the efficiency of star formation can be considered known, then the total star formation rate (SFR) can be estimated. In our Galaxy the total mass of molecular clouds is about 2×10^9 $M_\odot$ (Solomon *et al.* 1987) and the typical lifetime of these clouds is estimated to be of the order of 2×10^7 yrs (Larson 1981). The rate of cycling matter through the molecular gas must then be of the order of 100 $M_\odot$/yr, and if 5% of this mass goes into stars, the predicted SFR for our Galaxy is ≈ 5 $M_\odot$/yr.

The formation of stars evidently requires the prior formation of molecular clouds. The processes that are probably the most important in the formation of giant molecular clouds are:

Large-scale gravitational instabilities

For a thin gas layer with a velocity dispersion c_g and an average surface density μ_g the growth time for a gravitational instability is

$$\tau \sim \frac{c_g}{\pi G \mu_g} \sim 5 \times 10^7\ yrs \tag{1.5}$$

where the local values $c_g \sim 6$ km s^{-1} and $\mu_g \sim 8$ $M_\odot$/pc^2 have been substituted (Larson 1987).

Density-wave compression of the interstellar medium

The time-scale for processing gas through density-wave arms is approximately

$$\tau \sim \frac{2\pi R}{V} \sim 2 \times 10^8\ yrs \tag{1.6}$$

where R and V are the galactic radius and rotation speed, and local values have again been used (Larson 1987).

Cloud coagulation by random collisions

Adopting conventional values for cloud parameters, the time required for random collisions to build up a cloud of mass M is

$$\tau \sim 7 \times 10^6 M^{1/3} \sim 3 \times 10^8\ yrs \tag{1.7}$$

for a cloud of mass 10^5 $M_\odot$ (Larson 1987); a short time-scale will apply in spiral arms where the space density of clouds is enhanced.

All of the cloud formation time-scales involved are of the order of 10^8 yrs. If 5% of the mass that goes into giant molecular clouds condenses into stars the time-scale, τ_{SF}, for processing interstellar matter into stars is then 20 times longer than the time-scale, τ_{CF}, for cloud formation, *i.e.*

$$\tau_{SF} = \epsilon^{-1}\tau_{CF} \sim 2 \ Gyrs. \tag{1.8}$$

If the efficiency of star formation is fixed, then the rate of star formation depends only on the rate of molecular cloud formation. The cloud formation processes discussed have time-scales that vary inversely with the surface density, μ_g, of the gas and we expect that, at least to a first approximation,

$$\tau_{SF} \propto \mu_g^{-1} \tag{1.9}$$

If the dependence on other parameters are not important then the star formation rate per unit area in a galactic disk satisfies

$$\frac{SFR}{area} = \frac{\mu_g}{\tau_{SF}} \propto \mu_g^2 \tag{1.10}$$

As the SFR/area is proportional to the square of the gas density then any region which increases its gas surface density will also have an increase in its rate of star formation. It has become clear that the gas surface density is high towards the nuclei of many IR-luminous galaxies and so we would expect that these circum-nuclear regions will have large rates of star formation (Henkel *et al.* 1991).

If the infrared luminosity, L_{IR}, is powered by young stars then the rate at which gas is being converted to stars is proportional to L_{IR}, *i.e.*

$$\dot{M}* = K L_{IR} \tag{1.11}$$

The value of K depends on the assumed form of the stellar IMF and, among other quantities, the temporal behaviour of the star formation. Models imply that modestly luminous galaxies, with $L_{IR} = (0.4\text{-}3)\times10^{10}$ $L_\odot$ are converting the gas in their central regions into stars at rates $\dot{M} = 2\text{-}12$ $M_\odot$ yr^{-1} (Telesco 1988). It has been recognised that star formation maintained at these levels will exhaust all of the gas in many active star-forming galaxies in much less than a Hubble time. For the typical values $\dot{M} = 3\times10^{-10}$ L_{IR} and $L_{IR}/M(H_2) = 10$, the time-scale to deplete the gas is $\tau_g(H_2) \equiv M(H_2)/\dot{M} = 3\times10^8$ yr (Telesco 1988). It is this relatively short duration which has led to many of the IR luminous galaxies being termed "starbursts". The time-scale for exhaustion of the molecular gas is crucially dependent on the initial mass function of the stars because if low mass stars do not form then the starburst could be sustained for far longer.

Towards the nuclei of some of these IR luminous galaxies the efficiency of converting molecular gas into stars appears to be higher than across the Milky Way, *e.g.* an efficiency of 50% has been inferred for M82 (Larson 1987). The requirement of a high efficiency of star formation may be satisfied if star formation takes place on a time-scale short compared with the time required for the negative feedback effect due to ionisation to become important. There is a delay time in the feedback provided by the finite evolutionary lifetimes of the ionising stars; if we define the delay time as the time required for the emission of half of the ionising photons that will ever be emitted, this time is about 3×10^6 yr for a cluster of O stars with a normal IMF (Larson 1987). If star formation occurs within a time interval shorter than this, less than half of the stellar ionising photons will be emitted whilst the stars are still forming, and the negative effect of ionisation will accordingly be reduced. The high surface density of the gas in the region will result in a reduced time-scale for cloud formation. This will also act to increase the efficiency of

star formation and in the limiting case where the surface density becomes high enough, that the time-scale for cloud formation becomes smaller than the time-scale for cloud disruption, then the efficiency of star formation will approach unity. Smith (1992) argues that the gas velocity dispersion is higher, though, in the nuclei of many IR luminous galaxies. An increase in the velocity dispersion increases the growth time for gravitational instabilities. An effect that would increase the efficiency of star formation is if the IMF is biased against the formation of the most massive stars as these are the stars which have the most damaging environmental impact.

1.3 The energetic interstellar medium

1.3.1 Understanding the dominant energy inputs into the interstellar medium

As discussed above, star formation occurs deep within molecular clouds and so if we are to have any theory of how stars form within galaxy nuclei we need to quantify how the physical nature of the molecular clouds depend upon their environment. Observations of CO 1-0 indicates that molecular gas is the dominant component of the ISM by mass in many galaxy nuclei, *e.g.* Scoville *et al.* (1985). The molecular gas is also much denser than other components of the ISM but has a much smaller volume filling factor than the other components, *e.g.* Carral *et al.* (1994). Furthermore, the molecular gas in galaxy nuclei is observed to have a higher average density than molecular clouds typically found in the local solar neighbourhood, *e.g.* Wall *et al.* (1991). Moreover, at larger radii clouds of atomic, rather than molecular, hydrogen start to dominate the mass budget of the ISM in galaxies, *e.g.* Scoville *et al.* (1985). Understanding the interface between molecular gas and atomic gas and the physics of what controls the relative fraction of these two phases is required if we are to understand how the mass of the ISM is distributed in galaxies, and why.

The efficiency of star formation is controlled by the competition of how quickly stars form within the clouds against how long the molecular gas can survive in a state where stars are able to form. Therefore, it is crucial to understand the physical mechanisms in the regions where clouds are being eroded. One obvious place where it would be expected that clouds are being destroyed is where strong UV fields impinge upon the edges of the molecular gas. Destruction of molecular hydrogen will result in atomic hydrogen and so the physics of these UV bathed regions will have an integral bearing on the interplay between the atomic and molecular phases on a galactic scale. Another obvious way to destroy molecular clouds is through shocks where energetic collisions dissociate the molecules.

The previous paragraph(s) spell out the reasoning behind the research in this thesis. The physics of the interface between molecular and atomic gas is crucial in any empirical model of star formation in galaxy nuclei. Below we discuss in more detail the physics of molecular regions bathed in UV and the physics of shocks impinging upon molecular gas.

1.3.2 Regions where UV photons dominate the heating of the gas

Photon dominated regions (PDRs), or also commonly called photodissociation regions, are, funnily enough, regions where far ultra-violet (FUV) (6 eV $< h\nu <$ 13.6 eV) photons dominate the heating and/or cooling of the gas.[4] They are typically observed to be at the edges of molecular clouds, in the interface region between ionised gas and the molecular gas. The basic

[4] Much of this section has been taken from Genzel (1991)

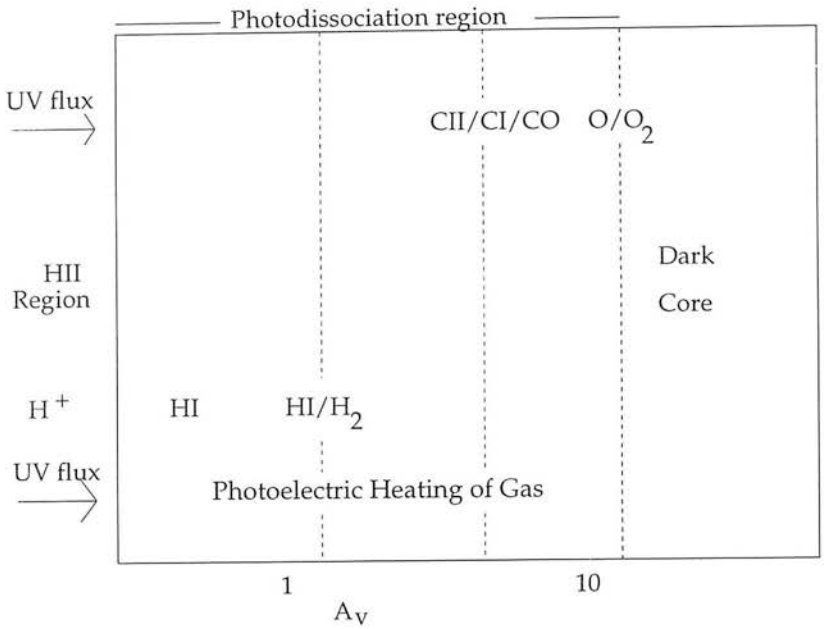

Figure 1.4: The chemical structure of a PDR

size scale of the dissociation region is given by the penetration depth of far-UV radiation. The most efficient broad-band absorber of far-UV radiation is dust[5] and because the column of dust is proportional to the visual extinction the local UV field, G, in the PDR is

$$G \propto e^{-A_v} \tag{1.12}$$

and the maximum thickness of a photodissociated region is given by the condition that the UV dust absorption optical depth be a few, or

$$d_{PDR} \approx \tau_{abs} \approx a\,few \tag{1.13}$$

corresponding to a hydrogen column density of[6]

$$N_0(H) \approx 6 \times 10^{21}\ cm^{-2} \tag{1.14}$$

Detailed theoretical models have been developed to describe PDRs, eg. Tielens & Hollenbach (1985), Black & van Dishoeck (1987) and Sternberg & Dalgarno (1989). Generally, the models consider a plane parallel slab illuminated from one side by an intense FUV field. The chemical structure in the PDR that is common to all models is displayed in Figure 1.4

The penetrating FUV photons create an atomic surface layer. At a depth corresponding to $A_v \sim 2$, the transition from atomic H to molecular H_2 occurs. This is a direct consequence of the fact that photodissociation of H_2 requires UV absorption from the $X^1\Sigma_g$ ground electronic state to the $B^1\Sigma_u$ and $C^1\Pi_u$ excited states, followed by a transition into the unbound continuum of the ground state. There is no direct continuum dissociation process. The UV transitions of H_2 (the Lyman and Werner bands) rapidly become optically thick and self-shielding sets in (Black

[5] With a typical atomic photoionisation cross section of 10^{-17} cm^2, a dust absorption cross section of $\sim 10^{-21}$ cm^2 per H nucleus (Savage & Mathis 1979), and an abundance ratio of $\sim 10^{-6}$ for the ionisable species, only 1% of the photons are absorbed by metal atoms.

[6] This immediately gives us a clue to understanding why atomic and molecular clouds are closely related. If a cloud has a column density above about 5×10^{21} cm^{-2} then there is enough dust to shield the interior of a cloud from far-UV radiation and molecules can form and survive. If the column density of the cloud is below this value then it is likely that most of the molecules will be dissociated and the cloud will be atomic.

& van Dishoeck 1987). The absorption of UV photons by H_2 is discussed in greater detail in chapter 3.

In this outer layer almost all of the gaseous carbon is in the form of C^+—see chapter 5 for further details. For a given value of n_H the CII intensity from a PDR saturates at large values of G_{UV} because for such radiation field intensities the total column density of CII is determined by the dust penetration depth of the UV photons which varies only logarithmically with G_{UV} (Stacey *et al.* 1991). In other words, a higher G_o results in a slightly larger column density of dust to the CII/CI/CO transition region, where the extra dust column reduces the far-UV flux to a relatively constant "transition" value.

At this transition region, which is typically at $A_v \sim 4$, the carbon balance shifts from C^+ to CO with only a small layer of atomic carbon produced in the transition region. The reason for the sharp transition can also be understood as follows. The dissociation potential for carbon monoxide, 11.09 eV, is very close to the ionisation potential for carbon, 11.25 eV. Carbon monoxide is a very stable molecule, not highly reactive. In a shielded environment in which chemical reactions can occur it is the endpoint of these reactions. Also, oxygen is more abundant that carbon. Therefore, in a shielded environment most of the carbon will be in the form of CO.

As ^{12}CO 1-0 rapidly becomes optically thick most of the emerging I_{CO} from a PDR is produced rather close to the C^+/CO transition region. The strength of the I_{CO} emission depends upon the local temperature. Wolfire *et al.* (1989) argue that as the gas temperature at the transition region depends on the local far-UV flux, and is therefore relatively constant, the intensity of emission of I_{CO} should be at a fairly constant level from all PDRs. Except for the O locked up in CO, essentially all the oxygen is in atomic form until very deep into the cloud, $A_v \sim 10$. In addition to these most abundant species, the photodissociation zone contains many less abundant ions, such as S^+, Mg^+, Si^+ and Fe^+ whose abundances depend heavily on depletion.

Besides the chemical composition, the FUV photons also control the energy balance of the gas through photoelectric heating and UV pumping of H_2. These mechanisms are highlighted in Figure 1.5. Far-UV photons absorbed by a dust grain will create energetic electrons within the grains. These electrons diffuse through the grain, reach the surface, overcome the work function of the grain and any Coulomb barrier if the grain is charged, and are ejected into the gas phase with excess kinetic energy. The photoelectric effect converts, typically, about 0.5% of the far-UV energy into gas heating in this way (Bakes & Tielens 1994). The rest of the energy is absorbed by the grain and emitted as far-IR dust continuum radiation. The gas in the surface layer is then much warmer ($\sim$ 500 K) than the dust (30-75 K).

UV pumping of H_2 molecules can convert a similar fraction of the UV energy into gas heating if the hydrogen density is sufficiently high (Sternberg & Dalgarno 1989). In this case, electronic excitation of H_2 molecules in the Lyman and Werner bands at 1000 $\AA$ leads to subsequent radiative decay into a vibrationally excited level of the electronic ground state (2 to 3 eV) in 9 out of 10 excitations, Figure 1.5. At densities greater than the critical density for collisional de-excitation of the vibrational states, ($n(H_2)_{crit} \approx 7 \times 10^4$ cm^{-3}), energy can again be converted into gas heating. In the UV transitions of H_2, the conversion efficiency of a single absorbed photon into kinetic energy can be as high as 30%. The total efficiency of converting far-UV photons into heating depends on the fraction of incident radiation absorbed by H_2 molecules throughout the cloud. This fraction depends on the dust to gas ratio and on the ratio of gas density to intensity of the UV field and is usually $\leq$ 10% (Sternberg & Dalgarno 1989).

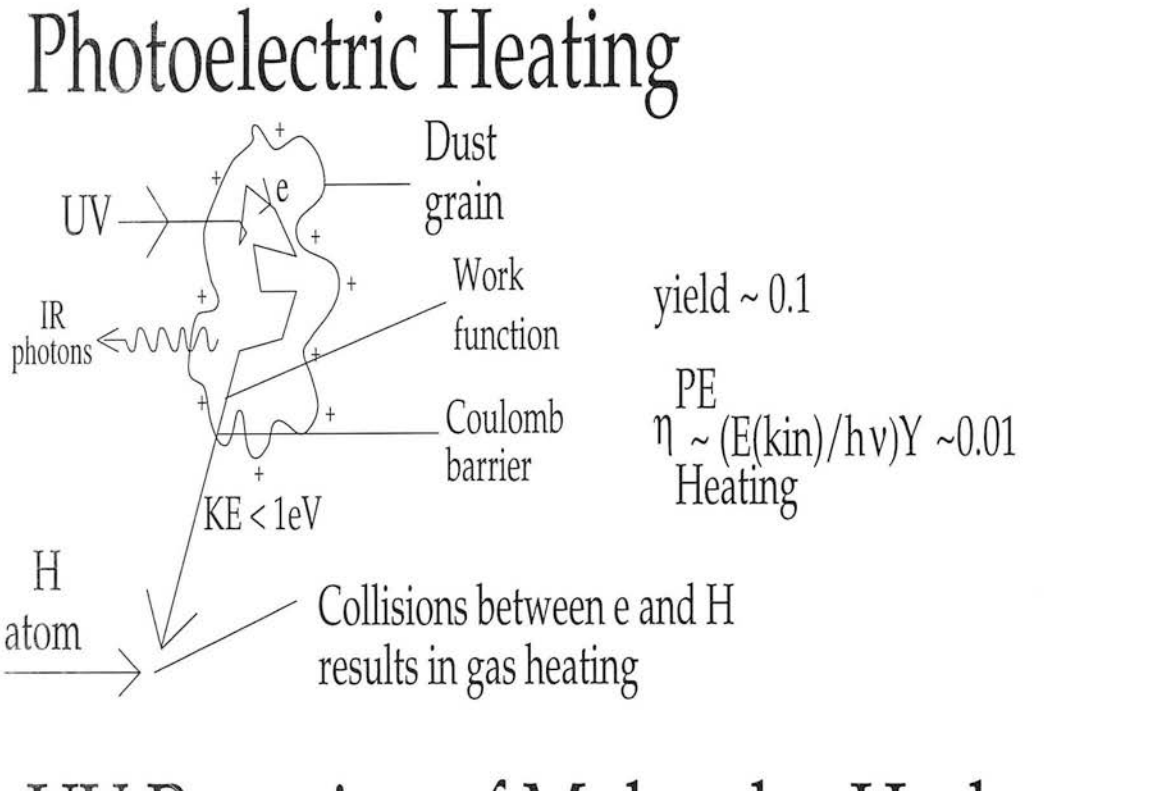

Figure 1.5: The dominant heating mechanisms in a PDR

Somewhat deeper into the cloud, $A_v > 4$, penetrating red and near-infrared photons keep the dust warm and gas-grain collisions couple the gas temperature to slightly below the dust temperature. Gas cooling of the photodissociation zone at $A_v \leq 5$ is primarily by the fine structure lines of OI 63 μm, CII 158 μm and SiII 35 μm). Of lesser importance are the H_2 ro-vibrational and rotational lines and the sub-mm fine structure lines of CI, largely because of the small column densities in the upper state and because of their small A-coefficients. The rotational lines of CO become important coolants deeper into the cloud.

The standard model of Tielens & Hollenbach (1985) is representative of dense photodissociation regions within a few tenths of a parsec of a massive O star, such as the HII region/cloud interfaces in Orion. The gas temperature in the PDR ranges between about 1000 K at the surface to about 100 K at the C^+/CO transition. Many of the important cooling lines in PDRs are at wavelengths in the far-IR which means that the atmosphere stops all attempts from observing the lines from the ground. It is only by going above the bulk of the absorbing layers in the atmosphere that it becomes possible to observe the far-IR lines. This has meant that much of the observational data on PDRs has come from the Kuiper Airborne Observatory.

1.3.3 Regions that are heated by shocks

Interstellar shock waves are generated by supersonic mass motions, such as colliding clouds, outflows from young stars, stellar winds and supernovae.[7] The kinetic energy of the supersonic motions is converted into thermal energy. In the process, shocks compress and accelerate gas and dust. Shocks radiate primarily in lines from the cooling gas behind the front where the flow motion is converted into random thermal motions (Hollenbach & McKee 1989). With the exception of high velocity shocks ($v_s > 50$ km s^{-1}) in dense ($n(H_2) > 10^6$ cm^{-3}) clouds, dust emission is small compared to line emission from hot gas. Shocks in dense molecular clouds often radiate mostly in the infrared and sub-millimeter lines of molecules, atoms and ions. High velocity, (J)-shocks dissociate most molecules and ionise atoms. Magneto-hydrodynamic (C)-shocks create large column densities of moderately warm molecular gas.

J-shocks

In cold gas (sound speed < 1 km s^{-1}) with no or weak magnetic fields, a fast (> 50 km s^{-1}) pressure disturbance creates a J-shock, where temperature, density and flow velocity suffer a virtually discontinuous jump across the shock front. Conservation of mass and momentum (and energy for an adiabatic shock) yield relations between preshock variables and downstream variables. These Rankine-Hugoniot relations are, for instance, discussed in Dyson & Williams (1980).

The thermal structure behind the front is shown in Figure 1.6 for the case of a 80 km s^{-1} shock into a $n = 10^5$ cm^{-3} pre-shock density gas (from Hollenbach & McKee 1989). Immediately behind a fast shock in a molecular cloud the temperature is high,

$$T_s \approx 1.5 \times 10^5 \left(\frac{v_{shock}}{100\,km\ s^{-1}}\right)^2 \ [K] \tag{1.15}$$

Consequently the molecules dissociate and ionise. The post-shock gas radiates in the UV and visible wavelength bands in resonance, semi-forbidden and forbidden lines of hydrogen, helium and the ions of oxygen, carbon, sulfur, and iron. Further downstream ($N_H \geq 10^{16}$ cm^{-2}), the hydrogen ionising photons are absorbed, creating a 10^4 K temperature plateau. Hydrogen

[7] Much of the section has been taken from Genzel (1991)

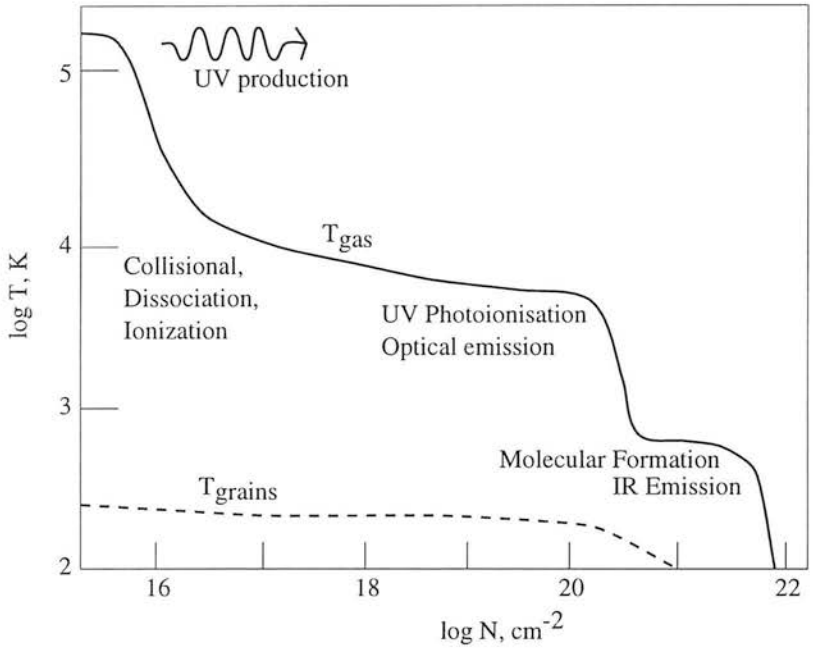

Figure 1.6: The post-shock temperature structure behind a fast molecular J shock ($n = 10^5$ cm^{-3}, $V_s = 80$ km s^{-1}). This figure is adapted from Hollenbach & McKee (1989). Three regions are delineated: 1) the hot, $T \sim 10^5$ K immediate post-shock region, where gas is collisionally dissociated and ionised and UV photons are produced which affect both the pre-shock and post-shock gas; 2) the "recombination plateau", where the Lyman continuum photons are absorbed, maintaining $T \sim 10^4$ K; and 3) the recombining and molecule-forming gas downstream, where chemical energy of H_2 formation can maintain a lower temperature plateau.

recombination lines and [NeII] fine structure lines originate there. Further downstream again ($N_H \approx 10^{20}$ cm^{-2}), the gas recombines and cools rapidly. Molecular formation sets in at temperatures of a few hundred K. As a result of the high temperatures, neutral-neutral chemical reactions proceed rapidly. Carbon is efficiently converted to CO. The remaining oxygen is converted to OH and H_2O. In at least moderately dense gas ($n(H_2) \geq 7 \times 10^4$ cm^{-3}), the H_2 formation energy is converted into gas heating and creates another temperature plateau at ≈ 400 K (Neufeld & Dalgarno 1989). This heating through the collisional de-excitation of H_2 is similar to the heating mechanism in dense PDRs, but this time the formation of H_2 provides the energy source, rather than UV photons. The calculations of Hollenbach & McKee (1989) show that much of the infrared emission from J shocks comes from this plateau and from the temperature region $< 10^4$ K, where the gas density is about 100 times greater than in the pre-shock gas. Typically 1-10% of the shocks energy emerges in infrared lines.

Hollenbach & McKee (1989) calculated the chemical and thermal structure and cooling of dissociative shocks with speeds between 40 and 150 km s^{-1} at preshock densities between 10^3 and 10^6 cm^{-3}. At medium densities ($\approx 10^4$ cm^{-3}) and velocities, the dominant coolants are OI 63 μm, OI 6300 $\AA$ and CI 9849 $\AA$, followed by H_2 and CO rotational and ro-vibrational line emission. At densities of 10^6 cm^{-3} or greater the rotational line emission of H_2O and OH dominates and grain cooling becomes important. The FeII lines at 1.3/1.6 μm, along with vibrational transitions of H_2, are the most prominent emission lines in the near-IR range. Depending on the gas phase abundance of silicon, SiII 35 μm emission may also be detectable. Sub-millimeter emission of highly excited rotational states of SiO, HCN, CN, SO and NO may be characteristic tracers of J-shocks in dense clouds (Genzel 1991).

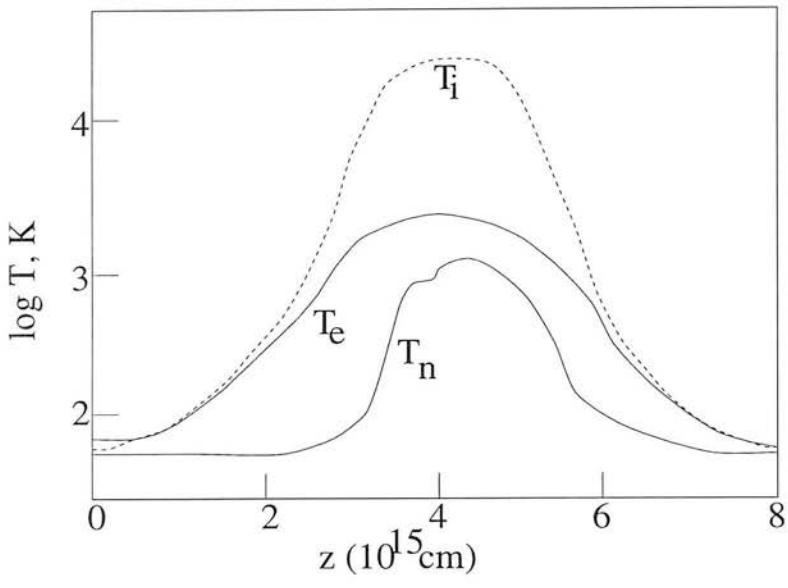

Figure 1.7: Temperature structure behind a C shock with shock velocity 25 km s^{-1} in a dense molecular cloud with $n_H = 10^6$ cm^{-3}, $x_e = 10^{-8}$ and $B_o = 1.0$ mG. The plot is adapted from Draine *et al.* (1983).

C-Shocks

A different type of shock occurs if shock velocities are less than about 40 km s^{-1}, and if there is a moderately strong magnetic field and the ionisation fraction in the cloud is moderately low (x_e = [electrons]/[hydrogen] $\leq 10^{-6}$). In the presence of a magnetic field, disturbances propagate at the Alfvèn speed, v_A, given by

$$v_A = \frac{B}{\sqrt{4\pi\rho}} = 22 \left(\frac{B}{1mG}\right) \left(\frac{n}{10^4\ cm^{-3}}\right)^{-1/2} \quad [km\ s^{-1}] \tag{1.16}$$

where ρ and n are the mass and number density of the gas. Shocks are possible for $v_A < v_{shock}$, otherwise the pressure disturbance is "communicated" and damped by Alfvén waves. In partially ionised gas, the ions react rapidly to changes in the magnetic field and then communicate those more slowly to the neutrals by ion-neutral collisions. Because of this difference in reaction speed, it is possible to transmit damped Alvén waves in the "ion" fluid at the ion magnetosonic speed, $v_A(\text{ion}) = (\rho/\rho(ion))^{1/2} v_A >> v_A$. In that case magnetic field and ion density ρ(ion) must vary continuously through the shock front. If the neutrals (because of their interactions with ions) also vary continuously, the shock is called a "C-shock".

The shock sends a message to the upstream gas via the ions and magnetic field. The ions begin to compress and accelerate, so that they drift relative to the neutrals and heat and accelerate them. The neutral gas can rapidly radiate its thermal energy away. In practise this happens if molecules are not dissociated (T < a few 10^3 K) and the efficient cooling of H_2, CO, OH and H_2O is available. The detailed structure of a 25 km s^{-1} C-shock into a 10^6 cm^{-3} pre-shock density cloud at a magnetic field of 1 mG is shown in Figure 1.7, adapted from Draine *et al.* (1983). C-shocks radiate nearly the entire energy of the shock in many molecular and atomic infrared lines[8] [OI] 63 μm dominates the cooling for slow (10 km s^{-1})

[8] There is very little far-IR continuum emitted by C-shocks because of the relatively low gas temperature immediately behind the shock. The gas is not hot enough to radiate in the UV, and so the line emission from the cooling post-shock gas tends to come out in the optical to near-IR. At these longer wavelengths the dust is less

shocks. Rotational and ro-vibrational line emission of H_2 is the main coolant for higher velocities ($10 < v_{shock} < 50$ km s^{-1}), but moderate pre-shock densities. For densities of 10^6 cm^{-3} or greater, H_2O and OH rotational emission becomes more and more important.

1.4 The philosophy behind this thesis

In an extra-galactic source, and particularly a starburst galaxy, the region of interest is invariably unresolved spatially and so only global information about the local energy inputs is available. The region of interest, the nucleus of the starburst, will contain a mixture of shocks, produced by collisions of molecular clouds, bipolar outflows and supernovae explosions, and PDRs, neighbouring the HII regions around O and B stars. What is therefore needed in extra-galactic studies is the determination of reliable diagnostics of either shocked gas or PDRs. If such diagnostics can be found then it would be possible to use the knowledge of the location of the shocks/PDRs in the nuclear region in order to see what effects the energy inputs are having on the emission from more "ambiguous" tracers of excited gas. Moreover, if the physics of the emission from the "reliable" diagnostics is understood, it is possible that the reliable tracers can be used to constrain physical parameters such as the density, temperature and either local UV flux or shock velocity, always assuming that PDRs and shocks are not coextensive. In particular, two discriminants between shocks and PDRs are atomic carbon and molecular hydrogen.

1.4.1 Fine-structure transitions of atomic carbon

PDRs are bright in the far-IR dust continuum, the far-IR fine-structure lines of OI and CII and the rotational lines of CO. Observations of several of these lines from the same region can be used to determine the physical conditions in the emitting gas. The far-IR fine-structure lines are particularly useful in that respect since the critical densities of the C^+ and O° lines (3×10^3-3×10^5 cm^{-3}) and excitation energies (100-300 K) span the range present in many PDRs. The CII 158 μm line, which is usually optically thin, can be used to determine the total mass of emitting gas. Of course, this analysis assumes elemental abundances (or abundance ratios). Often densities are inferred from the ratio of the total cooling rate (*i.e.* the OI + CII intensity) to the far-IR dust continuum. This subject is discussed in greater detail in chapter 5.

Shocks are expected to be bright in the far-IR fine-structure lines and in fact, unlike PDRs, most of the luminosity is emitted by lines rather than through continuum emission from dust. In PDRs the ratio of line to continuum luminosity is about 1%, the photoelectric efficiency, whereas in shocks the ratio is far higher.

Of particular interest is atomic carbon. The fine-structure lines from the ground electronic level are robust diagnostics of PDR gas. The predicted intensity from PDRs is fairly independent of both density and the UV field. In shocks the brightness of the CI emission may be considerable but shocks, because of the relatively low filling factors of the gas involved, do not dominate the carbon emission budget from a molecular cloud. Therefore, atomic carbon is expected to be a reliable tracer of PDR gas in starbursts, particularly in regions where the ratio of total line luminosity to continuum luminosity is about 1%, indicative that the dominant emission source is PDRs. This subject is discussed in greater detail in chapter 5.

efficient at absorbing the radiation and so most of this line radiation is not absorbed and reprocessed to longer wavelengths.

1.4.2 Line ratios of molecular hydrogen

Far-UV photons directly excite H_2 electronically (Burton 1992). The interpretation of fluorescent H_2 emission is complicated by the need to consider two processes, radiative excitation of the H_2 molecule by far-UV, and its collisional de-excitation, mainly by H atoms. H_2 absorbs photons in the 11-13.6 eV range and is excited to an electronic state above ground. The decay back to the ground electronic state leads to the vibrational continuum (H_2 photodissociation) 10% of the time and to a bound, vibrationally excited state 90% of the time (typically at ~ 2 eV above ground). In pure radiative fluorescence (Black & van Dishoeck 1987), the molecule cascades down the vibrational-rotational ladder, emitting near-IR photons. In low-density clouds ($n < 5\times10^4$ cm^{-3}; Goldschmidt & Sternberg 1995) the relative intensities of the IR fluorescent emission lines are insensitive to the cloud conditions because they are determined primarily by the branching ratios of the purely radiative quadrupole ro-vibrational transitions which are molecular constants. The relative line intensities are characterised by large vibrational excitation temperatures and small rotational temperatures (Black & van Dishoeck 1987). A discrepancy in the measured vibrational and rotational temperatures, therefore, is a signal that H_2 is excited by UV photons. In a shock the two temperatures are the same because H_2 is thermalised. This subject is discussed in greater detail in chapter 3.

1.4.3 The rest of this thesis

In order to test whether it is possible to reliably trace the amount of PDRs, using carbon, and discriminate between shocks and PDRs, using molecular hydrogen, in a starburst's nucleus it is important that they are calibrated against each other for at least one source. In order to do this, the nearby starburst NGC 253 was chosen as the control object. Much of the previous work on atomic carbon has compared its abundance directly with that of carbon monoxide and so it was decided to study NGC 253 in the light of CO, particularly $C^{18}O$.

In the next chapter I discuss previous observations of the starburst galaxy NGC 253. The chapters after that discuss H_2, $C^{18}O$ and CI, in that order. Finally, I summarise the main conclusions that have been reached and suggest future lines of research.

Chapter 2

A review of previous observations of NGC 253

2.1 Introduction

The Sculptor galaxy NGC 253, a nearly edge-on spiral (i=78°, Pence 1981) of type SAB(s)c (de Vaucouleurs *et al.* 1991) or Sc(s) (Sandage & Bedke 1995), is perhaps the best example of a nearby nuclear starburst (Rieke *et al.* 1988). There is a large scatter in published distance estimates towards NGC 253 (Mauersberger *et al.* 1996). Graham (1982) suggested that the Sculptor group is considerably extended in the line-of-sight and that NGC 253 is more distant than other members of the group, for which good distance estimates exist (NGC 55: 1.4±0.1 Mpc, NGC 300: 1.6±0.2 Mpc; see van den Bergh 1992 and references therein). Blecha (1986) observed 24 of the brightest globular clusters and estimated a distance of 2.4 to 3.4 Mpc, while David & Pritchet (1990) analysed a colour-magnitude diagram of stars in the halo of NGC 253 and concluded that the distance is 1.7 to 2.6 Mpc. Other estimates include Sandage & Tammann (1975), who estimated a distance of 3.4 Mpc. The distance I have adopted for NGC 253 is 2.6 Mpc.

NGC 253 is among the most prominent extra-galactic sources from the radio range, *e.g.* Antonucci & Ulvestad (1988), to the infrared, *e.g.* Telesco *et al.* (1993), to X-rays, *e.g.* Fabbiano & Trinchieri (1984). The rest of this chapter discusses the observations of NGC 253 across the electromagnetic spectrum and concludes with an attempted synthesis of what is known about one of the most comprehensively studied galaxies.

2.2 Gamma-ray observations

Gamma-ray observations of starburst galaxies have the potential to detect supernovae signatures through the dense starbust nuclear regions. Such observations could be used as a direct estimator of supernova rates and discern between different types of supernovae (SN) occurring in the starburst cores. Extra-galactic γ-ray astronomy is still in its infancy and to date γ-rays have been detected from only 2 starburst galaxies. One of these galaxies is NGC 253.

Bhattacharya *et al.* (1994) detected γ-rays in the energy range 0.05-10 MeV using the Oriented Scintillation Spectrometer Evolution (OSSE) on the Compton Gamma-Ray Observatory. NGC 253 was detected in continuum up to 165 keV with a total of 4 sigma confidence and an estimated luminosity 3×10^{40} erg s^{-1}. The spectrum is best fitted by a power law of photon index 2.5. It is not clear what emission mechanism is responsible for the high energy gamma rays.

Extrapolating the Ginga photon fluxes, reported by Ohashi *et al.* (1990), to the energy range in which OSSE detected emission, yields fluxes an order of magnitude below the OSSE detections. This is the case even if a power law spectrum is assumed. Thus, there is another emission mechanism other than the very hot thermalised gas responsible for the emission detected by Ginga (Ohashi *et al.* 1990), which produces the emission detected by OSSE.

Bhattacharya *et al.* (1994) argue that the inverse Compton scattering of relativistic electrons off the far-IR photon field may only provide about 10% of the flux but Goldschmidt & Rephaeli (1995) have argued that inverse Compton scattering may be responsible for all the γ-ray flux from NGC 253. Bhattacharya *et al.* (1994) argue that thermal bremsstrahlung, from fast moving cosmic rays interacting with nuclei, provides approximately 3% of the observed luminosity. To derive this value, Bhattacharya *et al.* (1994) assumed that the cosmic ray flux in the circum-nuclear region of NGC 253 is about 160 $\times$ the local value[1] and the average particle density of the interstellar medium in NGC 253 is $\sim$ 30 cm^{-3} (Rieke *et al.* 1980). Mauersberger *et al.* (1995) estimate that the average particle density is $\sim$ 2000 cm^{-3}. The estimate of Mauersberger *et al.* (1995) may be a factor of 5 or so too high (see the discussion in section 2.9, on millimetre studies of NGC 253) but it is clear that the number density assumed by Bhattacharya *et al.* (1994) is probably an order of magnitude too low. As the estimate of the thermal bremsstrahlung luminosity scales directly with the number density (Bhattacharya *et al.* 1994) it is likely that thermal bremsstrahlung provides a significant contribution to the γ-ray flux detected by OSSE.

Summarising, γ-ray continuum emission has been detected from NGC 253. Thermalised hot gas (7×10^7 K) is only responsible for a few % of the observed flux. Other mechanisms which may be responsible for the γ-ray emission are inverse Compton scattering of relativistic electrons off the far-IR photon field and thermal bremsstrahlung between cosmic rays and nucleons. It is not clear which is the dominant process. The luminosity of the γ-ray emission from NGC 253, few $\times$ 10^7 L$_\odot$, is negligible when compared to the bolometric luminosity of NGC 253, few $\times$ 10^{10} L$_\odot$.

2.3 X-ray studies

Unlike active galactic nuclei, where the luminosity in the X-ray band can rival or even dominate the luminosity in other bands, the X-ray luminosity of starburst galaxies tends to be modest in comparison with their optical or infrared luminosity, a few percent or less. Nevertheless, the character of the information provided by the X-ray emission is unique as it probes the "high energy" phenomena in a galaxy, particularly those phenomena associated with the endpoints of stellar evolution: supernova remnants and the diffuse interstellar medium heated by them, and X-ray binary systems containing a compact object, either a neutron star or black hole. Below is a summary of what is known about the X-ray emission from NGC 253.

Fabbiano & Trinchieri (1984) observed NGC 253 with the High Resolution Imager (HRI) on the Einstein satellite and argued that the X-ray emission is made up of 4 components: eight bright pointlike sources; diffuse emission in the inner disk; a more intense region associated with the inner region; an extension along the southern portion of the minor axis. The pointlike sources are confined to the galactic bulge region and based on their high X-ray luminosities these are thought to be X-ray binaries (Petre 1993). The southern component along the minor axis, it was suggested, indicates the presence of shock-heated gas associated with, and outflowing from,

[1] The cosmic ray flux in NGC 253 is assumed to be the value derived for M82 by Völk *et al.* (1989).

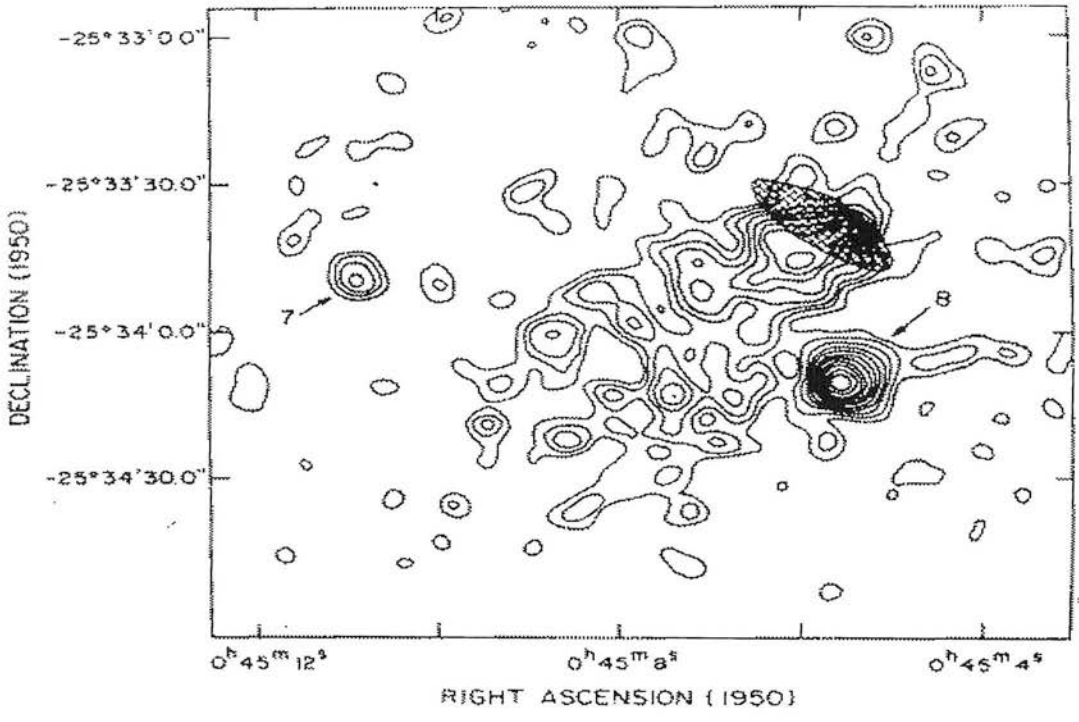

Figure 2.1: The X-ray plume emanating from the nucleus of NGC 253, adapted from Fabbiano & Trinchieri (1984). The shaded area approximates the size of the 2 cm radio emission reported by Turner & Ho (1983).

the starburst nucleus, Figure 2.1.

Fabbiano (1988) observed NGC 253 with the Imaging Proportional Counter (IPC) on Einstein. The X-ray emission shows an extended feature which is only seen to the north of the galaxy. This feature has no optical or radio counterpart and might be due to gaseous clouds ejected from the nucleus (Fabbiano 1988). Fabbiano (1988) suggested that the IPC observations provided evidence for a bipolar outflow of gas from the nuclear region, along the minor axis. The suggestion of a bipolar outflow is supported through the observations of an OH plume by Turner (1985). Given the inclination of NGC 253, the absence of a northern plume in X-ray emission can be understood in terms of absorption of the soft X-ray photons by the interstellar medium in the disk of NGC 253. Fabbiano (1988) derived the mass of hot gas showing up through its X-ray emission to be $\sim 3 \times 10^7\,M_\odot$, under the assumption that the gas has a filling factor of unity.

Ohashi *et al.* (1990) took an X-ray spectrum of NGC 253 in the 2-20 keV range using Ginga. Ohashi *et al.* (1990) suggest that a major fraction of the X-ray emission is from hot gas that has a temperature of ~ 7 keV (7×10^7 K). This temperature is inconsistent with the much higher temperatures characteristic of massive X-ray binaries (Petre 1993). Petre (1993) notes that while this temperature is consistent with that of low mass X-ray binaries the X-ray emission is unlikely to be solely generated by X-ray binaries for two reasons. First, citing the likelihood that the strong X-ray activity is presumably due to the starburst (Fabbiano & Trinchiere 1984) there is an inconsistency in the age of the starburst of NGC 253 ($\sim 10^7$ yrs) and the ages of low mass X-ray binaries ($\sim 10^9$ yrs). Secondly, the extended halo is evidence for a large amount of diffuse gas. If the temperature of this gas is $\sim 7 \times 10^7$ K, which is substantially higher than can be confined gravitationally, this provides a natural explanation for the extended X-ray halo

(Petre 1993). Ohashi *et al.* (1990) failed to detect iron K-emission and they suggested that this was due to a depletion of iron if most of the continuum emission is of thermal origin. Ohashi *et al.* (1990) suggested that maybe the iron is initially contained in dust grains which have not been ionised or destroyed. Ohashi *et al.* (1990) derived a similar mass of gas to Fabbiano (1988) ($\sim 2 \times 10^7\,\mathrm{M}_\odot$).

Petre (1993) reviewed the observations of NGC 253 made with the X-ray observatories BBXRT and ROSAT. Petre (1993) argues that a two component model of X-ray emitting gas is required to explain the BBXRT observations. The best fit spectrum includes a hot ($\sim 8 \times 10^7$ K) thermal bremsstrahlung component and a warm component ($\sim 4 \times 10^7$ K). The ROSAT image above 500 eV appears very similar to the IPC image but in the 0.1-0.5 keV band, an extensive halo, surrounding the entire galaxy is visible. Petre (1993) suggests that the combined result of the BBXRT and ROSAT data is that the hot $\sim 10^7$ K emission arises in or near the bulge, and that the extended halo is substantially cooler ($\leq 2 \times 10^6$ K). Petre (1993) argues that the complex and spatially varying spectra of NGC 253 suggests multiple components to the emission. In the 0.2-4.0 keV band approximately 30% of the flux comes from resolved X-ray sources and most of the remaining flux arises in the extended halo. Petre (1993) notes that it is a mystery why the iron line is missing in the X-ray spectra of several starbursts, including NGC 253, especially if the hot gas is the product of many supernovae explosions.

2.3.1 Discussion of X-ray results

It appears that X-ray observations of NGC 253 show evidence for a plume of hot gas, generated on the nucleus, which is flowing away from NGC 253 as a "superwind". Several authors have attempted to derive the physical conditions in the superwind and its likely impact on the evolution of the starburst region of NGC 253. Fabbiano (1988) estimated the nuclear mass loss rate to be of the order of $1\,\mathrm{M}_\odot\ \mathrm{yr}^{-1}$ whereas Ohashi *et al.* (1990) estimates the mass loss rate to be of the order of $20\,\mathrm{M}_\odot\ \mathrm{yr}^{-1}$. The difference arises because Ohashi *et al.* (1990) argue that the hot gas will be escaping with its sound speed whereas Fabbiano (1988) argues that the hot gas is escaping as a free-flowing wind. The derive supernovae rate in NGC 253 is of the order of $0.1\ \mathrm{SN\ yr}^{-1}$ (Ulvestad & Antonucci 1994) and so it is likely that, with an ejecta of the order of $10\ \mathrm{M}_\odot$ per SN, the estimate of Fabbiano (1988) may be closer to the true mass loss rate of NGC 253.

Absorption of the X-ray flux by foreground material means that the observed X-ray fluxes have to be corrected for absorption when deriving the X-ray luminosity. This correction means that there are significant uncertainties in the X-ray luminosity of NGC 253. The electron density, n_e, in the gas is given by

$$n_e = 1.11\sqrt{\frac{3L_x}{4\pi R^3 \Lambda(T)}} \tag{2.1}$$

where the value 1.11 is the Gaunt factor, L_x is the X-ray luminosity, R is the radius of the region of interest and Λ(T) is the cooling function of the gas at a temperature T, (Nulsen *et al.* 1984). At temperatures of $\sim 7 \times 10^7$ K the bulk of the cooling is from bremsstrahlung and so the rate is fairly independent of metallicity (Raymond *et al.* 1976). Unfortunately, none of the X-ray telescopes provide beam matched observations at several wavelengths and so it is not clear how you should derive a luminosity at a certain position in a galaxy given that the X-ray fluxes are from several components, all of which may undergo differing amounts of absorption. To derive the conditions in the nuclear region it is unsuitable to use the observations made

with Ginga due to its very large beam size ($1.1° \times 2°$). The Einstein observations of Fabbiano & Trinchieri (1984) are more suitable due to the detection cell size of $12'' \times 12''$ of the HRI. Fabbiano & Trinchieri (1984) argued that the X-ray feature along the minor axis is relatively well collimated, suggesting an approximately conical emission region of $\sim 70''$ height and $20''$ radius. Inspection of Figure 2.1 reveals that there is X-ray emission from a "rectangular blob" with dimensions $70'' \times 20''$. Fabbiano & Trinchieri (1984) derive a luminosity for the blob equal to 6×10^{38} erg s^{-1}. To derive this luminosity, they assumed that the gas temperature is $\sim 6 \times 10^6$ K. Ohashi *et al.* (1990) argue, though, that a gas temperature of $\sim 7 \times 10^7$ K is more realistic. Without a detailed understanding of the HRI response function it is impossible to know what effect this different temperature will have on the derived luminosity. To derive the electron density of the X-ray emitting gas in the central $20''$ of NGC 253 I have assumed that the response function of the HRI is flat over the energy range 0.5-7 keV. Assuming that 2/7 of the blobs luminosity is in the central $20''$, and with a Raymond *et al.* (1976) cooling function for gas at 7×10^7 K, I derive an electron density of ~ 0.1 cm^{-3} in the central $20''$ (~ 250 pc) of NGC 253. This assumes that the X-ray gas has a filling factor of the order unity. This should be realistic for the starburst in NGC 253 (Carral *et al.* 1994). The pressure in the X-ray gas ($P \approx 7 \times 10^6$ K cm^{-3}) is similar to that of other components of the ISM in the starburst (Carral *et al.* 1994).

Summarising, X-ray observations of NGC 253 have revealed the presence of hot gas associated with both supernova remnants in the bulge, and the extended halos around the galaxy. Imaging observations have revealed a number of un-resolved sources. Broad band X-ray spectroscopy indicates that the dominant emission component has a thermal bremsstrahlung spectrum with $T \sim 7 \times 10^7$ K. The origin of this component is probably supernovae-produced gas but it is a mystery why such gas does not have emission from iron. Much of the hard X-ray emission may be produced by an ensemble of X-ray binaries (Heckman 1993). Inverse Compton scattering of IR photons off relativistic electrons may also contribute substantially to the hard X-ray emission and could also explain the γ-ray emission from NGC 253 (Goldschmidt & Raephelli 1994). Heckman (1993) suggests that a composite thermal plus non-thermal origin for the hard X-rays could explain the X-ray continuum observations and the relative weakness of the 6.7 keV Fe K line in NGC 253. Observations in the range 10-500 keV are required before it can be established whether inverse Compton scattering is indeed important in generating the high energy photons observed towards NGC 253. The pressure in the hot gas within the nuclear starburst region is similar to other colder components of the ISM. The hot gas shows evidence for the ejecta of $\sim 1\,M_\odot$ yr^{-1} from the circum-nuclear region of NGC 253. The luminosity of the X-ray emission from NGC 253 (a few $\times 10^7\,L_\odot$) is negligible when compared to the bolometric luminosity of NGC 253 (a few $\times 10^{10}\,L_\odot$). The mass of hot gas emitting X-rays is of the order of $10^7\,M_\odot$.

2.4 Optical studies

McCarthy *et al.* (1987) took optical images and spectroscopy of ionised gas towards, and away from, the nuclear region of NGC 253. The optical images appear to show emission cocooning the X-ray emission reported by Fabbiano & Trinchieri (1984), particularly along the southern minor axis of the galaxy, Figure 2.2. McCarthy *et al.* (1987) provided possible explanations for the origin of the energy source which generates the optical emission. Their favoured model was that clouds in a superwind are photoionised by far-UV radiation that leaks out of the central starburst. McCarthy *et al.* (1987) note that the principle difficulty with this model is that the

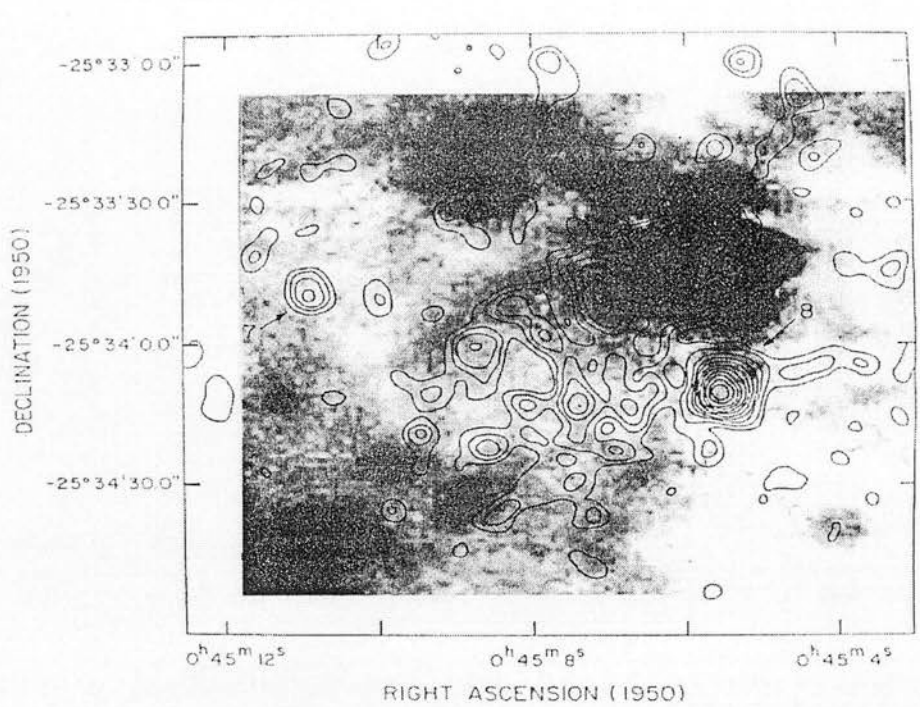

Figure 2.2: A narrow-band Hα + [NII]λ6548,6584 image of NGC 253, adapted from McCarthy *et al.* (1987). The contours of the X-ray plume are superimposed. The faint filamentary line emission appears to cocoon the X-ray emission

observed spectra of NGC 253 are dissimilar to models of gas photoionised by O and B stars. Such a difficulty can be removed by postulating a population of very hot stars (T $\geq$ 56,000 K), known as "warmers", in the starburst region of NGC 253. The existence of a population of warmers seems unlikely as Carral *et al.* (1994) suggest that the effective temperature of the stars in NGC 253 is $\sim$ 35,000 K. McCarthy *et al.* (1987) argue that shocks driven by the winds ram pressure are unlikely to provide enough energy to produce the observed optical emission and similarly for X-ray heating, because the X-ray luminosity is a small fraction, $\sim$ 0.1%, of the bolometric luminosity. This resulted in McCarthy *et al.* (1987) noting that it is not at all clear what energy source produces the optical emission.

Heckman *et al.* (1990), in a seminal work on the nature and implications of the superwind phenomenon, discussed optical spectroscopic data and images of 14 galaxies which included NGC 253. Heckman *et al.* (1990) noted that the morphology of the ionised gas along the SE minor axis of NGC 253 is strongly limb brightened, which suggests that the outflowing gas defines a hollow cylinder or conelike structure. There is a region of split line (double-peaked) emission in the SE ionised nebulae, Figure 2.3. The region of split lines begins about 130 pc from the nucleus and extends out an additional 450 pc. At a position 250 pc SE of the nucleus a slit spectrum along the major axis position angle of NGC 253 shows that the region of split lines extends about 350 pc. There is no corresponding region of split lines that was detected to the NW of the nucleus, presumably because the emission region is on the far side of the slightly tipped dusty disk. The velocity separation of the split lines ranges from about 250 km s^{-1} at positions nearest to the nucleus to about 450 km s^{-1} at the SE extremity of the nebulae. The split lines consist of a weak blue-shifted component (velocity ranging from -200 km s^{-1} to nearly -400 km s^{-1} relative to the adopted systemic velocity of 236 km s^{-1}) and a red-shifted component (velocity ranging from -50 to +100 km s^{-1} relative to systemic) that is typically 2

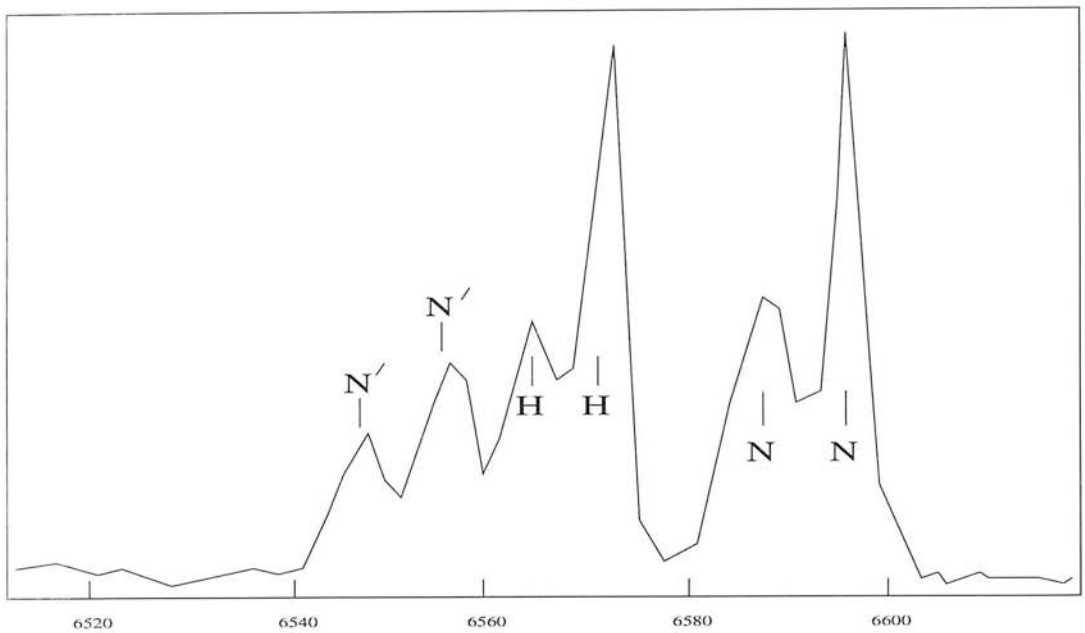

Figure 2.3: An example of the line splitting of the optical spectra to the SE of NGC 253. The components in the spectrum are denoted N′ for [NII] λ 6548, H for Hα and N for [NII] λ 6584. The figure is adapted from Heckman *et al.* (1990)

times brighter. Each of the two components is about 200 km s^{-1} wide (FWHM).

Heckman *et al.* (1990) explained their observational results in terms of a cone of outflowing gas which is tipped at +15° to the plane of the sky, Figure 2.4. The front surface at the near side of the cone produces the blue-shifted component while the component near the systemic velocity comes from the back. Similarly the front surface of the far side of the cone produces a component near the systemic velocity and the back surface produces a red-shifted component. Heckman *et al.* (1990) suggested that the red-shifted component is stronger than the blue-shifted component because the surface brightness of the emitting material along the cone wall declines with distance from the nucleus. Hence, along a given line of sight through the tipped cone, the kinematic component near the systemic velocity will always be produced by gas that is actually closer to the nucleus than gas producing the second kinematic component. With this kinematic description of the outflowing gas Heckman *et al.* (1990) suggested that the optical emission lines originate from gas that has an outflow speed of $\approx$ 340 km s^{-1}.

By measuring the [SII] λ 6717, 6731 emission line doublet flux ratio Heckman *et al.* (1990) derived electron densities, n_e, and, by assuming that the emission lines arose from gas at T = 10^4 K, they were able to infer pressures. They derived n_e = 630 cm^{-3} within 100 pc of the nucleus of NGC 253 which corresponds to a gas pressure of P = 6.3×10^6 K cm^{-3}, very similar to the pressure in other components of the ISM within the starburst region.[2] The densities/pressures decline systematically with radius from the starburst. The radial density/pressure profile is shallow at small radii (less than a few hundred parsecs) but steepens at large radii. Heckman *et al.* (1990) argued that this radial density profile agrees well with the superwind model in which the gas within the starburst (inside the wind's sonic radius) is confined by the thermal pressure of very hot (T $\sim$ 10^8 K) thermalised stellar ejecta, and the gas at large radii is confined

[2] The electron density derived by Heckman *et al.* (1990) is comparable to the value of 400 cm^{-3} derived by Carral *et al.* (1994).

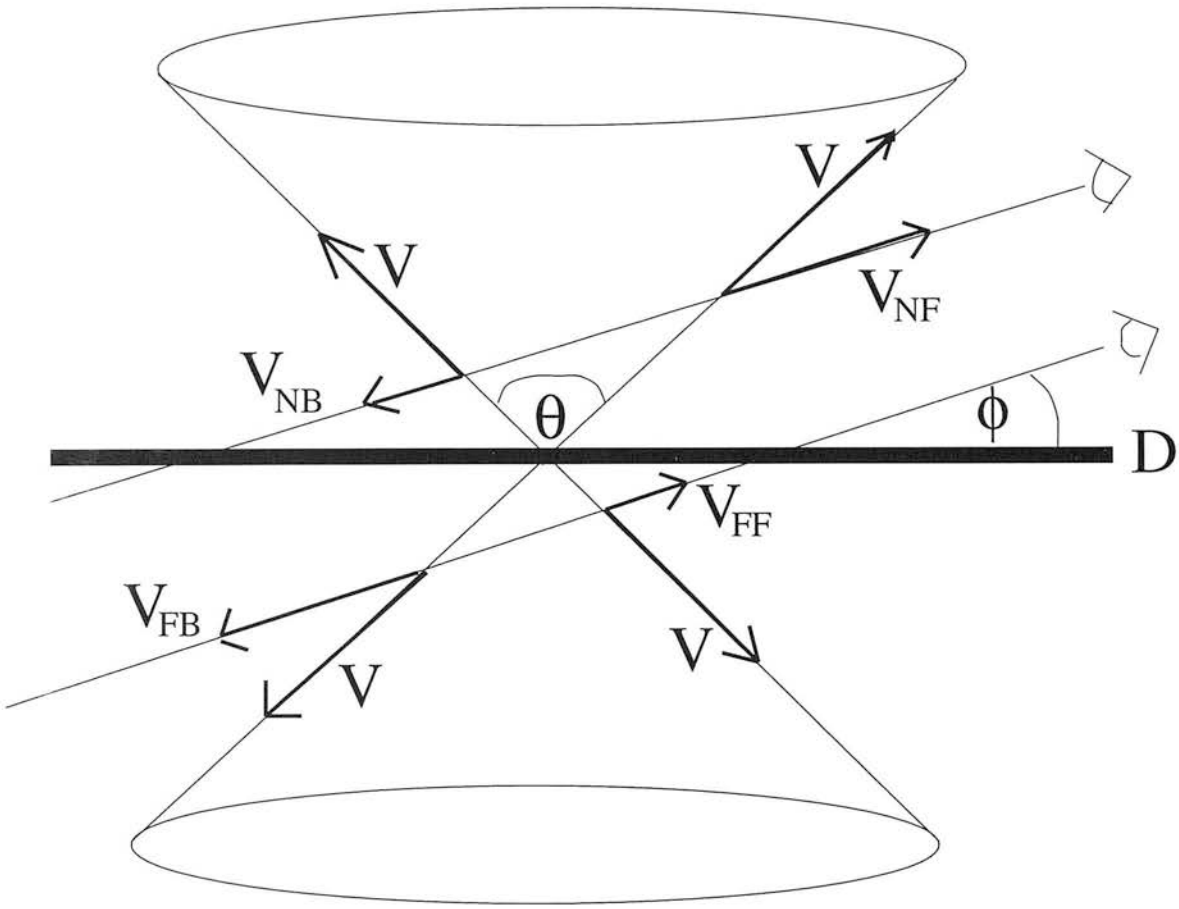

Figure 2.4: Schematic of outflow along a bi-conic surface centred on the nucleus of NGC 253, with the cone's symmetry axis along the minor axis of the disk. The disk is indicated by the rectangular region labelled "D" and the structure is viewed at an angle ϕ to the plane of the disk. The opening angle of each cone is θ, and the gas flows along the surface of the cone at a uniform velocity, V. The line of sight through the cone on the near side of the galaxy disk yields a double-peaked emission line with the gas on the front surface, producing a component that is strongly blue-shifted, labelled V_{NF}, and the gas on the back side producing a component near the systemic velocity, labelled V_{NB}. Similarly, the gas on the surface of the far-side cone produces a component near systemic velocity, labelled V_{FF}, as well as a strongly red-shifted component, labelled V_{FB}. Optical emission from the far side suffers high extinction with respect to the near side and so only two components of the emission lines are observed. If the surface brightness of the gas drops rapidly as a function of distance from the nucleus, the component at velocity V_{NB} is brighter than the component with velocity V_{NF}. The figure is adapted from Heckman *et al.* (1990)

by the ram pressure of the superwind. The actual outflowing wind, of which the bulk of the mass and volume is in the form of the hot rarefied X-ray emitting gas, was estimated by Heckman *et al.* (1990) to have a terminal velocity of about 2000 km s^{-1}.

Heckman *et al.* (1990) derived the optically emitting gas mass in the superwind to be of the order of 10^5 $M_\odot$. This mass is much smaller than the masses of both cooler molecular gas ($\sim 10^8$ $M_\odot$, Canzian *et al.* 1988) and hotter X-ray emitting gas ($\sim 10^7$ $M_\odot$, Fabbiano 1988). Heckman *et al.* (1990) derived a filling factor of $\sim 10^{-3}$ for the Hα-emitting gas. Thus, the optical emission-line gas must consist of small clouds or thin sheets. This is consistent with Figure 2.2, where the optical emission appears to cocoon the X-ray emitting gas in a thin "knotty" layer.

Heckman *et al.* (1990) noted that the optical emission from the outflowing wind has a spectrum similar to the spectra of galaxies which have been designated a Low Ionisation Nuclear Emission Region (LINER). The optical emission line luminosity of NGC 253 in the nebula is $\sim 4\times10^8$ $L_\odot$, which is about 1% of the bolometric luminosity. Heckman *et al.* (1990) suggest that the mass loss rate of the nuclear region is around 1 $M_\odot$ yr^{-1}. Heckman *et al.* (1990) have also noted that the derived parameters of the superwind in NGC 253 means that it is energetically capable of powering the nebulae. Firstly, the cooling time in the gas which is observed through its optical emission is much shorter than the superwind dynamical time, *i.e.* the shocks driven into the ambient gas should be strongly radiative. For the densities derived from the [SII] doublet Heckman *et al.* (1990) argue that the post-shock cooling times ranges from a few hundred years to about 10^4 yrs for shock velocities in the range 100-300 km s^{-1}. The radiative cooling time only becomes comparable to the dynamical times of $\sim 10^7$ yrs when the shock velocities exceed 800 km s^{-1}. Secondly, the estimated kinetic energy flux in the superwind was derived by Heckman *et al.* (1990) to be $\sim 5 \times 10^8$ $L_\odot$ which implies that $\sim$ 100% of the superwind's energy needs to be converted into optical emission if the superwind is directly responsible for generating the optical emission. Heckman *et al.* (1990) suggest though that it is unlikely for the impact of the superwind upon its environment to be solely responsible for the optical emission. They argue that if shocks are responsible for the Balmer photons then for an outflow speed of 340 km s^{-1} shock models imply that 250 $M_\odot$ yr^{-1} of ambient material is being shocked. This implies that over the dynamical lifetime of $\sim 10^7$ yrs, about 3×10^9 $M_\odot$ must be shocked or entrained by the superwind. Furthermore, models of 340 km s^{-1} shocks into densities that are similar to those observed in the nebulae produce a Hα surface brightness which, given that the surface area of the optical emission region is $\sim$ 0.75 kpc^2 (a cylinder with length 600 pc and diameter 250 pc), can only account for about 5% of the observed Hα luminosity. Heckman *et al.* (1990) also argue that it is very unlikely that the optical emission is from gas that is photoionised by the central starburst. The spectrum of the nebula is that of a LINER rather than a typical HII region. Also, to explain the observed strength of the [OI] line with respect to the Hα emission requires stars that have very high effective temperatures of $\geq 56,000$ K. Such high effective temperatures are inferred only for HII regions which are extremely metal deficient (5% solar metallicity) and which contain very little dust (Heckman *et al.* 1990). This is not the case in the dusty nucleus of NGC 253. Moreover, Carral *et al.* (1994) derive an effective temperature of $\approx$ 35,000 K for the stars in NGC 253. Heckman *et al.* (1990) also argued that photoionisation by an AGN is unlikely by comparing the nebula in NGC 253 to nebulae in other starbursts, such as M82, where there is not a large radial gradient in the [OIII]/Hβ ratio which would be expected for a point source size such as an AGN. Heckman *et al.* (1990) proposed the optical emission was generated by 2 mechanisms, shock excitation by the superwind dominating

at radii greater than 250 pc, and photoionisation by the starburst at radii less than 250 pc

Schulz & Wegner (1992) took long-slit spectra and images of NGC 253 and note that the off-nuclear spectra are consistent with the lens-shaped spatio-kinematic pattern of an expanding shell, similar to the model suggested by McCarthy *et al.* (1987). Schulz & Wegner (1992) suggest that nitrogen is overabundant in the centre of the galaxy. They also suggested that most of the emission lines came from photoionised regions with a small contribution from shocked gas to the emission. Schulz & Wegner (1992) propose that UV radiation from the nucleus escapes through outflow induced cavities and it is this UV radiation which photoionises the gas.

2.5 Near-IR observations

Wynn-Williams *et al.* (1979) took a K-band spectrum of NGC 253. The spectrum shows strong Brγ emission and the 2.3 μm CO stellar absorption feature.[3] Wynn-Williams *et al.* (1979) suggest that the presence and strength of the CO feature indicates that late-type giant stars produce most of the 2.2 μm continuum emission, while the rate of ionisation implied by the strength of Brγ indicates that most, if not all, of the far-IR luminosity originates from O and B stars. This means that compared to our Galaxy, the number of massive young stars in the central 150 pc of NGC253 is $\sim 30\times$ greater, but the total mass of stars is the same.

Rieke *et al.* (1980) suggest that the 2 μm flux is dominated by the light of supergiant stars. This is in contrast to Wynn-Williams *et al.* (1979) who argue that red supergiants account for less than 1% of the 2 μm flux by assuming that the ratio of M supergiants to ionising flux is the same in the nucleus of NGC 253 as found in 30 Doradus. However, the ionising flux in 30 Doradus is apparently generated by stars from a population that is so young (3×10^6 yrs) that there are as yet no red supergiants associated with it, while the M supergiants in the nebulae are the result of an earlier burst of star formation (Rieke *et al.* 1980). Thus, the ratio of red supergiants to ionising flux in 30 Doradus reflects the history of the nebulae much more strongly than it does the intrinsic ratio expected in a larger region of space which is undergoing an extended phase of rapid star formation.

Beck & Beckwith (1984) observed the near-IR hydrogen recombination lines, Brα and Brγ, towards the nucleus of NGC 253. Beck & Beckwith (1984) note that the spatial distribution of the recombination lines is similar to the 10 μm flux, which suggests a similar origin in young stars. The 2 μm continuum is not as well correlated with the young stars. This is not too surprising as there are significant extinction variations across the nucleus which will distort the 2 μm map (Sams *et al.* 1994). Furthermore, the 2 μm emission is produced by giant and supergiant stars. The 2 μm emission may, therefore, be associated with an earlier episode of star formation and so it need not be distributed in the same manner as the youngest stars. Beck & Beckwith (1984) estimate the luminosity of newly formed stars to be comparable with the bolometric luminosity of NGC 253.

Scoville *et al.* (1985) took near-IR images of the J,H and K continuum of NGC 253 and mapped the CO 1-0 intensity profile along the major axis. The CO 1-0 intensity was used to measure the H_2 column density. The derived H_2 column density radial profile, along with the HI column density radial profile, is shown in Figure 2.5. Towards the nucleus, and throughout the inner disk, the H-K colour is redder (by 0.2 mag) than a normal stellar disk, or even a disk enriched in late-type giant stars and suffering foreground extinction. Scoville *et al.* (1985) suggest that the enhanced emission at 2 μm in NGC 253 requires a significant contribution of

[3] Much of this section is repeated in chapter 3. It is included here for completeness.

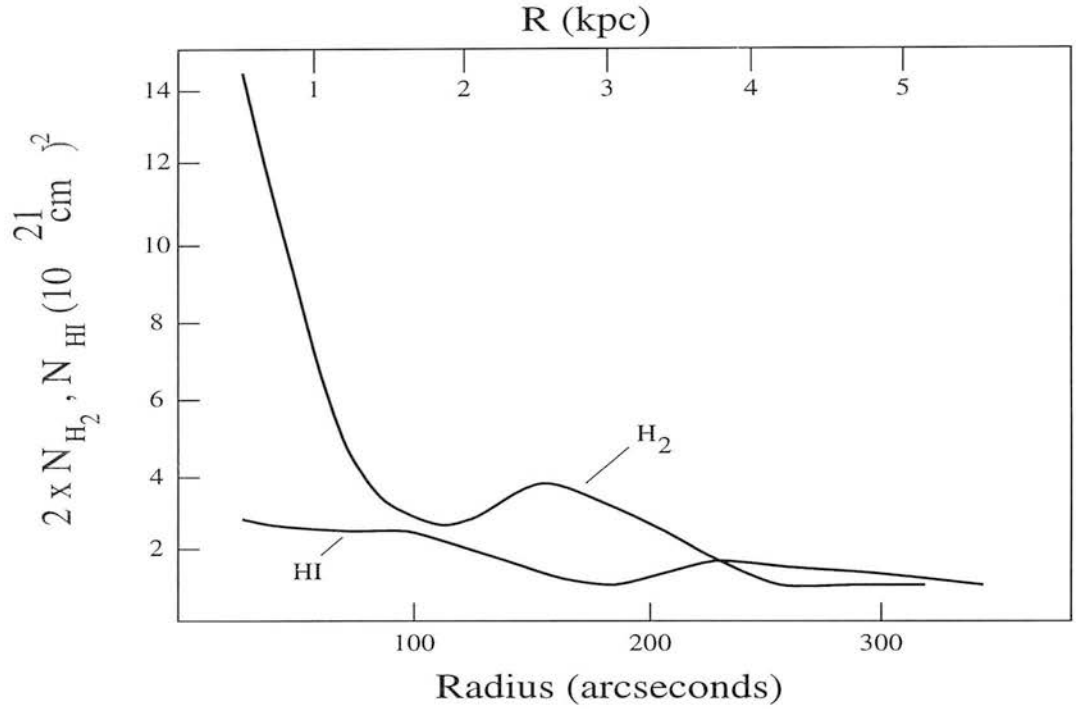

Figure 2.5: The surface densities of atomic and molecular hydrogen are shown along the major axis of NGC 253. The molecular hydrogen column densities are measured indirectly through observations of the CO 1-0 line. The figure is adapted from Scoville *et al.* (1985)

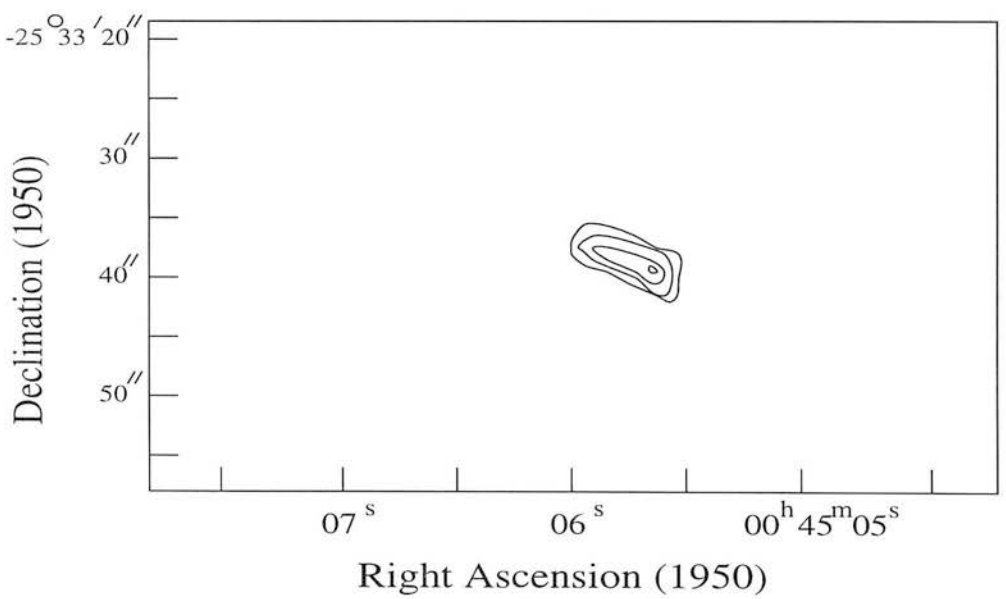

Figure 2.6: An illustration of the 2 μm emission from the centre of NGC 253. The figure is adapted from Rieke *et al.* (1988). The 2 μm emission is centrally concentrated with a FWHM of $\sim 4'' \times 2''$.

hot dust at 2 μm. The combination of 4 magnitudes of visual extinction plus 40% hot dust at 2 μm accounts for the nuclear colours. The picture of Scoville *et al.* (1985) agrees with the measurements of Becklin *et al.* (1973). The 3.5 and 10.1 μm fluxes of Becklin *et al.* (1973) give a colour temperature of $\sim$ 500 K for circular regions centred on the nucleus of radii from 5″ to 30″ diameter. Scoville *et al.* (1985) suggest that since the hot dust will not be isothermal, its hotter components near 1000 K produces a 2 μm excess and this 2 μm excess combined with the 3.5 μm flux has a colour temperature slightly below 1000 K.

Rieke *et al.* (1988) has argued that if hot dust contributed at K then we would expect the stellar CO bands to be diluted in strength by dust, which would lie predominantly at the long-wavelength end of the K window. However, the features in NGC 253 are stronger than is typical for normal galaxies. Rieke *et al.* (1988) suggest that the peculiar JHK colours are the results of optical depth effects arising because the stars and dust are intermingled and because of inhomogeneous extinction across the source. Rieke *et al.* (1988) note that the central 3″ of the nucleus is significantly bluer in H-K than the surrounding regions which occurs if the surrounding regions are subject to strong extinction. This may not be so clear cut as Puxley (1991) has noted that the JHK colours of a starburst population will be significantly bluer than those of old stars, principally because of the significant contribution of hot young stars to the near-IR continuum. Rieke *et al.* (1988) argued that the emission from molecular hydrogen in NGC 253 is indicative of shocked gas and they proposed that the shocked gas is produced directly by supernovae and by collisions of dense molecular clouds accelerated by supernovae in the starburst region. They argued that H_2 is not excited by the far-UV field in NGC 253 because of the relative weakness of the 2-1 S(1) line with respect to the 1-0 S(1) line.

Forbes *et al.* (1993) observed the nucleus of NGC 253 in the light of [FeII], Brγ and H_2 1-0 S(1) at 1″ resolution. The emission appears to predominantly arise from "hot spots". The hot spots are compact star-forming regions containing a mixture of HII regions, SN remnants and supergiants. Forbes *et al.* (1993) suggest that Brγ and H_2 are excited in star-forming regions, whereas [FeII] traces the distribution of SN.

Sams *et al.* (1994) observed the nucleus in J, H and K continuum with 0.5″ resolution. They proposed that the "true" nucleus of NGC 253 is not associated with the intensity peak in the J, H and K maps but is located 2.2″ NE of the peak and corresponds to the brightest 2 cm radio point source detected by Turner & Ho (1985). Sams *et al.* (1994) suggest that the hot spots discussed by Forbes *et al.* (1993) are in fact holes in the extinction. Sams *et al.* (1994) argue that the near-IR intensity peak has substantial emission arising from hot dust of at least 500 K.

Prada *et al.* (1996) measured the H_2 1-0 S(1) and Brγ velocity curves along the major axis and compared them with optical and mm measurements. The near-IR rotation curves are consistent with the mm measurements reported by Canzian *et al.* (1988) but show a central velocity gradient that is 7 times steeper than that shown by the optical velocity curve, Figure 2.7. This was interpreted by Prada *et al.* (1996) as being due to optical depth effects caused by dust, *i.e.* to the SW of NGC 253, which is on the far side the optical emission only traces the kinematics of gas that is in the foreground with respect to the nucleus. Hence, Prada *et al.* (1996) conclude that the optical emission is of limited use when trying to study kinematics in dusty galaxy nuclei, such as found in NGC 253. A very similar conclusion was reached by Puxley & Brand (1995). Prada *et al.* (1996) also compared the spatial variations of the H_2 1-0 S(1) line to that of ^{12}CO 1-0 along the major axis and suggested that the fraction of shocked gas due to SNRs increased towards the nucleus.

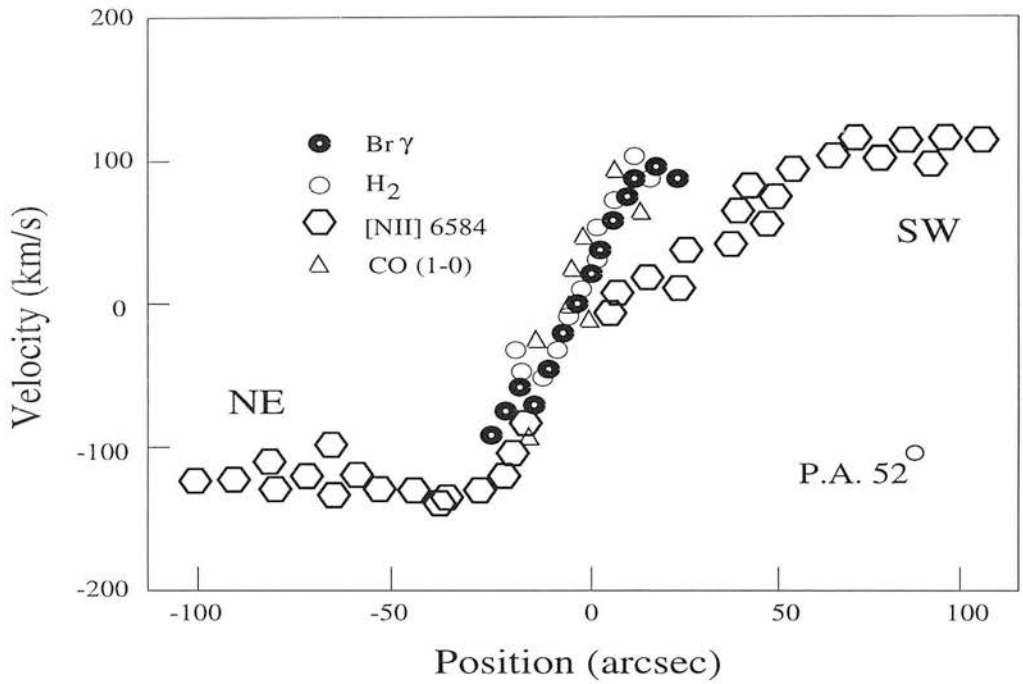

Figure 2.7: The measured radial velocities in Brγ and H_2 1-0 S(1) along the major axis of NGC 253, compared with the [NII]λ = 6584 $\AA$ data of Ulrich (1978) and the CO data of Canzian *et al.* (1988). The optical emission from the SW of the galaxy, which is on the far-side and hence has high extinction, does not trace the kinematics of the nuclear region but only traces the kinematics of the gas in the disk of NGC 253. The figure is adapted from a similar figure shown in Prada *et al.* (1996).

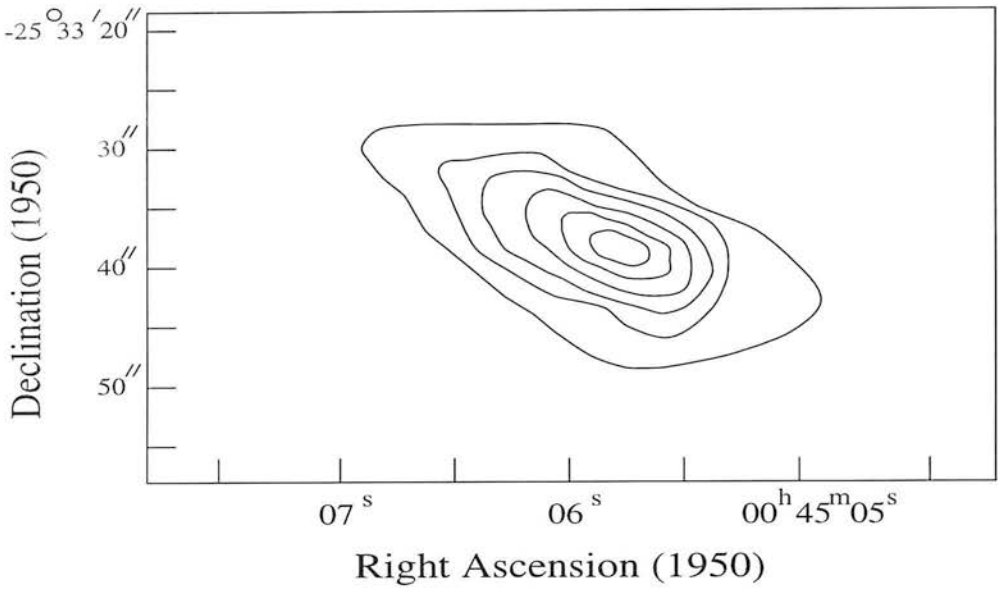

Figure 2.8: A map of the 10.8 μm emission from the centre of NGC 253. The figure is adapted from Telesco *et al.* (1993).

2.6 Mid-IR observations

Piña *et al.* (1992) imaged the nucleus of NGC 253 at 12 and 20 μm with a spatial resolution of 0.8″. Their positional uncertainty is 1.6″. The proposed "nucleus" - the dominant, bright, flat-spectrum radio source identified by Turner & Ho (1985), is not associated with the mid-IR peak but is located 2.2″ to the NE of the mid-IR peak. With this positioning, the mid-IR peak falls within 1″ of the 2 μm peak and a second weaker mid-IR source coincides with the brightest steep-spectrum 6 cm radio source.

Keto *et al.* (1993) made narrow band images at 8.5, 10 and 12.5 μm with 1.2″ resolution. Most of mid-IR flux, 80%, derives from a small region $\leq$ 10″ in diameter. Within this small region there are 3 spatially and spectrally distinct IR components - two bright compact sources and a surrounding envelope of low-level diffuse emission. The mid-IR and the 2 cm radio observations of Turner & Ho (1985) are loosely correlated in position but not in brightness which implies that the nuclear emission is emitted by more than one mechanism. They detect the same luminosity as previous observations and hence all the recent star forming activity is in the central 10″ and so 50% of the luminosity of the entire galaxy derives from the central 10″.

Telesco *et al.* (1993) made mid-IR maps of NGC 253 at 10.8, 19.2 and 30.0 μm with 4″ resolution. Figure's 2.8 and 2.9 show illustrations of the 10.8 μm and 30.0 μm maps of Telesco *et al.* (1993). The peaks lie within 1″ of the 2 μm nucleus of Rieke *et al.* (1988). The half-intensity size of the source is the same throughout the range 10-30 μm: 7″ $\pm$ 1″ along the major axis and less than 4″ along the minor axis. This lack of increasing source size with increasing wavelength out to 30 μm suggests that the distributions of flux at $\lambda \sim 100\,\mu$m resembles the maps and so the maps delineate the distribution of the bolometric luminosity of the starburst. The flux at the lowest 10.8 μm contours is elevated (the map appears bigger) compared with that at longer wavelengths because emission from small, transiently heated grains is relatively more important at the lower energies of the starburst periphery. Deep in the starburst region of NGC 253, where the UV energy density is high, small grains are more easily destroyed and larger grains which are in thermal equilibrium with the UV field are relatively more important

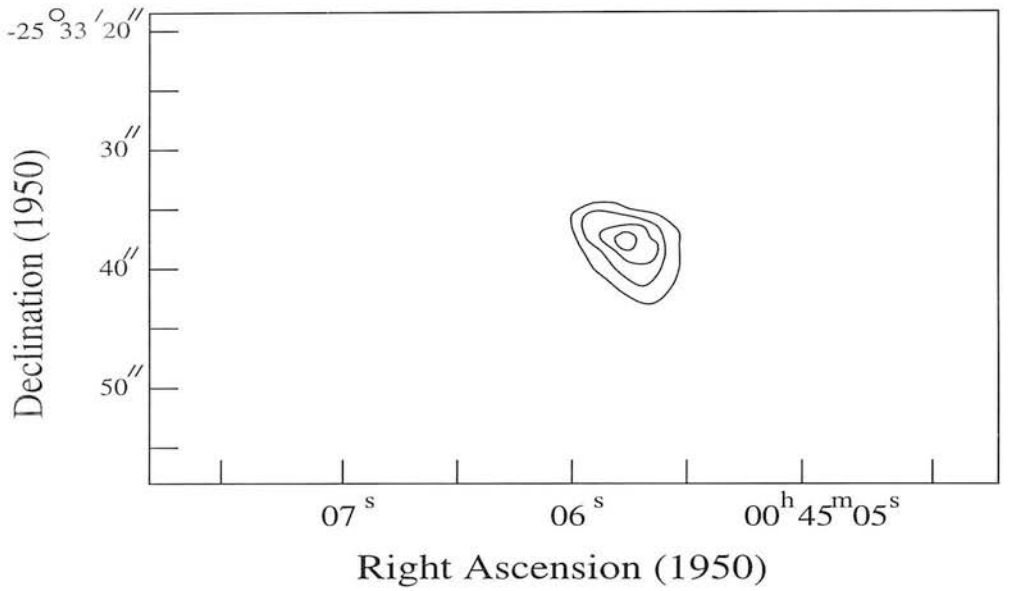

Figure 2.9: A map of the 30.0 μm emission from the centre of NGC 253. The figure is adapted from Telesco *et al.* (1993).

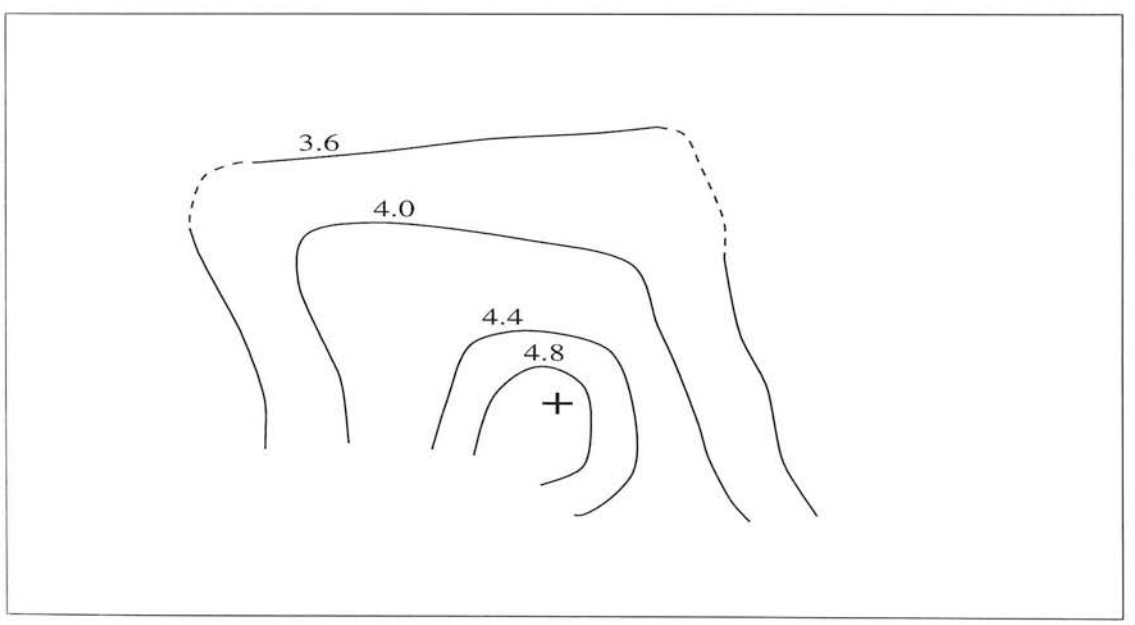

Figure 2.10: Spatial distribution of the ratio of 19.2 and 10.8 μm flux densities in the centre of NGC 253. The plus sign is the 10.8 μm peak. The contours are drawn only for regions with signal-to-noise ratios greater than 2. The figure is adapted from Telesco *et al.* (1993).

contributors to the IR emission. An implication of this is that heavy elements of the interstellar medium that are usually depleted onto small dust grains will be enhanced in the starburst region. The 19.2/10.8 ratio drops off towards the centre. Telesco *et al.* (1993) interpret the flux ratio as a measure of the dust temperature and so the spatial variations imply that the dust is cooler near the starburst centre than in the surrounding regions. Telesco *et al.* (1993) argue that the 10 μm flux arises from star-forming regions and does not come from collisionally heated dust in supernova remnant shocks, as suggested by Ho *et al.* (1989).

2.7 Far-IR studies

Telesco & Harper (1980) observed the broad-band continuum of NGC 253 between 30-300 μm. At these wavelengths NGC 253 resembles HII region/molecular cloud complexes in the galaxy; the continuum is thermal re-radiation by dust at T $\sim$ 30-50 K. The far-IR flux substantially exceeds that expected for stellar photospheric emission from late-type stars at IR wavelengths and so an additional power source, probably O and B stars, is needed. NGC 253 is unresolved at 60 μm with a 28″ beam. The continuum has a slope that is steeper than a blackbody long-ward of maxima and less steep at shorter wavelengths, Figure 2.11. These characteristics are similar to those associated with the IR spectra of Galactic HII region/molecular cloud complexes (caused by dust). The spectrum deviates from a blackbody spectrum long-ward of the peak because of the low long-wavelength emission efficiency of dust grains. It deviates short-ward of the peak because of the presence of grains hotter than those dominating the emission near the peak. Approximately 80% of the power from the centre of NGC 253 is emitted at $\lambda > 30\,\mu$m. The mass of gas associated with the dust is $\sim$ 2 orders of magnitude greater than the mass of ionised gas. The neutral gas in molecular clouds, rather than ionised gas, must constitute the predominant environment of the dust grains emitting the far-IR radiation. The mass of ionised gas is comparable to the mass of gas which could be coextensive with those grains emitting the IR power at $\lambda \leq 30\,\mu$m. A lower limit to the source size at 60 μm is $\approx 7''$, which is derived by assuming optically thick thermal emission from dust grains with temperatures of $\approx$ 40 K. This picture, and source size, is supported by Telesco *et al.* (1993) who argue that the source size does not increase from 10-30 μm. An alternative description of the data of Telesco & Harper (1980) is that the far-IR source is larger than the 10 μm source, which could result from a large-scale temperature gradient such that the dust temperatures are smaller at large radial distances. This alternative picture is not supported by the work of Telesco *et al.* (1993), who argue that the hottest dust is not in the nuclear region.

Carral *et al.* (1994) detected the [CII] 158 μm, [OI] 63 μm, [SiII] 35 μm, [OIII] 52,88 μm and [SiII] 33 μm fine structure lines from the central 45″ of NGC 253. They derive the gas phase silicon abundance to be nearly solar which they interpret as evidence for grain destruction in NGC 253. To derive the conditions in the photodissociated atomic gas, Carral *et al.* (1994) used the ratios of $(I_{CII} + I_{OI})/I_{FIR}$ and I_{CII}/I_{OI}. They derived a PDR density of 10^4 cm^{-3} and T $\approx$ 300 K. Using the [CII] line flux to estimate the amount of gas in the PDR phase, Carral *et al.* (1994) suggested a figure of about 2%. The derived area filling factor of the PDR gas was $\sim$ 1.5. For the HII regions in NGC 253 they used the ratio of the [OIII] 52 μm and 88 μm lines to derive an electron density of $n_e = 400$ cm^{-3}. The derived thermal pressure of the HII regions is similar to the pressure in the PDRs and so Carral *et al.* (1994) argue that the HII gas is in pressure equilibrium with PDRs at the surfaces of molecular clouds. The HII gas fills a significant fraction, $\sim$ 10%, of the volume between the clouds. Assuming a lower limit to

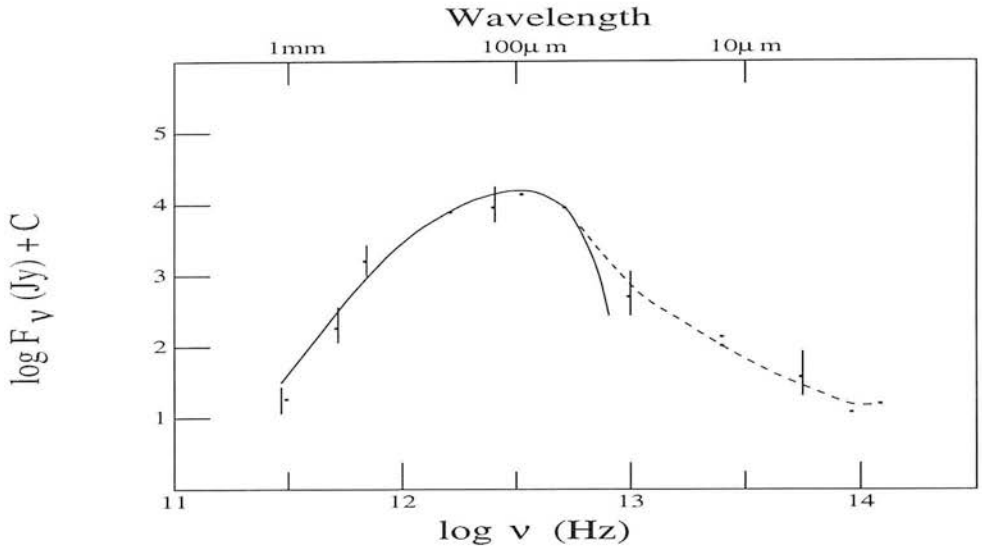

Figure 2.11: The infrared spectrum of NGC 253, adapted from Telesco & Harper (1980). The dashed curve was drawn through the data by Telesco & Harper (1980). The solid curve is of the form $\nu^n B_\nu(T_d)$, where ν^n is the spectral dependence of the dust grain emission efficiency and $B_\nu(T_d)$ is the Planck function. The parameters chosen by Telesco & Harper (1980) were dust at a temperature of 45 K with $n = 1.5$.

the oxygen abundance O/H = 5.6×10^{-4} they used the [OIII] 52 μm line, in conjunction with measurements of the Brα flux and the 3.3 mm continuum, to derive an effective temperature of the ionising stars to be $\geq 34,500$ K. By applying the models of Wolfire *et al.* (1990) to NGC 253 they suggest that the molecular gas in NGC 253 is distributed in large numbers ($5\times10^3 - 5\times10^5$) of small (0.5-2 pc) dense (10^4 cm^{-3}) clouds with a volume filling factor of $10^{-3} - 10^{-2}$. Carral *et al.* (1994) suggest that in the starburst of NGC253, the molecular clouds and HII gas are in pressure balance with a supernova-shocked, hot $\sim 2 \times 10^6$ K, low density (~ 1 cm^{-3}), all pervasive medium.[4] An illustration of how Carral *et al.* (1994) envisage the ISM in the nucleus of NGC 253 is displayed in Figure 2.12. The temperature of the X-ray gas derived by Carral *et al.* (1994) is about an order of magnitude smaller than that derived by Ohashi *et al.* (1990), $\sim 5 \times 10^7$ K, and the derived volume filling factor of the X-ray gas is much larger in the picture of Carral *et al.* (1994), $\sim$ 100%, than the $\sim$ 5% suggested by Ohashi *et al.* (1990).

[4] After reviewing the X-ray observations and their implications for the density and temperature, and hence pressure, of the hot all pervasive medium, I think that it is unlikely that the conditions assumed by Carral *et al.* (1994) will be applicable to NGC 253. This arises because there is higher temperature, but lower density, gas in NGC 253 than suggested by Carral *et al.* (1994). For a temperature of $\geq 10^7$ K and n $\sim$ 0.1 cm^{-3}, the cooling rate of the gas is long, $\sim 5\times10^7$ yrs. Carral *et al.* (1994) suggest that the pressure, P, in the hot component can be estimated from P = 2/3 S E t where t is the cooling time, S is the SN rate per volume and E is the energy per SN. Assuming there are 0.1 SN yr^{-1} within a radius of 200 pc and each SN produces an energy input of 10^{44} J, I derive a pressure of P $\sim 3\times10^{10}$ K cm^{-3}, four orders of magnitude larger than the pressure in the other components. In otherwords the rate of SN is so high in NGC 253 that there is runaway heating of the hot gas. The pressure estimate of Carral *et al.* (1994) for the X-ray gas can be lowered by reducing the cooling time of the hot gas, through decreasing its temperature and increasing its density. For gas as cool as 10^6 K, the cooling time is still long enough that the predicted pressure is an order of magnitude larger than the pressure in the other components. I conclude that the pressure of the X-ray gas is maintained at $\sim 5\times10^6$ K cm^{-3} because there is a pressure sink, *i.e.* the pressure is so high that the hot-gas expands and escapes. Thus, the pressure in the X-ray gas drives a superwind, *i.e.* the superwind is energy driven. In this case the pressure in the hot gas is not simply P = 2/3 S E t but should include terms due to the loss of gas, and hence pressure, out of the nucleus of NGC 253. An analysis of this problem has been made by Chevalier & Clegg (1985) and Tomisaka & Ikeuchi (1988).

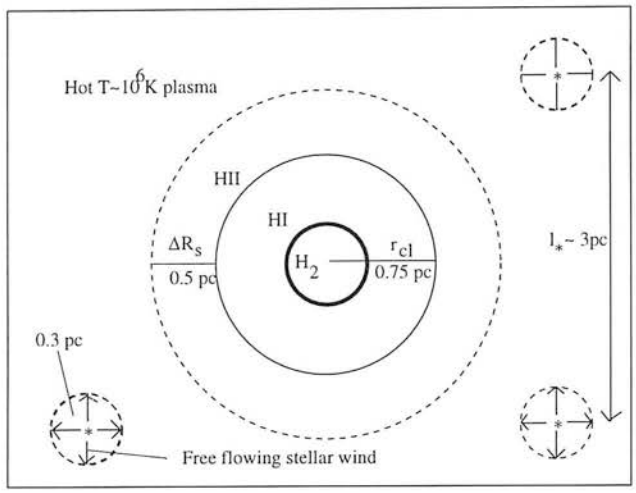

Figure 2.12: A schematic of the ISM in the central 250 pc of NGC 253, as suggested by Carral *et al.* (1994). Most of the volume is filled with T$\sim 1-3\times10^6$ K plasma with a density of $n_I \sim 1-3$ cm^{-3}. Neutral clouds of radius $r_{cl} \sim 0.75$ pc (or sheets, shells or filaments of thickness $\sim$0.75 pc) are embedded in this gas, They have dense ($n_m \sim 10^5$ cm^{-3}) molecular cores, labelled "H_2", and thick atomic PDR surfaces labelled "HI" with $n_a \sim 10^4$ cm^{-3} and $T_a \sim 200-300$ K. The HII gas ($n_e \sim 400$ cm^{-3}, $T_e \sim 8000$ K) was envisaged to form shells of thickness $\Delta R_s \geq 0.5$ pc around the neutral clouds. The O stars are ~ 3 pc apart, and their free-flowing winds penetrate $\sim$0.3 pc into the hot plasma.

2.8 Sub-millimetre observations

Harris *et al.* (1991) detected CO 6-5 emission from NGC 253. The J = 6 level is 116 K above ground and has a critical density of 10^6 cm^{-3} and so the CO 6-5 detection provides direct evidence for large amounts of warm dense molecular gas in NGC 253. Harris *et al.* (1991) claim that the intensity distribution of the 6-5 line is similar to the $40'' \times 9''$ CO 1-0 bar (Canzian *et al.* 1988) but more extended than the $4'' \times 2''$ FWHM 2.2 μm, 10 μm and radio continuum distribution. The CO 6-5/1-0 brightness temperature ratio is 2.5. This could be emitted by optically thin gas with an excitation temp of 41 K but this would not be consistent with the CO 2-1/1-0 ratio: one implication of this is that there could be physical components with a range of temperatures and densities and different spectral lines probe different regions. Harris *et al.* (1991) argue that as the 6-5 emission region FWHM is larger than the near-IR FWHM size this suggests that mechanisms other than star formation may heat the molecular gas. Harris *et al.* (1991) suggest possible heating processes are a cosmic-ray flux a few hundred times the local Galactic rate, or turbulence. It is not clear, though, whether there is any need to invoke heating mechanisms other than stars to explain the observed CO 6-5 in NGC 253. The near-IR FWHM could be just due to old stars (see Chapter 3) and so it's not clear why one would expect the hot, molecular gas to follow the old stellar distribution. Also, Telesco *et al.* (1993) argues that the 10 μm FWHM is $7''\times4''$, larger than that discussed by Harris *et al.* (1991). As Harris *et al.* (1991) only detected CO 6-5 in 3 positions along the major axis of the CO bar, it may be premature to argue that there is hot molecular gas not associated with star formation in NGC 253.

Güsten *et al.* (1993) detected CO 4-3 towards NGC 253. The J = 4 level is 55 K above ground and has critical density of the order of $10^{4.5}$ cm^{-3} and so its detection provides further evidence for large amounts of warm dense molecular gas in NGC 253. They could explain the

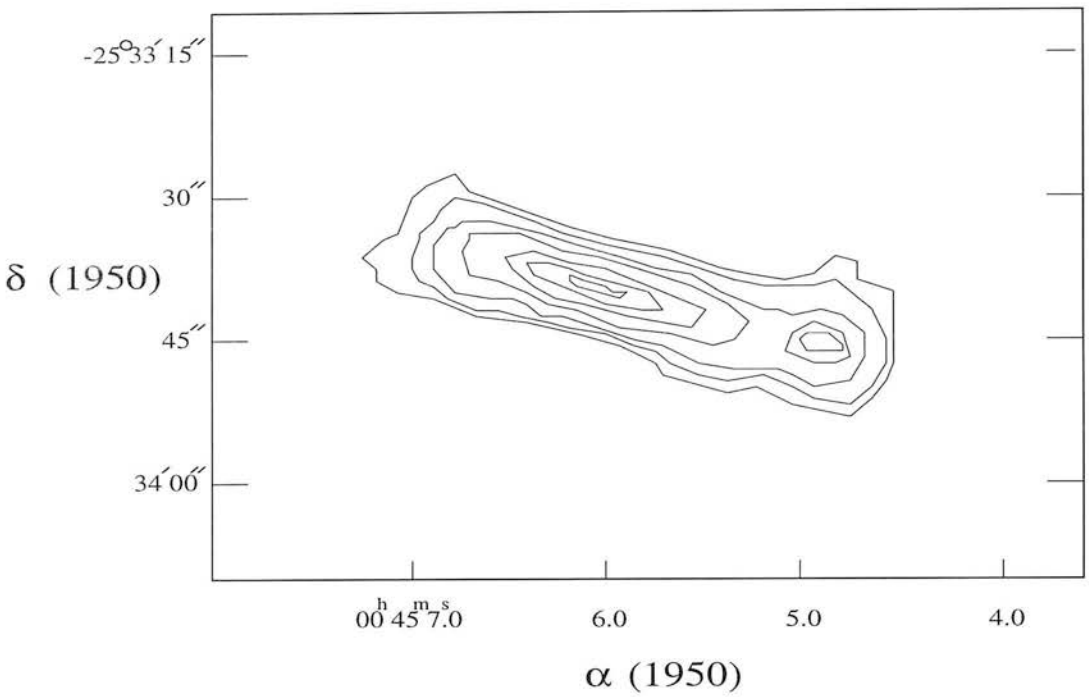

Figure 2.13: An illustration of the observed CO emission from the centre of NGC 253. The figure is adapted from Canzian *et al.* (1988).

observations with a single component model of the gas having n = 2×10^4 cm^{-3} and T = 50 K but their inhomogeneous data set inhibits detailed analysis.

2.9 Studies in the millimetre

Canzian *et al.* (1988) imaged the ^{12}CO emission from a "molecular bar" with $5'' \times 9''$ resolution, Figure 2.13. The bar has an angular extent of $39'' \times 12''$ with a derived mass of molecular gas of 4.8×10^8 M$_\odot$. The gas in the bar appears to be rotating as a rigid body with a steep rotation curve, indicating a large central mass. Canzian *et al.* (1988) argued that their observations implied a small radial inflow of gas into the nucleus. The dynamical mass in the nuclear region of NGC 253 is 1.3×10^9 M$_\odot$ which implies a gas to dynamical mass ratio of 0.4.

Carlstrom *et al.* (1989) used an interferometer to map the 1-0 line of HCO$^+$ and HCN as well as the 3 mm continuum. HCO$^+$, HCN and CO have similar distributions which suggests that the gas associated with the starburst is dense. There are two components of dense gas, separated by approximately $9''$. Carlstrom *et al.* (1989) suggested that the components are due to limb brightened emission from a molecular torus of gas. The 3 mm emission is distributed similar to emission at longer wavelengths which are dominated by non-thermal emission. The 3 mm continuum peaks at the base of the optical filamentary emission and X-ray emission and is "bracketed" by the dense molecular gas.

Nguyen-Q-Rieu *et al.* (1989) detected HCN 1-0, HCO$^+$ 1-0 and CS 2-1 in 5 positions along the major axis of NGC 253. Nquyen-Q-Rieu *et al.* (1989) argue that the line strengths require a large fraction of the molecular gas to reside in small dense clumps with a low volume filling factor. To estimate the degree of clumping they assume that the gas at a uniform density of 10^5 cm^{-3} uniformly fills the beam and that the path length is roughly the diameter of the beam ($\sim$ 300 pc). This implies a mass of gas of $\approx 10^{11}$ M$_\odot$, which is about 1000$\times$ larger than

the estimated mass of gas of Canzian *et al.* (1988). Nguyen-Q-Rieu *et al.* (1989) argue that this indicates that the volume filling factor must be of the order of 0.001, but this argument is uncertain because there may be differences in the abundances in NGC 253. Nguyen-Q-Rieu *et al.* (1989) note that as the line profiles of the molecules agree with CO it is likely that the dense gas and more diffuse gas share the same kinematics. The dense gas traced by HCN and HCO^+ is more compact and more intimately associated with the starburst region than the bar of CO (Canzian *et al.* 1988). Nquyen-Q-Rieu *et al.* (1989) suggest that because the HCO^+/HCN abundance ratio in M82 is higher than in NGC 253, there is a higher cosmic ray flux in M82 than in NGC 253.[5]

Mauersberger & Henkel (1989) mapped NGC 253 in CS 2-1. The map is consistent with the CO 1-0 line and there is evidence for two peaks. They also detected $C^{34}S$ 2-1, CS 3-2 and CS 5-4. The derived density of the molecular gas in the CS emitting regions is $10^{5\pm0.4}$ cm^{-3} and the 2-1 emitting gas has a clumping factor of ~ 0.2 within the central 11″ beam. To derive the column density of CS they assumed a relative $^{32}S/^{34}S$ abundance of 23, which is the terrestrial value. They derive the clumping factor by comparing the observed line temperature with the predicted line temperature for a beam filling factor of unity.

Mauserberger *et al.* (1990) detected HC_3N in 6 transitions towards NGC 253. Several of the lines show two separate velocity components which were associated with hot-spots on the molecular bar of Canzian *et al.* (1988), Figure 2.14. By comparing the line-intensities with a large velocity gradient (LVG) model, Mauersberger *et al.* (1990) suggest that the bulk of the gas observed in HC_3N has densities of the order of 10^4 cm^{-3} and a beam-filling factor of $> 10\%$. There is a second component of molecular gas with a lower filling factor but much higher excitation ($n \geq 10^5$ cm^{-3}, $T \geq 60$ K). The relative abundance of HC_3N in NGC 253 is comparable to that in the Orion hot core and TMC1 but is larger than in quiescent clouds.

Mauersberger & Henkel (1991) mapped N_2H^+. The spatial distribution follows that of CS. The map shows weak evidence for two peaks because the integrated intensity over the blue and red-shifted intervals changes with velocity. N_2H^+ has a high dipole moment and so traces dense gas ($n \geq 10^4$ cm^{-3}) but if $n > 10^5$ cm^{-3} then N_2H^+ is destroyed through the reaction

$$N_2H^+ + CO \rightarrow HCO^+ + N_2$$

So N_2H^+, unlike most other molecules, is confined to a very narrow range of densities. This will happen for all molecular density tracers that are ions, eg HCO^+. Mauersberger & Henkel (1991) also detected the 3-2 and 2-1 lines of SiO plus $H^{13}CO^+$, $H^{13}CN$ and $HN^{13}C$. SiO can only form if the first excited fine structure level of the Si atom is populated. As this is 111 K above ground SiO must be tracing hot gas. SiO is probably optically thin and as the SiO 3-2/2-1 ratio is 1.02, the density must be low. An LVG model predicts that $n = 10^{4-5}$ cm^{-3} and densities $n > 10^5$ & $< 10^4$ are excluded. SiO is extended (>> 1 pc) and the intensity of SiO relative to that of other high density tracing molecules approaches that of hot, dense Galactic cloud cores like e.g. Orion KL. The SiO intensity is much lower towards M82, by factors of 2-5. CH_3OH shows a similar behaviour to that of SiO and, since the abundances of SiO and CH_3OH increase with temperature, Mauersberger & Henkel (1991) argue that the molecular gas is hotter in NGC 253 than in the other galactic nuclei. The molecular gas in NGC 253 may be warm without being exceptionally dense. Tracers for "quiescent" gas, eg N_2H^+, and "violent" gas, *e.g.* SiO and CH_3OH, may well coexist in the nuclear region of NGC 253 because N_2H^+ and

[5]This conclusion is in conflict with Paglione *et al.* (1996) who suggest that the cosmic ray flux is higher in NGC 253 than in M82.

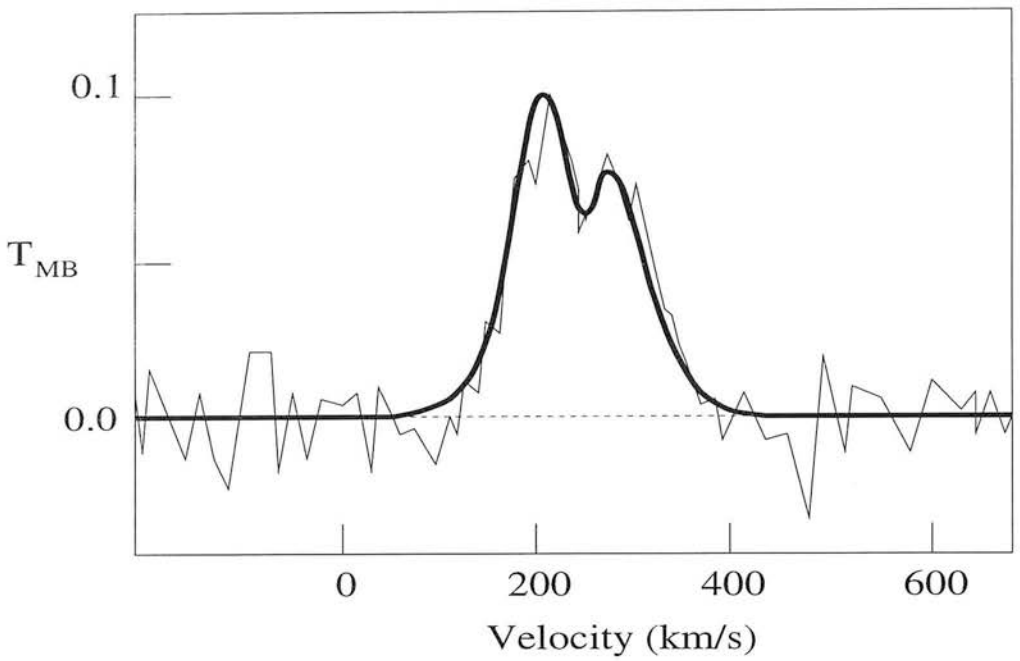

Figure 2.14: An illustration of the observed HC_3N 9-8 emission from the centre of NGC 253. The figure is adapted from Mauersberger *et al.* (1990).

SiO arise from gas with similar densities and the observed linewidths and velocities are similar for the two molecules. So unlike our Galaxy, N_2H^+ and SiO are coextensive—in our galaxy, clouds that are both warm and dense normally destroy N_2H^+. To explain the SiO brightness Mauersberger & Henkel (1991) claim that a large scale heating mechanism is required that isn't directly associated with the O and B stars and such a mechanism could be the dissipation of tidal energy. Mauersberger & Henkel (1991) argued that the heating is not due to supernovae because otherwise SiO should have been readily detectable from M82, which it wasn't. They discount UV heating because it is only efficient on the surface of the clouds and they did not think that most of the gas in NGC 253 is at low A_v. It is likely that the gas phase abundance of Si may be enhanced in NGC 253 (Carral *et al.* 1994) and so it is not clear whether the bright SiO highlights the efficiency of tidal heating or highlights the enhanced gas phase abundance of Si. Furthermore, it is not ruled out that the bulk of the molecular gas could well be at low A_v, given that the bulk of the gas is possibly in small compact clouds (Carral *et al.* 1994).

Mauersberger *et al.* (1991) detected four transitions of CH_3CCH (methyl acetylene) and derived an abundance which is similar to Galactic values. They also detected three transitions of CH_3CN (methyl cyanide) and derived a "normal" abundance. They derive densities of $\sim 3 \times 10^4$ cm^{-3} for the emitting gas. They failed to detect CH_3CN in M82 which shows that the chemical compositions between the two galaxies are different. Figure 2.15 illustrates the reported chemical abundances in the galaxies NGC 253, M82 and IC 342. Mauersberger *et al.* (1991) suggested that the differences in abundances are possibly due to the size of the molecular gas region because in M82 the region of circum-nuclear molecular gas is large and clouds are less effectively heated by shocks and dissipation of tidal energy than the more compact circum-nuclear structure of NGC 253. They also suggested that the dense molecular clouds will be destroyed and regenerated much more frequently in NGC 253 than in M82.

Sage *et al.* (1991) observed $C^{17}O$ and $C^{18}O$ in the 2-1 and 1-0 transitions towards NGC 253.

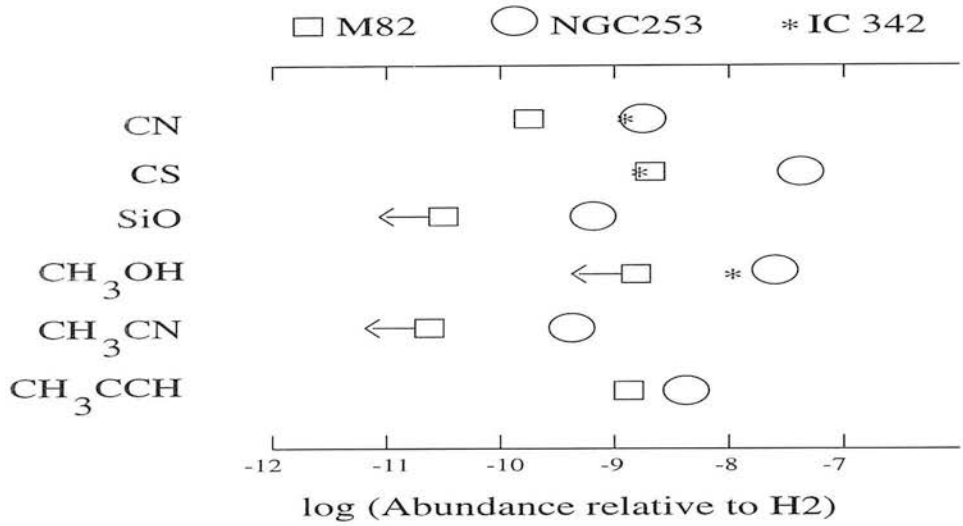

Figure 2.15: The relative abundances, and upper limits, of a number of molecules in M82, NGC 253 and IC 342, adapted from Mauersberger *et al.* (1991). The abundances are normalised to H_2 and so are prone to uncertainties due to the indirect approach of measuring the H_2 abundance. Even so, NGC 253 shows a higher abundance in many molecules, showing the richness of the chemistry in the starburst.

They observed the 2-1 lines with the IRAM 30 m (13″) and the 1-0 lines with the NRAO 12 m (57″). The $C^{18}O$ 1-0 line is blended with a line of HNCO. Sage *et al.* (1991) derive the $^{18}O/^{17}O$ ratio to be 10 ± 3 (the solar system ratio is 5.5). They explained this increase of $^{18}O/^{17}O$ in terms of nucleo-synthesis enhancement with high mass stars producing ^{18}O but little ^{17}O.

Nguyen-Q-Rieu *et al.* (1992) detected HCO^+ 3-2, HCO^+ 1-0 and HCN 1-0 emission from NGC 253. The 3-2/1-0 line ratio of HCO^+ and HCN is ≤ 2.5. Nguyen-Q-Rieu *et al.* (1992) suggest that the HCO+ and HCN lines are not highly excited ($T_{ex} \leq 30$ K) and the lines are optically thick.

Petuchowski & Bennet (1992) detected SO and SO_2 in NGC 253. SO is enhanced in regions where there are shocks or UV photons. As SO and SO_2 constitute the major repository of gas-phase sulphur in an oxygen-rich environment, whilst, if oxygen is depleted most-gas phase sulphur resides in CS, the SO/CS ratio is potentially a sensitive probe of the O abundance. They derive an abundance ratio of $N(SO)/N(CS) \geq 8 \times 10^{-2}$ from which they derive the fractional abundance of oxygen in NGC 253 to be $\geq 10^{-7}$.

Henkel *et al.* (1993) derived the $^{12}C/^{13}C$ isotopic ratio in NGC 253 from observations of six molecules (CO, CN, CS, HCN, HCO^+ and HNC) They derive $^{12}C/^{13}C \sim 40$ and claim that the $^{16}O/^{18}O$ ratio was ≈ 200 because the line intensity ratio of $^{13}CO/C^{18}O$ is ≈ 5.

Mauersberger *et al.* (1995) detected 3 lines of OCS towards the nucleus. The abundances of OCS are consistent with models for warm, dense clouds which have not yet reached chemical equilibrium or with models of the frequent erosion of grain mantles by C-shocks. They claim that OCS is emitted by gas with $n = 10^{3.4}$ cm^{-3} and that this component makes up the bulk of the molecular gas mass. Mauersberger *et al.* (1995) claim that all molecular studies of NGC 253 can be reconciled if there are two molecular density components, the first one with $n = 10^{3.5-4.5}$ and the second one with $n = 10^{5-5.5}$. They derive the mean H_2 density to be 2000 cm^{-3} and say that as this is close to the density of the OCS emitting gas then the volume filling factors of the CO and OCS emitting gas are close to unity. The brightness temperature of ^{12}CO 2-1 averaged over the central 11″ of NGC 253 is about 15 K. At densities ≥ 2000 cm^{-3}, brightness

temperatures of CO are predicted to be 25-45 K if CO is optically thick for kinetic temperatures of 30-60 K and so Mauersberger *et al.* (1995) claim that the area filling factor of CO is 30-50%. It is not clear how reliable the analysis of the volume filling factor of the molecular gas is by Mauersberger *et al.* (1995). They derive the mean H_2 density by assuming a ^{12}CO 2-1/1-0 ratio of $\sim$ 0.9 which is the average value for a number of spiral galaxies (Braine *et al.* 1993). As the largest ^{12}CO 1-0 temperature is 9 K when observed with a $9'' \times 5''$ beam (Canzian *et al.* 1988) and Mauersberger *et al.* (1995) argue that, with an $11''$ beam, the 2-1 line is $\approx$15 K, it is clear that extrapolating an average of the observed properties of spiral galaxies to derive the properties of starbust nuclei, such as NGC 253, may produce misleading results. Furthermore, to derive the number density of the OCS emitting gas Mauersberger *et al.* (1995) used the brightness ratio of the 8-7 to the 11-10 line. Inspection of the observed spectra shows that there are deep absorptions and confusion with other lines which means that both the baseline removal and the fitting of lines with gaussians may be tricky and, furthermore, give an unreliable result.

Hüttemeister *et al.* (1995) mapped NGC 253 in the emission from the 1-0 line of HNC. The map resembles the CS 2-1 map of Mauersberger & Henkel (1989). The double horned spectra, as seen in HC3N, are not seen in the broad spectra of HNC, HCN and CO. The relative abundance is smaller than 10^{-8} obtained for dark clouds and smaller than in the Orion KL region and Hüttemeister *et al.* (1995) suggest that this may be because the gas in the starburst is dense and warm, possibly caused by frequent shocks.

Paglione *et al.* (1995) used the Nobeyama Millimeter Array to map the HCN 1-0 line across the starburst with $2'' \times 4''$ resolution. The HCN emission lies along the molecular bar in several unresolved ($r \leq 30$ pc) complexes, Figure 2.16. Paglione *et al.* (1995) claimed a rough association between the molecular peaks and radio sources. In particular, Paglione *et al.* (1995) suggested that the flat radio nuclear source was a very luminous HII region (the nuclear source is about 100 times more luminous than W49, the most luminous HII region complex in the Milky Way).[6] The other flat radio sources were also assumed to be thermal sources which are 10 times less luminous than the radio peak but still many times brighter than W49. Paglione *et al.* (1995) used the ratio of HCN to CO to infer the density, which they claimed was $\sim 10^4$ cm^{-3} averaged over the central 120 pc of NGC 253.

2.10 Radio studies

Turner (1985) mapped the four 18 cm lines of OH with a resolution of $17.7'' \times 9.5''$. The lines are seen in emission and absorption. There is a steep rotation curve in the inner 125 pc radius which yields a nuclear mass of 5×10^8 M$_\odot$. The OH absorbing gas is seen at broader velocities than the HI and optical (60-550 km s^{-1}). The clumping of the absorbing gas implies individual entities $\sim$ 15 pc in size, which is suggestive of Giant Molecular Clouds (GMCs) in the Milky Way. The absorbing gas appears to be distributed in a toroid of mean radius 150 pc from the nucleus. There is a plume of OH emission which extends 1.3 kpc above the equatorial plane. There is no apparent velocity gradient, and no significant intensity gradient, over the projected extent of the plume. The lack of velocity gradient over the plume indicates that it is not involved with the rotation curve, and so does not lie in or close to the plane of the galaxy.

[6] As is discussed below, the brightness temperature of the radio nucleus is about 90,000 K (Turner & Ho 1985) and so the radio nucleus is unlikely to be entirely thermal in origin. Jim Jackson & Jim Ulvestad (private communications) claim that, after subtraction of a synchrotron component, the thermal component of the nuclear source is consistent with a very luminous HII region. The other flat radio sources are also consistent with the picture that they contain luminous HII regions.

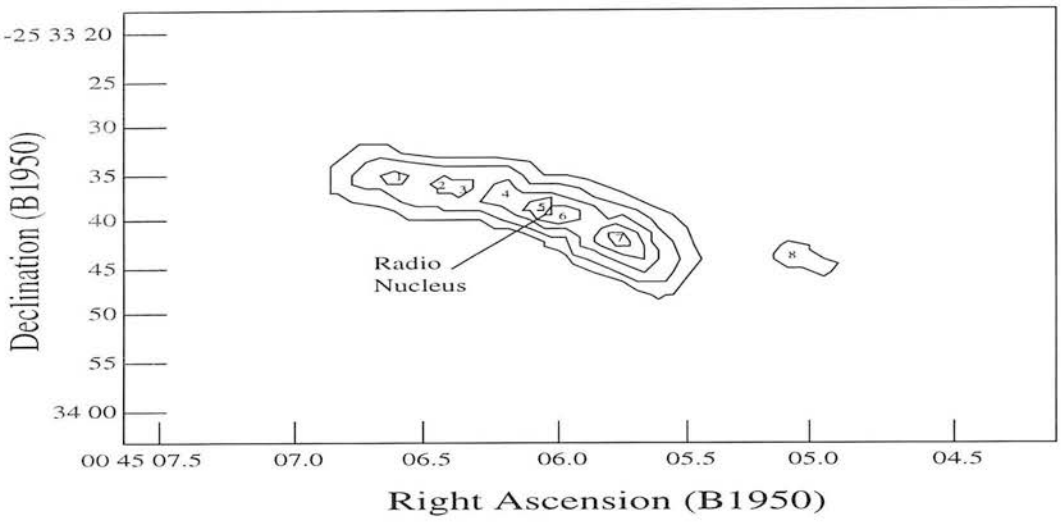

Figure 2.16: A map of the HCN 1-0 emission towards the nucleus of NGC 253, adapted from Paglione *et al.* (1995). The numbers label various emission peaks which are presumably molecular complexes.

The peak velocity of 278 km s^{-1} and the northern projected direction indicate that the plume is ejected from the nucleus. If it is ejected perpendicular to the plane with an opening angle of 45° then the ejection velocity, V_{ejec} is 168 km s^{-1} with a range of velocities of ± 70 km s^{-1}. Steady mass loss from the nucleus, and not an impulsive explosive event, is responsible for the plume because there is no velocity gradient in the plume and there is not the same range of velocities in the plume as there is the range of distances in the plumes extent. The projected N-S extent of the plume is ~ 1.2 kpc which gives the dynamical lifetime for steady-state ejection as 1.2 kpc / V_{ejec} = 6.5×10^6 yrs. Over this time a few % of the total nuclear mass has been ejected and this mass shows up in the plume. The relative intensities of the lines are not like galactic OH masers. Pumping involving collisions, near-IR or UV radiation are ruled out, by Turner (1985), on grounds of inadequate rates. Only far-IR pumping has a sufficient rate and may explain two of the three lines seen in emission.

Turner & Ho (1985) made a radio map at 2 cm with 0.2″ × 0.1″ angular resolution. They barely resolved the central radio source, 0.05″ × 0.04″, which implies it has a brightness temperature of ≥ 9 × 10^4 K, indicative of non-thermal activity. The radio properties of this source are only just consistent with those of a SN remnant as the source is ~ 50× the luminosity of the strongest Galactic supernova remnant, Cas A, in a region less than a parsec in extent. Radio emission from a recent supernova may explain the large flux and small size of the core source. It could also be a compact synchrotron source similar to those found in active galaxies and quasars. The total radio luminosity of the source is ~ 10^4 $L_\odot$ which is comparable to M81 but a 1000× more luminous than the Galactic centre. The central source is surrounded by compact knots (≥ 0.1″) with relatively flat spectral indices (α ~ -0.3) and brightness temperatures of a few thousand, Figure 2.17. These knots may represent emission associated with star forming regions or they may be related to ejection from the nuclear source as the knots are highly collimated over the central 9″ to within 1° in projection. The radio structure is orientated perpendicular to the bar.

Antonucci & Ulvestad (1988) made a VLA map at 6 cm which shows at least 35 compact radio sources, Figure 2.18. Most of the sources are unresolved, or only marginally, with typical

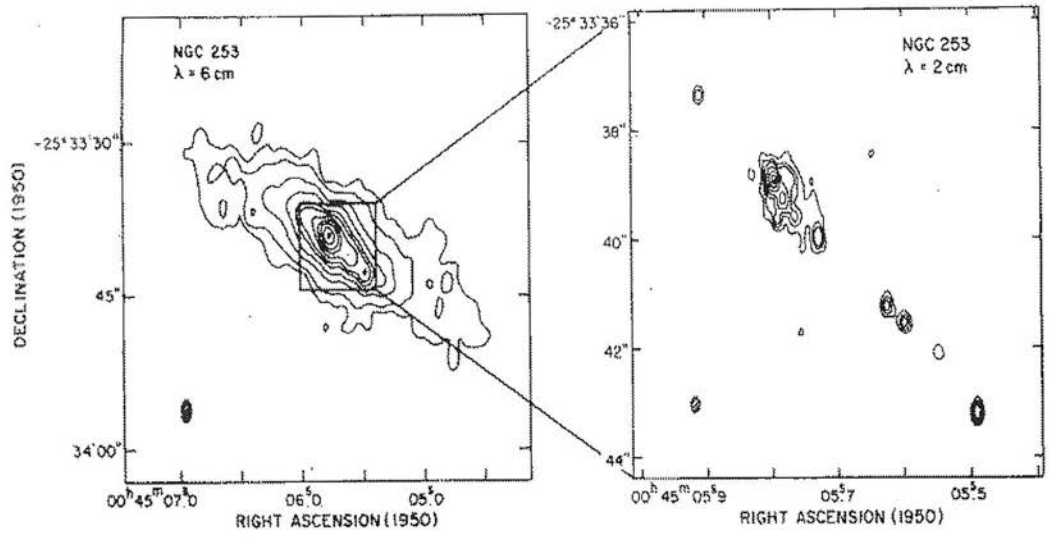

Figure 2.17: The radio sources towards the nucleus of NGC 253, reported by Turner & Ho (1985). The nuclear source is non-thermal and the other knots appear to be aligned.

diameters no greater than 2.5 pc. The 35 sources are distributed amorphously over 600 pc, which is in contrast to the 120 pc line of sources in Turner & Ho (1985). Some of the radio sources missed by Turner & Ho (1985) are brighter at 6 cm than Turner & Ho's source 1. The bright central source appears to have the flattest spectrum and was claimed to be a self-absorbed synchrotron source. There may be 2 populations of radio sources.

Ulvestad & Antonucci (1991) reported a second epoch observation of NGC 253 at 6 cm which showed no new compact radio sources stronger than 3 mJy. None of the 6 cm sources stronger than 1 mJy underwent significant flux decreases in 18 months. The strongest source showed an increase of 6.5% in flux density. They also observed NGC 253 for the first time at 3.6 cm. The 3.6 cm map identifies new sources because of the reduction of confusion. There are $\sim$ 100 compact sources present within a few hundred parsecs. A few of the resolved sources may be HII regions but most of the unresolved sources have steep spectra.

Ulvestad & Antonucci (1994) observed NGC 253 for a third epoch at 6 cm and for a second epoch at 3 cm. No new sources have appeared at both wavelengths and none of the sources are fading. The limits on source fading indicate that the current radio SN rate is no greater than 0.25 yr^{-1}. Several of the sources have flat spectra (the Turner & Ho sources) and so it is likely that there are two types of compact radio sources in the nucleus of NGC 253, not just young supernovae and supernova remnants.

2.11 A synthesis of the main results from the observations

NGC 253 shows emission characteristic of starburst activity across the entire electromagnetic spectrum. The main results are, in no particular order:

- NGC 253 is showing starburst activity, rather than activity expected from an Active Galactic Nucleus, because

    1. X-ray images show that the bulk of the emission is from extended diffuse gas, rather than from a point source in the galaxy.

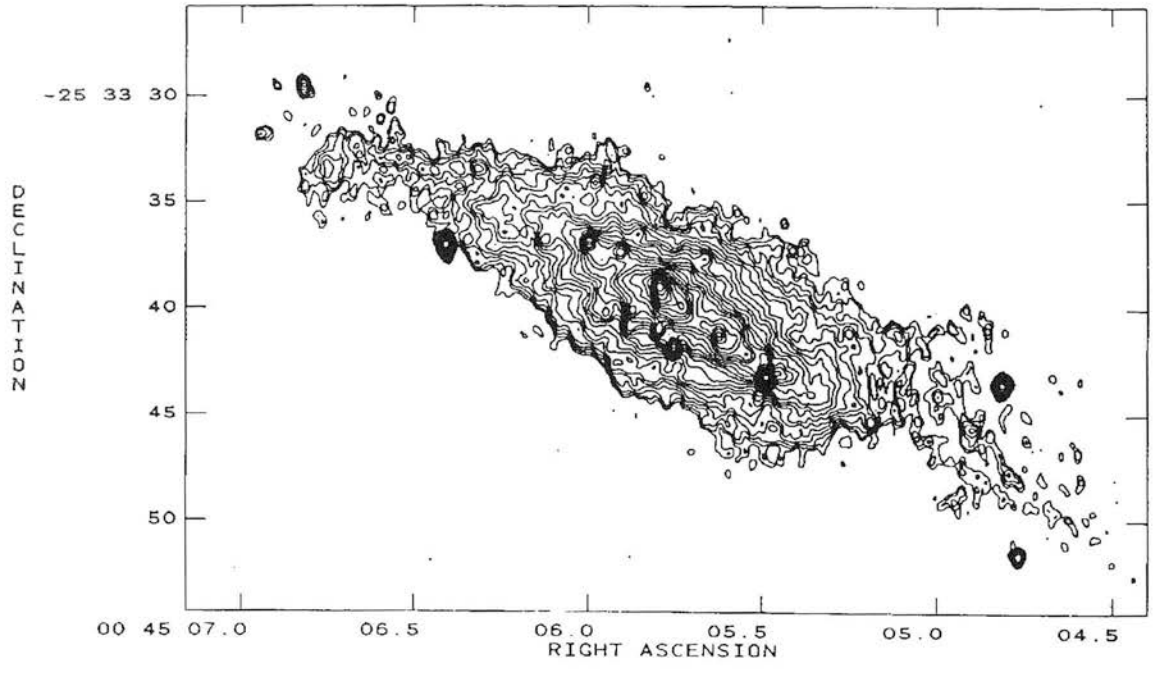

Figure 2.18: The radio emission from NGC 253, as reported by Antonucci & Ulvestad (1988). There are many sources in no particular structure and so it is likely that the alignment of Turner & Ho's sources is not highlighting a jet.

2. the radio images show many sources in the nucleus rather than just a point source or jet. Some of the first VLA images did show images consistent with a jet but later deeper images with the VLA showed that the jet structure was coincidental. It should be noted, though, that the radio nucleus does show evidence for non-thermal activity although it could be just due to a supernova remnant.
3. the optical spectrum shows no evidence for a photoionising AGN.
4. there are no high-excitation near-IR lines and the CO depth looks stellar, which suggests that there is no AGN continuum dilution.
5. there are no large line-widths
6. the bolometric luminosity compared to the number of Lyman continuum photons is consistent with star-formation

- The bolometric luminosity of the starburst is generated by a population of massive stars still undergoing nucleo-synthesis. The luminosity is not generated by supernovae remnants because the derived SN rate is ≤ 0.1 yr^{-1}. This means that, with an average energy per SN explosion of 10^{44} J, the SN remnants can only account for about 5% of the bolometric luminosity.
- The starburst was presumably triggered by a bar potential. There appears to be no evidence for any merger or interaction between NGC 253 and any other galaxy. Evidence for a bar comes from

1. interferometric imaging of CO 1-0, which shows a molecular bar on the scale of a few hundred parsecs
2. K band imaging, which shows evidence for a stellar bar, on the larger scale of a few kilo-parsecs.

- The central few hundred parsecs appear to be undergoing solid body rotation. Optical emission to the SW of the galaxy arises from the foreground disk of NGC 253, rather than from the nuclear region, and hence does not trace the kinematics of the circum-nuclear gas.
- The main starburst in NGC 253 is centrally concentrated, covering a region of size only about one hundred parsecs. The evidence for the compactness of the starburst comes from
  1. mid- to far-IR images, which show that the bolometric luminosity is on this scale
  2. recombination lines of atomic hydrogen, which show quite a rapid fall-off in brightness outside the nucleus
- There is some activity, either past or present, in the gas outside the central starburst. This is supported through
  1. radio images which show several point sources, which are either HII regions or supernovae remnants, in an extended region across the bar
  2. molecular tracers which show that some large scale heating process produces extended warm dense gas across the molecular bar
  3. observations of the hottest dust, which shows a halo of activity around the main activity.
- The starburst is estimated to be about 10^7 yrs old because of estimates of both the size of the superwind and the velocity with which the wind is estimated to be expanding

Chapter 3

Molecular hydrogen in NGC 253

3.1 Introduction

Molecular hydrogen makes up the bulk of the mass of molecular clouds but emission from H_2 only traces the location of energetic events within or around the clouds. The molecule's low moment of inertia means its rotational levels are well separated, with no excited levels populated in cold clouds ($T \leq 100$ K). Thus, it does not radiate in quiescent clouds, unlike other molecular species such as CO (Chapter 4). The molecule is homo-nuclear and so it's centre of mass spatially coincides with it's centre of charge. Thus, it has no permanent electric dipole moment and therefore radiates through quadrupole transitions. This results in relatively weak line strengths, but has the great advantage of producing optically thin line radiation. This is because the optical depth of an H_2 line is given by

$$\tau_\lambda = \frac{1}{8\pi}\left(\frac{A\lambda^3}{\Delta V}\right) exp\left(\frac{hc}{k\lambda T_{ex}}\right) N_{upper} \tag{3.1}$$

where A is the transition probability of a line occurring at wavelength λ, ΔV is the characteristic velocity width of the line, T_{ex} is the gas excitation temperature, N_{upper} is the column density of the upper level of the transition, h is the Planck constant and k is the Boltzmann constant. Substituting in typical parameters results in a value of τ equal to

$$\tau = 10^{-23} N_{upper}[cm^{-2}] \tag{3.2}$$

for the 1-0 S(1) transition.[1] Commonly observed column densities of emitting H_2 are of the order of 10^{18} cm^{-2} which indicates that these regions are essentially transparent to the H_2 radiation. Therefore, observation of a line leads straightforwardly to a determination of the level column density, which can then be directly compared with model predictions for the excitation process at work. A useful aid in illustrating how the H_2 is excited is a column density diagram.

3.1.1 Column density versus energy level diagrams

If the emitting gas is in local thermodynamic equilibrium (LTE) then the column density in each level, N_j, is described by

[1] A rotational-vibrational transition is commonly identified by the upper and the lower vibrational number of the transition followed by the letters S(J), Q(J) and O(J) depending on whether the rotational quantum number J of the lower level of the transition is smaller than, equal to, or greater than that of the upper level of the transition. For example, the 2-1 S(1) transition occurs from a transition from level (v=2, J=3) to level (v=1, J=1), 1-0 Q(3) is a transition from level (v=1, J=3) to level (v=0, J=3) and 2-0 O(2) is a transition from level (v=2, J=0) to level (v=0, J=2).

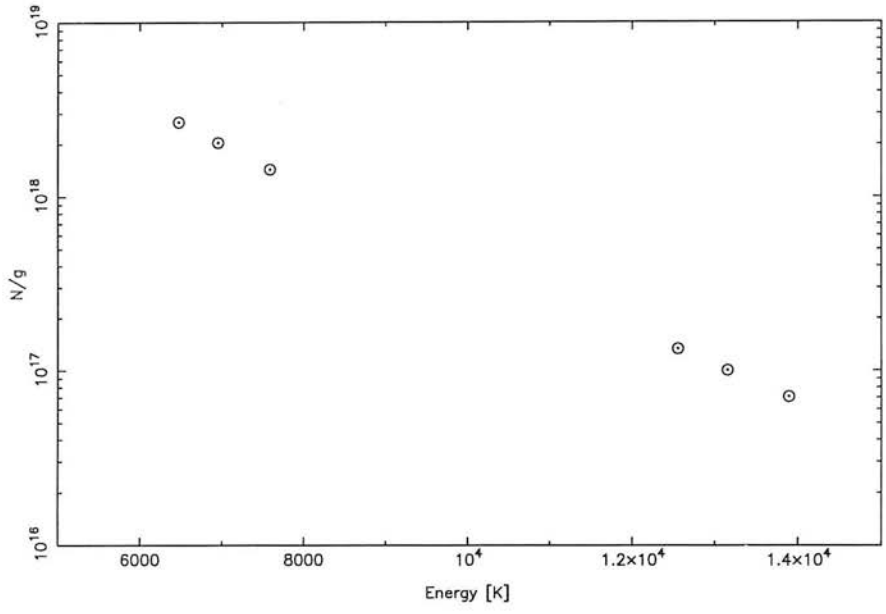

Figure 3.1: A column density diagram for H_2 expected towards a C shock in HH 7.

$$N_j = N_{H_2} g_j \frac{exp(-E_j/kT_{ex})}{Z} \tag{3.3}$$

where N_{H_2} = total column density in all the levels; g_j = statistical weight of the upper energy level of the transition; Z = partition function which is written as

$$Z = \sum_j g_j exp(-E_j/kT_{ex}) \tag{3.4}$$

The intensity of radiation from a level j, I_j, is given by

$$I_j = \frac{1}{4\pi} \frac{hc}{\lambda_j} N_j A_j \tag{3.5}$$

where λ_j = wavelength of the transition; A_j = spontaneous radiative decay rate of the transition; N_j = column density of the upper energy level of the transition; h = Planck's constant; c = speed of light. The statistical weight of a level is $g_j = g_s g_J$, where $g_J = (2J + 1)$ is the rotational degeneracy and g_s is the spin degeneracy ($g_s = 1$ if J is even, $g_s = 3$ if J is odd). It follows that the column density in the upper energy level is simply (neglecting extinction)

$$\left(\frac{N_j}{g_j}\right) = \frac{4\pi I_j \lambda_j}{hc A_j g_j} \tag{3.6}$$

Through measuring the intensity of radiation from several transitions, equation 3.6 can be used to compare the observed population of levels with model predictions of the population distribution. A useful tool in illustrating the population of H_2 is a column density diagram. Figure 3.1 shows such a plot of the column densities of several transitions expected towards HH 7.

The nature of the emission process can be characterised by the appearance of these level population diagrams. The two most common processes of exciting H_2 in the ISM, particularly towards star forming regions are thermal collisions and the absorption of UV photons. Collisionally excited H_2 emission has been observed in a variety of Galactic sources including bipolar

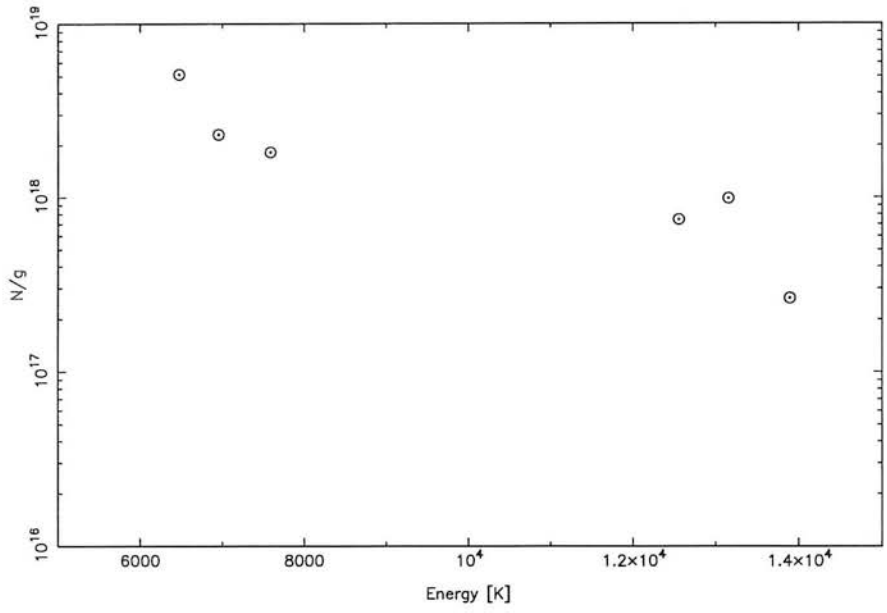

Figure 3.2: A column density diagram for H_2 observed towards the planetary nebula Hubble 12. The measurements are those of Ramsay *et al.* (1993)

outflows (Fernandes 1993) and supernova remnants (Graham *et al.* 1987). Although the exact shock process is uncertain in many cases, be it C-shocks or J-shocks (see Burton 1992 for a review), the excitation of H_2 is through collisions and hence is a thermal process. The population of the vibrational and rotational levels all lie along one curve (see Figure 3.1) indicating that the H_2 emission traces gas at the temperatures from which it arises, typically observed to be $\sim$ 2000 K in shocked regions.

Figure 3.2 shows a population diagram of a region that is excited by UV photons (adapted from Ramsay *et al.* 1993). To understand why Figure 3.2 differs from Figure 3.1 a knowledge is needed of how H_2 is excited by UV photons.

Fluorescent H_2 emission

Fluorescent H_2 is generated in a two step "far-UV pumping" process, Figure 3.3. Incident far-UV (11-13.6 eV) photons upon a molecular cloud are absorbed by H_2 in its Lyman and Werner electronic states which then decay to the ground electronic state (Black & van Dishoeck 1987, hereafter B&vD). It should be noted that H_2 absorbs UV photons with specific frequencies rather than through broad band absorption of a range of frequencies. Approximately 10% of the time, the relaxation back to the ground electronic state results in the H_2 being in a vibrational level higher than 14 in which case the molecular is unbound and so dissociates (Solomon 1966, Stecher & Williams 1967). The other 90% of the time, the relaxation back to the ground state results in H_2 being in a vibrational level less than 14. In this case the molecule is bound and will decay through electric quadrupole transitions in the infrared (B&vD).

As the fluorescent excitation of H_2 is coextensive with the photodissociation of H_2, due to them both resulting from the same initial UV absorption, the total abundance of H_2 in a region exposed to far-UV photons and its excited state populations are closely coupled (B&vD). In the region where H_2 can be fluorescently excited, near-IR emission lines are generated as the molecules cascade down the vibrational-rotational ladder, with a time-scale of typically 1 year

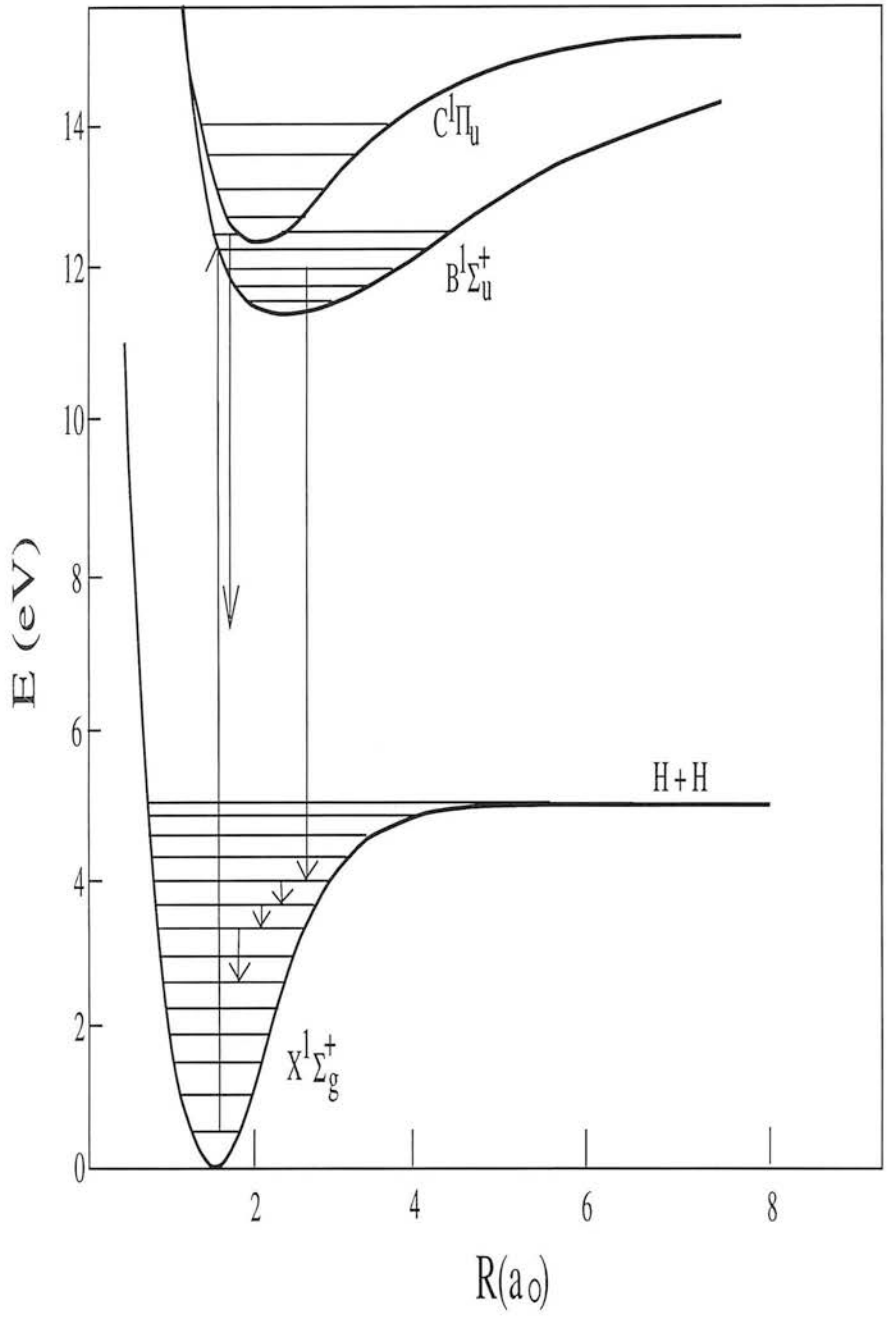

Figure 3.3: The processes of ultraviolet pumping and dissociation of molecular hydrogen. H_2 in the ground electronic state absorbs a UV photon and makes a transition to an excited electronic state, either to the Lyman band, $B^1\Sigma_u^+$, at 11.2 eV or to the Werner band, $C^1\Pi_u$, at 12.3 eV. The relaxation back to the ground state results in H_2 being in a vibrational level of ≤ 14 90% of the time, in which case an IR cascade results as the molecule relaxes down the vibrational-rotational ladder. The other 10% of the time, the relaxation back to the ground electronic state results in H_2 being in a vibrational state > 14 in which case the molecule is unbound, and so dissociates into two H atoms.

per quadrupole decay. The H_2 spectra produced in low-density PDRs ($n < 3 \times 1000$ cm^{-3}) all have the same characteristic non-thermal shape with relative line intensities that are insensitive to the cloud parameters including the gas density and intensity of the incident UV radiation. This is because the intensities are determined primarily by the branching ratios of the purely radiative quadrupole ro-vibrational transitions, which are molecular constants.

The population diagrams thus highlight that the higher energy levels are overpopulated, with respect to that expected from a Maxwell-Boltzmann distribution, because these higher levels are being filled by the radiative cascade, rather than through collisions. Observationally, this results in the line ratio of 2-1 S(1)/1-0 S(1) being far higher in low density fluorescent regions (B&vD) than it is in shocked gas (Brand *et al.* 1988).

In denser PDRs the interpretation of fluorescent H_2 emission is complicated by the need to consider collisional de-excitation of the H_2 molecule, mainly through collisions with H atoms (Sternberg & Dalgarno 1989). If $n \geq n_{crit}$, collisional de-excitation proceeds faster than radiative decay and much of the vib-rotational energy is transformed into heat.[2] The spectrum is modified as the levels are pushed toward LTE and can resemble the thermal spectrum seen in shocks. Observationally, this results in the 2-1 S(1)/1-0 S(1) line ratio being similar in both dense PDRs and shocked gas (Burton *et al.* 1990). It is still possible to discriminate between shocks and dense PDRs by observing transitions from the higher energy transitions, such as 3-2 S(4), because these levels only have significant populations in PDRs. Unfortunately, these high energy transitions are very weak and so need particularly sensitive observations to detect them.[3]

Due to the difficulties of discriminating between dense PDRs and shocks there is currently no consensus of what is the dominant excitation mechanism of H_2 in external galaxies (for NGC 253, Puxley *et al.* 1990 suggest that H_2 is excited in PDRs whereas Rieke *et al.* 1988 favour shocks). It is desirable that a method be found to discriminate between the various mechanisms as this would then allow a check on the validity of other ways we have of deciding between shock and UV excitation of the molecular phase of the ISM, where inferences have to be made about metallicity and elemental ratios. The rest of this chapter describes how, by using several characteristics of the differences between fluorescent and shock excited H_2, information derived from the column density diagrams can be used to discriminate between the two mechanisms.

3.2 The significance of the ortho to para ratio of molecular hydrogen

3.2.1 Measuring the rotational and vibrational temperatures

From the intensity ratio of any two transitions it is possible to derive an excitation temperature. One can hope to characterise the nature of the H_2 emission by deriving the excitation temperatures between different rotational and vibrational levels, T_{rot} and T_{vib}. To calculate rotational or vibrational excitation temperatures the following conditions must be met:

i) for a rotational excitation temperature, the two transitions must have the same upper vibrational level and different upper and lower rotational levels, *i.e.* between the two transitions,

$$\Delta v = 0 \ \ \Delta J \neq 0 \tag{3.7}$$

[2] n_{crit} is the critical density of the molecule and defined as the density at which the rate of collisions, which induces a change in energy level, is equal to the rate of radiative decay. For the levels of H_2, n_{crit} is 10^{4-5} cm^{-3} (Sternberg & Dalgarno 1989).

[3] In extra-galactic studies, detection of these weak lines is not possible in practice, due to the intrinsic uncertainty in the nature of the underlying continuum around the lines.

ii) for a vibrational excitation temperature, the two transitions must have different upper and lower vibrational levels and the same rotational level, *i.e.* between the two transitions,

$$\Delta v \neq 0 \;\; \Delta J = 0 \tag{3.8}$$

From the points shown in Figures 3.1 and 3.2, it is possible to derive a rotational temperature using the transitions 1-0 S(1) and 1-0 S(0), and to derive a vibrational temperature using the transitions 1-0 S(1) and 2-1 S(1). Inspection of Figures 3.1 and 3.2 highlights the difference in these temperature measures between the shock and PDR case. In the shocked case, all of the transitions fall on or close to a straight line and the derived rotational temperature is close to the derived vibrational temperature, as would be expected from gas in LTE. Contrary to this is the PDR case where the transitions do not fall on a straight line. The derived rotational temperature is much lower than the derived vibrational temperature. Furthermore, it should be noted that the derived rotational temperature is lower in the PDR case than in the shocked case.

The derived vibrational and rotational temperatures in a PDR do not measure the physical kinetic temperature. The reason for this is that, by its nature, the fluorescent process is non-thermal. The radiative cascade induced by UV photons overpopulates the highest energy levels with respect to a Maxwell-Boltzmann population. It is this overpopulation which gives the measured vibrational temperature in a PDR to be $\sim$ 5000 K whereas the kinetic temperature of the gas is $\sim$ 10% of this (Sternberg & Dalgarno 1989).

In the preceding discussion we have argued that the ratio of the 1-0 S(1) and 1-0 S(0) transitions can be used to measure a rotational temperature. The 1-0 S(0) line is a transition between two para states and the 1-0 S(1) line is a transition between two ortho states. The normalisation of the levels on the diagram implicitly assumed that the ortho to para ratio of H_2 is equal to three, the high temperature limit. However, in most PDRs the observed ortho to para ratio is less than 3 (Chrysostomou *et al.* 1993). Thus, rotational temperatures derived using neighbouring ortho and para transitions may give misleading answers. Below we discuss how we can measure the ortho to para ratio of the excited H_2 directly and how this allows us to measure the dominant excitation mechanism of H_2 in a starburst galaxy.

3.2.2 The physics of molecular hydrogen

The ground electronic state of molecular hydrogen is labeled $X^1\Sigma_g^+$.[4] The symbol, Σ, denotes the total electron angular momentum projected onto the internuclear axis, k (eg. Σ=0,Π=1, $\Delta = 2$ etc, in units of Plancks constant h). The total spin angular momentum quantum number for the two electrons takes the value of S = 0,1; the value of (2S + 1) is the left superscript of the term symbol. The subscript g (and u), and the superscripts + (or -) are concerned with the overall symmetry properties of the electronic wave-function.

In a diatomic molecule any plane through the internuclear axis is a plane of symmetry. For a Σ state, the electronic eigenfunction remains unchanged (+) or changes sign (-) when reflected in any plane passing through both nuclei. Similarly, if the two nuclei in the molecule have the same charge the field in which the electrons move has a centre of symmetry. As a consequence of this symmetry, the electronic eigenfunctions remain unchanged (g) or change sign (u) when reflected about this centre of symmetry.

[4] The various electronic states are labeled alphabetically, with capital letters for singlet states and lower case letters for triplet states: thus, the ground state of H_2 is $X^1\Sigma_g^+$ and the repulsive lowest triplet state is $b^3\Sigma_u^+$.

Each electronic state is split into a series of energy levels by the vibrational and rotational motion of the nuclei. The nuclear rotation, together with the electronic angular momentum and the total electron spin combine to form the total angular momentum vector, J. For H_2, whose nuclei are identical fermions, the total wave-function must be antisymmetric with respect to an interchange of the nuclei. The total wave-function of the molecule is given by

$$\Psi = \psi_{el}\, \psi_{vib}\, \psi_{rot}\, \psi_{nuc} \tag{3.9}$$

The ground electronic state of H_2 has symmetry $^1\Sigma_g^+$, and so the electronic and vibrational wave-functions are left unchanged by exchange of nuclei. Similarly, the rotational wave-function is symmetric for even values of J and antisymmetric for odd values. Each hydrogen nucleus has spin I = 1/2. Thus, there are three alternative nuclear wave-functions, ψ_{nuc}, which have a total resultant nuclear spin T = 1 (degeneracy of 2T + 1), and are symmetric, and only one wave-function which has a nuclear spin T = 0 and is antisymmetric. In order that the total wave-function shall be antisymmetric to exchange of nuclei, as required by Fermi-Dirac statistics, the rotational levels for which J is even are associated with the total nuclear spin T = 0 and those with odd values of J are associated with the total nuclear spin T = 1. The total degeneracy, or statistical weight, of each level is given by g_j = (2J + 1) (2T + 1), where T = 0,1 is the total nuclear spin.

The selection rules for the electronic dipole transitions are summarised by Field *et al.* (1966). The rules are: the electronic angular momentum changes by Δ = 0,±1; the electron spin does not change; states with subscript g combine only with states with subscript u and vice versa; states with + or - symmetries combine only with like states. In the ground electronic state, dipole transitions between different vibrational and rotational levels are forbidden. However, much slower quadrupole transitions are allowed. The selection rules for the rotational quantum number are ΔJ = (J"-J') = +2,0,-2 and these transitions are labeled O(J"), Q(J") and S(J") respectively. These selection rules preserve the ortho or para nature of each molecule.

Summarising, H_2 exists in two states, ortho or para, which are dependent on whether the rotational angular momentum J is even (para) or odd (ortho). Emission from H_2 preserves the ortho or para state of each individual molecule. Furthermore, collisions between two hydrogen molecules preserves the sum of ortho and sum of para molecules. The ground state of H_2 is para (J = 0).

3.2.3 Measuring the ortho to para ratio of H_2 from the population diagrams

The key to measuring the ortho to para ratio of molecular hydrogen can be seen from examining the population diagrams shown in Figures 3.1 and 3.2. Comparison of Figure 3.1 and 3.2 shows the large differences between thermal and fluorescent emission and shows that the nature of the dominant excitation mechanism can be characterised by the appearance of the level populations. In shocked regions, the population of the vibrational and rotational levels all lie along one curve. For the ultraviolet excitation of H_2 molecules, the series of rotational levels of each vibrational level are described by separate curves.

Deriving the ortho to para ratio

From measured H_2 line intensities it is possible to calculate the ortho to para ratio. The rotational excitation temperatures for each vibrational level are calculated using two levels

with the same spin to accommodate our initial ignorance of the ortho to para ratio. Ratioing two transitions from separate ortho and para states then allows the ortho to para ratio to be calculated. However, care must be taken because the rotational excitation temperature changes with J; it gets higher with increasing J. To cater for this fact it is best to calculate the ortho to para ratio with the level which is straddled by the levels used to calculate the rotational excitation temperature. For instance, for v = 2, the 2-1 S(0) and 2-1 S(2) transitions can be used to calculate the rotational excitation temperature, and to calculate the ortho to para ratio the 2-1 S(0) and 2-1 S(1) transitions would be used.

The degeneracy for each level is $g_j = g_s g_J$, where g_J is the rotational degeneracy given by $g_J = 2J + 1$. Using equations 3.3 & 3.5 and leaving the spin degeneracies for the ortho and para states as free parameters, the ortho to para ratio is calculated with the equation

$$\frac{g_s^O}{g_s^P} = \frac{(2J_P + 1)}{(2J_O + 1)} \frac{I_O \lambda_O A_P}{I_P \lambda_P A_O} exp\left(\frac{-\Delta E}{kT_{rot}}\right) \tag{3.10}$$

where g_s^O, g_s^P = spin degeneracies for ortho and para states; J_O, J_P = rotational quantum number for ortho and para states; I_O, I_P = intensity of ortho and para transitions; A_O, A_P = spontaneous radiative decay probability of ortho and para transitions; ΔE = energy difference between the para and ortho states. The following section discusses how measurements of the ortho to para ratio in different astrophysical environments have shown systematic differences between shocked regions and PDRs, and hence can be used to discriminate between these two excitation mechanisms.

3.2.4 The ortho to para ratio of H_2 in an astrophysical context

It is believed that H_2 is formed on dust grains with the ratio of ortho H_2 to para H_2 (the o/p ratio) equal to the high-temperature limit of 3 to 1. This is because the formation reaction is exothermic and once the molecule is formed it is ejected into the gas, with one-third of the binding energy ($\sim$ 1.5 eV) going to the kinetic energy of the molecule, one-third to the grain lattice and one-third to the internal energy of the molecule, producing so-called "hot" molecules, *e.g.* Black & Dalgarno (1976). However, the picture is complicated because the molecule may remain on the grain for some time before being ejected into the gas and will be thermalised at the lower temperature of the grain (Chrysostomou *et al.* 1993). Once the ortho/para ratio is determined, conversion between the two states occurs in the gas phase by spin exchange reactions with H and H^+ (Takayanagi *et al.* 1987) or with excited H_2 (Willacy & Brand 1996). Conversion between the two states via radiative or collisional transitions is very inefficient. In thermal equilibrium the ortho/para ratio is dependent on the temperature, increasing with T to its maximum value of 3 at a temperature of a few hundred K.

The ortho to para ratio in PDRs

In PDRs one might expect to see o/p = 3 since the temperatures are generally > 300 K. However, the observed values are considerably less than this, ranging from 1.7 to 2.3, *e.g.* Chrysostomou *et al.* (1993) and Ramsay *et al.* (1993).

Several ideas have been suggested to account for these low values of the ortho/para ratio. Chrysostomou *et al.* (1993) suggested that in a clumpy PDR the gas will not be in pressure equilibrium with its surroundings and will therefore not be static, as assumed in most models. The UV radiation falling on the surface of a clump will heat it, increasing its pressure relative to its surroundings and causing the surface layers of gas to stream away. The photodissociation

front advances into the clump and excites colder material which was previously deep inside the clump. This gas will have a lower ortho/para ratio reflecting its lower temperature and if the outflow of gas is faster than the alteration of the ortho/para ratio by spin exchange reactions the observed ratio will be lower than expected from the temperature of the PDR.

Takayanagi *et al.* (1987) explained the low ortho to para ratio towards NGC 2023, 1.7, by assuming that the observed ratio was equal to the initial ortho to para ratio, set up during formation. This would imply that the H_2 had a formation temperature of $\sim$ 65 K, far lower than expected for a "hot" molecule. Chrysostomou *et al.* (1993) considered the time-scale for the newly formed hydrogen molecule to reside on the grain. The longer the grain resides, the more energy is lost to the grain, and the lower the ortho to para ratio of the H_2 molecule once it is ejected. Currently, it is not clear whether H_2 resides on the grains long enough for this proposal of Chrysostomou *et al.* (1993) to work.

Alternatively, several groups have argued that the ortho/para ratio is mainly affected by the different UV photoabsorption rates of the two species, *e.g.* Sternberg & Dalgarno (1989) and B&vD, and is independent of the formation value. In PDRs, ortho and para H_2 acts as two independent species with different electronic transitions which can absorb UV photons. In PDRs there is a sharp transition between atomic and molecular hydrogen which occurs where the H_2 becomes optically thick to the impinging UV and self-shields. The different transitions of the ortho and para H_2 mean that the photodissociation fronts for the two forms are slightly displaced and the ortho/para ratio is mainly affected by the different UV photoabsorption rates of the two species. This may be understood as due to the independent self-shielding of each of the ortho- and para-H_2, rather than the ortho/para abundance ratio of the predissociated H_2. The ortho/para ratio that is measured is in an excited state. If the molecule is in an ortho state in the ground vibrational level, the absorption of a photon will result in it being in an ortho state of the excited level. However, the ortho/para ratio of the excited H_2 is not the same as in the ground state because of differences in the rate of photoabsorption of the ortho and para forms. Ortho H_2 is more plentiful and will self-shield first, which results in a lower abundance in the excited state and hence a lower measured ortho/para ratio. Willacy & Brand (1996) have included the spin exchange between excited H_2 and H as well as the different rates in ortho- and para- photoabsorption and derive ortho/para ratios close to the measured values.

The ortho to para ratio in shocked gas

Interstellar shock waves are generated by the supersonic injection of mass into the ISM, usually from young stellar objects, stellar winds, supernova remnants or colliding clouds. Since the bulk of the kinetic energy of the impact goes directly into heating the gas and is then radiated as the gas cools, shock waves are strong line emitters accessible to spectroscopic observations. Shock waves in molecular clouds have mostly been observed when outflowing gas from a young stellar object impacts upon ambient molecular material. The H_2 is heated to 1000 K or higher and, since it cools within a year, the observations of H_2 line emission directly trace the locations where supersonic material interacts with the ambient gas. Since the gas is hot ($T > 300$ K) the ortho para ratio will saturate at a value of 3, since collisions will rapidly bring the states to a thermal equilibrium. Measurements of the ortho/para ratio in shocked gas have produced the value 3 as expected (Brand *et al.* 1988).

3.2.5 Summary

To summarise, observations of Galactic PDRs indicate that the ortho to para ratio in excited H_2 is around 2 and not the hot thermal limit of 3. Such a value has been explained in several ways and may indicate that H_2 is formed at a low temperature on dust or that the ortho- and para- H_2 self-shield at different depths into a PDR. Measurements of the ortho/para ratio in shocked gas reveals the value 3.

By measuring the ortho/para ratio in a system of unresolved sources of H_2 emission, such as towards the nuclei of galaxies, we will have a clean measure of whether the molecular hydrogen is predominantly excited by UV photons or by thermal collisional processes. To test whether the ortho to para ratio of H_2 could be measured in a starburst nucleus, the circum-nuclear region of NGC 253 was observed. H_2 transitions with $\Delta v = \pm 1$ have energies ~ 0.5 eV and occur near $2\,\mu$m. Moreover, H_2 has a small moment of inertia and so the rotational lines are well spaced.[5] In particular, the near-IR K-window is rich in several bright H_2 lines and so is well suited for this science.

In principle, once the dominant excitation mechanism of H_2 is determined then it should be possible to compare this result with observations of other tracers in the hope of extracting information about the physics of the starburst. In particular, K-window spectra of galaxies show the bright hydrogen recombination line, Brγ. This line will arise from regions in which hydrogen is predominantly ionised, *i.e.* HII regions. In recent years, mainly because of the uncertainty over the dominant excitation mechanism of H_2 in galaxy nuclei, there has been controversy over what the ratio of 1-0 S(1) to Brγ traces. Lester *et al.* (1990) suggested that radial variations in the ratio of shocks to PDRs within starbursts resulted in changes in the 1-0 S(1)/Brγ ratio. An alternative picture has been proposed by Puxley *et al.* (1990), who suggested that the efficiency with which PDRs turn far-UV photons into IR H_2 emission is responsible for the scatter in the ratio of 1-0 S(1)/Brγ. A resolution of this issue, at least for NGC 253, is presented in section 3.5.

3.3 Observations and data reduction

K band spectra of the circum-nuclear region of NGC 253 were observed on the nights of 19-21 November 1993 with the United Kingdom Infrared Telescope (UKIRT) on Mauna Kea, Hawaii. The instrument used was the cooled grating spectrometer, CGS4, which had a long slit (90″) projected onto a 62×58 pixel InSb array. In the configuration employed, the instrument had a spatial resolution of 3″ per pixel which resulted in only the middle 30 rows of the array being illuminated. The width of the slit was also 3″. The angle of the slit was fixed at 51° east of north so that the slit was placed along the major axis of NGC 253, Figure 3.4.

We observed 4 distinct wavelength bands within the K window in order to get higher spectral resolution than a single band covering the entire K window. The sub-bands observed covered the wavelength regions: 1.98-2.08 μm (labeled 203); 2.06-2.16 μm (labeled 211); 2.14-2.24 μm (labeled 219); 2.22-2.32 μm (labeled 227). The velocity resolution of the sub-bands was 107 km s^{-1} pixel^{-1} and the spectral dispersion was 220 km s^{-1} at 2.2 μm.[6] The spectral resolution was measured from a calibration spectrum of an argon arc lamp, using a 150 lines / mm grating in the 2nd order.

[5] This is unlike heavier molecules, such as CO, where the rotational lines are so close that they produce a band head.

[6] Alternatively, the sub-bands had a resolution of $R = \lambda/\Delta\lambda \approx 1350$

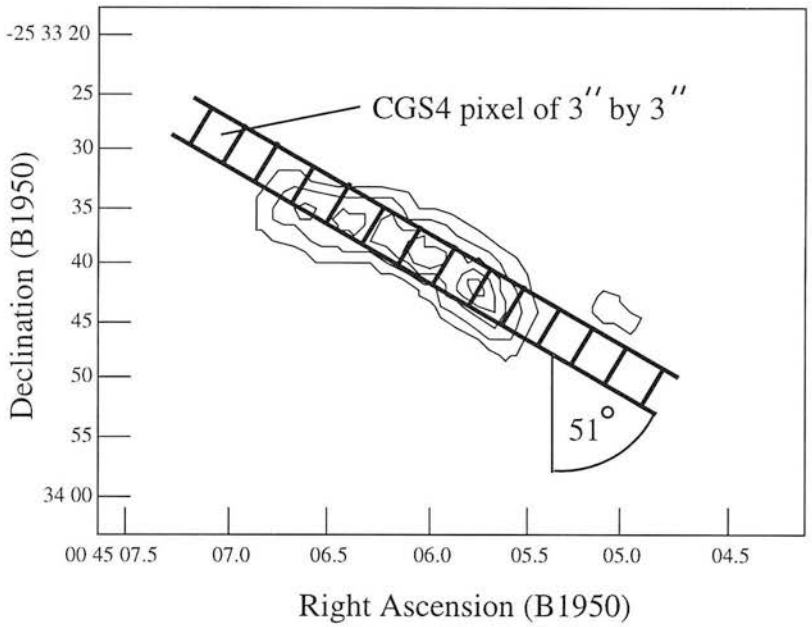

Figure 3.4: The position of the slit was along the major axis of NGC 253, at a P.A. of 51°. The contours are a schematic of the HCN 1-0 emission reported by Paglione *et al.* (1995).

We also took a lower resolution spectrum of the K window, in order to normalise the absolute fluxes of the individual high resolution spectra so they could be matched up. The low resolution spectra had a velocity resolution of 454 km s^{-1} $pixel^{-1}$ and the spectral dispersion was 980 km s^{-1} at 2.2 μm[7]. The spectral resolution was measured from an argon arc lamp taken with a 75 lines / mm grating.

The observations were sampled spectrally by moving the detector by half a pixel over 2 pixels giving integrations at 4 detector positions. This mode of sampling, *i.e.* over 2 pixels, was used so as to minimise the effects of bad pixels on the array. With this mode the spectral positions sampled by bad pixels will also be sampled by adjacent good pixels, and hence recovering the data. Only pairs of bad pixels on the array which happen to be adjacent will give a "bad" spectral position.

3.3.1 Data reduction procedure

Producing spectra for each position

Each object and sky frame were flat-fielded using the dedicated CSG4 data reduction software.[8] The first step in the procedure is to acquire a "reduced" version of a bias frame. The flat-field frame in CGS4 is obtained by observing an internal blackbody source which uniformly fills the slit via an integrating sphere. The bias and dark current is removed from this frame and the resultant image (normalised by a low order polynomial) is the intrinsic pixel-to-pixel gain variation of the array as a function of wavelength. The reduction software then reduces all the object, sky and arc lamp observations using this flat-field.

Bad pixels, *e.g.* saturated or noisy, are also treated by the reduction software. A bad pixel mask is created by plotting a histogram of the errors on the pixel values of relatively short exposure (a few seconds) of the dark current. Points which are beyond the main distribution

[7] Alternatively, the sub-bands had a resolution of $R = \lambda/\Delta\lambda \approx 300$

[8] Much of this subsection has been taken from Chrysostomou (1993).

by 3σ are flagged as bad and are incorporated into a separate image which forms the bad pixel mask. Another mask is created of all the dead pixels, those that show no noise and so don't show up in the histogram stage. The dead and bad masks are then "OR"-d together to produce another mask. This mask then informs the reduction procedures which pixels are either bad or dead and should therefore be ignored.

Once the data was flat-fielded further reduction was carried out using FIGARO and SPECDRE routines. Firstly, a routine is used which takes all the the object and sky pairs (each sky observation is taken immediately before or after the object observation to make consecutive pairs), and subtracts the sky emission from the object observation. This also effectively removes the dark current from the object frame, because the object and sky have the same dark current. The intensity of sky lines are known to vary with a period of $\sim$ 10 minutes (Ramsay *et al.* 1992) and since the time difference between our object and sky position was small ($\sim$ 80 seconds), the subtraction of sky emission in this manner should be good.

The same pixel from each row in the sky subtracted frames was extracted and placed into a separate frame. This gave frames which contained spectra at the same pixel position from all sky subtracted object frames. These spectra were then co-added.

Calibrating the wavelength and flux of the spectra

The wavelength scales of the spectra were calibrated by making observations of the known transitions from either an argon or krypton lamp. The wavelengths of the transitions were identified using the list published by Outred (1978). The calibrated wavelength scales from the lamp observations were used to replace the estimated wavelength scale in the observations.

Flux calibration was carried out by making observations of the standard star HR 12 (spectral type = A3V, $m_k = 5.74$). Because of seeing, the emission from the standard star is distributed over several pixels about the centre. To measure all the flux from the star the central 5 pixels were added together. Before adding, some of the pixel positions needed to be de-rippled.[9]

Our observing routine was to observe standard, then object and finally a standard again. In some cases we actually measured standard, object, standard, object, standard. This was required because the flux calibrated standards actually differed slightly in flux and spectral shape. This was put down to atmospheric effects which to first order would scale with airmass. To produce our final standard we therefore used the mean airmass at which the observation of NGC 253 was taken and used a linear interpretation of our two standards at known airmasses to produce a standard at that airmass. These "airmass corrected" standards were then used to flux calibrate the spectra of NGC 253.

Before the standards could be used to calibrate the flux, stellar absorption features needed to be removed. The spectra of A-type stars, at $2\,\mu$m, only have the Brγ feature in absorption. The feature in the star will be Lorentzian broadened. To a high order, the Lorentzian profile can be approximated by the sum of 3 gaussians and so the Brγ feature was removed by fitting the absorption with a 3 gaussian sum. Atmospheric absorption features are not removed because

[9] Ripples on the spectra are caused by the standard moving in and out of the slit between integrations (*i.e.* detector positions) so that the absolute fluxes on each integration differ. When the reduction software comes to interleave these integrations, the differences manifest themselves as a ripple pattern on the spectrum. The image motion occurs as a consequence of wind bouncing the telescope, or seeing effects. The rippling was removed by selecting a region of the spectrum where the ripple pattern is most evident. The mean of this region is calculated and the ripple spectrum is defined by the deviation of each point from this mean at the ripple period, from which a maximum and minimum amplitude are defined. From this information, the ripple spectrum is extended so that it has the same coverage as the standard spectrum at the pixel of interest. The ripple is divided into this standard spectrum thus removing the ripples. The 5 de-rippled spectra were then added together to produce the complete standard which is now flux calibrated.

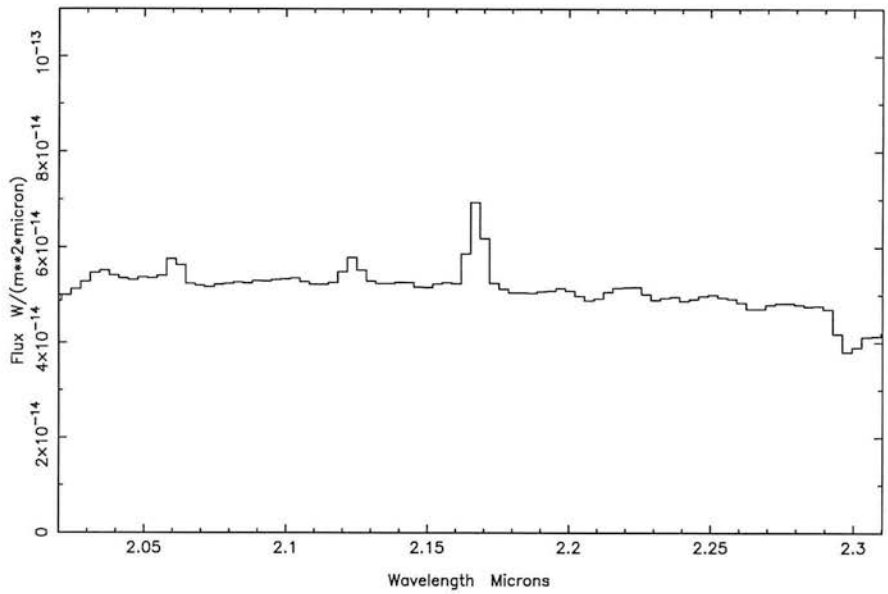

Figure 3.5: The low resolution spectrum at the nuclear position

they are intrinsic to the atmosphere and so will also be present in the spectra of NGC 253 and division of the NGC 253 spectra by the standard spectra will remove these features. The stellar spectrum was divided by a blackbody function at the effective temperature of the star (T_{eff} = 8709 K), which is normalised so that only the slope of the stellar spectrum is removed. The flux density from the star as a function of wavelength was then calculated from the magnitude at K, and divided into the stellar spectrum. The resultant spectrum was then divided into the object spectrum converting the number of data counts into a flux density.

3.3.2 Normalising and overlapping the spectra

At this point in the reduction process we had flux calibrated several separate spectra on separate nights for each of our sub-bands. To increase the S/N we needed to join these bands together. On November 20th we took a low resolution spectrum of NGC 253 which gave us the flux across the entire K window, Figure 3.5.

Each of the separate night's data was normalised to the relevant wavelength region in the low resolution spectrum through multiplication of the flux. We used multiplication, rather than adding offsets, because the line to continuum ratio of the brightest line for each of the separate sub-bands was constant from night to night and so the scaling offsets were caused by something that affected both the H_2 lines and the continuum, rather than just the lines alone (Figures 3.6, 3.7, 3.8 & 3.9).

As can be seen from Figures 3.6, 3.7, 3.8 & 3.9 there are variations from point to point in the band which shows either a maximum or minimum at or around a position which is about + 30 $\rightarrow$ 60 parsecs from the nucleus.[10] Some understanding of why this maximum occurs here can be understood from Figure 3.10. Figure 3.10 shows the flux measured around the 1-0 S(1) line in the low resolution spectrum and shows a peak in the flux at a position + 30 $\rightarrow$ 60 parsecs from the nucleus. Moreover, the gradient of flux change with distance will be at a maximum at

[10] It should be noted that +ve values indicate positions to the SW of the nucleus, -ve values indicate positions to the NE of the nucleus.

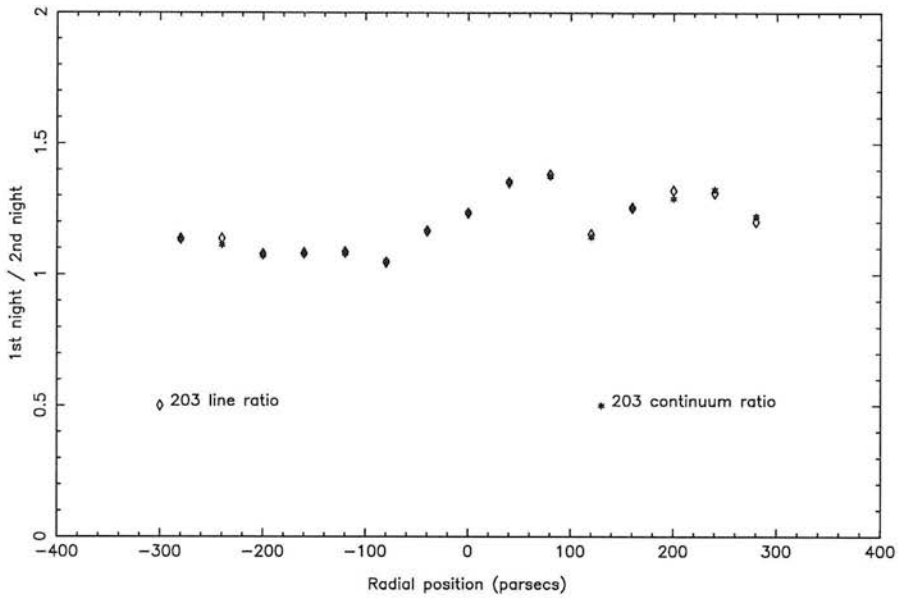

Figure 3.6: The variations in line to continuum ratio for the 203 sub-bands. The line variations scale linearly with the continuum variations which indicates that normalising the different nights by multiplication rather than addition will not cause errors in the absolute line fluxes of the emission lines.

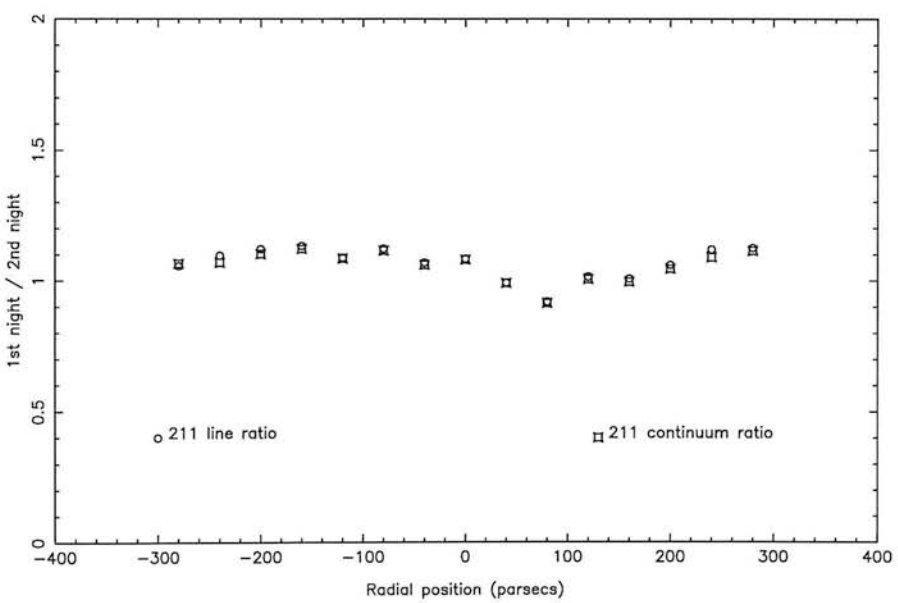

Figure 3.7: The variations in line to continuum ratio for the 211 sub-bands.

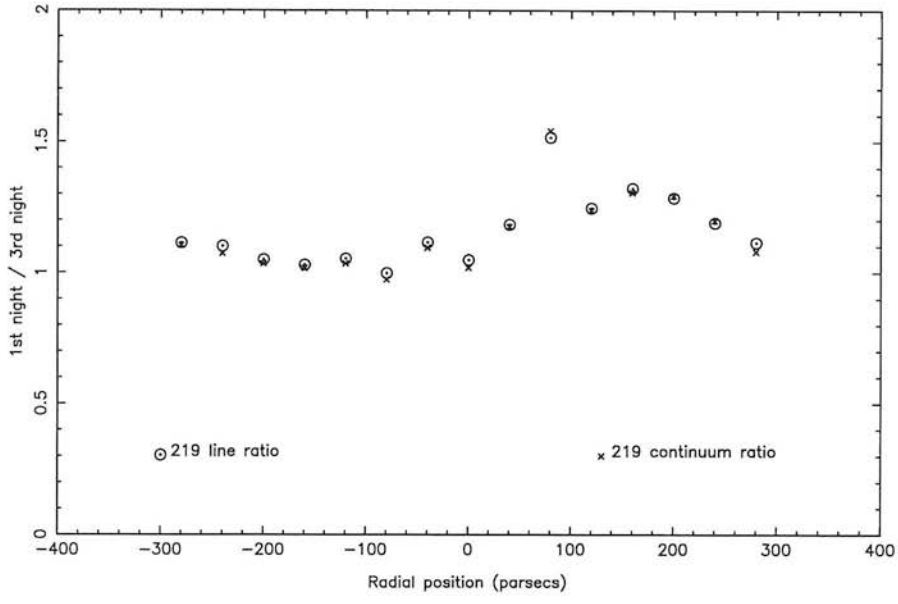

Figure 3.8: The variations in line to continuum ratio for the 219 sub-bands.

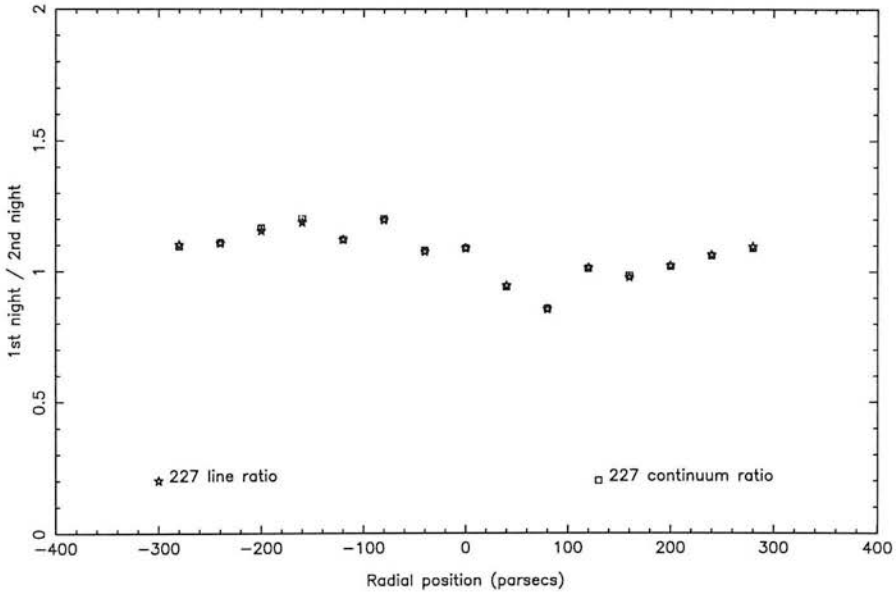

Figure 3.9: The variations in line to continuum ratio for the 227 sub-bands.

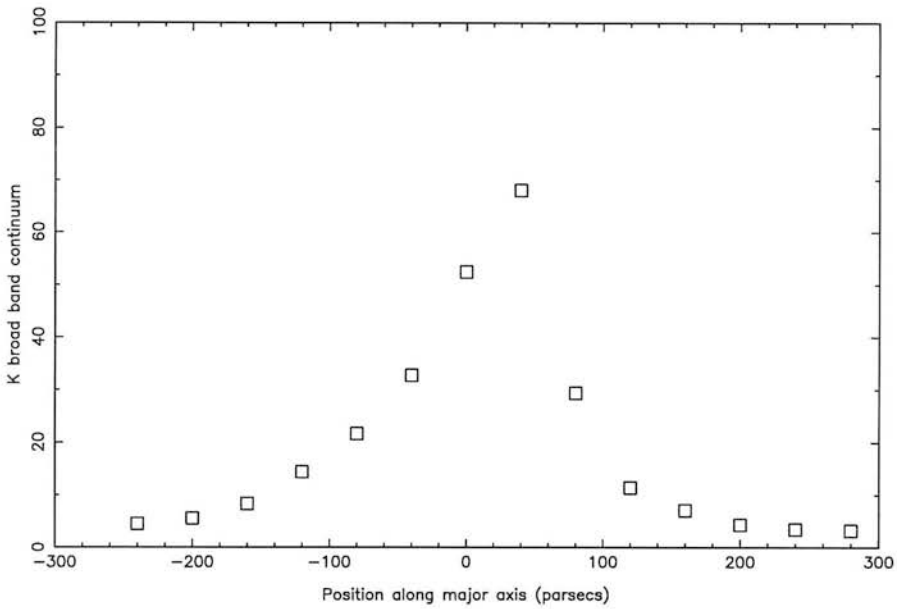

Figure 3.10: The continuum flux measured in our low resolution spectrum.

these points and so slight pointing offsets between different integrations on different nights will cause variations in the measured fluxes at each position along the slit. Furthermore, inspection of Figures 3.6 → 3.9 reveals seeing variations from night to night. Figures 3.7 and 3.9, which are comparisons of observations from the 1st and 2nd night, resemble each other, as do Figures 3.6 and 3.8, which are comparisons of observations from the 1st and 3rd night. Variations in seeing will mean that more, or less, of the flux from NGC 253, arising from outside the 3″ width of the slit, will be observed.

Once the spectra from each sub-band was normalised, the individual spectra were combined through a weighted mean to produce a final sub-spectrum. Each of the separate sub-spectra were then joined together by choosing a reasonable overlap region and taking the weighted mean of the points within this region. We now had a complete high resolution spectrum of the entire wavelength region $2.02\,\mu$m → $2.31\,\mu$m. Figure 3.11 shows the nuclear spectrum.[11] The signal to noise ratio of this spectrum is $\sim$ 400 per pixel. Figure 3.12 shows the typical errors in an expanded part of Figure 3.11, the region around the 1-0 S(1) line. This highlights that all the features in the continuum in Figure 3.11 are real, caused by absorption features in the atmospheres of cool stars. To measure the emission lines of interest it is important to model the continuum, as several absorption features coincide in wavelength with emission lines produced in the ISM. The next section discusses how this was performed.

3.4 The K band spectra in NGC 253

3.4.1 Modeling the underlying continuum

Before we can measure the H_2 lines of interest we need to subtract the underlying continuum. The near-IR emission from NGC 253 has been the subject of several detailed studies. The K-band of the galaxy contains emission lines, *e.g.* molecular hydrogen, ionised hydrogen and helium, and absorption lines, *e.g.* carbon monoxide. Below is a summary of previous work on

[11] The spectra from other locations along the slit are plotted in Appendix A

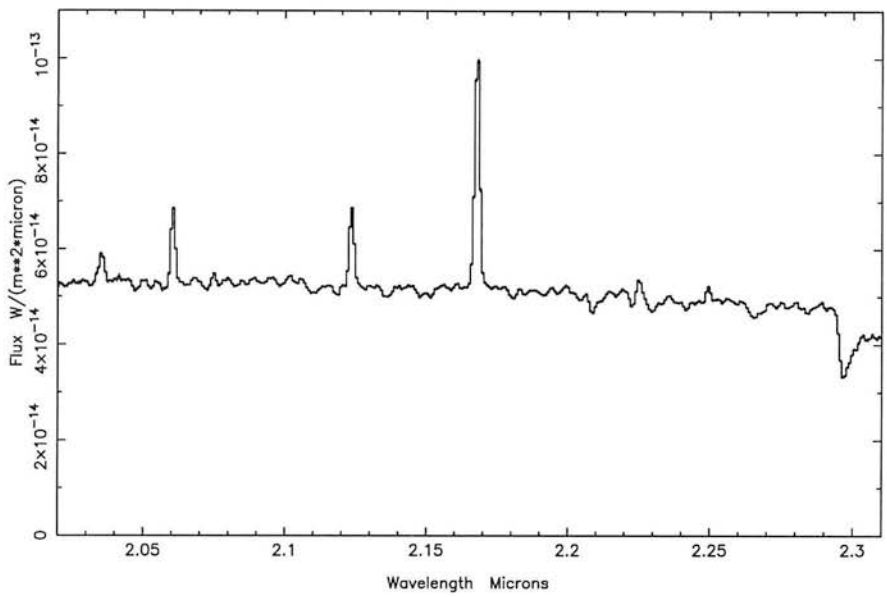

Figure 3.11: The nuclear spectrum of NGC 253. The figure highlights the small photometric uncertainty in each pixel.

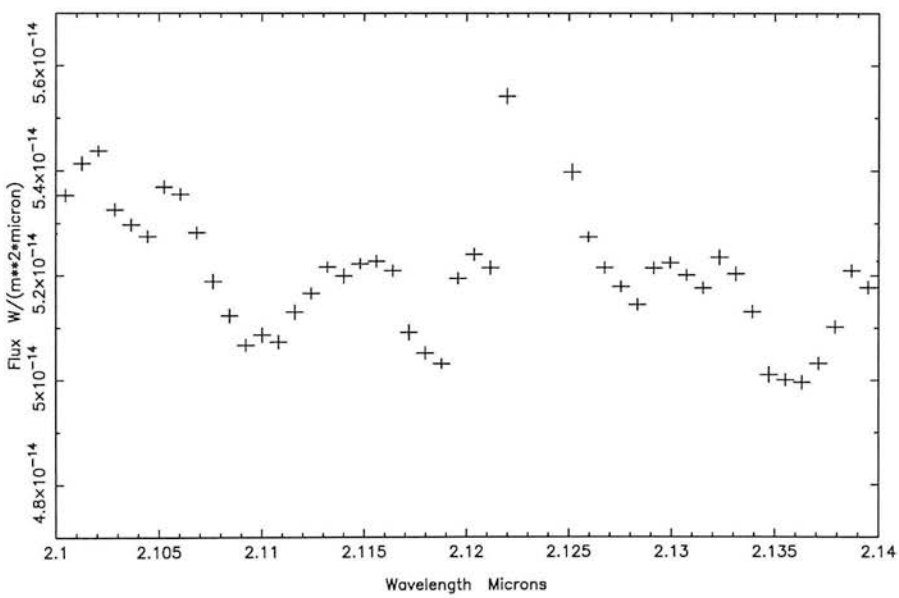

Figure 3.12: The high S/N of the spectra highlights that all the features in Figure 3.11 are real. Note that the ordinate scale of the cross is the size of the error at that position.

the K-band emission from NGC 253. The contribution of various components in producing the K-band emission in NGC 253 has been controversial with groups disagreeing on what is the dominant stellar type and what fraction of the emission arises from hot dust.

A summary of previous work

Wynn-Williams *et al.* (1979) took a K-band spectrum of NGC 253. The spectrum of Wynn-Williams *et al.* (1979) shows strong Brγ emission and the 2.3 μm CO stellar absorption feature. Wynn-Williams *et al.* (1979) suggested that the presence and strength of the CO feature indicates that late-type stars produce most of the 2.2 μm continuum emission. Wynn-Williams *et al.* (1979) suggested that the dominant contribution to the K-band flux is from giant stars and argue that red supergiants account for less than 1% of the 2 μm flux. They arrived at this conclusion through assuming that the ratio of M supergiants to ionising flux is the same in the nucleus of NGC 253 as that found in 30 Doradus in the Large Magellanic Cloud.

Rieke *et al.* (1980) suggested that the 2 μm flux is actually dominated by the light of supergiants, rather than giants, and they argued that the analysis employed by Wynn-Williams *et al.* (1979), in deriving the contribution of supergiants in NGC 253 by comparison to 30 Doradus, is flawed. Rieke *et al.* (1980) argued that the ionising flux in 30 Doradus is apparently generated by stars from a population that is so young, 3×10^6 yrs, that there are as yet no red supergiants associated with it, while the M supergiants in the nebulae are the result of an earlier burst of star formation. Furthermore, Rieke *et al.* (1980) argued that, when corrected for extinction, the CO index for NGC 253 is anomalously large and indicates the presence of supergiants.

Beck & Beckwith (1984) observed the near-IR hydrogen recombination lines, Brα and Brγ, towards the nucleus of NGC 253. Beck & Beckwith (1984) note that the spatial distribution of the recombination lines is similar to the 10 μm flux which suggests a similar origin in young stars. The 2 μm continuum is not as well correlated with the young stars. This is not too surprising as there are significant extinction variations across the nucleus which will distort the 2 μm map (Sams *et al.* 1994). Furthermore, the 2 μm emission is produced by giant and supergiant stars and may be associated with an earlier episode of star formation and so need not be distributed in the same manner. Beck & Beckwith (1984) estimated the luminosity of newly formed stars to be comparable with the bolometric luminosity of NGC 253.

Scoville *et al.* (1985) argued that towards the nucleus, and throughout the inner disk, the H-K colour is redder (by 0.2 mag) than a normal stellar disk, or even a disk enriched in late-type stars and suffering foreground extinction. Scoville *et al.* (1985) argued that the colours of giants and supergiants are very similar and so it is hard to tell what stellar type is dominating the near-IR emission. Scoville *et al.* (1985) argued that to explain the enhanced emission at 2 μm in NGC 253, compared to that expected purely from a population of late-type stars, required a significant contribution of hot dust at 2 μm. Scoville *et al.* (1985) suggested that the combination of 4 magnitudes of visual extinction plus 40% of the 2 μm emission produced by hot dust could account for the nuclear colours. Scoville *et al.* (1985) argued that this picture agreed with the measurements of Becklin *et al.* (1973). Becklin *et al.* (1973) measured 3.5 and 10.1 μm fluxes which give a colour temperature of $\sim$ 500 K for circular regions centred on the nucleus of radii from 5″ to 30″ diameter. Scoville *et al.* (1985) suggested that since the hot dust will not be isothermal, its hotter components, near 1000 K, produce a 2 μm excess and this 2 μm excess combined with the 3.5 μm flux has a colour temperature slightly below 1000 K.

Rieke *et al.* (1988) has argued that there is little evidence for a significant fraction of the

emission in the K-window to arise from any other source than late-type stars. Rieke *et al.* (1988) argued that if hot dust contributed at K then we would expect the stellar CO bands to be diluted in strength by dust, which would lie predominantly at the long-wavelength end of the K window. However, the features in NGC 253 are stronger than is typical for normal galaxies. Rieke *et al.* (1988) suggested that the peculiar J H K colours observed by Scoville *et al.* (1985) are the results of optical depth effects, arising because the stars and dust are intermingled, and inhomogeneous extinction across the source. Rieke *et al.* (1988) note that the central 3″ of the nucleus is significantly bluer in H-K than the surrounding regions which occurs if the surrounding regions are subject to strong extinction. It is not clear whether this difference in H-K colours is due to differing extinction or the evolutionary state of the starburst as Puxley (1991) has noted that the J H K colours of a starburst population will be significantly bluer than those of old stars, principally because of the significant contribution of hot young stars to the near-IR continuum. Rieke *et al.* (1988) also argued that the emission from molecular hydrogen in NGC 253 is indicative of shocked gas and they proposed that the shocked gas is produced directly by supernovae and by collisions of dense molecular clouds accelerated by supernovae in the starburst region. They argued that H_2 is not excited by the far-UV field in NGC 253, because of the relative weakness of the 2-1 S(1) line with respect to the 1-0 S(1) line.

Forbes *et al.* (1993) observed the nucleus of NGC 253 in the light of [FeII], Brγ and H_2 1-0 S(1) at 1″ resolution. The emission appears to arise from "hot spots". The hot spots are compact ($\leq$ 12 pc) star forming regions containing a mixture of HII regions, SN remnants and supergiants. Forbes *et al.* (1993) suggest that Brγ and H_2 are excited in star forming regions whereas [FeII] traces the distribution of SN.

Dust grains in close proximity to O and B stars may achieve equilibrium temperatures of several hundred degrees and thus radiate in the mid- and near- IR. Also, small particles may be transiently heated to high temperatures by absorption of single UV photons. Telesco *et al.* (1993) have imaged NGC 253 in several mid-IR broad-band filters. Towards the nuclear position the mid-IR colours suggest that the dust is cooler than at the edge of the starburst. Telesco *et al.* (1993) argues that the smallest grains which should also be the hottest may be destroyed in the starburst through the action of strong shocks and UV. Hence the contribution of non-stellar emission to our spectra may well become more important as we move away from the nucleus.

Sams *et al.* (1994) observed the nucleus in J, H and K continuum with 0.5″ resolution. They proposed that the "true" nucleus of NGC 253 is not associated with the intensity peaks in the J, H and K maps but is located 2.2″ NW of the peaks and corresponds to the brightest 2 cm radio point source detected by Turner & Ho (1985). Sams *et al.* (1994) suggest that the hot spots discussed by Forbes *et al.* (1993) are in fact holes in the extinction. Sams *et al.* (1994) argue that the near-IR intensity peak has substantial emission arising from hot dust of at least 500 K.

Subtraction of the continuum

From the preceding discussion it is clear that there is uncertainty in what makes up the K-band continuum emission in NGC 253. There will almost certainly be variations in the relative stellar contribution from supergiants and giants across the starburst nucleus. Furthermore, emission from hot small grains may make a non-negligible contribution to the 2 μm flux from specific regions in NGC 253, particularly towards the edge of the starburst nucleus.

From evolutionary models, it is expected that the average temperature of the red stars should

Table 3.1: Stellar types chosen from the Kleinmann & Hall (1986) atlas

Star	Spectral type
SU Per	M3-M4 Iab
R Lyr	M5 III
SW Vir	M7 III
χ Peg	M2 III
BK Vir	M7 - III
γ Dra	K5 III
HR 8726	K5 Ib
μ Cep	M2 Ia

be related to the age of the starburst. Up to t $\approx 10^{6-7}$ yr the temperature will be at its lowest (Renzini & Buzzoni 1986). However, there may be a significant contribution to the K band emission from hot young stars still on the main sequence. Such a population dominates the near-IR emission from the blue dwarf galaxy II Zw 40 (Joy & Lester 1988).

Younger clusters are expected to be dominated by red supergiants whilst older ones contain only red giant branch (RGB) stars. A convenient parameter used in measuring the stellar class is the CO Δv = 2 bands ($\lambda \geq 2.29\,\mu$m). These bands are strongly saturated in cool stars and so the strength of the band-head is little dependent on variations of the CO column density in the stellar photospheres but increases strongly with the micro-turbulent velocity, ξ (Origlia *et al.* 1993).[12] Kleinmann & Hall (1986), hereafter KH, produced an atlas of K band spectra of various stars. It was decided to use the CO (2,0) band-head, at 2.3 μm, that is also apparent in the spectra of NGC 253 to attempt to simulate various scenarios of stellar populations mixed with non-stellar emission.

We chose 8 different stars from the KH atlas, listed in Table 3.1, which covered the range of stars that may exist in all or part of the nuclear region and which could feasibly dominate the emission. Inspection of these stars revealed that the spectra of NGC 253 are flatter than all the KH stars and, furthermore, the CO band-head in NGC 253 is weaker than the bulk of the giant and supergiant KH stars, Figure 3.13. Therefore, there has to be a component to the overall luminosity in the K window that is not stellar and both fills in the CO band-head and makes the spectrum flatter. Such an extra component is likely to be warm/hot dust with T $\sim$ 600-1000 K, as suggested by Scoville *et al.* (1985). The warm dust will preferentially add emission to the red end of the K spectrum, over that of the blue spectrum, exactly what is needed to alter the KH standards to match the observed spectra of NGC 253. Dust is likely to be responsible rather than other emission mechanisms because the magnitude of the other emission processes acting at 2 μm will only have a small effect on the KH spectra.[13]

In particular, free-free emission, which is fairly flat across the K window and hence could mimic dust, will only provide about $\sim$ 3% of the K emission in NGC 253. Joy & Lester (1988) have tabulated the near-IR free-free continuum and recombination line coefficients. In the nuclear spectrum of NGC 253, the Brγ flux is $\sim 1.5 \times 10^{-16}$ W m^{-2}. Using the calculations of Joy &

[12] Micro-turbulence increases with advancing spectral class and luminosity (McWilliam & Lambert 1984).
[13] See Puxley (1991) for details of the important 2 μm emission processes in M82.

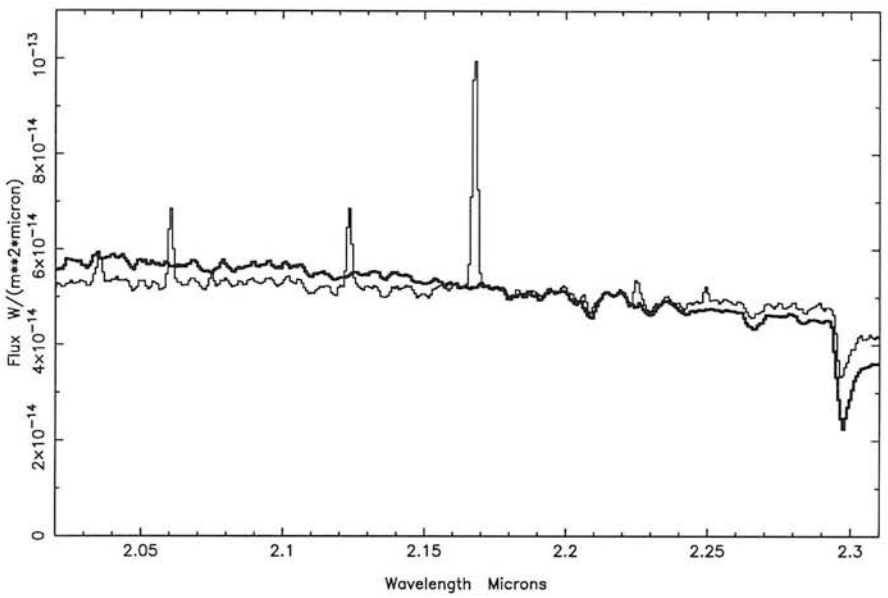

Figure 3.13: The KH standard SU Per overlaid on the nuclear spectrum of NGC 253. The CO band-head is deeper in SU Per than it is in NGC 253. Furthermore, the spectrum of NGC 253 is flatter than that of SU Per. It is therefore likely that some, $\sim$ 10-40%, of the 2 μm emission from NGC 253 is produced by warm dust.

Lester (1988) this indicates that the free-free flux density at 2.2 μm is $\sim 2\times10^{-15}$ W m^{-2} μm^{-1}. We measure the continuum flux density on the nucleus to be $\sim 6\times10^{-14}$ W m^{-2} μm^{-1}, a factor of 30 greater than the free-free prediction. The line-to-continuum ratio of Brγ is observed to fall off with distance in NGC 253 and so the maximum contribution of free-free emission is $\sim$ 3%.

The dust in NGC 253 and our galaxy, along the line of sight, will "redden" the spectrum of NGC 253. The magnitude and the shape of the reddening function is dependent on both the quantity of dust and its spatial location with respect to the stars. Puxley (1991) discusses the large range in extinction measures that can be obtained when it is uncertain whether the dust is foreground or is mixed within the stars in NGC 253. Sams *et al.* (1994) suggests that the typical extinction across the starburst is $A_v \approx$ 1-5, which translates to a typical extinction at 2 μm of $A_{2\,\mu m} \approx 0.3$.[14] Using the extinction law of Landini *et al.* (1984)

$$\frac{\tau_\lambda}{\tau_{Br\gamma}} = \left(\frac{\lambda}{2.166}\right)^{-1.85} \tag{3.11}$$

indicates that reddening will only change the spectra of the unreddened KH stars by 1-3%, not enough to account for the differences apparent in Figure 3.13. This conclusion is independent of whether the dust causing the extinction is foreground to the stellar population in NGC 253 or is mixed amongst the population.

It is difficult to constrain the absolute contribution of stars and dust at any point because of the uncertainties in the temperature and emissivity of the dust and the population of stars, which result in uncertainties in the CO depth and spectral shape. Furthermore, reddening and the small contribution of free-free emission should be included in any fit. Clearly, all these various uncertainties need to be taken into account in any quantitative model of the contribution to the near-IR emission in NGC 253. Rather than separate all the various contributions to the

[14] Note that Sams *et al.* (1984) argue for a much larger extinction at the location of the radio nucleus

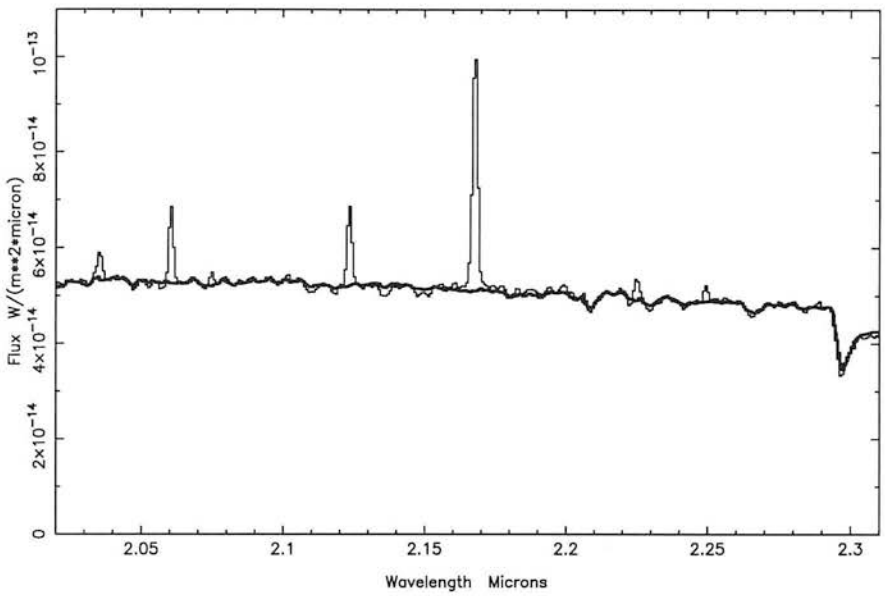

Figure 3.14: The adjusted KH standard SU Per overlaid on the nuclear spectrum of NGC 253. Note the good match between the stellar absorption features and the galaxy continuum.

continuum emission, we tried to simulate the addition of all the components by applying the following technique.[15] We first corrected the star for the recessional velocity of NGC 253, by measuring the wavelength difference between the minimum of the trough of the CO band-head in the KH star and the minimum of the trough of NGC 253. We then normalised the stellar CO depth to that of NGC 253 by adding a constant and multiplying by a constant to the flux. The slope of the corrected KH star was then multiplied by a 2nd order polynomial so that it matched the observed slope of NGC 253. This process matched the over-all spectra of NGC 253 to the corrected KH stars very well. Figure 3.14 highlights how this technique produces an accurate match between adjusted KH stars and the spectra of NGC 253.

When measuring the emission lines it is important to have the stellar velocity dispersion of the model of the continuum matched to the actual stellar dispersion in NGC 253. The stellar dispersion in NGC 253 will vary across the starburst. There is also a complication in that within the 3″ pixels we have used there could well be velocity dispersion gradients, particularly near the nucleus. Without observations designed to measure these dispersion variations it is hazardous to construct models of the dispersion. This may introduce systematic effects into measurements of the flux, dispersion and centroid of an emission line due to absorption features which coincide with part or all of an emission line being incorrectly smeared or sharpened. The present data-set is not optimised to measure the stellar velocity dispersion and therefore some arbitrary smoothing was needed to try to match the observations with the broadened KH stars. After a trial and error approach gave reasonable fits, it was decided to broaden the KH stars by a "gaussian function" of FWHM and a "coverage" of 5 pixels for the central 3 positions in NGC 253. For the surrounding positions, a gaussian function with a FWHM and coverage of 3 pixels was used.[16]

[15] The technique simulates the effects of red-shift, dilution and extinction as well as mimicing the addition of stars, warm dust and free-free emission.

[16] The smoothing routine had inputs parameters for the gaussian FWHM and for how many surrounding pixels about each point should the gaussian smoothing be applied, which I called the coverage. So strictly, I have not applied a full gaussian smoothing to the KH stars but the present approach should give a close resemblance to

3.4.2 Measuring the parameters of the 1-0 S(2), 1-0 S(1) and 1-0 S(0) H_2 lines

The nuclear spectrum shown in Figure 3.14 clearly shows several emission lines. In order to reliably measure the emission from these lines a technique was needed to subtract the underlying continuum. Much of the previous uncertainty in measuring the 1-0 S(0) and 2-1 S(1) emission lines of H_2 in galaxies has been due to the uncertainty in the underlying continuum. To measure the ortho to para ratio for any vibrational level, we needed the combination of either two para transitions and one ortho transition or two ortho transitions and one para transition. The 3 brightest emission lines of H_2 in the spectra of NGC 253 are the 1-0 S(2) (at 2.04 μm), the 1-0 S(1) (at 2.13 μm) and the 1-0 S(0) (at 2.22 μm). These 3 lines fill the requirement of a pair of para states with one ortho state and so they can be used to estimate the ortho to para ratio.

In any continuum subtraction there will be uncertainty over which wavelength region to fit the underlying continuum and the accuracy with which the continuum is fitted. The approach used was for each line in each position, subtract one of the eight fitted KH stars from the local continuum. The residuals left by the subtraction were then fitted with an arbitrary polynomial so as to mimic an extrapolation of the residuals under the line. The resulting emission line was then fitted with a gaussian in order to measure the flux, centroid and FWHM of the line. The same approach was applied with the remaining 7 fitted KH stars. This gave 8 different measures to each line at each position. A weighted mean of these 8 values may give a misleading result because a particular KH star may give a good fit, and hence a small error, to a particular line but this KH star may not be representative of the actual stellar population at that position. Thus, taking the average of the 8 values was thought a more reliable estimate of the true value of the emission line at that wavelength. The standard deviation of the eight different values should also closely match the uncertainty in that value.

The energy levels of the 3 H_2 transitions are close enough that the emission of all 3 lines should be coextensive. Thus, the FWHM of these lines should be very similar. Furthermore, these 3 lines should all have the same Doppler-shifted recessional velocity. Therefore, if a choice of parameters in the continuum subtraction resulted in one of the 3 lines having a FWHM or "centroid" velocity that differed noticeably from the other 2 lines then it was assumed that this was due to the continuum subtraction introducing an unwanted systematic error into the wayward lines measurements. Changing the continuum subtraction parameters, such as wavelength region fitted or polynomial order, eventually resulted in a closer match between the 3 lines.

This iterative technique resulted in the 3 emission lines being matched in centroid velocity and velocity dispersion at all the positions along the slit. Below is a discussion of the continuum subtraction for each of the 3 v = 1-0 lines.

The 1-0 S(2) transition

This line is the shortest wavelength line measured in the spectrum. Figure 3.15 shows the local continuum and the line. Shown in Figure 3.16 are the various KH fitted stars around the line.

The main uncertainty in measuring the line intensity is the choice of star. This is because the coolest fitted KH stars show quite deep absorption features near the line. This means that it is uncertain where the local continuum finishes and where the line starts. Because the absorption feature to the blue of the line varies from star to star, our technique of choosing an average

gaussian smoothing. I used this alternative approach, of arbitrarily choosing a coverage number to give a good fit, because the FIGARO routines only allow integer values for the input of FWHM— from trial and error it was clear that the best fit would require a non-integer choice.

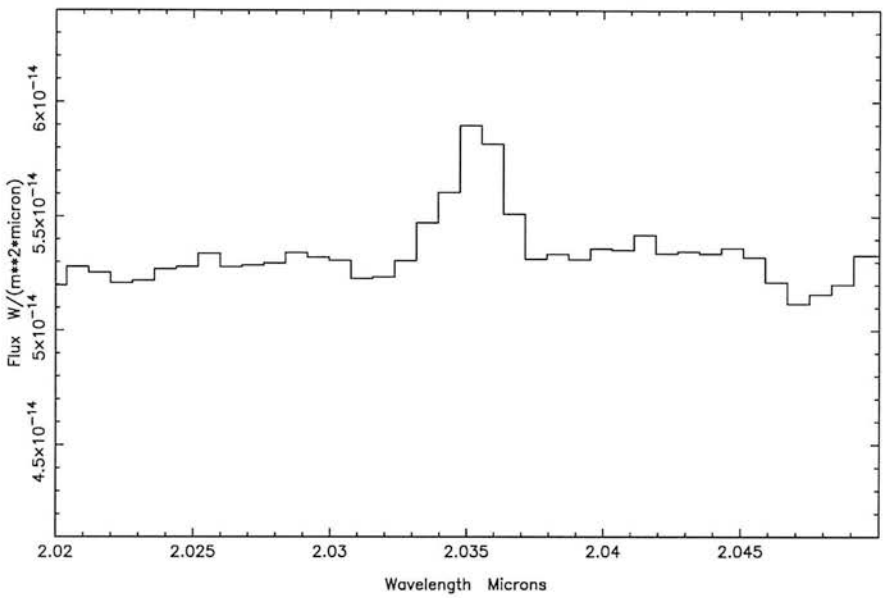

Figure 3.15: The line and continuum around 1-0 S(2).

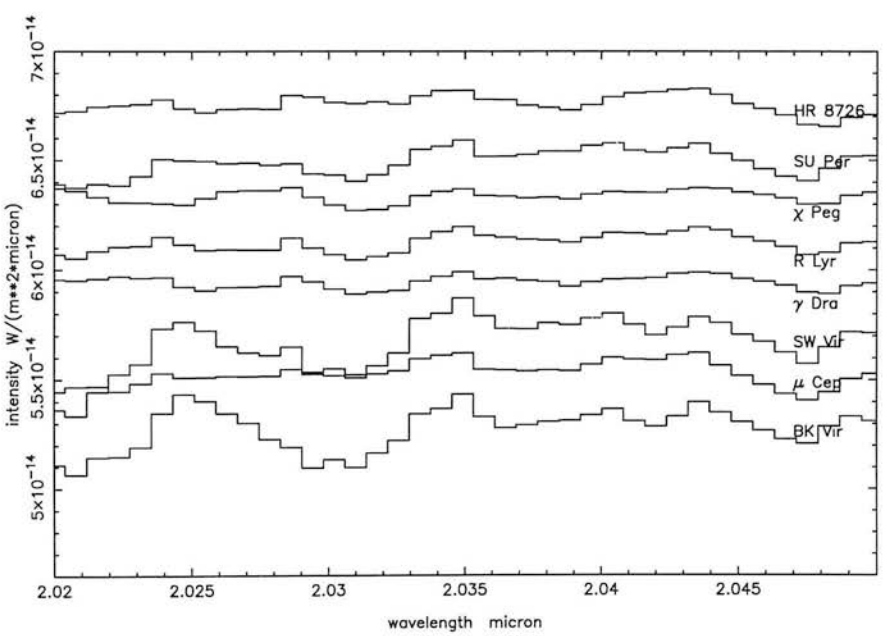

Figure 3.16: The "fitted" KH star around the 1-0 S(2) line. These stars are the KH stars after we applied the technique of fitting them to the observed spectrum of NGC 253. They are displayed as "star + constant".

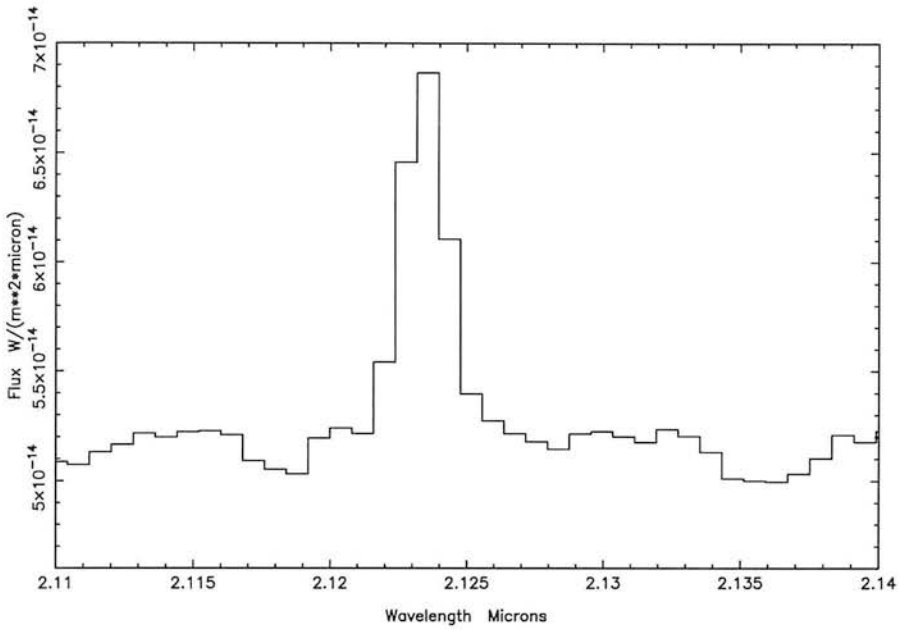

Figure 3.17: The line and continuum around 1-0 S(1).

over a range of possible stars may produce extra/less blue flux in the line. Hence this tends to make the centroid of this line uncertain. Furthermore, there is a gradient across the 2.02—2.05 μm emission, between the different stars. This is because the coolest giants, with their reduced CO band-head, have even cooler dust added to their flux which produces a continuum with a negative gradient over this region. The warmer supergiants have a positive gradient over the region. The observed spectra of NGC 253 actually show various gradients, with some positions showing negative slopes and others positive. The technique of applying a 2nd order polynomial across the entire wavelength region results in the variations at the blue end of the spectrum. If we had chosen a higher order polynomial then we could have removed, to some extent, the uncertainties in the slope at 2.04 μm. Unfortunately, this would then start removing the ambiguity caused by the uncertainty in the unknown stellar population which was actually needed in order to estimate the uncertainty in our measurements.

The 1-0 S(1) transition

This line is the brightest H_2 line in the spectrum. The line is bright and the continuum relatively flat and so the line measurements are the most secure. Figure 3.17 illustrates the line and local continuum. Figure 3.18 shows the fitted KH stars in the same wavelength region.

The 1-0 S(0) transition

This line coincides with a deep stellar absorption feature due to sodium. Another uncertainty in the measurement of this line in our data-set is that the wavelength where the line lies is within a region where two of our bands, 219 and 227, overlap. Thus, the slight differences in flux between the two bands produces an ambiguity in the flux, and hence local continuum, in the overlap region. Figure 3.19 illustrates the line and local continuum. Figure 3.20 shows the various stellar fits to this wavelength region. The uncertainty in this line meant that the FWHM and centroid were only measured, through tweaking the parameters that go into the continuum subtraction, after the values of dispersion and centroid velocity measured for the 1-0 S(2) and

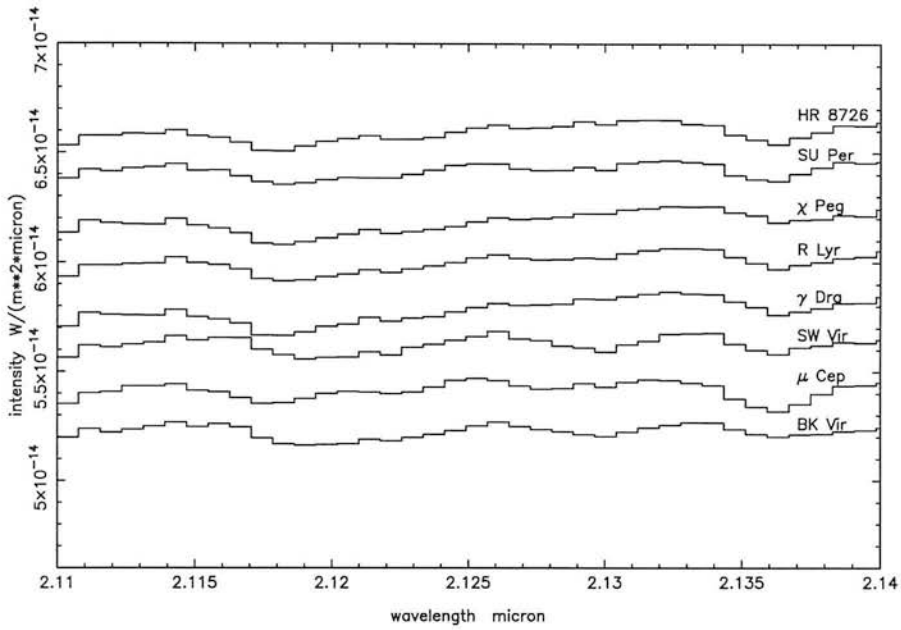

Figure 3.18: The "fitted" stars around the 1-0 S(1) line

1-0 S(1) lines were in close agreement with each other.

3.4.3 What are the likely systematic errors in the measurements?

There is always the danger when comparing line ratios that a systematic error in one or more of the line measurements will produce incorrect ratios. We are combining observations made on different nights and if there are slight variations in pointing between the different nights then we would be combining different regions of the galaxy. Such pointing offsets may be caused by mis-aligning the slit. If the emission lines of interest did not scale directly with the continuum, *i.e.* if the gas and stars have different distributions, then pointing offsets would cause the line flux and continuum flux to scale independently. As was mentioned previously it appears that there is no obvious change in the line to continuum ratio for each of the nights in each of the sub-bands—see Figures 3.6→3.9. So normalising the different nights by multiplication will not result in lines being differentially normalised with respect to the continuum. Each of the spectra from different nights have variations in the "calibrated" flux of up to 40%, caused by aggregate pointing and seeing variations. The systematic error introduced by combining these spectra is less than 40% because we have a measure, through the low resolution spectra, of the absolute flux for each position. It is estimated that combining spectra covering the same wavelength region, but observed on different nights, will result in a systematic uncertainty of $\leq 10\%$ in the flux of the line of interest.

To produce our final spectrum for each position we combined spectra of differing wavelength regions. The spectra of each of the separate wavelength regions were normalised to the low resolution spectra before being combined. In the overlap region, the weighted mean of the two adjoining spectra was used to produce the "true" spectrum. It is estimated that this technique could cause systematic uncertainties in the flux in the overlap regions of $\leq 10\%$. The only line that falls in one of the overlap regions is 1-0 S(0), at $2.225\,\mu$m.

The high quality of the spectra resulted in small photometric errors. At the position -240 pc to the NE of the nucleus, the position with the lowest line fluxes, the photometric uncertainty in

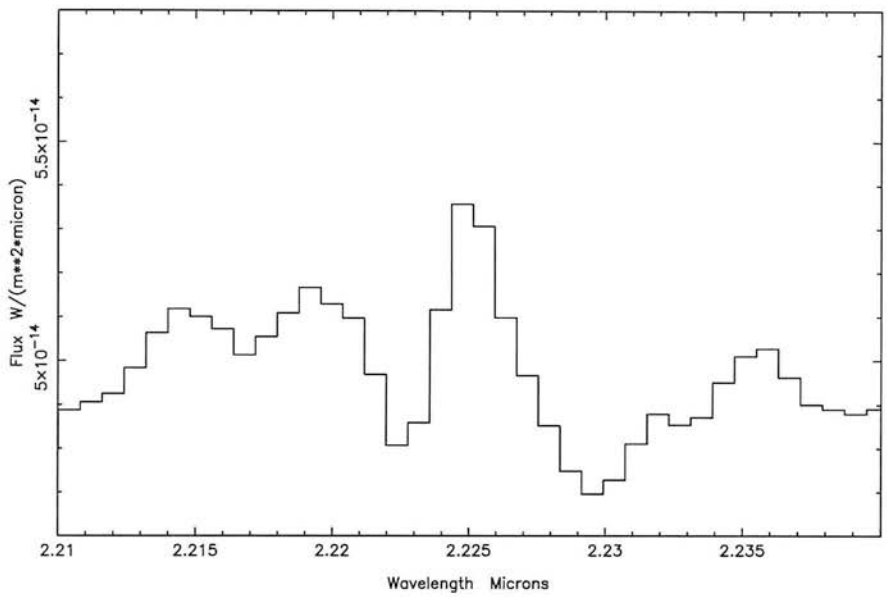

Figure 3.19: The line and continuum around 1-0 S(0)

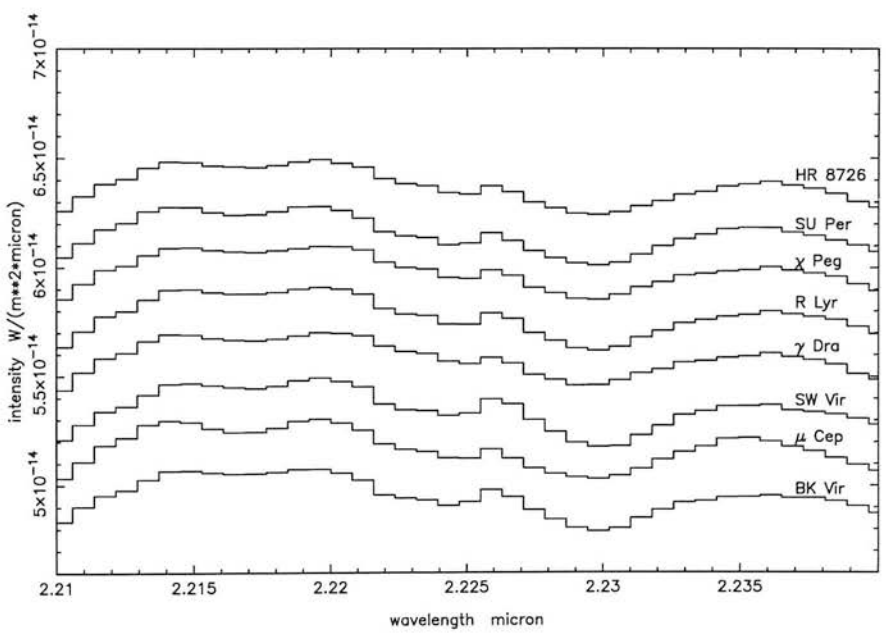

Figure 3.20: The "fitted" SU Per around the 1-0 S(0) line

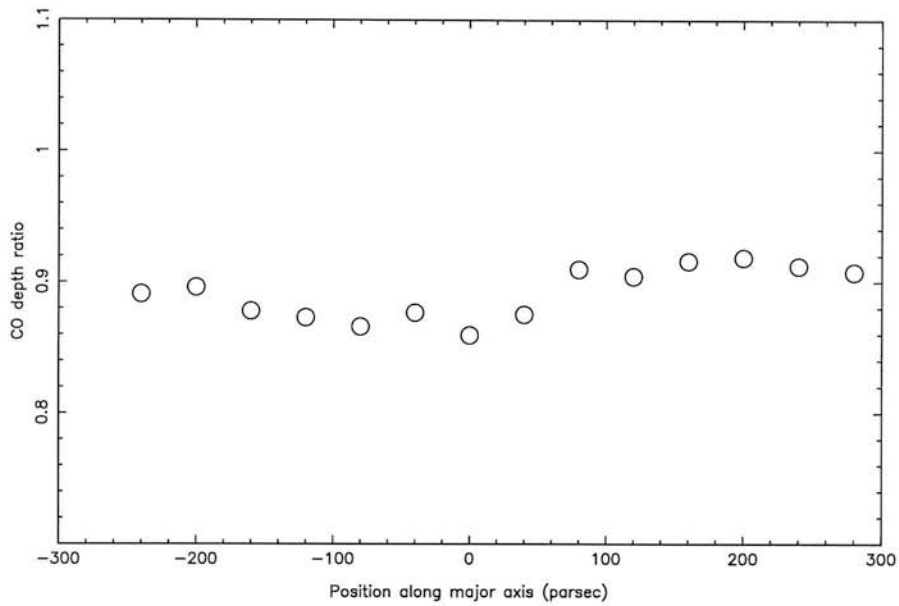

Figure 3.21: The normalised depth of the CO band-head across the starburst

the flux of each of the lines is only $\sim$ 15% for 1-0 S(2), $\sim$ 10% for 1-0 S(1) and $\sim$ 15% for 1-0 S(0). The percentage photometric uncertainty in the lines at other positions will be equal to the ratio of line fluxes at -240 pc to that of the other positions multiplied by the percentage uncertainty at -240 pc. The photometric errors are in fact smaller than the systematic uncertainty, resulting from combining spectra on different nights and over different wavelength regions, for all positions except at -240 pc.

It is plausible that the dominant spectral type in the stellar population will change across the starburst. Moreover, given that Telesco *et al.* (1993) suggest that small hot grains may be depleted in the starburst but survive in a halo then it is possible that the hot dust component to the K band flux may increase with radius. Figure 3.21 shows the ratio of the flux in the continuum to the blue of the CO band-head to the flux in the trough of the feature. There does not appear to be any systematic change in this ratio across the starburst which suggests that the normalisation of our fitted KH stars to that of NGC 253 should be constant across the region. A change in the dominant stellar population will have the largest effect on the 1-0 S(2) line measurement, due to this line being in a region in which the slope changes from star to star. It is difficult to measure this effect in the data-set. The policy of choosing the average from 8 different types of star should insure against the errors being dominated by the change of stellar population.

Figure 3.22 shows the position velocity diagram obtained using the approach of measuring the wavelength offset between the trough of the CO feature in the KH stars to that in the positions across NGC 253. As can be seen, the wavelength of the trough in the KH varies, at least at the spectral resolution we are measuring. This could feasibly result in absorption features at the wavelengths of the emission lines being offset slightly from star to star. Again, any such systematic error introduced by this variation, from a stellar population which changes with radius, is difficult to assess. The policy of choosing eight different stars will insure against any major problems incurred through this uncertainty.

Figure 3.23 shows how the line to continuum ratio of the 1-0 S(1) line varies across the

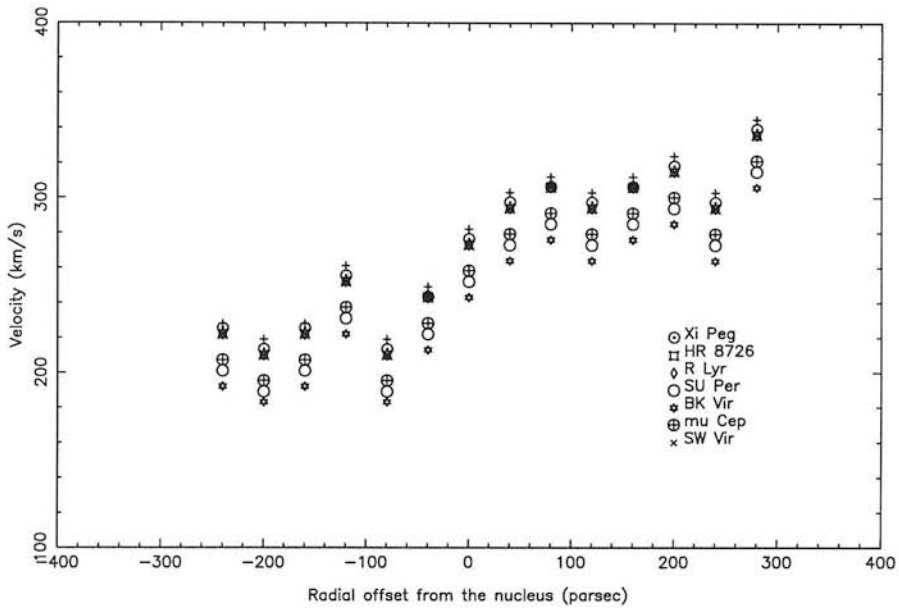

Figure 3.22: The position velocity diagram obtained from the CO band-head. This plot shows the red-shift between the trough of the CO absorption in NGC 253 with respect to the trough of the various KH stars.

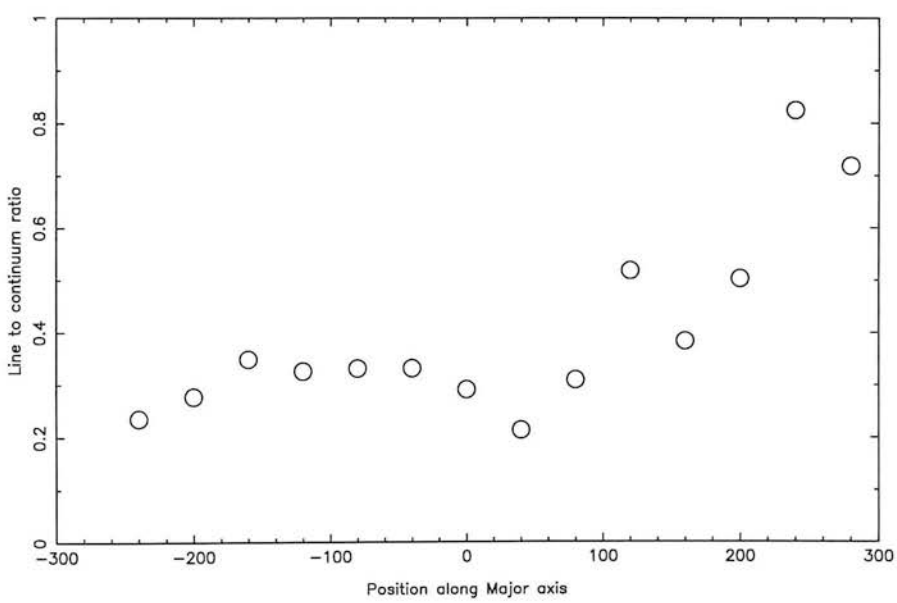

Figure 3.23: The line to continuum ratio of the 1-0 S(1) line

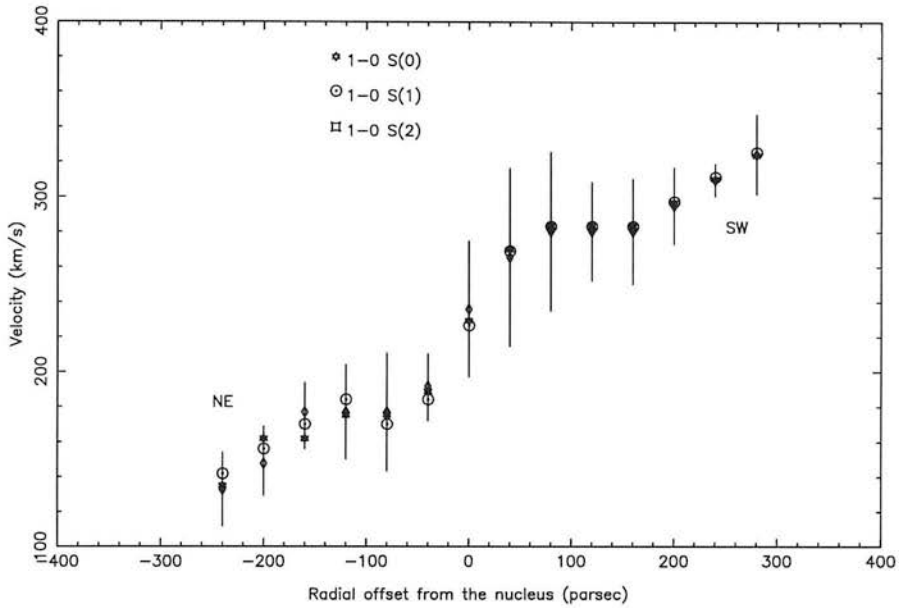

Figure 3.24: The rotation curve of molecular hydrogen. The reduction technique I applied was to match the red-shifts of the 1-0 S(2), 1-0 S(1) and 1-0 S(0) so as to minimise the scatter on this figure. There are 3 error bars actually superimposed on top of each other for every position, but at every position the largest error in velocity is that of the 1-0 S(2) line.

starburst. As can be seen, the ratio is close to being constant in the North East region but there is a systematic rise in the ratio from the nucleus to the South West.

Summarising, estimates of the systematic errors in our data reduction process result in uncertainties of $\leq 10\%$ in the fluxes of 1-0 S(2) and 1-0 S(1) and $\leq 15\%$ for the flux of 1-0 S(0). These systematic uncertainties are far larger than the random uncertainties of the measurements of each line.

3.4.4 Results of the kinematic fits to 1-0 S(2), 1-0 S(1) and 1-0 S(0)

Figure 3.24 shows the position velocity diagram obtained from the 3 H_2 lines. It is clearly showing lots of structure including solid body rotation towards the edge of the starburst. Closer towards the nucleus the rotation curve changes into either a spiral pattern or another region of solid body rotation. If the inner region is solid body then the faster rotation speed suggests that NGC 253 has a large extended mass distribution in the central 100-200 pc. If the inner region is a spiral pattern then it suggests that non-circular motions dominate the molecular gas kinematics on the starburst region. Unfortunately, only a single slit observation along the major axis was made and so we can not say for sure what is causing the structure evident in Figure 3.24. The rotation curve is consistent with kinematic measurements of the 1-0 S(1) line, reported by Prada *et al.* (1996), as well as the CO 1→0 rotation curve reported by Canzian *et al.* (1988).

Figure 3.25 shows the dispersion of the lines at various positions across the slit. No obvious trend is apparent although the dispersion may fall off towards the edge of the galaxy.[17] There

[17]The dispersion I measure is $\sim$ 200 km s^{-1}, a factor of $\sim$ 3 greater than the dispersion reported by Prada *et al.* (1996). Inspection of the Brγ spectra in Puxley & Brand (1995) indicates a velocity dispersion of $\sim$ 200 km s^{-1}, in close agreement with Figure 3.25 but not in agreement with Prada *et al.* (1996) (Phil Puxley, private communication). I thus note that there is a current disagreement in the velocity dispersion in NGC 253. Further observations, at higher spectral resolution than used here, could settle the issue.

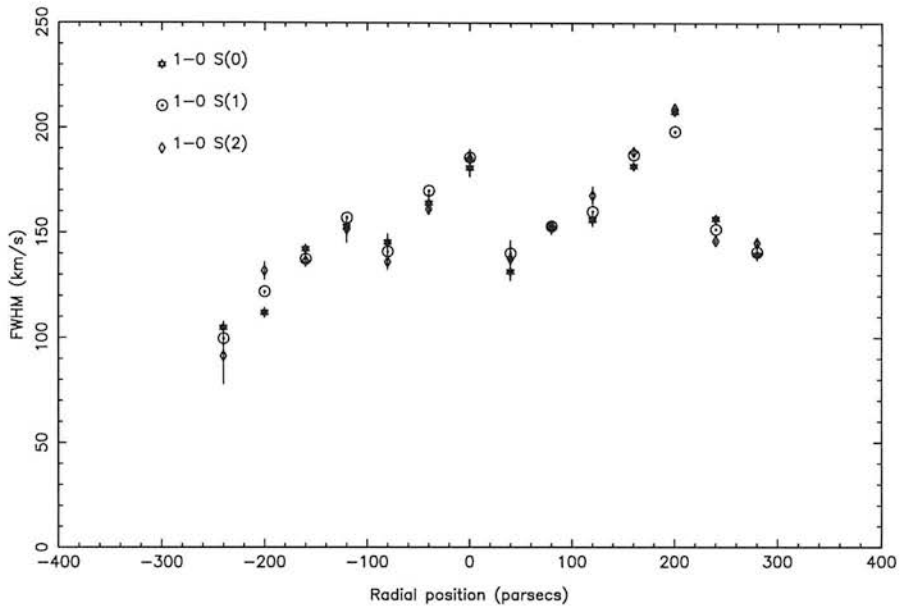

Figure 3.25: The velocity dispersion of molecular hydrogen. The reduction technique I applied was to match the dispersion of the 1-0 S(2), 1-0 S(1) and 1-0 S(0), so as to minimise the scatter on this figure. There are 3 error bars actually superimposed on top of each other for every position, but at every position the largest error in dispersion is that of the 1-0 S(2) line.

is a rise in velocity dispersion within the nuclear region. Again, we cannot study the dispersion off-axis and so we cannot tell for sure what the dispersion is saying about the gas kinematics in NGC 253.

3.4.5 Measuring the parameters of the 2-1 S(1) line

The K band also has several lines of H_2 emitted from the v = 2 level. Measuring the 2-1 S(1) line (at 2.25 μm) allows the determination of the vibrational temperature by comparing this line with the 1-0 S(1) line. Moreover, the ratio of these two lines has been used in the past as evidence that the H_2 is excited in either shocks or PDRs. The wavelength of the line coincides with a calcium absorption feature and so to measure the line accurately it is important to reliably subtract the local continuum. Figure 3.26 shows the line and local continuum and Figure 3.27 shows the various fitted KH stars.

By carrying out a similar analysis to that used to measure the 3 H_2 lines from the v = 1-0 series, it was discovered that the FWHM of the 2-1 S(1) is less than the FWHM of the v = 1-0 lines. Figure 3.28 shows the dispersion of the 2-1 S(1) overlaid on the dispersion measured from the 1-0 S(1) line. This is to be expected as the transition is $\sim$ 14,000 K above ground, compared with $\sim$ 7000 K for the 1-0 S(1), and so the regions which generate the 1-0 S(1) will be expected to have a higher velocity dispersion. The fact that the FWHM of the 1-0 S(1) is different to that of 2-1 S(1) means that the emission cannot be entirely coextensive. As the 1-0 S(1) FWHM is broader than 2-1 S(1), and the flux in the lines should scale with FWHM, it means that the flux ratio of these two lines will be lower than obtained from just comparing the heights of the two emission lines above the continuum, even after trying to model the underlying continuum.

The centroid of the line closely matches the rotation curve obtained from the 3 v = 1 lines. Figure 3.29 shows the rotation curve obtained from 2-1 S(1) overlaid on the curve measured

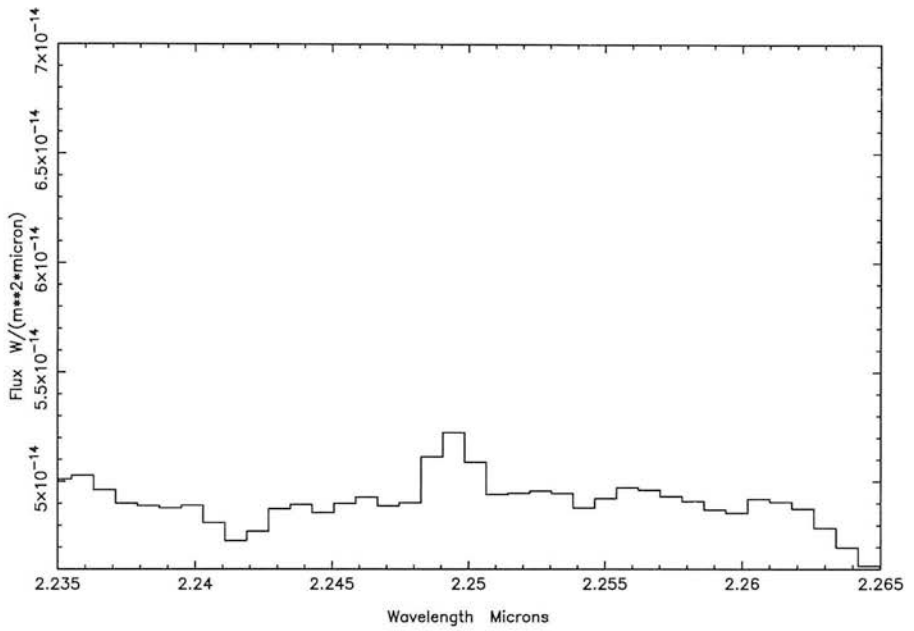

Figure 3.26: The line and continuum around 2-1 S(1)

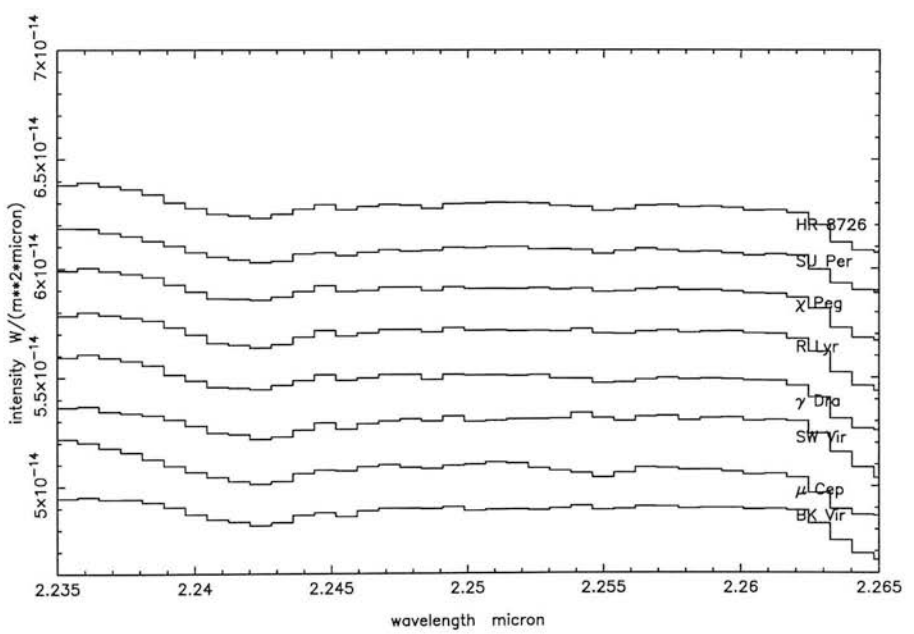

Figure 3.27: The fitted KH star around 2-1 S(1)

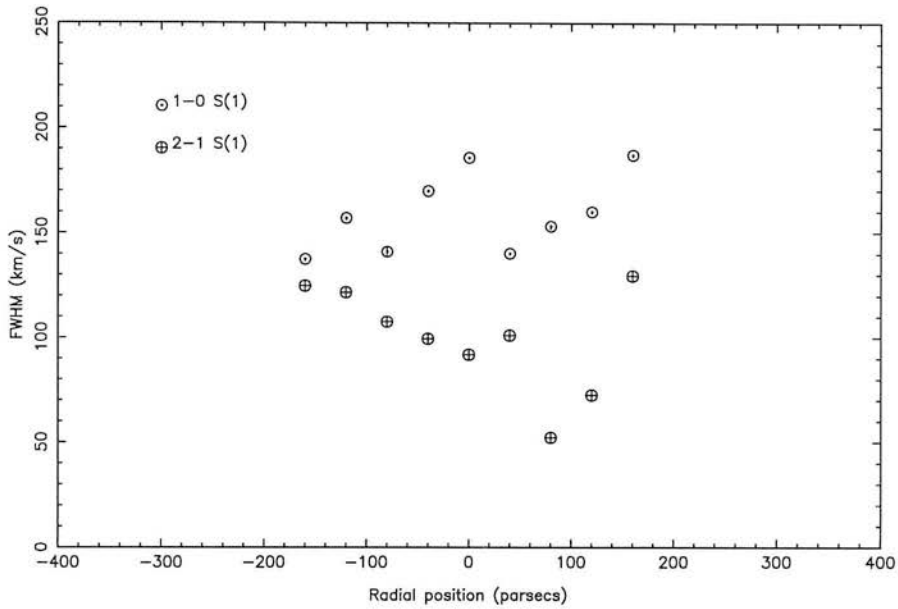

Figure 3.28: The difference in dispersion between 2-1 S(1) and 1-0 S(1)

using 1-0 S(1). As was discussed earlier, it is likely that the technique of combining spectra observed on different nights will introduce a systematic uncertainty of no more than 10% in the flux estimate of the 2-1 S(1) line. The maximum photometric uncertainty is $\sim$ 30% at -240 pc from the nucleus but for all the other positions, the photometric uncertainty in the 2-1 S(1) line is $< 10\%$.

3.4.6 Other H_2 lines

It was hoped that by measuring the 2-1 S(3), at 2.07 μm, and the 2-1 S(2), at 2.16 μm, lines we could measure the ortho to para ratio obtained from the v = 2 level and this could act as an independent confirmation.[18] Unfortunately, this could not be done with the existing data-set. Figure 3.30 shows the local continuum on and around the 2-1 S(3) line. The figure illustrates the 3 separate spectra we measured before combining. It is clear that there is a feature on the blue side of the line that is varying. Unfortunately, due to uncertainties in sky subtraction, there is a residual sky emission line at this point. This uncertainty in the blue continuum means that we cannot reliably measure the flux of this line.

The 2-1 S(2) line is the weakest line in the series and correspondingly the hardest line in which to reliably measure the underlying continuum. With the uncertainty in the continuum subtraction near 2-1 S(1) and the uncertain sky emission around 2-1 S(3), we cannot be sure of the 2-1 S(2) FWHM at any point. It was therefore decided that trying to measure the 2-1 S(2) line would be prone to many systematic uncertainties and therefore the line, along with 2-1 S(3), was not used in the analysis.[19]

[18] The o/p ratio from the v = 2-1 series should be $\leq$ the o/p ratio from the v = 1-0 series.

[19] It is noted that for galaxies with a higher H_2 line to continuum ratio than NGC 253, observations of the ortho to para ratio obtained from the v = 2 level can be used as an independent confirmation and to check for systematic errors in the o/p ratio measured from the v = 1 level.

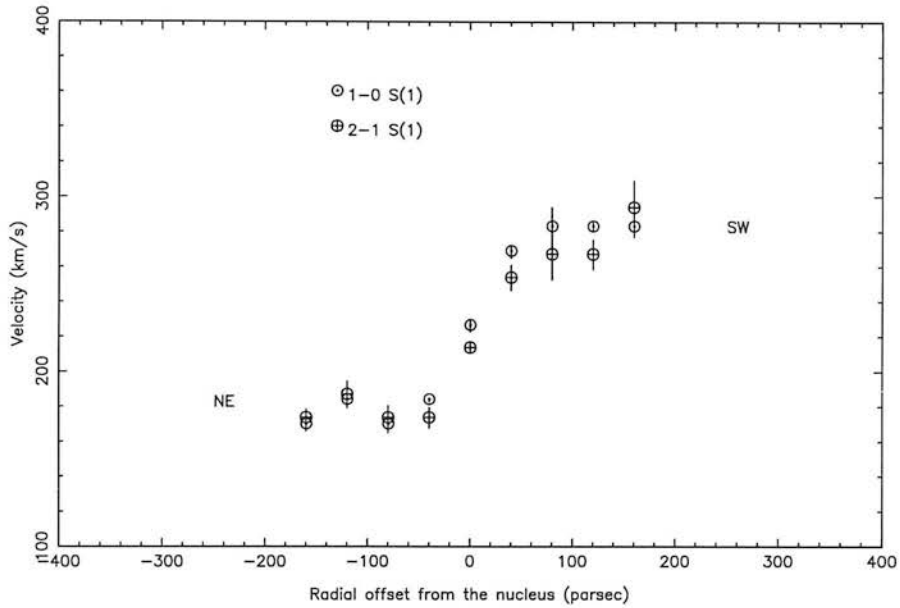

Figure 3.29: The 2-1 S(1) rotation curve

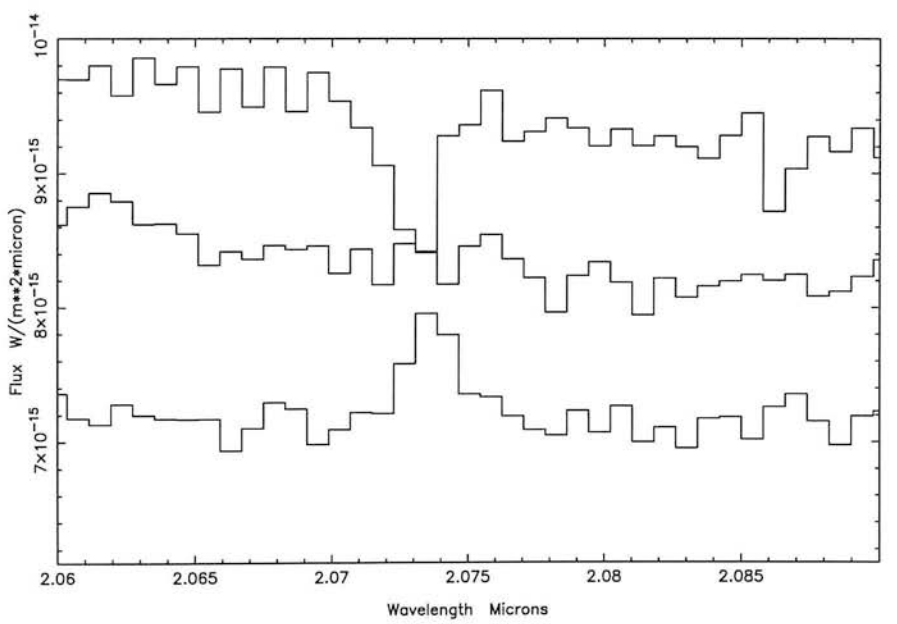

Figure 3.30: The 3 observations of the local continuum around the 2-1 S(3) line (at +120 pc from the nucleus). The fluctuations of the sky line, centered on 2.073 μm, swamp the 2-1 S(3) line, which is centered on 2.076 μm.

3.5 The excitation of molecular hydrogen emission in NGC 253

3.5.1 Results of H_2 measurements and their implications

In the preceding section we have discussed how we obtained measurements of the 1-0 S(2), 1-0 S(1), 1-0 S(0) and 2-1 S(1) emission lines of molecular hydrogen across the starburst in NGC 253. Although we have only measured 4 lines it is possible to constrain the excitation mechanism: the rotational temperature can be determined using 1-0 S(2) and 1-0 S(0); the vibrational temperature can be determined using 1-0 S(1) and 2-1 S(1); the all-important ortho to para ratio can be determined using 1-0 S(2), 1-0 S(1) and 1-0 S(0).

Table 3.2 lists all the measured fluxes of lines towards NGC 253 and Table 3.3 lists the relevant line parameters of the H_2 lines. The flux of a line divided by the pixel size gives the intensity, which from equation 3.6 gives the normalised column density in the upper level. Figure 3.31 illustrates the column densities observed at the nuclear position. As mentioned above, the FWHM of the 2-1 S(1) line is systematically lower than that of the 3 v = 1 H_2 lines and most of the uncertainty in the 2-1 S(1) flux results from the uncertainty in the FWHM.

Figure 3.32 shows the rotational temperatures, measured using 1-0 S(2) and 1-0 S(0), and vibrational temperatures, measured using 1-0 S(1) and 2-1 S(1). As can be seen, the rotational temperatures are $\sim$ 1000 K across the galaxy and the vibrational temperatures are $\sim$ 3000 K. This non-thermal discrepancy between the rotational and vibrational temperatures is entirely consistent with fluorescent excitation of molecular hydrogen in NGC 253.[20]

Figure 3.33 shows the ortho to para ratios measured from the v = 1 level across the galaxy. The values are around 2 everywhere, and nowhere is it measured to be 3 within the errors.[21] Thus, H_2 emission from NGC 253 traces PDRs, not shocks.

Figure 3.34 shows the profile of how the ratio of molecular hydrogen emission, the 1-0 S(1) transition, to ionised hydrogen emission, Brγ, varies. The profile shown here is consistent with a similar plot of the 1-0 S(1)/Brγ ratio in NGC 253 reported by Prada *et al.* (1996). The U structure, with a minimum in the 1-0 S(1)/Brγ ratio near the nucleus, has been observed in similar plots of several other galaxies, notably M82 and NGC 4945 (Prada *et al.* 1996).

Lester *et al.* (1990) argued that the rise in the 1-0 S(1)/Brγ ratio towards the molecular ring of M82 suggested that molecular gas was being shocked in the ring of gas around the starburst. They suggested that shocked gas would generate H_2 emission but little Brγ. This scenario suggests that radial variations in the ratio of shocks to PDRs within starbursts results in variations in the 1-0 S(1)/Brγ ratio. Puxley, Hawarden & Mountain (1990), hereafter PHM, suggested that the efficiency with which PDRs transform far-UV photons into IR H_2 emission was responsible for the scatter in the ratio of 1-0 S(1)/Brγ, observed in a number of galaxies.

[20] The error in the derived excitation temperature is given by

$$\delta T = \frac{T^2}{E_1 - E_2}\sqrt{\left(\frac{\delta N_1}{N_1}\right)^2 + \left(\frac{\delta N_2}{N_2}\right)^2}$$

where N_i is the population and E_i is the energy level (K).

[21] The fractional error in the o/p ratio is given by

$$\left(\frac{\delta o/p}{o/p}\right)^2 = \left(\frac{\delta N_{1-0S(1)}}{N_{1-0S(1)}}\right)^2 + \left(\alpha\frac{\delta N_{1-0S(2)}}{N_{1-0S(2)}}\right)^2 + \left((1+\alpha)\frac{\delta N_{1-0S(0)}}{N_{1-0S(0)}}\right)^2$$

where $\alpha = \frac{E_{1-0S(1)} - E_{1-0S(0)}}{E_{1-0S(0)} - E_{1-0S(2)}}$.

Table 3.2: The fluxes measured for all the positions (in units of 10^{-19} W m^{-2}).

Position along slit		1-0 S(2)	1-0 S(1)	1-0 S(0)	2-1 S(1)	Brγ
(arcsecs)[a]	(parsecs)[b]					
+21	+280	20.2±0.1[c]	48.5±0.1	17.2±0.3	—	—
+18	+240	41.6±0.2	60.7±0.1	19.1±0.1	—	9.1±0.2
+15	+200	30.6±0.3	51.6±0.3	20.4±0.2	—	7.1±0.2
+12	+160	31.4±0.5	62.4±0.1	23.9±0.1	12.4±0.1	19.0±0.3
+9	+120	50.1±0.9	128.1±0.3	51.9±0.8	22.7±0.1	55.6±1.3
+6	+80	93.1±1.8	196.7±0.4	74.5±1.3	34.4±0.4	291.9±3.9
+3	+40	127.4±6.6	299.1±0.8	125.4±3.0	74.4±0.5	1408.9±2.9
0	0	127.1±3.8	340.9±0.6	130.0±2.6	68.8±0.5	1150.0±3.1
-3	-40	101.7±1.9	236.2±0.5	88.2±1.7	39.8±0.7	484.6±0.9
-6	-80	52.4±1.5	145.3±1.1	54.8±1.3	31.6±0.6	269.3±1.0
-9	-120	38.9±0.5	98.5±0.4	38.2±0.7	19.2±0.2	103.0±0.6
-12	-160	24.1±0.7	58.5±0.3	23.7±0.3	17.3±0.5	40.4±0.5
-15	-200	20.4±0.7	30.3±0.2	13.1±0.3	—	24.0±0.1
-18	-240	14.0±1.0	20.1±0.2	9.8±0.2	—	10.5±0.1

[a] +ve values are to the SW, −ve values are to the NE

[b] 3″=40 pc when NGC 253 is at a distance of ∼2.75 Mpc.

[c] All the quoted errors are the random errors in our flux measurements. The systematic uncertainties of 10—15% are far larger than the random errors.

The models of B&vD and Sternberg (1988) indicate that the H_2 excitation efficiency, that is, the ratio of output IR line to incident UV continuum flux, depends primarily on the intensity of the incident ultraviolet radiation (χ), and the gas density ($n = 2n_{H_2} + n_H$), Figure 3.35. The efficiency of H_2 excitation is maximised for small χ/n, when the attenuation of UV radiation is dominated by line absorption. For larger values of χ/n, the efficiency is reduced because of removal of UV photons by dust. Thus, the extent to which the stellar radiation is diluted by geometry is pivotal in determining the relation between the molecular hydrogen luminosity and the UV luminosity.

Across the starburst of NGC 253, we measure the ortho to para ratio of H_2 to be ~ 2, not 3. This highlights that shocks cannot dominate the excitation of molecular hydrogen emission in NGC 253. PDRs dominate in producing the H_2 emission from NGC 253. Therefore, the radial variation of the ratio of 1-0 S(1)/Brγ in NGC 253 is related to the physics of PDRs, as suggested by PHM. The ratio is not related to the relative role of shocks and PDRs in producing H_2 and Brγ emission. In the next section I discuss the physics of the efficiency of converting UV radiation into emission from H_2. I then apply this physics, in conjunction with the calculations of PHM, in order to constrain the spatial relationship between O and B stars and PDRs in NGC 253.

Table 3.3: Line parameters for the observed H_2 lines.

Transition label	Wavelength (μm)	Energy (Kelvin)	g_j[a]	A 10^{-7} s^{-1}
1-0 S(2)	2.0338	7584	9	3.98
1-0 S(1)	2.1218	6956	21	3.47
1-0 S(0)	2.2235	6471	5	2.53
2-1 S(1)	2.2477	12550	21	4.98

[a]Assumes an ortho/para ratio of 3

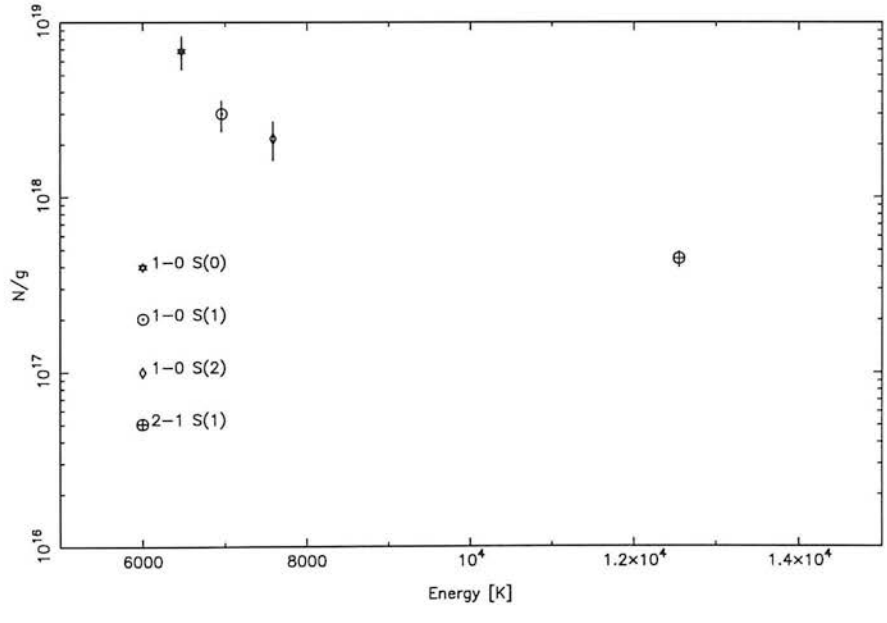

Figure 3.31: The column density diagram for the nuclear position.

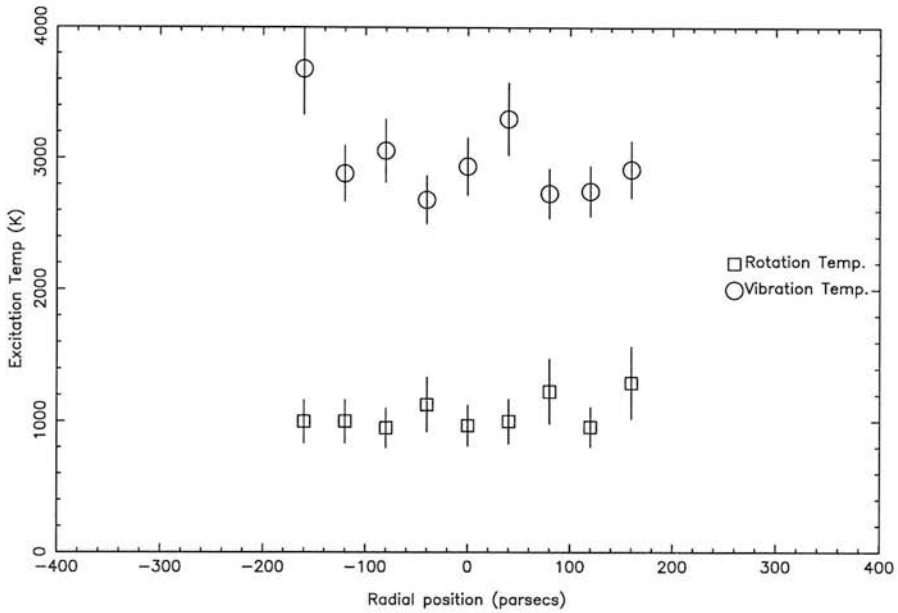

Figure 3.32: The rotational and vibrational temperatures across the starburst. The rotational temperature is derived from a comparison of the column densities in the 1-0 S(2) and 1-0 S(1) transitions. The vibrational temperature is derived from a comparison of the column densities in the 1-0 S(1) and 2-1 S(1) transitions.

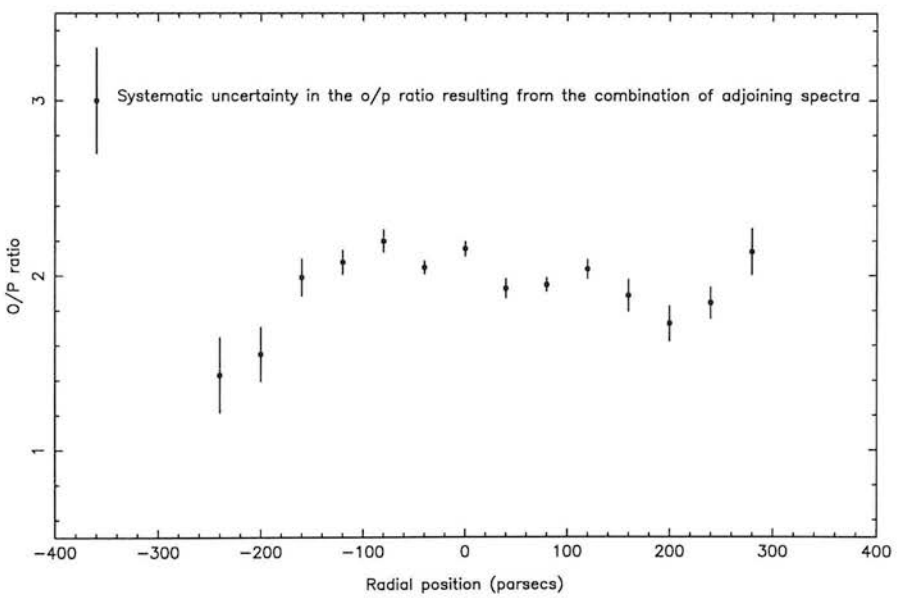

Figure 3.33: The ortho to para ratios across the starburst. The value is fairly constant at all positions suggesting that the excitation mechanism is the same throughout the inner regions of NGC 253. The derived ratio of $\sim$ 2, not 3, indicates that the H_2 emission arises from PDRs, not from shocked gas. As can be seen, the systematic error in the o/p ratio, resulting from the combination of adjoining spectra, dominates over the random errors, resulting from the photometric uncertainty of the pixels in the spectra and the subtraction of the underlying continuum around each of the lines.

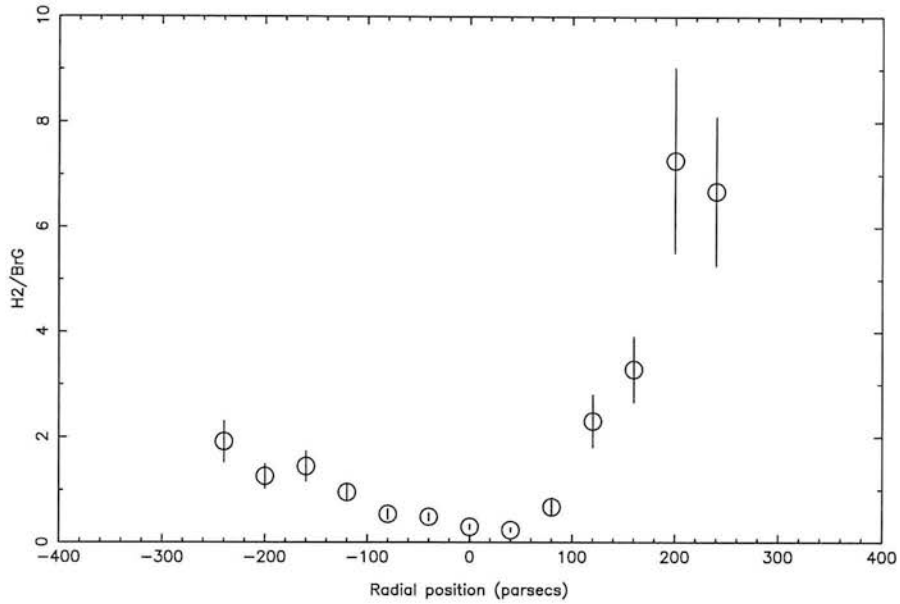

Figure 3.34: The ratio of 1-0 S(1)/BrG across the starburst

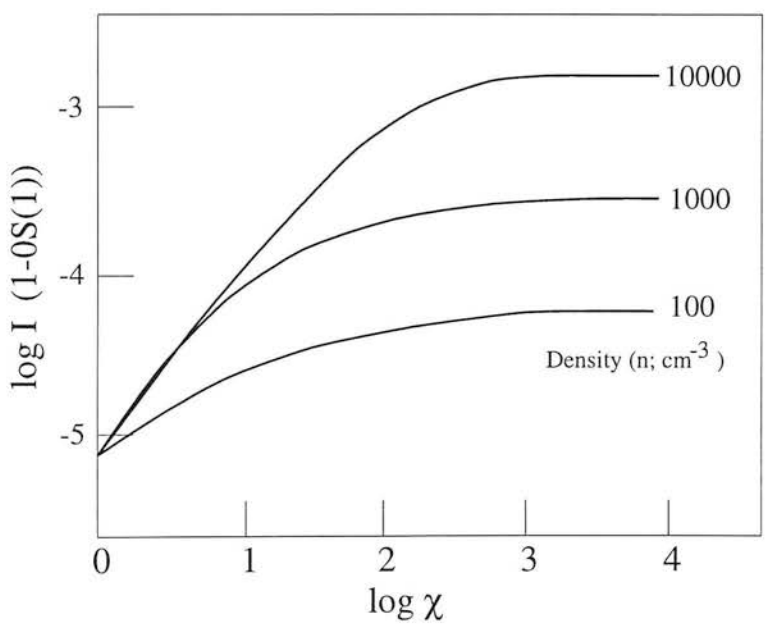

Figure 3.35: The emitted intensity in the 1-0 S(1) line of H_2, in units of ergs cm^{-2} s^{-1} sr^{-1}, as a function of the incident UV radiation (given relative to the background in the solar neighbourhood) for various values of the total gas density. The figure is adapted from B&vD.

3.6 The efficiency of generating H_2 emission in NGC 253

3.6.1 The efficiency with which far-UV is turned into H_2 IR emission

The efficiency, η, with which the UV flux impinging upon a molecular cloud, I_{UV}, is converted into a flux of IR photons, I_{IR}, has been discussed in detail by several groups, including B&vD and Sternberg (1988). For a given density of the gas, I_{IR} initially increases almost linearly with increasing I_{UV} but eventually saturates at some asymptotic value, Figure 3.35. This limit to fluorescent emission results from the competition between grains and molecules for absorbing the ultraviolet photons. If H_2 absorbs all the incoming UV photons then H_2 will be excited at maximum efficiency. There is a limit to this efficiency, though, because eventually the H_2 will go optically thick to the UV photons (B&vD). Once the far-UV photons which cause fluorescence are exhausted, then H_2 is no longer photodissociated, even though there well may still be far-UV photons available to ionise and dissociate other species. The rates of photodissociation and fluorescence of H_2 are severely depth-dependent due to the lines of ultraviolet absorption becoming rapidly optically thick to the UV. This results in the state of hydrogen towards the edge of a cloud switching from almost pure atomic, with a small fraction of H_2, to almost pure molecular hydrogen, over a small range of column density (Sternberg 1988). This sharp transition occurs when there is a sufficient column density of molecular hydrogen to completely self-shield itself against the UV, typically at a column density of $\sim 10^{15-16}$ cm^{-2} (Sternberg 1988).

If the dust becomes optically thick to the UV before H_2 goes optically thick then an increase in the UV field or density will not result in a larger column of excited molecular hydrogen. The depth into the cloud at which dust becomes optically thick to UV is fixed at a specific column density of gas whereas the depth into the cloud at which H_2 becomes optically thick depends primarily on the ratio of the intensity of the incident ultraviolet radiation, χ, and the gas density, $n = 2n_{H_2} + n_H$. The efficiency of H_2 excitation is maximised for small χ/n, when the attenuation of UV radiation is dominated by line absorption.[22] In this regime all the incoming UV photons dissociate and excite H_2. For larger values of χ/n, the efficiency is reduced because of the removal of UV photons by dust. PHM concluded that the extent to which the stellar radiation is diluted by geometry is pivotal in determining the relation between the molecular hydrogen luminosity and the UV luminosity from a starburst.

Another important factor which determines the efficiency of H_2 excitation is the duration of the PDRs exposure to UV photons. Goldschmidt & Sternberg (1995) and Hollenbach & Natta (1996) have modeled the time-dependent emission from molecular hydrogen in PDRs and they find that at "early-times", immediately following the onset of radiation, the emission is far more intense than at later times, Figure 3.36, when equilibrium is reached. This is because at early times, H_2 at the front of the cloud is exposed to UV. This results in both IR emission, through the cascade down the vibrational-rotational ladder of an excited molecule, and dissociation of H_2.[23] As the cloud evolves, most of the H_2 at the front of the cloud is dissociated and so at

[22] The excited H_2 column density, and hence the intensity of photons produced in the IR cascade, is limited by the depth to which the UV can penetrate, *i.e.* the depth at which the optical depth of the UV begins to saturate. The optical depth in turn is related to the column density of H_2, which is controlled by a balance between the formation and destruction of H_2. χ/n is the important parameter because the rate of photodissociation, and similarly the rate of exciting H_2, is $\propto \chi$ n whereas the rate of formation is $\propto n^2$. If the depth at which the UV goes optically thick to absorption by H_2 is larger than the depth at which the UV is absorbed by dust then the efficiency of producing H_2 emission will be at its maximum. Alternatively, if dust absorbs the bulk of the UV before it has gone optically thick in the H_2 lines then the efficiency will be reduced.

[23] It should be remembered that the dissociation of H_2 and its fluorescent excitation are intimately linked - when H_2 absorbs a far-UV photon, ~90% of the time results in an IR cascade whereas the remaining ~10% results in dissociation of the molecule.

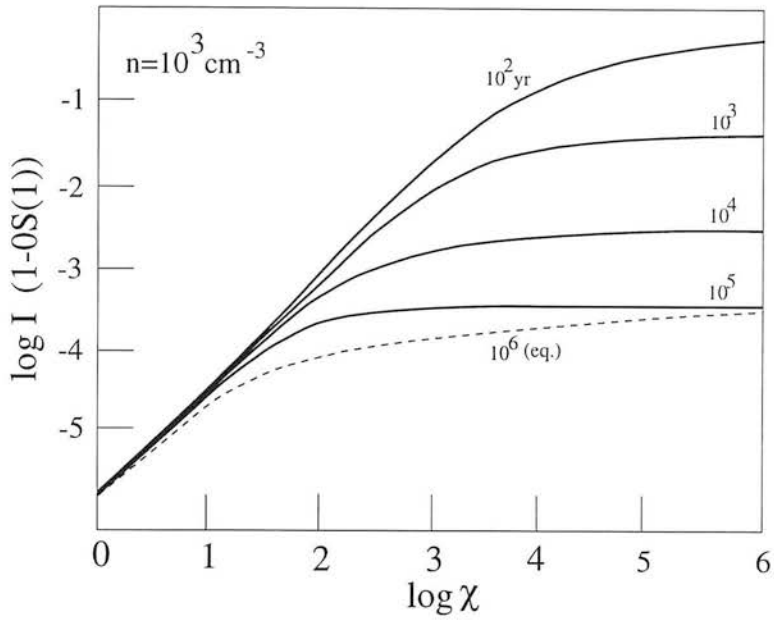

Figure 3.36: The emitted intensity in the 1-0 S(1) line of H_2, in units of ergs cm^{-2} s^{-1} sr^{-1}, as a function of the far-UV intensity, χ, at various times. The model is for a cloud of density 10^3 cm^{-3}. The figure is adapted from Goldschmidt & Sternberg (1995).

later times there is a much smaller equilibrium quantity of H_2 that produces IR emission. Thus, the total IR emission from the cloud drops as a dissociation front travels into the cloud.

Besides the UV photon flux, gas density and age, there are several other factors which can affect the strength of the molecular hydrogen emission from a PDR. An enhanced H_2 formation rate may increase the UV-to-IR efficiency by up to a factor of 2.5 for high UV intensities and low-gas densities (χ/n > 0.1 cm^{-3}). This rate depends in an uncertain way on grain properties such as temperature and chemical composition. Raising the gas temperature can also increase the H_2 formation rate and alters the lower level populations through collisions. The gas-to-dust ratio affects the excitation efficiency since dust competes with H_2 for UV photons.

There are several possibilities for the radial rise of the H_2 emission efficiency in NGC 253. As discussed above, this rise could be due to a change in the χ/n ratio. A scenario in which the PDRs at the edge of the starburst are freshly exposed to UV would be exciting in that we would be seeing time dependent effects in NGC 253 and as such, seeing an animated evolution of the starburst, albeit in physics space. Metallicity and variations in the H_2 formation rate could also explain the observed increase in efficiency. Below I concentrate on the first possibility, a change in the χ/n ratio, and discuss the implications of the ratio regarding the geometry of O and B stars and PDRs in NGC 253.

3.6.2 The ratio of UV flux / gas density decreases radially in NGC 253

The UV energy density scales with Brγ

The fact that the Brγ flux falls so dramatically with radius suggests that the UV energy density would fall at the same rate. If the initial mass function (IMF) of the forming stars is constant across the starburst, then the UV energy density will scale directly with the Brγ photon density. Spaans *et al.* (1994) explored how the colour of the radiation field affected a PDRs structure. Spaans *et al.* (1994) argued that the abundance of UV pumped excited H_2 is sensitive to the UV flux and could decrease by several orders of magnitude in a cooler radiation field. Thus, if the

IMF changed with radius in NGC 253, so that fewer of the most massive stars were generated towards the edge of the starburst, this would increase the Brγ/UV energy density ratio. If the geometry of the massive stars and PDRs were constant, the changing IMF would actually reduce the efficiency with which the UV field is turned into IR emission from H_2. In this case the 1-0 S(1)/Brγ ratio would not show such a pronounced upturn towards the edge of the starburst, as is observed. Contrarily, a radial variation in IMF in NGC 253 which generates a halo around the starburst rich in massive stars will have a hotter radiation field. This is not ruled out but such a model has to explain why the rate of star formation in NGC 253 drops with radius, so as to explain the reduced Brγ flux, but the ratio of massive stars to all stars produced actually increases with radius.

The radial falloff in Brγ strength in NGC 253 could also indicate that the starburst halo has a stellar population that is ageing - the O stars in this ageing population are starting to be removed from the population. The cooler B stars could still be producing copious amounts of UV radiation with energies below 13.6 eV. Such a population could still generate intense H_2 emission from the PDRs around B stars but would produce little or no Brγ from HII regions. If this was the case then it would suggest that the starburst in NGC 253 has evolved inwards into the nucleus of NGC 253. It is likely however, that a scenario of a young nuclear starburst surrounded by an ageing starburst, is unlikely to explain all the observations towards NGC 253. Telesco *et al.* (1993) suggests that the warm dust associated with the active star formation is centrally concentrated. The observations of Telesco *et al.* (1993) indicate that there is little warm dust generated by the hypothetical ageing population, even in the PDRs which would presumably be close to the UV-producing B stars.[24] Furthermore, images of the radio emission in NGC 253 by Ulvestad & Antonucci (1991) show a central concentration of supernovae remnants (SNRs). There is little or no evidence from the radio images of a significant population of SNR at the edge of the starburst.

It is likely, therefore, that across the region observed in NGC 253 the number density of UV photons with energy between 6 and 13.6 eV should scale almost linearly with the number density of ionising photons with energies above 13.6 eV. As discussed in PHM, the UV flux impinging upon PDRs is then dependent on the geometry between the young stars and the molecular gas.

The variation of PDR density across the starburst

Wall *et al.* (1991) suggest that there are two components to the CO-emitting gas in NGC 253: a hot dense core which dominates the emission towards the nucleus, and a bar of colder and more tenuous gas which dominates the emission away from the nucleus. Nguyen-Q-Rieu *et al.* (1989) observed that gas traced by HCN and HCO^+ is more centrally concentrated than the more diffuse gas traced by CO. Of course, it may be that the millimetre-wave observations are tracing the bulk of the molecular gas and may not be sampling the conditions within PDRs. But to first order, the molecular gas has a dense central concentration and shows a gradual falloff in density outside the core.

The radial variation of the χ/n ratio in NGC 253

In the preceding discussion it has been argued that both the UV energy density and gas density show a radial falloff in NGC 253. The falloff in Brγ appears steeper than the falloff in density.

[24] Telesco *et al.* (1993) argue that there is evidence for an extended halo of small grains that are heated by UV but they conclude that the bulk of the far-IR luminosity from NGC 253 is produced in a small compact region.

PHM explored how various geometries of the molecular gas and O and B stars would change the ratio of UV flux, χ, impinging upon PDRs.[25]

PHM explored 3 scenarios for the different geometries between the HII regions and PDRs. The geometry is crucial in determining the emitted 1-0 S(1)/Brγ ratio. When this ratio is less than 0.4, as observed towards the nucleus of NGC 253, then the PDR models of B&vD indicate that $\chi/n > 1$, that is, when the UV field is intense or the gas density low. As discussed above, the gas density is likely to be greater than 10^4 cm^{-3} in the nucleus, *i.e.* not low, and thus it is probable that the 1-0 S(1)/Brγ ratio is low because the UV intensity is high in the nuclear region. PHM suggested that such a high UV intensity could be readily generated by a large cluster of O and B stars, Figure 3.37. If we assume that the nuclear cluster of O and B stars resides within a communal HII region and the molecular gas envelops the Strömgren sphere of the HII region, then PHM describe how to estimate the UV intensity, χ, impinging upon the PDRs.

The radius of the Strömgren sphere is,[26]

$$R_s = \left(\frac{3 S_{Lyc}}{4\pi n^2 \beta_2(T_e)} \right)^{1/3} \tag{3.12}$$

where n is the gas density within the HII region, S_{Lyc} is the number of Lyman continuum photons emitted by the central star(s) and $\beta_2(T_e)$ is the total recombination coefficient at an electron temperature, T_e. Dyson & Williams (1980) suggest that a good approximation for $\beta_2(T_e)$ is

$$\beta_2(T_e) = 2 \times 10^{-16} T_e^{-3/4} \; m^3 s^{-1} \tag{3.13}$$

The incident UV intensity at the edge of the Strömgren sphere, χ, is

$$\chi = \frac{S_{uv}}{4\pi R_s^2} \tag{3.14}$$

where S_{uv} is the number of UV photons emitted by the central star(s). Towards the nucleus of NGC 253, Carral *et al.* (1994) estimated that the electron density in the ionised gas is 430 cm^{-3} and the electron temperature is 8000 K. Using these values, the UV flux, normalised to the local value, is

$$\chi = 5.8 \times 10^{-14} \left(\frac{N_{NUV}}{s^{-1}} \right) \left(\frac{N_{Lyc}}{s^{-1}} \right)^{-2/3} R^{-2} \tag{3.15}$$

where N_{Lyc} and N_{NUV} are the ionising and non-ionising photon fluxes and R is a dimensionless cloud-radiation source separation in units of the Strömgren radius. The ionising photons produce ionisations/recombinations throughout the volume of the HII region whereas PDR emission arises from the surface of the volume. PHM noted that if the O and B stars are tightly grouped near the centre of the HII region then the relative ionising and nonionising UV photon fluxes can be characterised by an effective temperature (T_{eff}) set by the stellar mass function.

The intensity of the UV radiation is then

[25] It should be noted that χ is the 91.2-110.8 nm photon flux per unit surface area relative to the mean starlight background in the solar neighbourhood: 2.0×10^{11} photon s^{-1} m^{-2}, from Draine (1978). The χ quoted above is from the Draine (1978) radiation field, not from the misquoted value by Roberge, Dalgarno & Flannery (1981) —see B&vD for further details. Various geometries result in different scalings between the UV energy density and χ impinging upon PDRs.

[26] see Dyson & Williams (1980) for the full derivation.

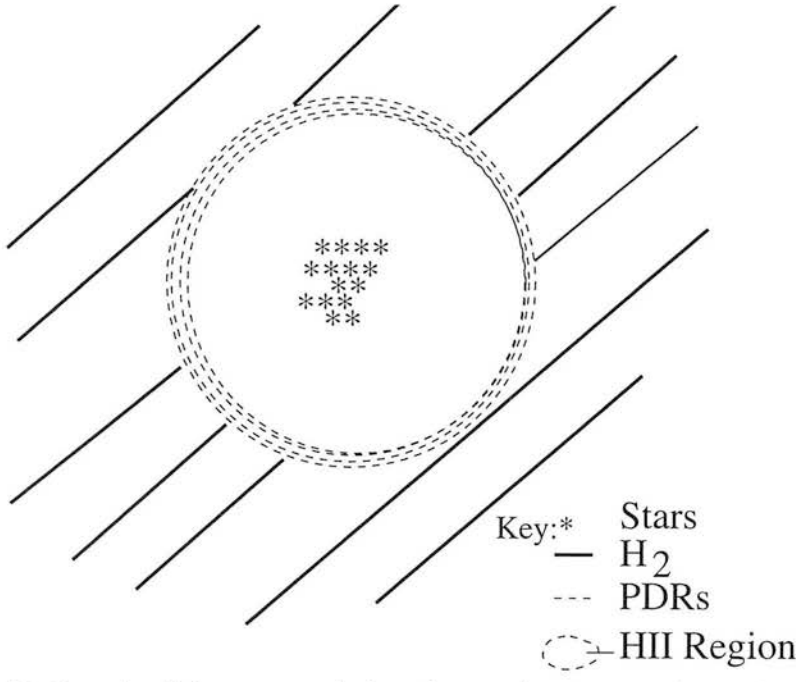

Figure 3.37: One plausible geometry is that the massive stars are clustered within one, or more, giant HII region(s).

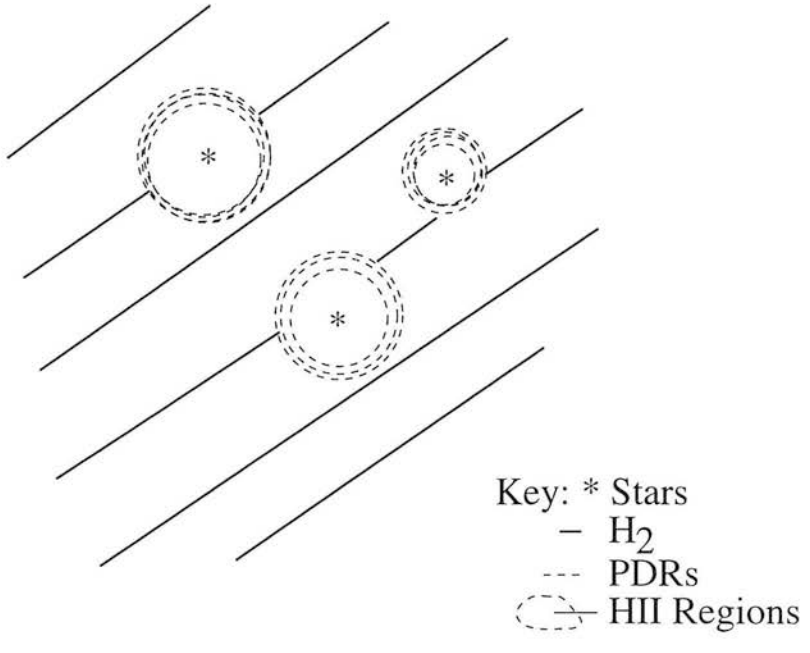

Figure 3.38: Another plausible geometry is that the massive stars are within their own individual HII regions.

$$\chi = 5.8 \times 10^{-14} \Theta(T_{eff}) \left(\frac{N_{Lyc}}{s^{-1}} \right)^{1/3} R^{-2} \tag{3.16}$$

where $\Theta(T_{eff})$ is the ratio of nonionising to ionising photon fluxes. PHM have tabulated $\Theta(T_{eff})$ for various IMFs and the corresponding effective temperatures. From the central few pixels we measure the average flux of Brγ to be $\sim 1 \times 10^{-16}$ W m^{-2}, with the main uncertainties resulting from how much the observed flux is reduced by extinction. Hummer & Storey (1987) have tabulated the recombination coefficients of atomic hydrogen for a range of densities and temperatures. Using the results of Hummer & Storey (1987) for electron densities of 10^{2-3} cm^{-3} and $T_e = 7500$ K, every 64 Lyman continuum photons result in 1 Brγ photon. Hence, the number of Lyman continuum photons generated in the nuclear region of NGC 253, N_{Lyc}, is $\sim 1 \times 10^{52}$ s^{-1}. Carrall *et al.* (1994) suggest that the effective temperature in NGC 253 is about 35,000 K. PHM calculate Θ(35,000 K) to be about two and thus we find that the average UV flux impinging upon the PDRs surrounding the cluster is

$$\chi \approx 2.2 \times 10^4 R^{-2} \tag{3.17}$$

PHM also considered the scenario in which individual stars are surrounded by their own Strömgren spheres, Figure 3.38. Each star has its own associated PDR and because each star produces a much smaller number of Lyman continuum photons than a cluster the intensity of radiation at the Strömgren sphere is less.

PHM tabulated the N_{NUV} and N_{Lyc} photon fluxes for different stars. For a star with an effective temperature of 35,000 K the number of Lyman continuum photons per second is $10^{48.34}$ and the number of UV photons per second in the range 91.2-110.8 nm is $10^{48.60}$. Thus, the intensity expected at the edge of each individual Strömgren sphere is

$$\chi \approx 1400 R^{-2} \tag{3.18}$$

With all the uncertainties with extinction corrections, the IMF and the exact geometry it is clear that χ is greater than 10^3 times the value of the Draine (1978) radiation field in the starburst nucleus of NGC 253. As is discussed in chapters 4 and 5, it is probable that most of the PDR emission from the starburst arises from gas at a density of 10^4 cm^{-3} or greater. With this constraint, the calculations of PHM suggest that to explain the fact that the measured ratio of 1-0 S(1)/Brγ is low, around 0.3 on the nucleus, the geometry of OB stars to PDRs is that of giant O and B clusters surrounded by large PDRs, Figure 3.37, rather than that of individual O and B stars surrounded by their own individual PDRs, Figure 3.38. Therefore, it is likely that χ is at least 10^4 within the active part of the starburst.

3.7 The clustering of star formation in the circum-nuclear region of NGC 253

The typical UV field in the starburst of NGC 253 is greater than 10^4 times the local value. The high observed ratio of Brγ/1-0S(1) in the circum-nuclear region of NGC 253 suggests that the O and B stars have to be clustered, so as to produce a large HII region enveloping many individual O and B stars. There is also other observational evidence for giant O and B clusters in the nucleus of NGC 253.

Paglione *et al.* (1995) discussed the spatial coincidence between several of the HCN 1-0 peaks and unresolved radio continuum sources. Many of the conspicuous radio sources have spectral

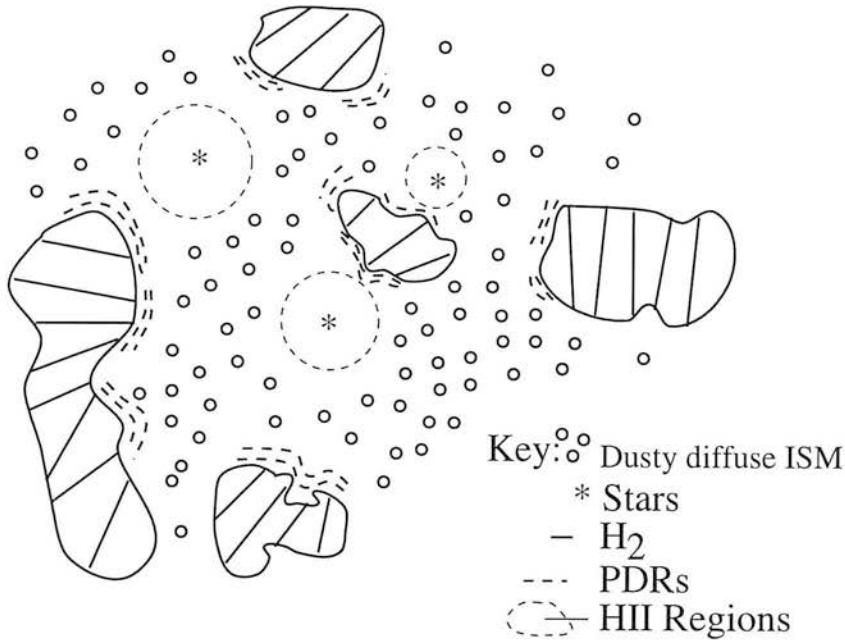

Figure 3.39: One plausible geometry is that the UV radiation field impinging upon PDRs is relatively diffuse.

indices typical of optically thin synchrotron emission from supernova remnants (Ulvestad & Antonucci 1991). However, from their flat spectra between 3.6 and 6 cm, roughly half of these radio sources may be thermal or have a significant thermal component. Although a nonthermal radio continuum source can have a flat spectral index due to gradients in density and magnetic field strength (Marscher 1977), or free-free absorption, the simplest interpretation is that the flat spectrum sources are thermal HII regions (Paglione *et al.* 1995). If these radio continuum sources are indeed HII regions, they must contain lots of O and B stars. Based on its 3.6 cm flux density (Ulvestad & Antonucci 1991), the radio continuum peak at the nucleus is nearly 100 times more luminous than W49, the most luminous HII region complex in the Milky Way (Bania *et al.* 1987). Since W49 contains $\sim$ 10 O and B stars, a simple scaling from the 3 cm radio flux suggests that the HII regions in NGC 253 contain $\sim$ 1000 O and B stars in a volume $\leq$ 6 pc across, far in excess of even 30 Doradus and M82 A (Paglione *et al.* 1995).[27] The other possible thermal sources along the central bar in NGC 253 are up to 10 times less luminous than the nuclear radio continuum peak but are still many times brighter than W49.

High-resolution images in the near-IR (Sams *et al.* 1994) and the mid-IR (Piña *et al.* 1992 and Keto *et al.* 1993) have revealed a bright IR peak that is evident across the entire 1.5-20 μm wavelength region. Careful pointing measurements have revealed that the location of the IR peak is not coincident with the radio nucleus but is located $\sim$ 2-3″ SW of the bright radio source. The far-IR luminosity of the IR peak was estimated by Piña *et al.* (1992) to be $\sim 4\times10^9$ $L_\odot$ from a region with a FWHM of 2.1″ (25 pc) at 19.5 μm.

Recently, Watson *et al.* (1996) observed the nucleus of NGC 253 with the Hubble Space

[27] As I discussed in Chapter 2, the brightness temperature of the radio nucleus is about 90,000 K (Turner & Ho 1985) and so the radio nucleus is unlikely to be entirely thermal in origin. Jim Jackson & Jim Ulvestad (private communications) claim that, after subtraction of a synchrotron component, the thermal component of the nuclear source is consistent with a very luminous HII region. The other flat radio sources are also consistent with the picture that they contain luminous HII regions.

Telescope (HST). Watson *et al.* (1996) reported four young, luminous compact stellar clusters in the starburst. The brightest cluster is located at the IR peak, within pointing errors. Watson *et al.* (1996) claim to have spatially resolved the size of the cluster, which has a half-light radius of about 2.5-3 pc, if it has a radial profile similar to a Galactic globular cluster. Watson *et al.* (1996) derived a luminosity of 1.3×10^9 $L_\odot$ for the main cluster, a factor of 3 smaller than Piña *et al.* (1992). The difference of 3 was accounted for by Watson *et al.* (1996) postulating that there are additional sources of background in the coarser beam of Piña *et al.* (1992).

Sams *et al.* (1994) claimed that many of the peaks in the IR images, including the ones which coincide with the HST clusters, except the brightest one, were actually holes in extinction through which the smooth underlying disk of NGC 253 was viewed. The clusters of Watson *et al.* (1996), judging from the analysis of the near-IR colours by Sams *et al.* (1994), are in regions of particularly low extinction. Puxley (1991) discussed various estimates of extinction, including near-IR colours, and noted that the J H K colours of a burst population are significantly bluer than those of the old stars, principally because of the significant contribution of hot young stars to the near-IR continuum. Consequently, the assumption of Sams *et al.* (1994), that the average colours of a typical Sc galaxy (Frogel 1988) can be used to estimate extinction, is incorrect. The near-IR colours of the clusters of young stars detected by Watson *et al.* (1996) may be bluer than an Sc galaxy and so the extinction to these clusters cannot be estimated from a colour-colour diagram. Therefore, the assertion by Sams *et al.* (1994) that the underlying near-IR light in NGC 253 is smooth, and we are looking at this light through patchy extinction, may not be true. In fact, much of the near-IR light could be generated in relatively small compact star clusters which have bluer colours than those of a Sc galaxy. As discussed by Puxley (1991), estimates of extinction from the ratios of hydrogen recombination lines may shed light on the underlying light distribution in NGC 253.

Summarising, observations made in the radio show a population of luminous flat radio sources across the nucleus of NGC 253. If these are HII regions, then their brightness indicates that they each one must contain many hundreds, possibly thousands, of O and B stars. Images of NGC 253 in the IR show one particular strong emitter that is located at, within pointing errors, a flat spectrum source. This particular source appears to have a bolometric luminosity of $\sim 2\times10^9$ $L_\odot$, generated by a cluster of stars with a half-light radius of ≤ 3 pc. HST images also show several other young clusters in the starburst, which are less luminous than the main cluster. The HST clusters spatially coincide with several of the near-IR peaks (Sams *et al.* 1994) although it appears that some of the clusters may be spatially offset from the flat radio sources. It is possible that source confusion in the radio images and pointing offsets in the optical and IR images may partially account for the apparent difference in positions between the radio and optical counterparts. With the discovery that much of the power of the starburst in NGC 253 is generated in compact clusters, each containing many O and B stars, this leads to several questions and lines of research that may shed insight into the physics of many, if not all, starbursts. In particular: why and how do the clusters form?; what controls their size and luminosity?; how will they evolve?; have they formed at a special location in the starburst? This final question may be answered, along with possible clues to the answers of the other questions, from detailed studies of the kinematics of the starburst in NGC 253.

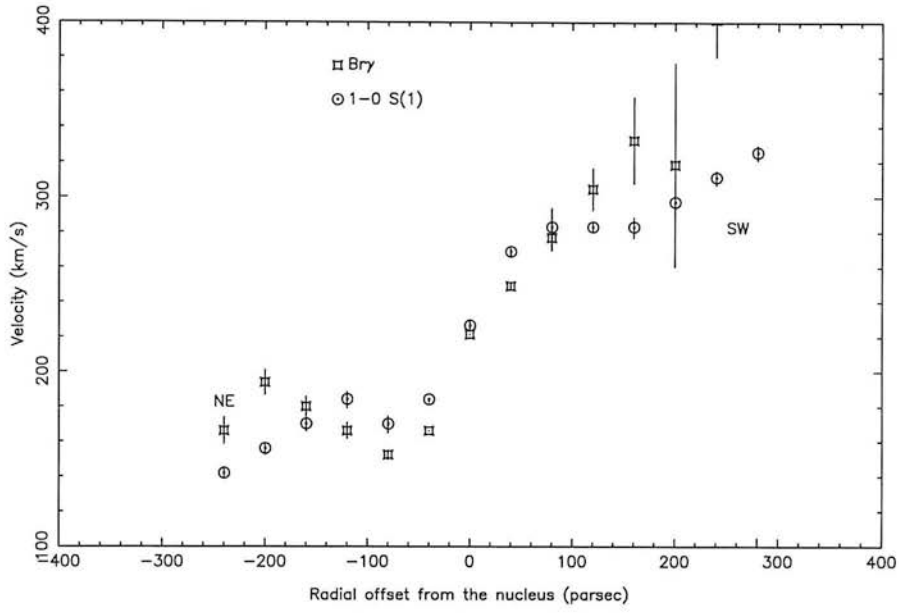

Figure 3.40: The velocity of 1-0 S(1) and Brγ across the starburst. The plot is consistent with a similar plot shown in Prada *et al.* (1996).

3.8 The kinematics of the ionised and molecular gas in NGC 253

Figure 3.40 shows the position velocity diagram of ionised gas, traced by Brγ, compared with the PDR gas, traced by 1-0 S(1). As can be seen there is a dramatic difference between the two tracers indicating that as we travel away from the nucleus the HII regions and PDRs are not coexistent in velocity space. The difference in kinematics between the Brγ and 1-0 S(1) is consistent with the work of Prada *et al.* (1996). Thus, within 3″ pixels, the bulk of the PDRs generating H_2 emission are not coexistent with the bulk of the HII regions generating Brγ emission. Moreover, Figure 3.34 highlights that the ratio of 1-0 S(1)/Brγ emission shows an increase in the regions that show such a discrepancy in velocities between H_2 and Brγ.

The ratio of 1-0 S(1)/Brγ shows a rise with radius and shows values approaching 10 towards the edge of the region observed. PHM argued that the most likely geometries of regions exhibiting 1-0 S(1)/Brγ ratios of these values are PDRs that are bathed in a relatively diffuse field, Figure 3.39. In the case of diffuse ultraviolet radiation, the UV-to-IR conversion efficiency tends to a maximum value. The efficiency becomes independent of the gas density provided that $\chi/n \ll 0.1$ cm^{-3}

As was mentioned before, the rotation curve of H_2 and Brγ indicate that the molecular gas and HII regions are two separate kinematic identities. The separation between the young stars and nearby molecular gas will dilute the radiation field impinging upon PDRs and, at least in NGC 253, the dilute radiation field enhances the observed 1-0 S(1)/Brγ ratio towards the edge of the starburst region. Unfortunately, NGC 253 was only observed along a single strip along the major axis and so it is hazardous to model the kinematics and explain why the HII regions and PDRs are not coextensive towards the edge of the starburst. It would be enlightening to map the kinematics of Brγ and 1-0 S(1) across the entire starburst and to see how the difference in kinematics between the ionised gas and PDR gas correlate with the 1-0 S(1)/Brγ ratio.

PHM note that there is a tendency for the 1-0 S(1)/Brγ ratio in starbursts to rise with the observed beam-size. Furthermore, in nearby starbursts such as M82 and NGC 4945, the 1-0 S(1)/Brγ ratio shows a rise towards the edge of the regions observed. If variations in the kinematics of the molecular gas and ionised gas are responsible for the variations in the 1-0 S(1)/Brγ ratio in NGC 253, then it may be that kinematics may help to explain the observed ratio in other galaxies as well. Such possibilities await further observations before they can be explored.

3.9 Conclusions

In this chapter I have presented measurements of several near-IR emission lines from NGC 253. In particular, I have been able to measure 4 H_2 lines across the starburst which has allowed an estimate of the ortho to para ratio of H_2. The ratio is observed to be close to 2, and not 3, which indicates that the bulk of the H_2 emission arises in PDRs rather than shocks. This is the case across the entire starburst.

As the H_2 emission arises from PDRs, it is likely that the ratio of Brγ to 1-0 S(1) is a measure of the geometry of O and B stars to PDRs, as originally suggested by PHM. Towards the nucleus of NGC 253 the geometry is tightly clustered O and B stars in a few giant HII regions which are encompassed by PDRs. Away from the nuclear region, the geometry becomes that of PDRs bathed in a relatively diffuse UV radiation field. The UV flux impinging upon the nuclear PDRs is high, $> 10^4$ times the local value.

The rotation curves of H_2 and Brγ suggest that the ionised gas is tracing a different kinematic system to that of the molecular gas, particularly away from the nucleus where it is likely that the PDRs are bathed in a relatively low UV field. Further observations should be able to confirm whether the disparity between the kinematics of PDRs and HII regions in NGC 253 is real.

3.10 Acknowledgements

I would like to thank Peter Brand, Henry Buckley, Mike McCartney, Steve McNally, Phil Puxley, Suzie Ramsay, Milagros Ruiz, Adrian Russell, Ewine van Dishoeck and Karen Willacy for their helpful and patient discussions.

Chapter 4

Carbon monoxide in NGC 253

4.1 Carbon monoxide as a tracer of molecular gas

The study of the spatial distribution, mass, physical condition and kinematics of molecular gas is vital, as it is the raw material for star formation, and the dominant component of the interstellar medium (ISM) in the star-forming regions of a galaxy. Molecular hydrogen naturally makes up the bulk of the molecular ISM but as the lowest quadrupole transition of H_2 occurs 510 K above the ground level it means that H_2 is unsuitable as a tracer of relatively cool (T $<$ 100 K) gas which makes up the bulk of the molecular component in a galaxy, even in galaxies with large scale energy inputs. This means that it is important to find tracers which are intimately mixed with the H_2. The most widely used tracer for both Galactic and extra-galactic observations of the physical conditions of the molecular gas is carbon monoxide (CO). An energy level diagram of CO is displayed in Figure 4.1. CO has been used to trace H_2 for a number of reasons:

- CO is the next most abundant molecule after H_2, being $\sim 10^4$ times less abundant
- the first vibrationally excited state of CO is too high above ground, Figure 4.1, to be strongly populated in the molecular phase of the ISM and therefore CO excited in the ISM emits almost exclusively a pure rotational spectrum which is straightforward to describe
- the rotational ladder of CO has transitions in the millimetre and sub-millimetre region, all but one of the seven lowest transitions being in atmospheric windows observable from the ground
- the transitions correspond to temperatures easily attained in molecular clouds ($h\nu/k$ = 11.1 K for the J=2-1 line) and are excited, by collisions with hydrogen molecules, at densities $n(H_2) \sim$ 100-300 cm^{-3}, again typical of the densities derived for molecular clouds
- due to the high abundance of CO and the low number of energy levels populated, the absolute population of the individual levels is high, making the emitted or absorbed line relatively strong and readily detectable from numerous existing telescopes.

Appendix B lays out the theory for why measurements of the intensity / brightness temperature of several rotational lines of CO can be used to constrain the column density, number density and temperature of the molecular gas.

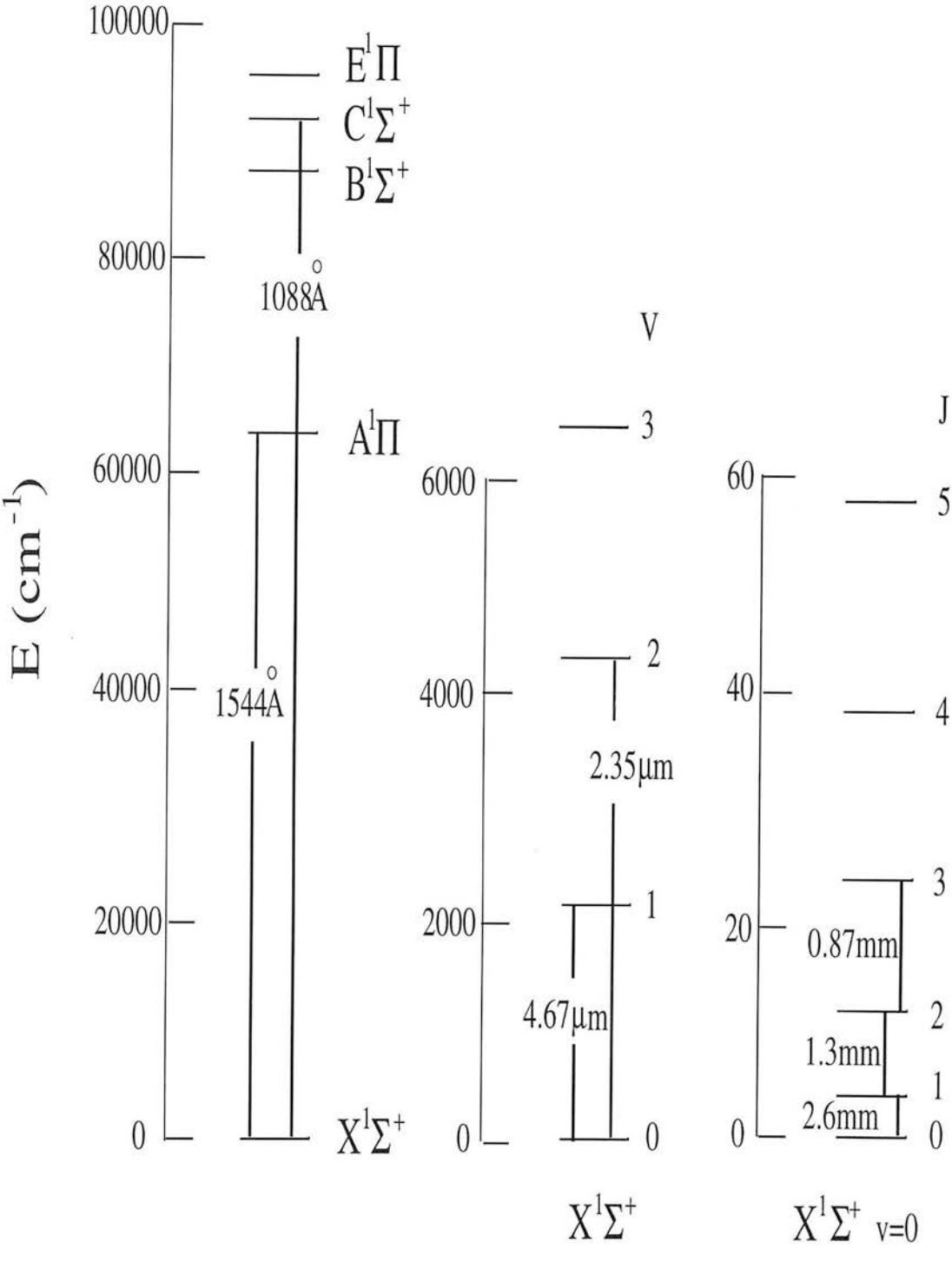

Figure 4.1: The electronic, vibrational and rotational energy levels of the CO molecule. Note the difference in energy scale; in order to convert the energy scale into K, multiply by 1.438768. The figure is adapted from Jansen (1995).

4.2 The case for observing $C^{18}O$ in NGC 253

In this section I review how the theory, outlined in Appendix B, has been applied to estimate the physical conditions of the molecular gas in NGC 253. As is discussed, there are still uncertainties in the nature of these conditions, and in particular the column density of CO. These uncertainties led to observations being undertaken in order to constrain the amount of carbon monoxide in NGC 253.

4.2.1 Previous observations of CO in NGC 253

Canzian *et al.* (1988) imaged the ^{12}CO J=1→0 emission[1] from a "molecular bar" with an interferometer beam of $5'' \times 9''$. The bar is illustrated in Figure 2.13. Canzian *et al.* (1988) claim that the molecular gas appears to be rotating as a solid bar but with a small radial inflow of gas, ~ 8 km s^{-1}, into the nucleus. Canzian *et al.* (1988) estimated the molecular gas mass to be 4.8×10^8 M$_\odot$ by assuming a linear conversion from the integrated CO temperature to the H_2 column density of

$$N_{H_2} = \alpha \int T_{MB}\, dV \tag{4.1}$$

where $\alpha = 3.6 \times 10^{20}$ H_2 cm^{-2} (K km s^{-1})$^{-1}$ has been derived from a sample of giant molecular clouds (GMCs) in the Galaxy (Scoville *et al.* 1987). Canzian *et al.* (1988) noted that as the dynamical mass in the central $39''$ of NGC 253 is 1.3×10^9 M$_\odot$, which they estimated from the slope of their rotation curve, the gas to dynamical mass ratio is 0.4.

Wall *et al.* (1991) observed ^{12}CO and ^{13}CO in the 3→2 and 2→1 transitions, and ^{12}CO 1→0, towards NGC 253. Wall *et al.* (1991) argued that there are two components to the CO emitting gas in NGC 253: a hot dense core of size $< 15''$, which dominates the emission towards the nucleus, and emission from gas in the bar which is colder and more tenuous. Towards the central $\sim 22''$ of NGC 253, Wall *et al.* (1991) observed the the ^{13}CO 3→2/2→1 ratio to be between 2.0 and 2.8. Given the uncertainties in the calibration of the observations[2] this ratio is close enough to the limiting value of 2.25 to indicate that most, if not all, of the ^{13}CO emitting gas is hot (T ~ O(100 K)), optically thin and thermalised ($n > 3\times10^4$ cm^{-3}, the critical density of the J = 3 state). The ^{12}CO lines also show evidence for warm molecular gas in the nucleus. The central $30''$-$40''$ has ^{12}CO 3→2 / 2→1 and 2→1 / 1→0 temperature ratios greater than unity.[3] This implies that warm (T > 20 K), not too optically thick gas dominates the emission in these lines. Furthermore, the brightness of the ^{12}CO lines, $T_{MB} = 6.2$ K, with the assumption of a beam filling factor of O(10%), implies that the temperature of the emitting gas is > 50 K. Wall *et al.* (1991) inferred that the temperature dropped away from the nucleus because of the small ^{13}CO 3→2 source size compared to the size of the emission region for lines of high dipole moment molecules such as CS 2→1.[4] Wall *et al.* (1991) also inferred that the density dropped with distance away from the nucleus because of the drop in the ^{12}CO 3→2 / 2→1 ratio. On the nucleus this ratio is ~1 and it declines to ~ 0.5 at positions $30''$ to the northeast and southwest. If the gas was in LTE then this requires that the molecular gas temperature falls to ~ 6 K.

[1] Hereafter, 1→0 signifies a rotational transition from J = 1 to J = 0, 2→1 signifies a transition from J = 2 to J = 1, *etc.*

[2] The data were taken from different telescopes, each with its own calibration uncertainties

[3] See however, Mauersberger *et al.* (1996) and the discussion below.

[4] The ^{13}CO 3→2 line is more temperature sensitive than the lower J lines of the higher dipole molecules because it is 32 K above ground whereas the CS J = 2 state is only 7 K above ground. In going from T = 100 K to T = 10 K the ^{13}CO 3→2 line strength decreases 5-6 times relative to the strength of the HCO^+, HCN and CS lines for a constant density and column density.

As the observed *Planck* brightness temperature is 6 K and it is unlikely that the gas fills the beam with a factor of order unity, it is likely that non-LTE effects are important in the CO emission away from the nucleus. This implies that the density of the CO emitting gas must be less than the critical density of the 3→2 transition [$n(H_2) < 5\times10^4$ cm^{-3}]. Wall *et al.* (1991) also noted that away from the nucleus the ^{13}CO 3→2 / 2→1 ratio is significantly less than the ^{12}CO 3→2 / 2→1 ratio which implies that ^{12}CO may be more fully thermalised than the ^{13}CO.

Harris *et al.* (1991) detected ^{12}CO 6→5 emission from the circum-nuclear region of NGC 253. To excite CO 6-5 requires gas temperatures of 116 K and densities of the order of 10^6 cm^{-3}, the critical density of the J=6 level, and so the detection reported by Harris *et al.* (1991) is direct proof that NGC 253 contains substantial amounts of gas that is both dense and warm. Harris *et al.* (1991) reported detections from 3 locations in NGC 253 and argue that the intensity distribution of the 6→5 line is similar to the CO 1→0 bar reported by Canzian *et al.* (1988), but more extended than the $4'' \times 2''$ FWHM of the 2.2 μm, 10 μm and radio continuum distribution. Harris *et al.* (1991) argue that the extent of bright CO 6→5 emission suggests that the warm molecular gas may be heated by mechanisms other than star formation in NGC 253 and suggested such mechanisms could be turbulence or a high flux of cosmic rays. I feel that it is a little premature to argue from the CO 6→5 observations that the molecular gas may be heated by processes not directly associated with star formation. Firstly, as I discuss in Chapter 3, the near-IR FWHM could be just due to old stars and so it's not clear why one would expect the hot molecular gas to follow the old stellar distribution. Secondly, Telesco *et al.* (1993) argues that the 10 μm FWHM is $7'' \times 4''$, with evidence for hot dust out to a radius of 30″ from the nucleus. Thirdly, the analysis presented by Wall *et al.* (1991) shows that the bulk of the warm and dense gas, that the CO 6→5 traces, is concentrated towards the nucleus of NGC 253 (within the central $\sim 20''$). Finally, as I discuss in Chapter 3, I measure the ortho to para ratio of H_2 to be ~ 2 towards the edge of the bar and this is direct evidence that UV photons from young stars are impinging upon molecular gas outside the main starburst. Moreover, CO 6→5 was only detected in 3 locations along the major axis and so it is not clear what distribution the warm dense molecular gas has.[5]

Sage *et al.* (1991) observed C^{17}O and C^{18}O in the 1→0 and 2→1 transitions towards NGC 253. Figure 4.2 shows the spectrum of C^{18}O 1→0 reported by Sage *et al.* (1991). The 1→0 observations of Sage *et al.* (1991) were made with the National Radio Astronomy Observatory (NRAO) 12m dish (55″ beam) and the 2→1 observations were made with the Institut de Radio Astronomie Millimétrique (IRAM) 30m dish (13″ beam). Sage *et al.* (1991) derive the ^{18}O/^{17}O ratio to be 10±3 (cf. the solar system ratio of 5.5). Sage *et al.* (1991) explained this high ^{18}O/^{17}O ratio in terms of nucleo-synthesis enhancement within the starburst. High mass stars produce a high ratio of ^{18}O/^{17}O and so a starburst that has an initial mass function biased towards the formation of high mass stars, Sage *et al.* (1991) claimed, steadily increases ^{18}O/^{17}O with time. The proposal of Sage *et al.* (1991), of differential isotopic enhancement in starburst nuclei, has been modelled in more detail by Henkel & Mauersberger (1993) and is discussed below.

Wall *et al.* (1993) reviewed the observations of NGC 253 reported by Wall *et al.* (1991) and also reported observations of ^{13}CO and C^{18}O 1→0 made with the NRAO 12m. Figure 4.3 shows the spectrum of C^{18}O 1→0 reported by Wall *et al.* (1993). Wall *et al.* (1993) claimed that, because they measured the temperature ratio ^{13}CO 1→0 / C^{18}O 1→0 to be 3.1±0.9, ^{13}CO 1→0 is optically thick in NGC 253. This interpretation by Wall *et al.* (1993) may not be so clear cut as inspection of Figures 4.2 and 4.3 reveals that observations of C^{18}O 1→0 are prone to

[5] At 690 GHz, sub-millimetre telescopes, such as the JCMT, have considerable error beams.

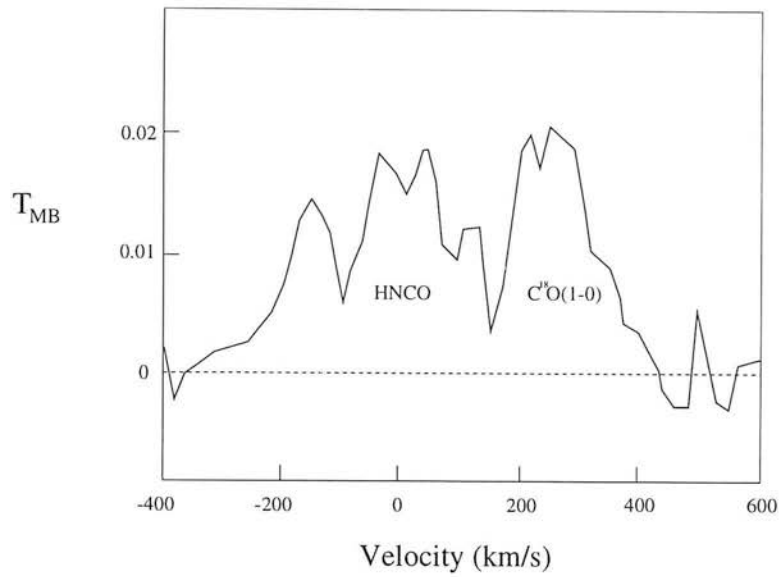

Figure 4.2: The nuclear spectrum of $C^{18}O$ obtained using the NRAO 12m, adapted from Sage *et al.* (1991).

uncertainties associated with subtracting baselines and spectral features (particularly HNCO).

Mauersberger *et al.* (1996) made an oversampled map in the ^{12}CO 2→1 line with the IRAM telescope. Mauersberger *et al.* (1996) argued that their data and the map of Canzian *et al.* (1988) can be reconciled with several geometries including a molecular bar, a molecular ring, a compact spiral or two unrelated GMCs. This latter case is analogous to the molecular clouds near the center of the Milky Way. Mauersberger *et al.* (1996) compared their observations of the 2→1 line with those of the 1→0 line made at several resolutions which shows that the 2→1 line is slightly weaker than the 1→0 line[6] and is consistent with optically thick emission. Mauersberger *et al.* (1996) suggested that their observations of the 2→1 line could be used to derive the molecular hydrogen column density. Braine *et al.* (1993) found that towards spirals the 2→1 line is, on average, a factor of 0.9 the strength of the 1→0 line. The data of Mauersberger *et al.* (1996) indicates that this appears to hold for NGC 253, at least on scales of 23″-55″. Using a CO-H_2 conversion factor $\sim$ 1.8 lower than that used by Canzian *et al.* (1988), Mauersberger *et al.* (1996) derived column densities of H_2 through

$$N_{H_2}(cm^{-2}) = 2.1 \times 10^{20} \int T_{MB}\, dv \tag{4.2}$$

Mauersberger *et al.* (1996) claimed that the molecular mass derived for NGC 253 in this way was $6.5 \times 10^8\, M_\odot$ within the central 50″. This value is about a factor of 5 larger than the molecular mass estimates made with observations of dust continuum and isotopic CO, in particular $C^{18}O$. Mauersberger *et al.* (1996) argued that this discrepancy was due to the assumption of a constant conversion factor between CO and H_2 in both the Galactic disk and extra-galactic circum-nuclear regions and they suggested that the conversion factor needed to be recalibrated in galactic nuclei to take into account the dynamical effects of stars. Mauersberger *et al.* (1996) derived a new conversion factor that took the effects of stellar dynamics into account and ar-

[6]This is in conflict with the data of Wall *et al.* (1991) who argue that, averaged over $\sim$ 40″, the ^{12}CO 2→1/1→0 temperature ratio is > 1. Given that the observations of Wall *et al.* (1991) were made with different telescopes whereas Mauersberger *et al.* (1996) derived their ratio from data with a single telescope (IRAM 30m) it is probably safer to trust the ratio of Mauersberger *et al.* (1996), but I note that there is currently a disrepancy in published estimates of the 2→1/1→0 temperature ratio towards the nucleus of NGC 253.

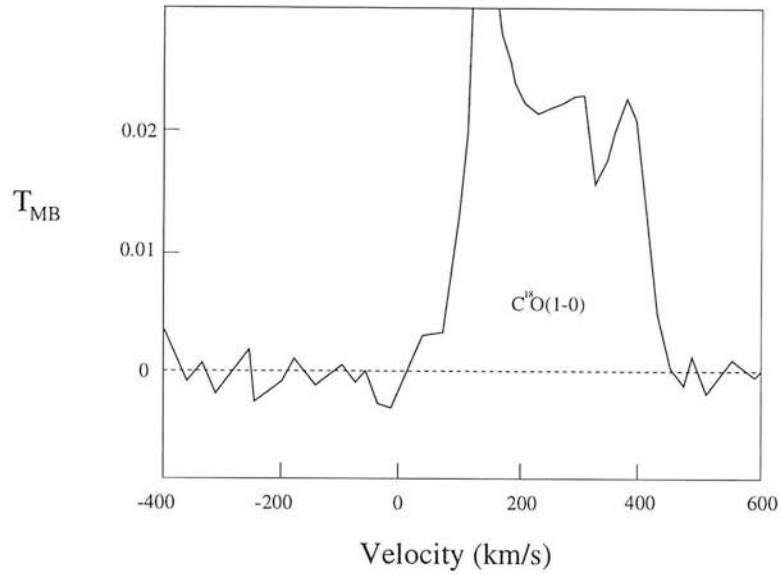

Figure 4.3: The nuclear spectrum of $C^{18}O$ obtained using the NRAO 12m, adapted from Wall *et al.* (1993). Wall *et al.* claimed that the spectrum had had a parabolic baseline removed, which increased the integrated temperature by 60%. Comparison with the spectrum reported by Sage *et al.* (1991) indicates that the parabolic baseline was probably confused with HNCO emission.

gued that using this new conversion factor resulted in gas mass estimates from the ^{12}CO 2→1 observations that were consistent with the estimates made using $C^{18}O$ and the continuum from dust emission. Mauersberger *et al.* (1996) derived the gas to dynamical mass in NGC 253 to be ~ 0.1, a factor of 4 or so less than the estimate of Canzian *et al.* (1988).

4.2.2 What can be learnt about CO in NGC 253 from multi-transitional observations of $C^{18}O$?

Carbon monoxide emission has been extensively observed by several groups towards NGC 253 and a picture, if somewhat uncompelling, can be made of the observational data to date. There appears to be at least two main sources of emission. There is a hot ($T > 50$ K) core of dense ($n > 10^4$ cm^{-3}) CO emitting gas which is spatially co-incident with the most-active region of star formation in NGC 253 (delineated by hot dust, HII regions and young supernovae remnants). There is also an elongated source of emission of size $\sim 35'' \times \sim 12''$. Due to the high inclination of NGC 253 it is not clear if this elongated emission is highlighting a bar, a spiral or a coincidence of discrete molecular clouds which mimics a large scale pattern. Away from the core, and along the elongated emission, both the density and temperature of the emitting gas fall away with distance. There may be evidence for warm and dense gas away from the core but further observations, preferably a map, are required in the mid-J CO lines before the evidence is compelling for the existence of such gas away from the starburst of NGC 253.

The starburst in NGC 253 may have differentially enhanced isotopes of both carbon and oxygen. This has been revealed by the anomalously high $^{18}O/^{17}O$ ratio observed in comparing both the 2→1 and 1→0 transitions of $C^{18}O$ and $C^{17}O$, although there is some uncertainty in this ratio due to confusion between spectral lines and baseline problems. Henkel & Mauersberger (1993) have discussed what types of stars are responsible for the enrichment of the ISM with the different isotopes of both carbon and oxygen: ^{18}O synthesis occurs in massive stars; ^{17}O is ejected

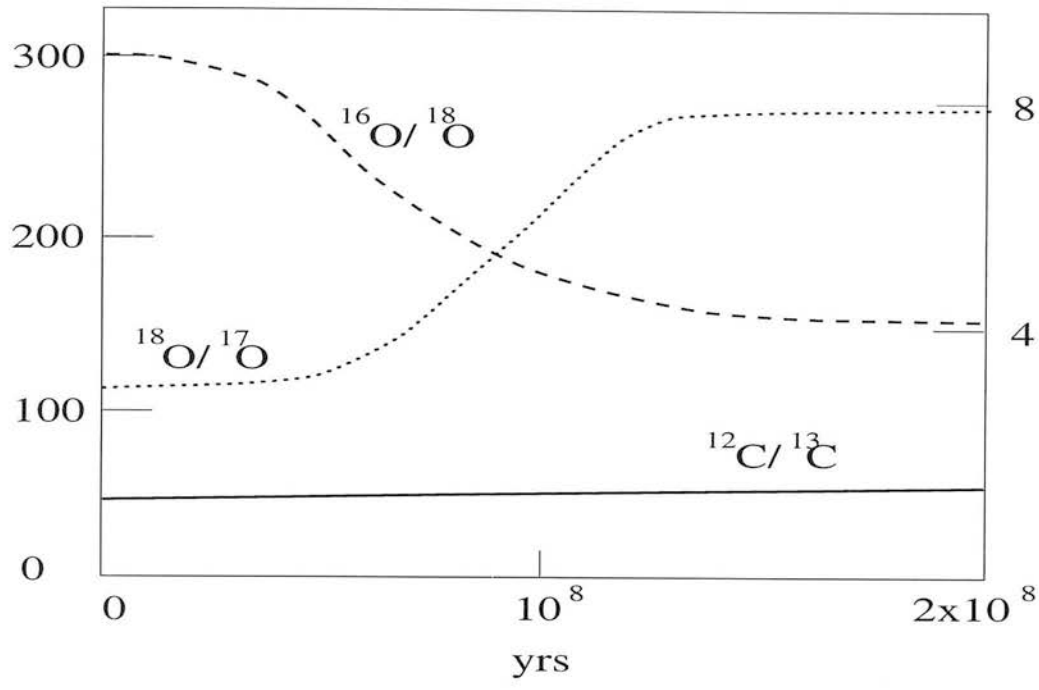

Figure 4.4: The evolution of the isotopes of C and O typically expected in a starburst, as a function of time. The figure is adapted from Henkel & Mauersberger (1993). For $^{12}C/^{13}C$ and $^{16}O/^{18}O$ values see the scale to the left; for $^{18}O/^{17}O$ values use the scale on the right hand side.

by intermediate mass giant stars; ^{16}O is synthesised by high mass stars only; ^{13}C is mainly a product of intermediate mass stars; ^{12}C is produced and ejected by intermediate ($\leq 8\,M_\odot$) and high mass ($> 8\,M_\odot$) stars. In a starburst, with a rapidly evolving stellar population and time-dependent enrichment of the ISM through supernovae and stellar winds the starburst will differently enhance the isotopes of carbon and oxygen. Henkel & Mauersberger (1993) modelled the isotopic evolution in starbursts, Figure 4.4, and concluded that it is to be expected that the $^{18}O/^{16}O$ ratio will be high in starbursts. This conclusion was supported by Henkel *et al.* (1993) who reported that, indeed, the $^{18}O/^{16}O$ ratio does appear to be high in NGC 253 ($\sim 200^{-1}$ cf. with the local value of $\sim 500^{-1}$).

There are several mechanisms, other than isotopic enhancement in starbursts, that can affect the isotopic ratios derived from carbon monoxide. UV photons, generated by the population of high-mass stars results in selective photodissociation of CO on the edges of clouds (see van Dishoeck & Black 1988 and the discussion below). Also, chemical fractionation of CO (van Dishoeck & Black 1988), particularly through the reaction

$$^{13}C^+ + {}^{12}CO \rightarrow {}^{13}CO + {}^{12}C^+ + 36K \tag{4.3}$$

results in the $^{13}CO/^{12}CO$ ratio being enhanced in cold clouds (T < 20 K) where the reverse reaction cannot overcome the activation barrier. Furthermore, infall of relatively unprocessed disk gas into the nucleus of NGC 253 will result in a $^{12}C/^{13}C$ enhancement (Henkel & Mauersberger 1993).

The hot dense core of NGC 253 is coincident with a vigorous star forming region and it is likely that in the core the molecular gas is bathed in a UV field about 10,000 times the local solar neighbourhood value (see Chapters 3 and 5). In such an environment the edges of clouds bathed in UV will have their heating dominated by the impinging UV field and the gas will be

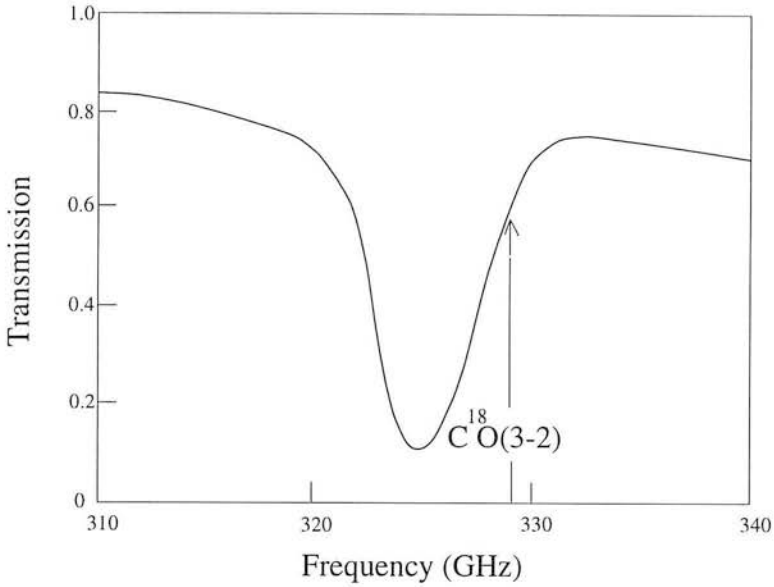

Figure 4.5: The atmospheric transmission expected above Mauna Kea, for a water content of 1.0 mm of precipitable water vapour. The $C^{18}O$ 3-2 frequency is close to a large dip in transmission, due to absorption by water. Thus, observations of $C^{18}O$ 3-2 are only feasible from a dry site like Mauna Kea.

heated, through the photoelectric effect (see Chapter 1), to temperatures of a few hundred K. In such a region it is expected that selective photodissociation is efficient. As $C^{18}O$ is destroyed at lower depths into a cloud than ^{13}CO, selective photodissociation is likely to reveal itself through $C^{18}O$ tracing more colder gas than ^{13}CO. Moreover, in NGC 253, the observed ^{13}CO $3\rightarrow2/2\rightarrow1$ temperature ratio is 2.0, which is close enough to the limiting value of 2.25 to indicate that ^{13}CO must be hot ($T \sim 100$ K), optically thin and thermalised ($n > 3\times10^4$ cm^{-3}).

Therefore, if ^{13}CO and $C^{18}O$ are coextensive in NGC 253, and selective photodissociation is not an efficient process, then we will know that $C^{18}O$ will also be thermalised and optically thin. Thus the observed $3\rightarrow2/2\rightarrow1$ temperature ratio will provide a measure of the temperature of the gas, and hence a check on whether $C^{18}O$ is coextensive with the hot ^{13}CO. If it can be shown that selective photodissociation is not important in changing the isotopic ratios then we can have some confidence that the models of Henkel & Mauersberger (1993) provide a realistic, but partial, description of the chemical evolution of a starburst. So by measuring the $3\rightarrow2/2\rightarrow1$ temperature ratio of $C^{18}O$ in NGC 253 we have a direct test of how efficient selective photodissociation is in NGC 253, and hence if it is likely to result in incorrect conclusions being drawn about CO and its isotopomers in a starburst environment.

The rest frequency of $C^{18}O$ $3\rightarrow2$ is $\sim$ 329 GHz which is within a large absorption trough, caused by water in the atmosphere. Figure 4.5 shows the atmospheric transmission for the relatively dry atmosphere above Mauna Kea. In a wetter atmosphere the trough would saturate, making observations of $C^{18}O$ $3\rightarrow2$ impossible because the atmosphere would be opaque. Thus it is only possible to perform this science at a dry site, such as found at the James Clerk Maxwell Telescope (JCMT) on the summit of Mauna Kea in Hawaii.

4.3 Observations and results

All the observations were made with the 15m JCMT and the data-reduction of the observations was carried out using the package SPECX. The back-end used was the Dutch Auto-correlation Spectrometer (DAS). The adopted map centre (0,0) was the nucleus of NGC 253, which was taken to be $\alpha(1950) = 0^h\ 45^m\ 06.0^s$, δ = -25° 33′ 36″. The observations were made by beam switching to a reference position 150″ north of the source.

A grid of 7 $C^{18}O$ 3→2 spectra was observed towards NGC 253 on 1-4 December 1994, using the receiver Rx B3i and with the DAS operated in 760 MHz bandwidth mode. The telescope efficiency was measured using Uranus and Saturn, as discussed in Appendix B, and assuming a single component 15.3″ diffraction beam. In short, the efficiency was measured by seeing what temperature the JCMT measured for a planet which is a radiating disk of a known size, and hence a known coupling, and a known brightness temperature. The efficiency with which the JCMT measured the planet is given by

$$\eta_{planet} = \eta_{planet\ coupling} \times \eta_{fss} \tag{4.4}$$

where η_{fss} is the main beam efficiency of the JCMT after losses due to forward scattering and spill-over are corrected, $\eta_{planet\ coupling}$ is the coupling of the JCMT dish to the planet and η_{planet} is the measured antenna temperature of the JCMT divided by the true radiation temperature of the planet. η_{fss} can then be used to measure the main-beam efficiency, η_{MB}, through

$$\eta_{MB} = \eta_{NGC\ 253\ coupling} \times \eta_{fss} \tag{4.5}$$

where $\eta_{NGC\ 253\ coupling}$ is the efficiency with which the JCMT beam couples to the emission from NGC 253. η_{fss} was found to be consistent with the values obtained from numerous observations of Jupiter and Mars as part of the JCMT maintenance (Adrian Russell, private communication) and so we take the standard value of η_{fss}=0.59. Saturn was used to check the pointing, which was good to 3″ (rms). Figure 4.6 shows a rotated RA-dec map at P.A. 53^0 of the 7 spectra on a T_A^* scale. We convolved our map of $C^{18}O$ 3→2 to a resolution of 23″. From the central 23″ the integrated temperature is $\int T_{fss} dV$ = 30 K km s^{-1}, where T_{fss} is the brightness temperature that has not been corrected for the coupling to NGC 253.

A single spectrum was taken of $C^{18}O$ 2→1 towards the (0,0) position in NGC 253 on 1994, December 2nd, using the receiver Rx A2 and with the DAS operated in 500 MHz bandwidth mode. The telescope efficiency was measured using Saturn, as discussed above, and assuming a single component 22.9″ diffraction beam. η_{fss} was found to be consistent with the values obtained from numerous observations of Jupiter and Mars as part of the JCMT maintenance (Adrian Russell, private communication) and so the standard value of η_{fss}=0.68 was used. Saturn was used to check the pointing, which was good to 3″ (rms). Figure 4.7 shows the single spectrum we observed of $C^{18}O$ 2→1 (at a resolution of 23″) towards NGC 253. We derive an integrated temperature[7] of $\int T_{fss} dV$ = 27 K km s^{-1}. Hence, we derive a $C^{18}O$ 3→2/2→1 temperature ratio of 1.1. This is clearly different to ^{13}CO, because Wall *et al.* (1991) found the ^{13}CO 3→2/2→1 temperature ratio to be between 2.0 and 2.8. It should be noted that I am deriving line ratios using T_{fss}, rather than the normal T_{MB}. This is because to convert from T_{fss} to T_{MB}, you need to correct for the coupling of NGC 253 to the JCMT beam. As I am comparing beam-matched observations, the ratio is independent of the coupling to NGC 253.

[7] Hereafter, I label integrated temperature as simply temperature.

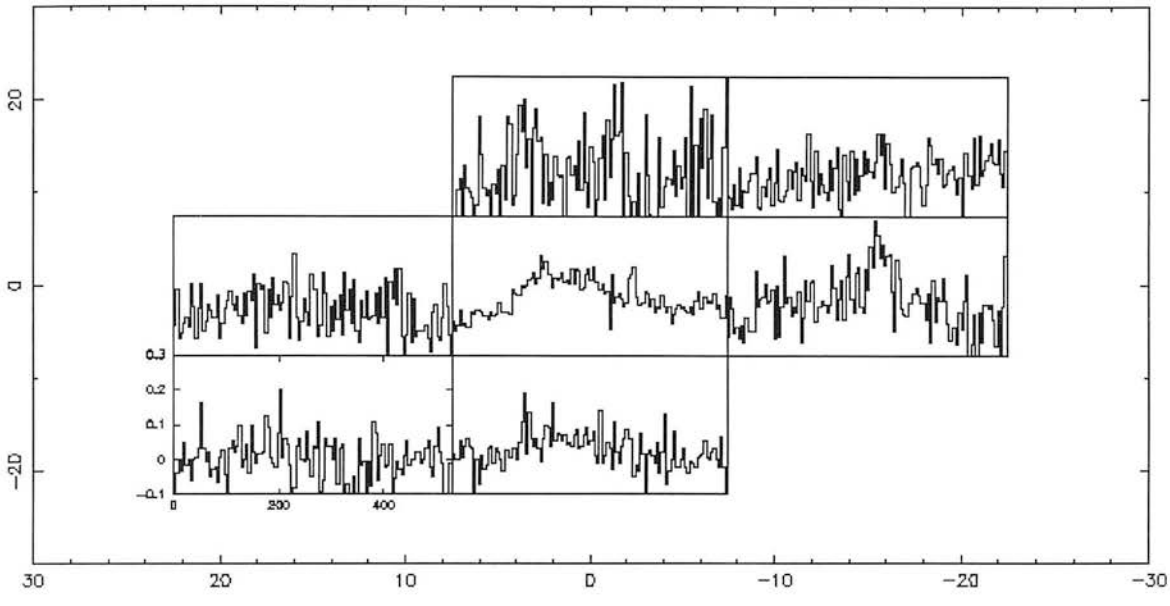

Figure 4.6: A grid map of the $C^{18}O$ 3-2 spectra observed towards NGC 253. The map is rotated by position angle ~53°. The centre of the map is RA (1950) 00 45 06.00, Dec -25 33 36.0 and the x,y scale units are arcseconds. The spectra are displayed on a T_A^* scale. To convert to the T_{fss} scale the spectra should be multiplied by η_{fss}^{-1}, where η_{fss} was measured to be 0.68

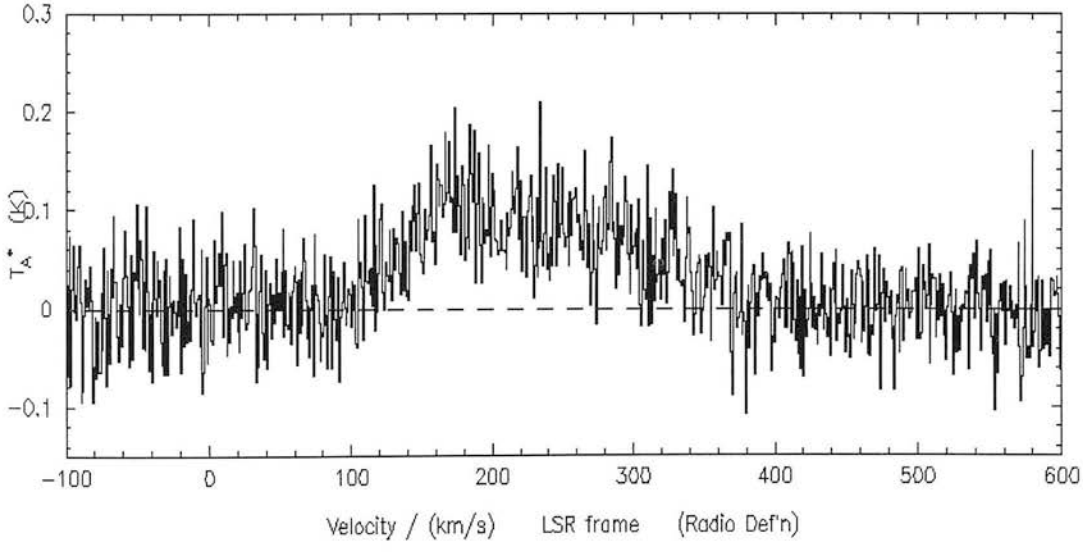

Figure 4.7: The spectrum of $C^{18}O$ 2-1 spectra observed towards NGC 253. The spectrum was taken at the position RA (1950) 00 45 06.00, Dec -25 33 36.0. The spectrum is displayed on a T_A^* scale. To convert to the T_{fss} scale the spectrum should be multiplied by η_{fss}^{-1}, where η_{fss} was measured to be 0.59

4.4 Discussion

4.4.1 ^{13}CO and $C^{18}O$ appear to be tracing different components of the molecular gas in the central 300 pc of NGC 253

Wall *et al.* (1991) argue that there are two components to the CO emitting gas in NGC 253: a hot dense core of size $< 15''$, which dominates the emission towards the nucleus, and a $40'' \times 10''$ bar, of colder and more tenuous gas, which dominates the emission away from the nucleus. This picture is supported by the observations of ^{13}CO and ^{12}CO made by Wall *et al.* (1991). The temperature ratio of ^{12}CO and ^{13}CO indicates that $\tau_{^{13}CO\ 3\rightarrow 2} \sim 0.2$. Wall *et al.* (1991) observed the ^{13}CO $3\rightarrow 2/2\rightarrow 1$ temperature ratio to be between 2.0 and 2.8 from the central $23''$ ($\sim$ 300 pc). Given the uncertainties in the observations (the data were taken from different telescopes) this ratio is close enough to the limiting value of 2.25 to indicate that most, if not all, ^{13}CO emitting gas is hot (T $\sim$ 100 K), optically thin and thermalised. A temperature ratio at the lower end of the observed range (^{13}CO $3\rightarrow 2/2\rightarrow 1 = 2.0$) can be explained by having a two component model of the ^{13}CO emitting gas with 90% of the emission from hot gas and 10% of the emission coming from cold (T $\sim$ 20 K) gas. Modification, due to a subthermal population of ^{13}CO or an increased optical depth (if the ^{13}CO and ^{12}CO emitting gas are not well mixed), must be small because otherwise the observed $3\rightarrow 2/2\rightarrow 1$ temperature ratio of ^{13}CO would be much closer to unity.

$C^{18}O$ paints a different picture of CO excitation towards the nucleus of NGC 253. Convolving our $C^{18}O$ $3\rightarrow 2$ spectra to the same resolution as our $C^{18}O$ $2\rightarrow 1$ spectrum, $23''$, we find that the temperature ratio of $C^{18}O$ $3\rightarrow 2/2\rightarrow 1$ is $\sim$1.1. $C^{18}O$ is almost certainly optically thin, given that ^{13}CO is optically thin, and, furthermore, the critical density of the energy levels of ^{13}CO and $C^{18}O$ are close enough that, if ^{13}CO is thermalised, $C^{18}O$ is thermalised. Hence, it would seem from the $3\rightarrow 2/2\rightarrow 1$ ratio, that the bulk of $C^{18}O$ emitting gas is cold (T $\sim$ 20 K) towards the nucleus of NGC 253; a temperature ratio of 1.1 can be explained with a two component model of $C^{18}O$ emitting gas but with only 10% of the emission arising from hot gas and 90% of the emission arising from cold gas. It appears that $C^{18}O$ and ^{13}CO may be tracing different components of the ISM towards the nucleus of NGC 253.

4.4.2 Selective photodissociation of CO

The photodissociation of a molecule in general can take place either directly by continuous absorption into the repulsive part of an excited electronic state, or indirectly by discrete absorptions into bound electronic states. The bound levels of the excited state then couple through a radiationless process with the continuum of a final dissociating state of a different symmetry. The dissociation energy of the ground state of CO is 11.09 eV, so that photodissociation of interstellar CO can only occur at wavelengths $911.75 < \lambda < 1117.8$ $\AA$. Hence, knowledge of the electronic states of CO lying 11.09-13.6 eV above the ground state is needed to understand the photodissociation of CO. The ionisation threshold of CO is at 885 $\AA$, so that photoionisation does not occur in the general interstellar radiation field.

Experimental work has revealed no continuous absorption of CO long-ward of 885 $\AA$ (Letzelter *et al.* 1987) and so the photodissociation of CO is dominated by discrete absorptions into excited states. Figure 4.8 shows a schematic of the photodissociation of CO, in which the bound potential curve is crossed by a repulsive state of a different symmetry. The cross-section, displayed in Figure 4.8, consists of a series of discrete peaks, broadened by the predissociation process. Because CO is dissociated by UV photons at specific frequencies, the depth-dependence

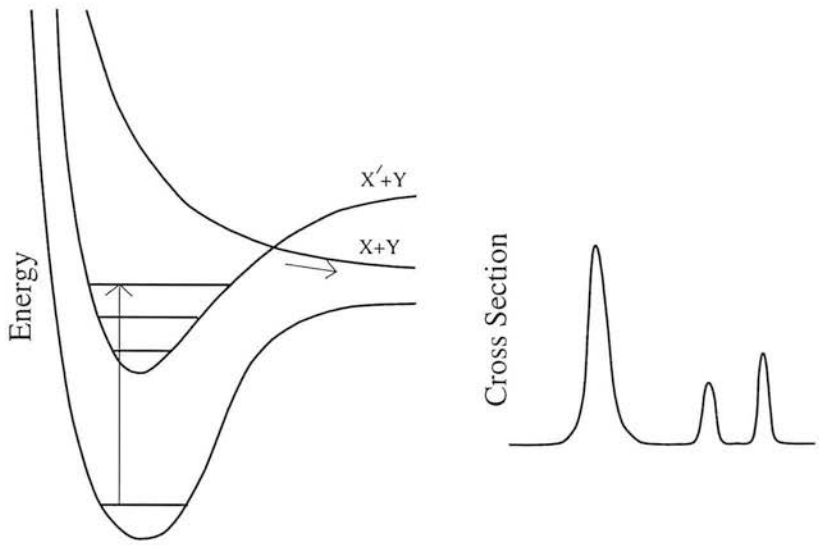

Figure 4.8: Potential energy curve and characteristic cross section for the process of predissociation. The photodissociation of CO occurs by this mechanism. The figure is adapted from van Dishoeck (1988).

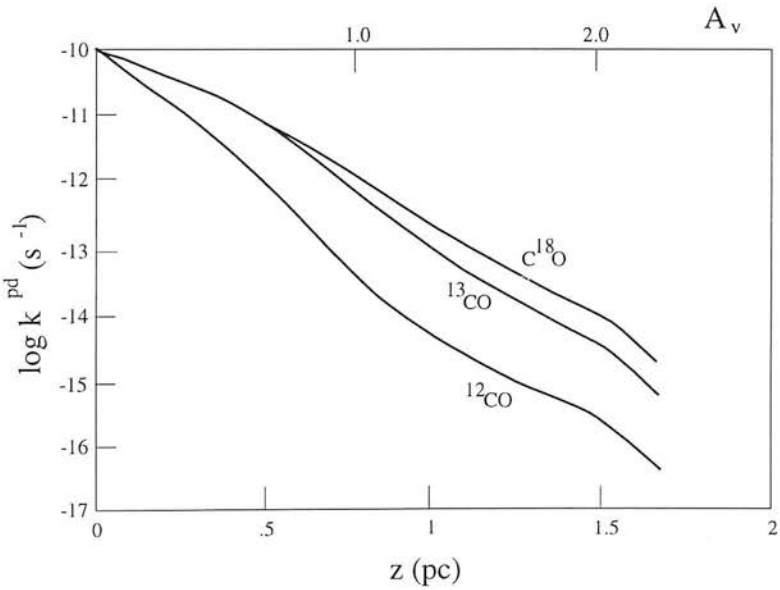

Figure 4.9: Photodissociation rates of ^{12}CO, ^{13}CO and $C^{18}O$ as functions of depth into a translucent cloud. The figure is adapted from van Dishoeck & Black (1988)

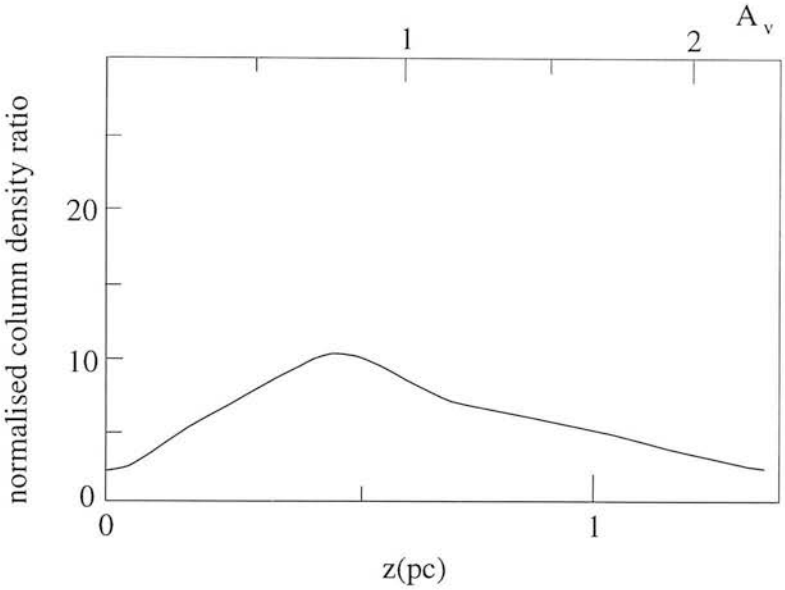

Figure 4.10: The cumulative isotopic column density ratio of $^{13}CO/C^{18}O$ normalised to the isotopic abundance, adapted from van Dishoeck & Black (1988). The curve is shown for a cloud of temperature 50 K and density 1000 cm^{-3}.

of the photodissociation rate is controlled by self-shielding, shielding by coincident lines of H and H_2, and by dust attenuation. In order to account for the first two effects, van Dishoeck & Black (1988) simulated the full absorption spectrum of CO at each depth into the cloud. Predissociation rates are rapid, $A^{pr} \sim 10^{11} - 10^{12}$ s^{-1}, and so the lines are intrinsically broad with line widths of 2-20 km s^{-1}. Some of the CO absorption bands are coincident with strong H or H_2 features and so are effectively blocked by them.

The depth dependence of the CO photodissociation rate is shown in Figure 4.9. The CO photodissociation rate decreases rapidly with depth into the cloud due to self-shielding and shielding by H and H_2. The calculation of the depth dependence of the photodissociation rate of the isotopic varieties ^{13}CO and $C^{18}O$ is complicated by the fact that lines in (0,0) bands can be effectively shielded by ^{12}CO inside the cloud, but not lines in (v',0) bands with v'$\geq$1, owing to the larger isotope shift when a non-zero vibrational quantum number is involved (van Dishoeck 1988). ^{12}CO is able to self-shield because it is relatively abundant whereas the rarer species of ^{13}CO and $C^{18}O$ cannot. Moreover, the photodissociation rate of $C^{18}O$ is higher than ^{13}CO throughout the cloud and indicates that ^{13}CO will be overabundant, with respect to $C^{18}O$ when normalised by isotope. This, I believe, is the key to understanding the line ratios in NGC 253. Figure 4.10 shows the ratio of ^{13}CO to $C^{18}O$ normalised to the isotopic values. The peak at about 0.5 pc is actually due to a rise in the importance of the ion-exchange reaction, shown in equation 4.3, which enhances the ^{13}CO abundance. If the gas has a higher temperature than 50 K, the temperature used in the model shown, as would be expected in dense PDRs where the temperature is around 300 K, the peak will be less pronounced but the important thing to note is that everywhere towards the edge of the cloud ^{13}CO is overabundant with respect to $C^{18}O$, *i.e.* the normalised column density ratio is greater than unity.

The effect of selective photodissociation of isotopic CO has been observed by several authors, e.g. Fuente et al. (1993), who find that the column density ratio of $^{13}CO/C^{18}O$ is enhanced towards the edge of a PDR. It is also to be expected that the temperature of the gas will

be higher towards the edge of the cloud, where UV heating will be more efficient, and thus, ^{13}CO 3→2/2→1 > C^{18}O 3→2/2→1. Thus, the ^{13}CO temperature ratio reported by Wall *et al.* (1991) indicates that, towards the nucleus of NGC 253, most of the gas is hot and, thus, at low visual extinction ($A_v < 5$). Such a low visual extinction indicates that most of the molecular gas in NGC 253 is either filamentary or clumpy in nature.

4.4.3 What are the values of the isotopic ratios in NGC 253?

The only observations of an ^{18}O bearing molecule in NGC 253 are those of the three lowest energy transitions of C^{18}O. Converting these observations into measures of ^{12}CO may be hazardous because C^{18}O appears to be tracing only a small fraction of the total CO column density, that which is in a cold state. This uncertainty in calculating ^{16}O/^{18}O is highlighted by the values derived for different lines. Henkel *et al.* (1993), using observations of several carbon bearing molecules towards the nucleus of NGC 253, derive ^{12}C/^{13}C ~ 40. Henkel *et al.* (1993) derive ^{16}O/^{18}O ~ 200 because the observed temperature ratio of ^{13}CO/C^{18}O in the 1→0 line is ~ 5. The observation of C^{18}O 1→0 was made by Sage et al. (1991) with the NRAO 12m. A similar observation of C^{18}O 1→0, made with the 12m by Wall et al. (1993), indicates that observations of C^{18}O 1→0 are prone to uncertainties associated with subtracting baselines and spectral features—see Figures 4.2 and 4.3. Using the beam-matched (23″) 2→1 observations of ^{13}CO, Wall et al. (1991), and C^{18}O (this work) we derive ^{16}O/^{18}O ~ 110-150 (the uncertainty is due to the brightness uncertainty reported by Wall *et al.* 1991). If we use the beam-matched (23″) 3→2 observations of ^{13}CO, Wall et al. (1991), and C^{18}O (this work) we derive ^{16}O/^{18}O ~ 280. The fact that the highest ^{16}O/^{18}O ratio is obtained for the 3→2 line is no surprise given that ^{13}CO is tracing hot gas whereas C^{18}O appears to be tracing cold gas. Thus, selective photodissociation of C^{18}O in NGC 253 means that it is not possible to use isotopomers of CO to give reliable estimates of the *intrinsic* ^{16}O/^{18}O ratio in the starburst region—we do measure the C^{18}O/^{13}CO ratio but this cannot be used to infer ^{16}O/^{18}O.

Henkel *et al.* (1993) argue that because H^{13}CN emission arises from dense UV-shielded cores, and τ(^{12}CO 1→0) ~ τ(H^{12}CN 1→0) ~ 3–4, if isotopic selective photodissociation is an important effect in NGC 253 then the ratio I(^{12}CO)/I(^{13}CO) will be much greater than I(H^{12}CN)/I(H^{13}CN). This is not the case because selective photodissociation does not have a dramatic effect on I(^{12}CO)/I(^{13}CO). Hence, even if selective photodissociation is important in NGC 253 this will not be highlighted by a comparison of ^{12}CO and ^{13}CO. If the bulk of molecular gas in NGC 253 exists in a region where the chemistry is dominated by a high UV field then selective photodissociation may affect the derived isotopic ratios from other molecules. Henkel *et al.* (1993) derived ^{12}C/^{13}C ~ 40 from observations of three carbon bearing molecules (CS, HNC and CN) and their respective ^{13}C isotopomer. In NGC 253 most of the gas is not shielded from UV photons and it is likely that CO and molecules such as CS are coextensive. van Dishoeck (1988) suggests that the photodissociation of interstellar CS probably proceeds by processes similar to those for CO, but with the difference that the dissociation energy and ionisation threshold is smaller by ~ 3 eV and the photodissociation rate of CS is larger than that of CO. Thus, with a lower abundance and higher photodissociation rate it is likely that CS will be unable to self-shield against the UV and hence will not undergo selective photodissociation of its isotopomers.

In the next section I calculate ^{12}CO column densities from ^{13}CO × 40 but I note that if selective photodissociation is important for the chemistry of HNC and CN then ^{13}CS may be

underabundant and the intrinsic value of $^{12}C/^{13}C$ will be < 40 in NGC 253.

4.4.4 The column density of CO in NGC 253

The ratio of ^{13}CO 3→2/2→1 may be as low as 2.0. Thus, there is some uncertainty in the nature of the ^{13}CO emitting gas. One hot component (T ~ 100 K) provides a good fit as does a two component model, with ~ 90% of the emission from very hot (T = 200 K) gas and ~ 10% of the emission from cold (T = 20 K) gas. If $\tau_{^{13}CO\,(3\rightarrow2)} \sim 0.5$ then this can also explain the observations but indicates that ^{12}CO and ^{13}CO are not coextensive and would require the gas that is partially optically thick to have a large column density ($N(H_2) > 10^{23}$ cm^{-2}) and be very hot (T >250 K). This latter possibility seems unrealistic. The derived ^{13}CO column densities are obviously dependent upon the chosen description of the gas that is emitting ^{13}CO. Fortunately, in NGC 253 it is clear that more than 90% of ^{13}CO is at T ≥ 100 K. There is less than 20% uncertainty in the derived ^{13}CO column density between the models of 100% at T = 100 K gas ($N_{^{13}CO} = 2.1 \times 10^{17}$ cm^{-2}), and 90% at 200 K and 10% at 20 K gas ($N_{^{13}CO} = 2.4 \times 10^{17}$ cm^{-2}). Given that $C^{18}O$ is tracing a cold component the second option, of a mixture of hot and cold CO, should be a reasonable description of the molecular gas in NGC 253.

There is little $C^{18}O$ in the hot gas towards NGC 253 which indicates that photodissociation plays an important role in the chemistry of the bulk of CO. The effects of photodissociation on the chemistry of CO have been studied in detail by van Dishoeck & Black (1988), for low density gas (10^3 cm^{-3}), and more recently by Köster *et al.* (1994), for denser gas (≥ 10^4 cm^{-3}). It appears, from these studies, that the effect of selective photodissociation on $CO/^{13}CO$ is a slight increase at intermediate depths due to the differences in self-shielding. The $^{13}CO/C^{18}O$ ratio appears more sensitive to self-shielding (van Dishoeck & Black 1988) and shows a much larger increase than the $CO/^{13}CO$. Hence, if the bulk of the molecular gas in NGC 253 is in an environment where self-shielding and photodissociation play a crucial role in determining the molecular abundances, particularly isotopic CO, the chemical models indicate that ^{13}CO will be a more reliable tracer of CO column density than $C^{18}O$.

So I find that, averaged over the central 23″ of NGC 253, by using the equations in Appendix B, the column density of carbon monoxide is $N(CO) = 2.4 \times 10^{17} \times 40 = 9.6 \times 10^{18}$ cm^{-2}.[8]

4.5 Conclusions

I have observed $C^{18}O$ 3→2 and $C^{18}O$ 2→1 towards the nuclear region of the starburst galaxy NGC 253. Observations of ^{13}CO by Wall *et al.* (1991) indicate that most of the molecular gas in the nuclear region is hot and dense. $C^{18}O$ appears to be tracing cold gas in NGC 253 and so it appears that $C^{18}O$ is only tracing a minor fraction (< 10%) of the total CO. The separation

[8] Israel *et al.* (1995) derive a column density of CO higher than the value I have quoted here. Inspection of Table 1 of Israel *et al.* (1995) reveals several numerical errors. An example of the numerical errors is the quoted measurements of ^{13}CO 3→2 by Wall *et al.* (1991). Wall *et al.* (1991) observed ^{13}CO 3→2 with a 23″ beam, not a 15″ beam. Furthermore, for the given ^{13}CO 3→2 integrated brightness temperature of 210 K km s^{-1}, this corresponds to an intensity of 8.8×10^{-9} W m^{-2} sr^{-1}—a factor of 2 greater than the value quoted by Israel *et al.* (1995). I agree with Israel *et al.* (1995) in the luminosity of ^{13}CO 3→2 but only under the assumption of a 23″ beam with an intensity I derived above. Israel *et al.* (1995) derive their column densities after correcting the observations of the various lines to a coupling of an assumed 36″×12″ source size, the approximate size of the CO 1→0 emission detected by Canzian *et al.* (1988). The source size of CO 1→0 may well be larger than the size of the region traced by the higher J lines. Wall *et al.* (1991) actually argued for a much smaller compact region of hot CO from their observations of ^{13}CO. This makes the coupling corrections of Israel *et al.* (1995) prone to uncertainties. Moreover, Israel *et al.* (1995) argue that there is no a priori reason to believe that ^{13}CO is fully optically thin and thermalised whereas I have argued that the 3→2/2→1 observations of ^{13}CO indicate that ^{13}CO is fully optically thin and thermalised.

between $C^{18}O$ and ^{13}CO may indicate that selective photodissociation of CO is efficient in NGC 253.

4.6 Acknowledgements

I take this opportunity to thank Peter Brand, Henry Buckley, Asuncion Fuente, Christian Henkel, Peter Papadopoulos, Phil Puxley, Adrian Russell and Ewine van Dishoeck for helpful and instructive discussions and an anonymous referee for a critical and insightful reading of a draft of some of this work when it was submitted for publication to MNRAS. I also thank Rachael Padman and John Lightfoot for help with SPECX and Bill Dent, Jeff Cox, Kimberley Pisciotta and Jim Pomeroy for help with the observations.

Chapter 5

Atomic carbon in NGC 253

5.1 Fundamental data and background

Molecular clouds contain approximately half of the Galaxy's total gaseous mass although they occupy only a small fraction of the volume of the Galaxy. The imbalance between mass and volume occurs because, except for dense self-gravitating clouds, the general interstellar medium (ISM) is approximately in pressure equilibrium and the other gas phases have higher temperatures and lower densities. Another small volume is occupied by cool neutral atomic gas, $T \leq 100$ K, concentrated in structures called "diffuse clouds" which may be associated with molecular clouds. About half of the volume of the Galaxy is occupied by neutral and ionised gas components with temperatures $T \leq 8000$ K, and the rest of it is occupied by a very hot, $T \sim 10^6$ K, highly ionised gas component.

The different phases of the ISM mean that ions, atoms and molecules exist in different states of excitation within the distinct phases of the ISM. A tracer of the various gas-phases of the ISM, particularly in the low excitation phases such as the cool neutral atomic gas and molecular clouds, is carbon, in its ionised, atomic and molecular form. The importance of carbon as a tracer can be understood from inspection of Table 5.1 which is a list of the most abundant elements, with their ionisation potentials (adapted from Keene 1990).
It is important to notice the following:

- carbon is the fourth most abundant element, with an abundance relative to hydrogen of $\sim 3{\times}10^{-4}$.

- carbon's ionisation potential, 11.26 eV, is the only one of the six most abundant elements lower than that of hydrogen. Only iron, which is a factor of 8 less abundant, has a lower ionisation potential. This means that, among atoms, carbon has virtually no competition for the interstellar ultraviolet radiation with photon energies between 11.26 eV and 13.6 eV and it will be easily ionised unless it is shielded by dust, an efficient continuum absorber of radiation.

- the dissociation potential for the carbon monoxide molecule, listed at the bottom of the table, is very close to the ionisation potential for carbon. Carbon monoxide is a stable molecule and not highly reactive. In a shielded environment in which chemical reactions can occur it is the endpoint of these reactions. As oxygen is more abundant than carbon it is reasonable to expect that, in an environment shielded from UV radiation, most of the carbon is in the form of CO.

Table 5.1: Cosmic abundances

Element	Abundance	Ionisation Potential (eV)
H	1.0	13.60
He	8.5×10^{-2}	24.59
O	6.6×10^{-4}	13.62
C	3.3×10^{-4}	11.26
N	9.1×10^{-5}	14.53
Ne	8.3×10^{-5}	21.56
Fe	4.0×10^{-5}	7.87
Si	3.3×10^{-5}	8.15
Mg	2.6×10^{-5}	7.65
S	1.6×10^{-5}	10.36
Molecule		Dissociation Potential (eV)
CO		11.09

The original calculations of an ultraviolet radiation field impinging upon the edges of clouds were discussed in terms of a kind of Strömgren-sphere problem for carbon, Werner (1970). It was soon realised that the distance over which the ionised carbon transformed to atomic carbon was sufficiently large that the bulk of the hydrogen in this region is expected to be molecular rather than atomic, Glassgold & Langer (1975). Ion-molecule reactions in regions containing mainly molecular hydrogen start to dominate over recombination in the removal of C^+ which results in most of the ionised carbon getting channeled into CO, rather than into an atomic form, Langer (1976). Recent calculations of the chemistry in the C^+/CO transition predict that most of the carbon outside the dense clouds is ionised (hereafter CII), most of it within dark clouds is in the form of carbon monoxide (CO), and, at the edges of the clouds between these two regions, there is a thin layer of atomic carbon (CI) (Tielens & Hollenbach 1985). Very little atomic carbon was expected deep within clouds. All other gas phase forms of carbon should be negligible compared with these. Observational support for the models came from studies of the diffuse and the shielded ISM. Studies of the diffuse, and hence unshielded, medium, from detections of UV absorption with the *Copernicus* satellite show that most of the gas phase carbon is ionised at low A_v, *e.g.* Morton *et al.* (1973). Furthermore, the major carbon-bearing constituent of the gas-phase in the dark, shielded regions of the molecular clouds is carbon monoxide (Keene 1990). The approximate picture of the state of carbon in the interstellar medium became CII in the diffuse medium, CI in dense cloud edges, and CO in the bulk of the dense clouds.

The orientation of the spins of electrons relative to their orbital angular momentum leads to "fine-structure" in the degeneracy of the electronic states of atoms and ions, with splittings in energy typically on the order of a few hundred K, well matched to the temperatures expected in the C^+/CO transition region, Tielens & Hollenbach (1985). Due to the fine-structure transitions being "forbidden", excited states are relatively long lived and so within the C^+/CO transition region, many of the fine-structure levels can have considerable column densities filled through collisions. The forbidden transitions between the various levels typically occur at frequencies of the order of 10^{12} Hz, namely in the sub-mm to far-IR region. In particular, atomic carbon

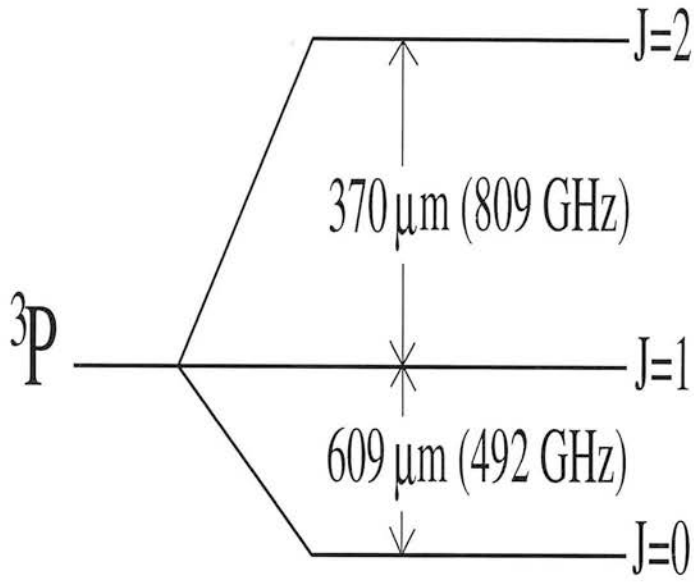

Figure 5.1: The fine-structure of the ground state of atomic carbon. Spin-orbit interactions split the ^{3}P state into three levels: the ground state $^3P_0$; the first excited state, $^3P_1$, which is 24 K above ground; the second excited state, $^3P_2$, which is 63 K above ground. The critical density of the $^3P_1$ level is 4.7×10^2 cm^{-3} and the critical density of the $^3P_2$ level is 2.8×10^3 cm^{-3}. The degeneracy of 3 results in two fine-structure transitions—the $^3P_1 \rightarrow {}^3P_0$ line is at 609 μm and the $^3P_2 \rightarrow {}^3P_1$ line is at 370 μm. The transition $^3P_2 \rightarrow {}^3P_0$ is a strongly forbidden magnetic quadrupole flip and is very weak.

has two fine-structure transitions in the sub-mm and so by observing these lines, as well as complementary transitions of other species such as ionised carbon, it is possible to extract information about the abundances and conditions within the C^+/CO transition region. In the next section I review the previous sub-mm observations of atomic carbon and discuss the theoretical interpretations of the observational results. In the following section I summarise the main observational and theoretical results and provide the reason for observing atomic carbon towards the nucleus of NGC 253.

5.2 A summary of previous observations of CI emission

Due to spin orbit interactions, the ground ^3P state of atomic carbon, CI, is split into three levels, at energies $E(^3P_2)/k = 62.5$ K, $E(^3P_1)/k = 23.6$ K and $E(^3P_0)/k = 0$ K, Figure 5.1. The two transitions, $^3P_1 \rightarrow {}^3P_0$ and $^3P_2 \rightarrow {}^3P_1$, are at frequencies of 492 and 809 GHz respectively. At low temperatures carbon can be considered a three-level atom because higher energy levels are nearly inaccessible ($E/k > 10^4$ K). The ground-state fine-structure levels of atomic carbon are easily collisionally excited; $n_{crit} \approx 1000$ cm^{-3} for collisions with H_2, Schröder *et al.* (1991). Atomic carbon is thus an efficient coolant of moderately dense ($n > 5\times10^2$ cm^{-3}), cool ($15 < T < 40$ K) interstellar material.

5.2.1 The widespread distribution of atomic carbon

Phillips & Huggins (1981), using the Kuiper Airborne Observatory (KAO) 90 cm telescope (3′ beam at 492 GHz), mapped the $^3P_1 \rightarrow {}^3P_0$ line in the Orion Molecular Cloud and argued that it appeared to be as extended as CO, even in regions of apparently high extinction. Furthermore, the carbon emission was brighter than expected and indicated that the abundance of atomic

carbon was of the order of the carbon monoxide abundance throughout the cloud. Moreover, the CI spectra appear to be of a similar shape to the CO spectra which suggests that CI and CO are coextensive. Towards the center of the Orion Molecular cloud the CI appears stronger at the edges than towards the center of the cloud with respect to ^{12}CO 1→0 emission, which suggests that CI emission avoids the densest cores.

Keene *et al.* (1985) observed $^3P_1 \rightarrow {}^3P_0$ emission from the edge-on ionisation fronts in M17 and S140 using the KAO. Keene *et al.* (1985) reported that the CI emission peaks farther into the ionisation front than the CO. The peak CI abundance in M17 was observed to be at an estimated 60 magnitudes of visual of extinction into the cloud from the ionisation front. Deep within these clouds Keene *et al.* (1985) derived the C/CO column density ratio to be ~ 0.1, again far higher than was expected. Moreover, towards M17 and S140 strips of CI and ^{13}CO 1→ 0 emission show very similar spectra in both velocity and line shape (Keene *et al.* 1985) which provided further support for the view that CI and CO are coextensive.

Genzel *et al.* (1988) mapped the $^3P_2 \rightarrow {}^3P_1$ emission from M17 and W51 with UKIRT (25″ resolution at 809 GHz). The CI emission was observed to be well correlated with the distributions of C^{18}O 2→1 and ^{12}CO 7→6 although the CI emission may peak slightly deeper into the clouds than the CO emission. Genzel *et al.* (1988) argued that there appeared to be a lack of CI 2→1 emission with respect to CO towards the densest cloud cores. The CI 2→1 emission appears to peak at a smaller depth into M17 than the observations of Keene *et al.* (1985). Genzel *et al.* (1988) noted a "remarkable similarity" in the profiles of CI 2→1, ^{13}CO 1→0 and ^{13}CO 2→1. Genzel *et al.* (1988) proposed that the bulk of the CI emission arose from the surfaces of clumps in photon dominated regions. In such a clumpy PDR the UV penetrates far deeper than in gas that is not clumpy. Genzel *et al.* (1988) suggested that mini-PDRs would be produced on the surface of clumps deep within the clouds and such mini-PDRs could explain the widespread CI emission.

Zmuidzinas *et al.* (1988) detected $^3P_2 \rightarrow {}^3P_1$ emission in seven sources using the KAO (80″ FWHM beam at 809 GHz). Zmuidzinas *et al.* (1988) failed to detect broad high-velocity wings in the Orion BN/KL region but their limit on the C/CO abundance ratio in the high velocity gas was not sufficiently restrictive to indicate a depletion of CI relative to CO in the shocked gas. They compared their CI 2→1 data with CI 1→0 observations and argued that both the CI lines are optically thin and the C/CO abundance ratio is around 0.1.

Frerking *et al.* (1989), using the KAO, observed $^3P_1 \rightarrow {}^3P_0$ emission towards six positions in the Ophiuchus molecular cloud and claimed that the CI emission bears a close resemblance in line shape, and spatial distribution, to the low J rotational lines of ^{13}CO. This resemblance was attributed by Frerking *et al.* (1989) to the similar opacities and excitation requirements of CI and ^{13}CO. Atomic carbon was observed to be less abundant at very high extinction ($A_v \sim 30$) than it is at intermediate A_v but its abundance is still high at least 10 magnitudes into the cloud, Figure 5.2.

White & Padman (1991) made maps of the CI emission in a single 1.3 km s^{-1} velocity channel towards M17, S140, Orion A and the Galactic Center using the JCMT (10″ beam at 492 GHz). The CI emission is concentrated towards the edges of the clouds but is also present at lower concentrations deeper within the clouds. CI was was not detected towards the Orion IRc2 outflow which seemed to indicate that shock dissociation of CO in the vicinity of outflows is not a principal source of CI. CI appears to avoid the densest regions and appears to reach a maximum on the edges of clumps revealed by C^{18}O. White & Padman (1991) argue that there is a general agreement between the CI distribution and CO tracers, such as ^{13}CO and C^{18}O,

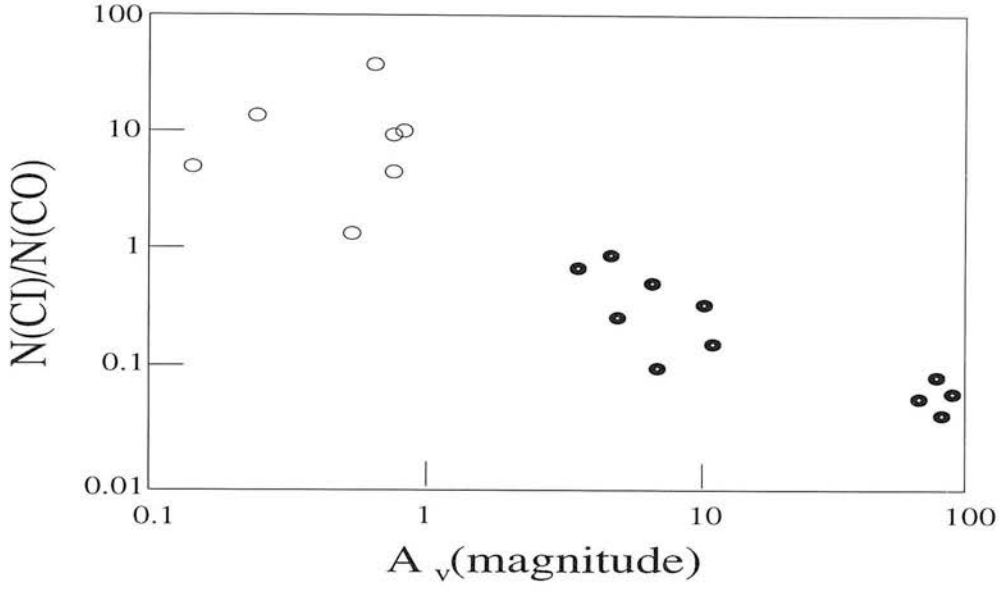

Figure 5.2: The ratio of N(CI)/N(CO) as a function of A_v, adapted from Frerking *et al.* (1989). The open circles are from UV measurements, the dark circles those of millimetre/submillimetre measurements.

but any formal correlation is poor.

Hernichel *et al.* (1992) used the Kölner Observatorium für Submm - Astronomie (KOSMA) 3 m telescope (55″ beam at 492 GHz) to observe CI emission towards S140, Figure 5.3. Hernichel *et al.* (1992) claimed that there are two components to the CI emission in S140: a narrow component, which traces the ambient cloud material, which is superimposed on a wider component (FWHM $\approx$ 15 km s^{-1}) which exhibits a line profile similar to that of the higher velocity material visible in CO. The wider component carries most of the CI column density and the velocity integrated CI emission peaks near the edge of the cloud facing the exciting star. The finding of Hernichel *et al.* (1992) is in contrast to Keene *et al.* (1985). The disagreement results from Keene *et al.* (1985) not observing a wide component in their observations. Furthermore, Hernichel *et al.* (1992) found that the high velocity CI emission extends over an area substantially larger than the molecular line wing emission and so may not be tracing the same gas as the outflow.

Walker *et al.* (1993) supported the conclusions of Frerking *et al.* (1989) by arguing that their observations of 11 molecular outflows show similar CI and low J ^{13}CO line profiles. Walker *et al.* (1993) argue that molecular outflows associated with young stellar objects show no evidence for shock enhancement of CI.

Plume *et al.* (1994) used a "Gaussian Focal Reducer" on the Caltech Submillimeter Observatory (CSO) which reduced the effective aperture to 60 cm. Plume *et al.* (1994) claim that towards S140 IRS 1 there is no evidence for the high-velocity CI emission reported by Hernichel *et al.* (1992), at a level a factor 5 below the reported intensity of Hernichel *et al.* (1992). An illustration of the spectrum of S140 IRS1 reported by Plume *et al.* (1994) is shown in Figure 5.4. The CI emission detected by Plume *et al.* (1994) is extended and follows the general morphology of the molecular gas as detected in the ^{13}CO 2$\rightarrow$1 line. In agreement with the scan of Keene *et al.* (1985), Plume *et al.* (1994) find that, along a cut through IRS1, the peak of the CI emission lies farther from the ionisation front than the peak of the molecular emission. Cross scans elsewhere across the I-front show the integrated strength of the CI and ^{13}CO lines peaking

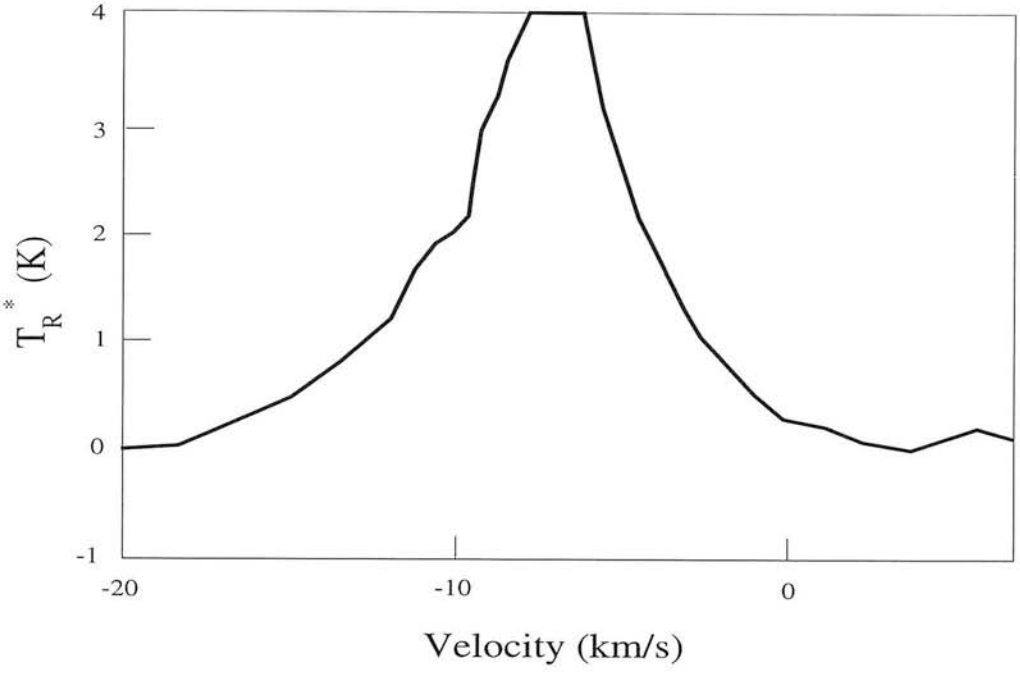

Figure 5.3: A schematic of the CI spectrum observed towards IRS1 in S140 by Hernichel *et al.* (1992).

at around the same distance from the front. Plume *et al.* (1994) claim that the CI line shapes and widths are similar to those of ^{13}CO.

Minchin *et al.* (1994) mapped the $^3P_1 \rightarrow {}^3P_0$ CI emission towards S140 using the JCMT. Minchin *et al.* (1994) detected broad line wing emission, Figure 5.5, and claimed that this supported the claim of Hernichel *et al.* (1992) but disagreed with the conclusions of Keene *et al.* (1985) and Plume *et al.* (1994). Minchin *et al.* (1994) argue that there appear to be two main sources of CI emission from S140, the PDR and an outflow source which is embedded within the cloud. The outflow source is about 70″ away from the PDR and Minchin *et al.* (1994) suggested that 3′ beams, used by Keene *et al.* (1985) and Plume *et al.* (1994), were too large to discriminate between the outflow and PDR. Minchin *et al.* (1994) claimed that the N(C)/N(CO) abundance ratio is 0.67 in the red-wing of the molecular outflow and suggested that this enhancement was due to carbon being produced by shocks within the outflow.

White (1994) argued that in the C-shocked region of IC443C atomic carbon is overabundant, by an order of magnitude, compared with quiescent molecular cloud cores. White (1994) claimed that this enhancement of CI in the supernova remnant could be caused by either the shock(s) or an enhanced cosmic ray flux density.

Minchin *et al.* (1995) have argued that their study of the line parameters, peak brightness temperature and linewidth, towards S140 indicate that there is *no* correlation between ^{13}CO 3—2 and CI. Minchin *et al.* (1995) attribute the lack of correlation as being due to the isotopic CO and CI emission emanating from different volumes of gas *i.e.* there are regions in S140 where CI and CO are not coextensive.

Towards the Orion bar, Tauber *et al.* (1995) claimed that there is a remarkable similarity in the distributions of the CI and ^{13}CO emission whereas in the Orion South region, which is the site of very dense gas, the ^{13}CO emission is strong whereas carbon emission is only average. Orion South appears as a vertical branch in the correlation plot of the ^{13}CO and CI integrated

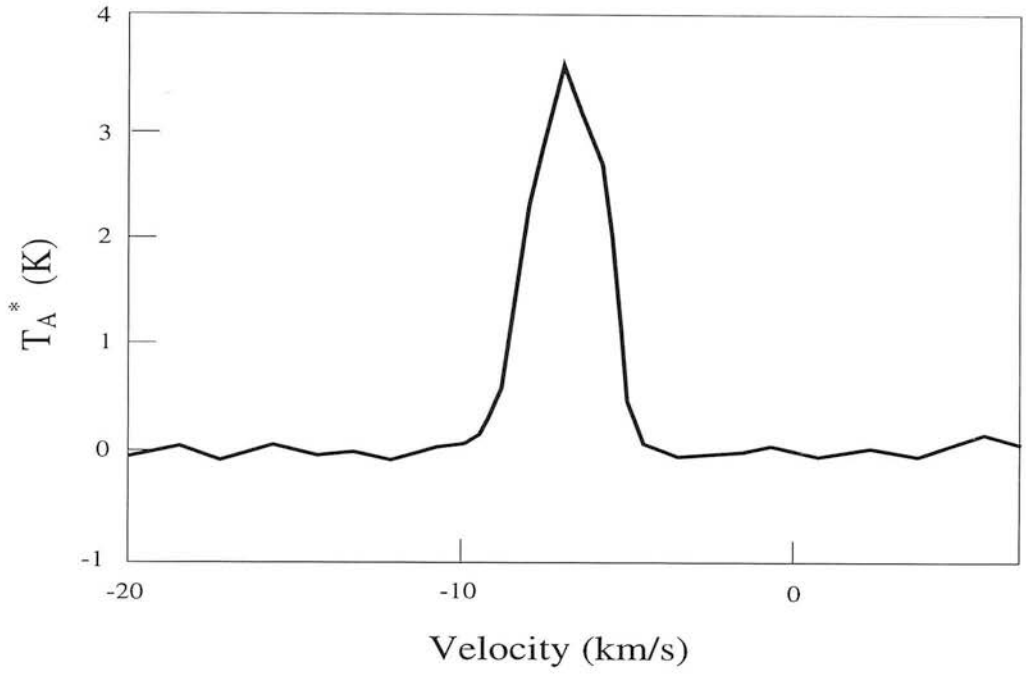

Figure 5.4: A schematic of the CI spectrum observed towards IRS1 in S140 by Plume *et al.* (1994).

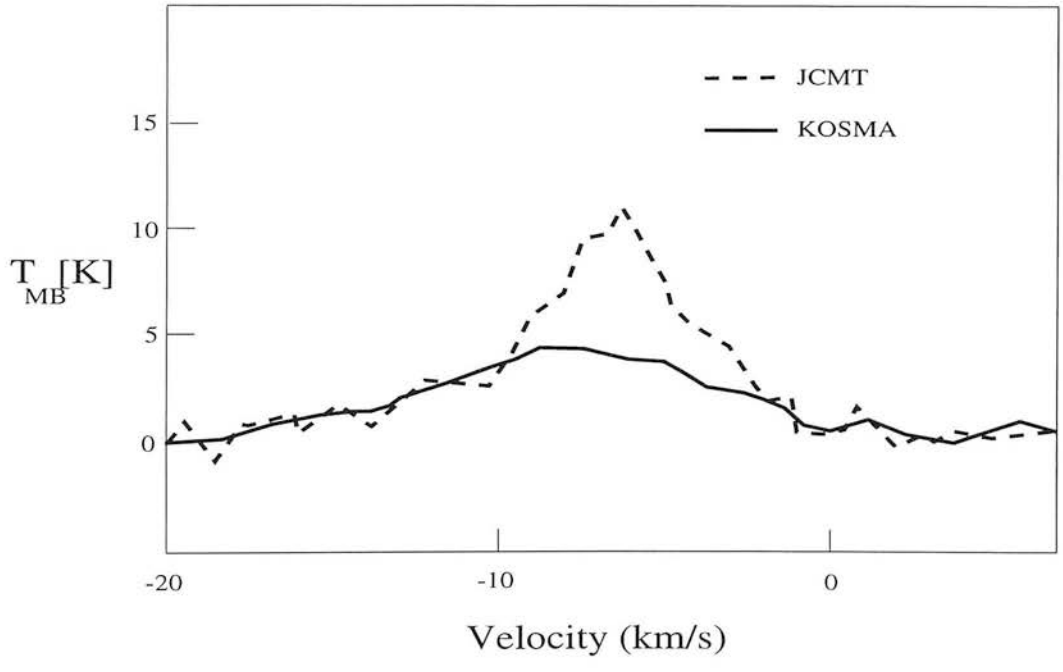

Figure 5.5: A schematic of the smoothed CI spectrum observed towards IRS1 in S140 by Minchin *et al.* (1994) with the JCMT—dashed line, compared with the spectrum obtained with KOSMA by Hernichel *et al.* (1992)—solid line. The observations are beam-matched yet the JCMT spectrum shows a brighter core.

intensities and would suggest that carbon comes up against a "brick wall" of dense gas. This would suggest that carbon is a very poor tracer of dense gas, supporting the interpretations of CI observations made by Phillips & Huggins (1981) and Genzel *et al.* (1988). The point that "CI avoids hot dense regions" has been made by Keene (1995) in her review of CI observations.

5.2.2 Theoretical explanations for the observed carbon

The initial chemical equilibrium models of molecular clouds, *e.g.* Langer (1976), predicted a CI abundance in a relatively thin layer near the cloud surface. The CI abundance was predicted to be below that of CO and so an integration of column density through a giant molecular cloud would result in a small N(CI)/N(CO) ratio, *i.e.* $\ll 0.1$.

Boland & De Jong (1982) suggested that, due to the turbulent nature of molecular clouds, parcels of molecular gas are circulated and every time a parcel reaches the outer layers of the core the dust grains have their mantels evaporated and/or photodesorbed. The various photoabsorption processes initiate the conversion of CO and carbon, contained in the grains, to CI which is then transported back into the interiors of the cloud on a circulation time-scale, t_{circ}. The time-scale to convert the free atomic carbon to CO in the center of a cloud is also of the order of t_{circ}. Boland & De Jong (1982) proposed that circulation of gas from the exterior to the interior of the cloud was the reason why there is an appreciable fraction of the gaseous carbon in an atomic form deep within clouds.

A role that shocks may play in enhancing the carbon emission deep within molecular clouds has been proposed by Williams & Hartquist (1984). Williams & Hartquist (1984) suggested that low velocity shocks in molecular clouds periodically return grain material, which is rich in carbon, to the gas phase of the ISM. Reactions of C with H_3^+ and HCO^+ are the most rapid loss routes for the free atomic carbon and these reactions ultimately leads to CO formation on a time-scale of 10^5 years. Williams & Hartquist (1984) criticised the mechanism suggested by Boland & De Jong (1982) on the grounds that the time-scale of circulating, through turbulence, the parcels of molecular gas, derived by Boland & De Jong (1982) was far too short. Williams & Hartquist (1984) further argued that the photoabsorption processes which Boland & De Jong (1982) used to remove the grain mantles were inefficient.

Leung *et al.* (1984) made pseudo time-dependent models of the gas phase chemistry within molecular clouds and hoped to mimic how the chemistry evolves as the cloud evolves. Large amounts of neutral atomic carbon exist at times well before steady state is achieved, Figure 5.6, but as steady state is approached the abundance of atomic carbon drops. The models of Leung *et al.* (1984) imply that for a large abundance of atomic carbon to exist deep within clouds, this chemistry has not reached steady state and so has been termed "early time". It should be noted that the time-scale of the chemistry is inversely proportional to the density of the gas.

Tielens & Hollenbach (1985) modelled the chemistry and heat balance of dense ($10^3 < n_o < 10^6$ cm^{-3}) PDRs on the edges of molecular clouds that are exposed to far-ultraviolet (far-UV) (6eV $< h\nu <$ 13.6eV) fluxes 10^3-10^6 times more intense than the ambient interstellar field, labelled G_o. These dense, highly illuminated photodissociation regions generally include a hot (T $>$ 100 K) atomic region (H, O and C^+) near the surface ($A_v < 3$), a warm (T $\sim$ 100 K) partially dissociated region (H_2, O, C and CO) at about $A_v \sim 4$, and a cooler (T $<$ 100 K) interior region ($A_v \sim 10$) where oxygen is still photodissociated to atomic form (H_2, CO and O). Tielens & Hollenbach (1985) predicted that the neutral carbon column density from PDRs should be about 5×10^{17} cm^{-2}. This value is fairly insensitive to the UV field—for a smaller

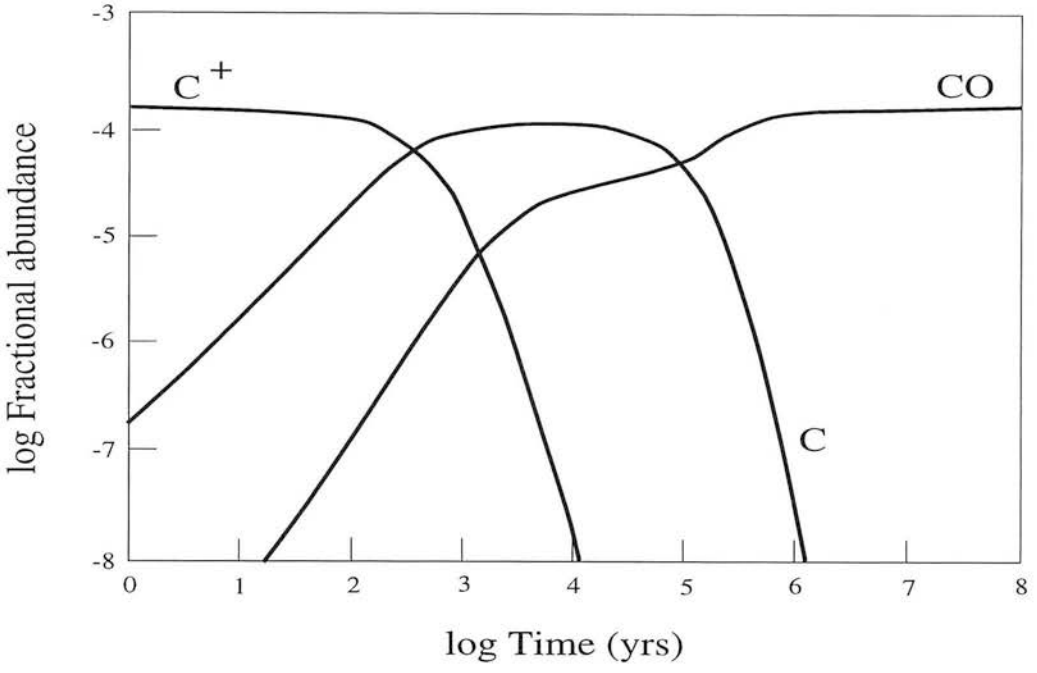

Figure 5.6: The abundances, relative to H_2, of C^+, C and CO as a function of time. The figure is adapted from Leung *et al.* (1984).

UV field fewer C atoms are photoionised but this is balanced by fewer molecules like CH, CH_2 and CO being photodissociated to produce C. The C column density is somewhat more sensitive to the gas density. There is an increase in the C column density for a decrease in the density because of the result of the competition between the different loss channels of C^+. For decreasing density relatively more C^+ is transformed to C rather than to CO, because the C^+-produced CH and CH_2 photodissociate rather than react with O to form CO. The column density of neutral carbon predicted by Tielens & Hollenbach (1985) is similar to what is observed in the ISM and is about 10 times larger than predicted in the original models of carbon chemistry in molecular clouds, *e.g.* Langer (1976). Part of this difference is due to a more detailed description of the chemistry by Tielens & Hollenbach (1985) and the rest is due to a higher choice of the elemental abundance of carbon.

Hollenbach & McKee (1989) discussed the gas-phase chemistry behind fast (30-150 km s^{-1}) interstellar shocks, and in particular the H,C and O network. Although CO has nearly three times the binding energy of H_2, CO dissociation often follows H_2 dissociation in shocks. This is because once H_2 is completely collisionally dissociated, CO is chemically dissociated at the high gas temperatures in the shocked gas through the endothermic reaction

$$H + CO \rightarrow C + OH. \tag{5.1}$$

Moreover, the photodissociation of CO proceeds by the line absorption of photons in the range $11\text{eV} < h\nu < 13.6\text{eV}$, and CO shields itself much like H_2.[1] CO is the first molecule to completely reform in the cooling post-shock gas. The formation of CO is initiated by the fast (at $T \geq 300$ K) reaction $H_2 + O \rightarrow OH + H$, with the resultant OH reacting with C^+ and C to ultimately form CO. CO destruction is by far-UV photodissociation, by endothermic reaction

[1] The photodissociation of CO is discussed in greater detail in chapter 4. The photodissociation of H_2 is discussed in greater detail in chapter 3.

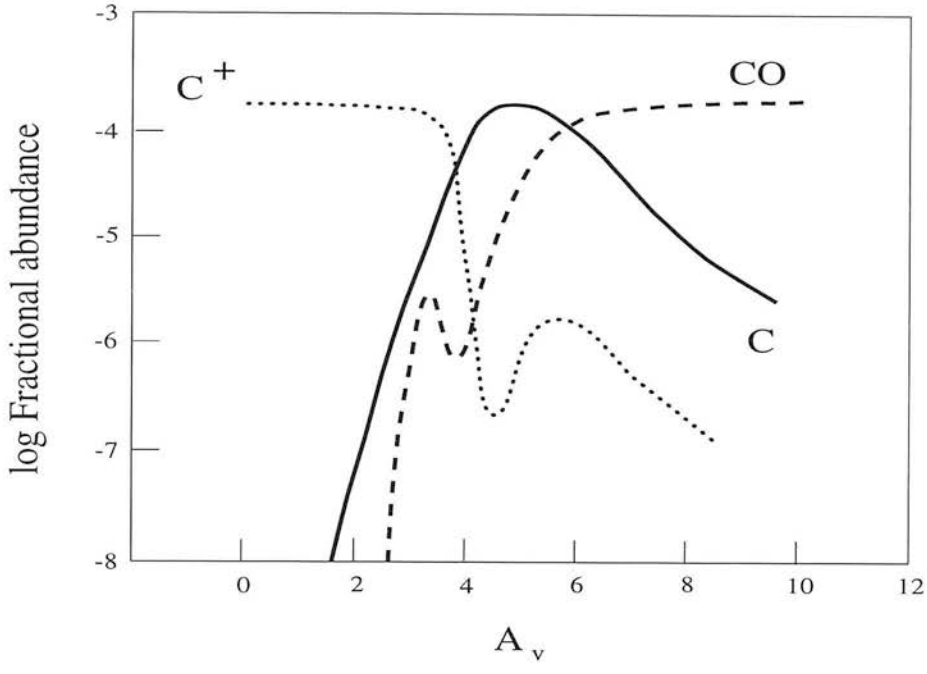

Figure 5.7: The abundances of C^+, C and CO as a function of visual extinction into a cloud. The model is that of a low density PDR, n = 10^2 cm^{-3}, exposed to a UV field of G = 10^2. The figure is adapted from Hollenbach *et al.* (1991).

with H, or by reaction with He^+. Once CO has self-shielded, at about a column density of N $\approx 10^{20}$ cm^{-2}, these reactions are sufficiently slow that all the carbon is efficiently channeled into CO, even when the H_2 abundance is low. Hollenbach & McKee (1989) used in their models a carbon abundance of $x_c = 2.3\times10^4$ and predicted that for shocks with pre-shock densities 10^{3-4} cm^{-3}, the CI (492 GHz) emission will have a brightness of $3-5\times10^{-6}$ erg cm^{-2} s^{-1} sr^{-1}. For higher density gas the CI emission falls below 10^{-6} erg cm^{-2} s^{-1} sr^{-1}. Although there may be small regions of reasonably bright CI emission produced by shocks, such shocks have a low volume filling within molecular clouds and so the models of Hollenbach & McKee (1989) rule out the chemistry directly following shocks as being responsible for the observed widespread distribution of atomic carbon.

Hollenbach *et al.* (1991) extended the models of Tielens & Hollenbach (1985) to lower densities ($10^2 \leq n \leq 10^5$ cm^{-3}) and lower UV fields ($1 \leq G_o \leq 10^4$). Hollenbach *et al.* (1991) discussed the carbon chemistry in their PDR models in some detail. In a low-density PDR, most of the carbon is neutral in the midsection ($4 \leq A_v \leq 6$), thus dividing the cloud into distinct regions of the three major carbon species C^+, C and CO. The abundance curve of neutral carbon generally shows one large peak, Figure 5.7. This contrasts with the two peak structure of a high-density PDR, Figure 5.8. The density dependence of the C curve can be understood in terms of the temperature sensitivity of the reaction chain which converts C^+ to CO. OH is a key intermediary in the formation of CO, reacting with C^+ to form CO^+, which ultimately forms CO, or reacting directly with C to form CO. However, the formation of OH is quite temperature sensitive, since it is initiated by the charge-exchange reaction

$$O + H^+ \rightarrow O^+ + H \tag{5.2}$$

whose reaction rate coefficient has a small activation barrier (230 K). The temperature at a

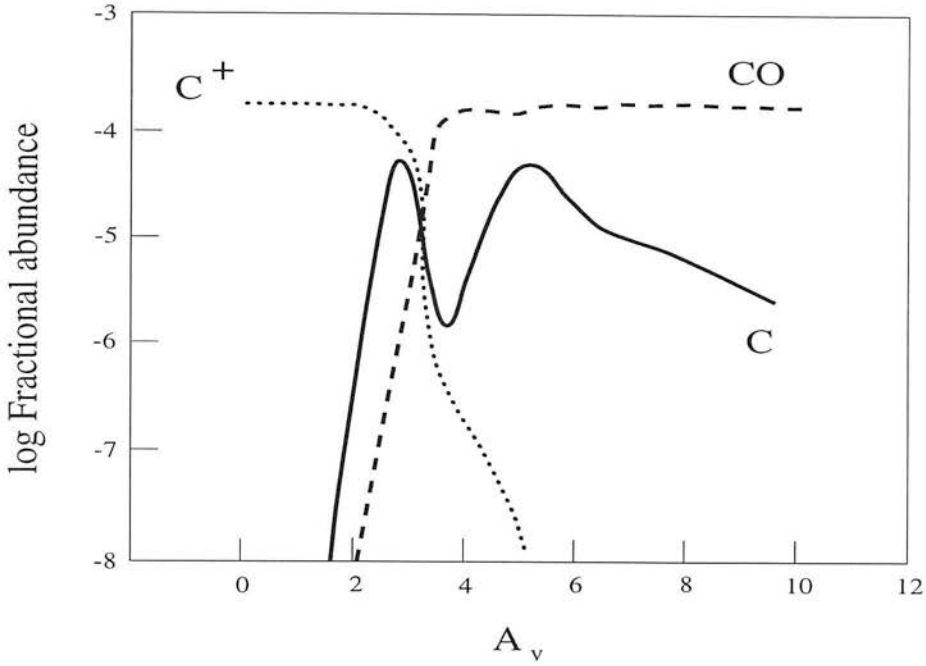

Figure 5.8: The abundances of C^+, C and CO as a function of visual extinction into a cloud. The model is that of a higher density PDR, n = 10^4 cm^{-3}, exposed to a UV field of G = 10^3. The figure is adapted from Hollenbach *et al.* (1991).

given depth in a PDR tends to increase with increasing n_0 because of the increased efficiency of photoelectric heating and collisional de-excitation of cooling transitions. Therefore, lower density, lower temperature PDRs have low rates of OH production and, consequently as A_v increases, C^+ recombines to form C, and CO only forms quite deep into the cloud. However, since the warmer, higher density models produce relatively high amounts of OH, a large fraction of CO can be formed via this reaction chain. As C^+ is channeled into CO in these models, the formation of C from the recombination of C^+ is reduced and the C abundance drops. This explains the first peak and subsequent decrease of the C abundance as a function of A_v. Further into the cloud the temperature drops and CO formation route through OH shuts off. Moreover, other reactions become important for channeling an increased amount of C^+ into C, *i.e.*

$$C^+ + S \rightarrow C + S^+ \tag{5.3}$$

which results in the second peak. The column density of atomic carbon, $N(C)$, was predicted by Hollenbach *et al.* (1991) to be of the order of 10^{18} cm^{-2}, relatively independent of n_o and G_o. Increasing G_o results in an increase of the depth into the cloud where the C^+/CO transition occurs but the column density across this transition remains constant. There is a small increase in $N(C\textsc{i})$ with decreasing density caused, as described above, by the drop in temperature with decreasing density, which tends to favour the formation of C rather than CO from C^+.

Chièze *et al.* (1991) suggested that dynamical mixing of gaseous material between diffuse regions and denser portions of molecular clouds was an efficient way of enhancing the atomic carbon abundance within the denser gas. Mixing leads to the chemical network being cyclic and obliterates the distinction between early time chemistry and steady state chemistry.

Pineau des Forêts *et al.* (1992) argued that models of the chemistry, due to the numerous linking of non-linear equations, produce two distinct phases of chemical equilibrium. The two

phases are dependent upon the local density, n_H, and the cosmic ray ionisation rate, ζ. While the rate (s^{-1}) of production of ions by cosmic rays, is independent of the density of the medium, the rate of their ultimate removal, by dissociative recombination, is proportional to the electron density. It follows that as $n_H = n(H) + 2n(H_2)$ decreases, the fractional ionisation of the gas, n_e/n_H, tends to rise. This rise in the electron density causes a decrease in the H_3^+ abundance through the dissociative recombination reaction

$$H_3^+ + e \rightarrow H + H_2 \tag{5.4}$$

H_3^+ can also be removed from the ISM through the reactions

$$H_3^+ + CO \rightarrow HCO^+ + H_2 \tag{5.5}$$

$$H_3^+ + O \rightarrow OH^+ + H_2 \tag{5.6}$$

Thus, as you increase the density these last reactions become more important than the first reaction in removing H_3^+. The ions HCO^+ and OH^+ quickly form O_2 and H_2O. Charge transfer with H^+ is the dominant means of destroying water and molecular oxygen through the reactions

$$H^+ + O_2 \rightarrow H + O_2^+ \tag{5.7}$$

$$H^+ + H_2O \rightarrow H + H_2O^+ \tag{5.8}$$

Reactions with O_2^+ and H_2O^+ decrease the electron abundance which means reactions with H_3^+ produces more HCO^+ and OH^+ which in turn produce more O_2 and H_2O which further decrease the electron abundance. This runaway means that there is a critical density, for a given cosmic ray ionisation rate, when the gas quickly switches from a high ionisation phase to a low ionisation phase. The state of ionisation of the gas plays a critical role in the chemistry of the medium. When the ionisation is high, at densities below the critical density of the phase transition, a higher fractional abundance exists for atomic carbon, Figure 5.9. The value of the critical density which separates the two regimes increases with ζ. When ζ is 2.5×10^{-17} s^{-1} the critical density is $n_H \approx 10^4$ cm^{-3}. The density of the transition between the two phases is influenced by the rate of dissociative recombination of H_3^+. This rate, experimentally, is uncertain but Pineau des Forêts *et al.* (1992) argued that recent measurements indicate that the rate is close to the high value they used.

Meixner & Tielens (1993) modelled theoretical clumpy PDRs in terms of two components, dense clumps (n $\approx 10^6$ cm^{-3}) embedded in a less dense interclump medium (n $\approx 10^3$ cm^{-3}). The UV radiation penetrates further into the clumpy region, by about an order of magnitude, and so can excite PDRs far deeper into the cloud than the plane parallel models of Hollenbach *et al.* (1991). Meixner & Tielens (1993) suggested that it is the interclump gas that dominates the emission from CI, not mini-PDRs produced on the surfaces of the embedded clumps. The clumpy model of Meixner & Tielens (1993) produces line intensities that are always higher than the homogeneous model. For CI emission the intensities are higher partly because the column density of the interclump PDR is larger than the homogeneous model column density and partly because they are the dominant cooling lines of the interclump medium.

Flower *et al.* (1994) computed models of the transition from a warm PDR to the cold, dark interior. Flower *et al.* (1994) find that the equilibrium value of the C/CO ratio in the

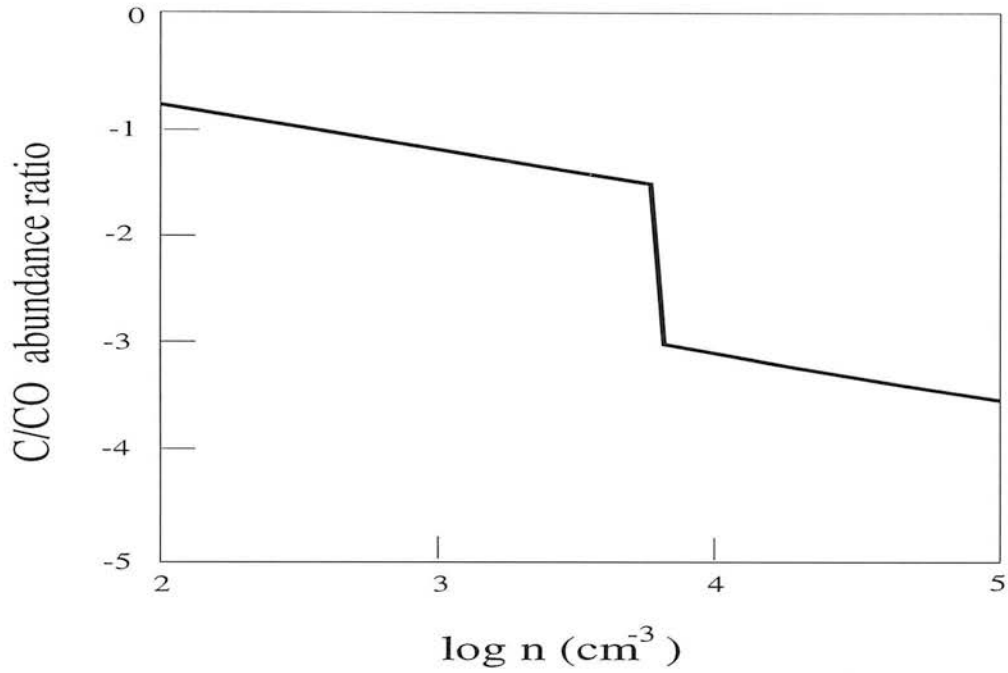

Figure 5.9: The dark-cloud abundance ratio of C to CO as a function of density, adapted from Pineau des Forêts *et al.* (1992). The phase transition in the equilibrium abundance, at a density of about 5×10^3 cm^{-3}, is due to a corresponding change in the equilibrium ionisation fraction. The ionisation fraction in turn is controlled by the cosmic ray flux.

interior is crucially dependent on the fractional ionisation of the gas, which depends upon the cosmic ray flux and the kinetic temperature. When the degree of ionisation in the cloud center exceeds a critical value, the $n(C)/n(CO)$ ratio increases by about two orders of magnitude to $n(C)/n(CO) \approx 0.1$. However, a high atomic carbon content in the interior is not reflected in the intensity of the CI emission because the high abundance is partially offset by a lower kinetic temperature in the region where CI contributes to the cooling of the medium. Furthermore, the bulk of the CI emission arises from the PDR, not from the cloud interior.

5.2.3 Extra-galactic observations of atomic carbon

Two extra-galactic sources, IC 342 and M82, have been observed in the light of CI emission. Büttgenbach *et al.* (1992), from a single spectrum of the nucleus, model the CI emission from IC 342 in terms of PDRs but which have, however, higher gas densities than are typically found in the Milky Way. In M82, Schilke *et al.* (1993) observed 5 spectra at selected positions in the nuclear region. White *et al.* (1994) have complemented the work of Schilke *et al.* (1993) by making a map of the whole region. Both groups find that the CI emission from M82 is about an order of magnitude brighter than predicted by the PDR models of Wolfire *et al.* (1990). They also find that N(CI)/N(CO) is $\sim$ 0.6 (hereafter, N(CI)/N(CO) represents the ratio of total column densities of CI and CO). Both groups find that they can explain the enhanced carbon emission by invoking the chemical models of Flower *et al.* (1994), which predicts a high abundance of CI deep in the interiors of clouds even in the absence of UV radiation. The equilibrium value of C^0/CO depends on the fractional ionisation of the gas and allow CI production in the presence of a strong cosmic ray flux. Both groups argue that there is a high cosmic ray rate (300 times the local solar neighbourhood value) in the centre of M82 and suggest

that the high carbon abundance can then be explained by these chemical models.

5.3 A summary of what is known about atomic carbon and the case for observing NGC 253

5.3.1 The present observational picture

Claims that carbon may be enhanced by shocks in S140 by Hernichel *et al.* (1992) and Minchin *et al.* (1994) have been disputed by Plume *et al.* (1994). A comparison of the spectra of Minchin *et al.* (1994) with those of Hernichel *et al.* (1992), Figure 5.5, indicates that although the strength of the wing emission appears to be of similar strength, there is a discrepancy in the peak brightness temperature of the two spectra. Furthemore, there is a discrepancy with the high S/N spectra of Plume *et al.* (1994), Figure 5.4. Moreover, inspection of the red wing of the CI spectrum of Minchin *et al.* (1994), Figure 5.5, shows that it is not of sufficient S/N to argue for a high C/CO ratio in the shocked gas. A much deeper spectrum is required before the claim can be supported, given that there are three data-sets of CI emission from S140 IRS1 which, are currently inconsistent.

Minchin *et al.* (1995) have claimed that there is no correlation between the parameters of CI emission, *e.g.* peak brightness temperatures and linewidth, with emission of isotopic CO. Such a lack of correlation would indicate that the atomic carbon and carbon monoxide are not coextensive which is contrary to what has been claimed by many investigators, *e.g.* Keene *et al.* (1985), Frerking *et al.* (1989) and Plume *et al.* (1994), who report that the spectra of CI and the low J lines of ^{13}CO are very similar. As mentioned above, the existing picture of CI emission towards S140 is controversial. It is of no surprise that Minchin *et al.* (1995) found no correlation in peak brightness temperature, as there are regions along any line of sight with different abundance ratios. It has been noted by several investigators, *e.g.* Phillips & Huggins (1981) and Keene (1995), that atomic carbon emission is reduced with respect to CO emission in the densest regions, which suggests that the C/CO ratio will be highest in low density gas. Furthermore, the critical densities of ^{13}CO 3$\rightarrow$2 and C^{18}O emission is about 3×10^4 cm^{-3} whereas the critical density of CI emission is around 10^3 cm^{-3}. It could be that towards S140, the CI emission is arising from low density gas which is not traced by the isotopic CO in the 3$\rightarrow$2 line. In such a scenario, there should be a far closer correlation in S140 by comparing the parameters of the 2$\rightarrow$1 and 1$\rightarrow$ 0 lines of isotopic CO with CI.

Previous investigators, *e.g.* Genzel *et al.* (1988), have argued that the CI emission arises from the surfaces of clumps within molecular clouds and as the UV photons can reach clumps deep within the clouds then this can explain the widespread CI emission. An alternative picture is that the bulk of the CI emission comes from the interclump medium. Such an alternative picture is attractive as this would explain the close correlation between the low J lines of CO and CI and the lack of correlation of the high J lines of CO and CI. Furthermore, this would account for why carbon is a poor tracer of dense regions. It is to be expected that there will be large regions of low density interclump gas within clouds at high extinction. Moreover, the PDR models of Hollenbach *et al.* (1991) suggest that the brightness of CI emission is independent of density. It is to be expected then that in a clumpy medium, in which the high density clumps have low volume filling factors and the interclump gas has a high filling factor, the low density gas will dominate in producing the total CI emission from the cloud.

It appears that the existing observational picture indicates that CI emission may trace rela-

tively low density gas. Furthermore, the bulk of CI emission arises towards the edges of clouds, most noticeably towards PDRs. There is still trace amounts of atomic carbon existing towards the centers of clouds, but usually in low density gas rather than in high density gas.

5.3.2 The present theoretical interpretations

Such an observational picture can be partially accounted for by several theoretical groups. Meixner & Tielens (1993) have suggested that the bulk of CI emission should arise from an interclump medium within PDRs. Flower *et al.* (1994) do not include clumps within their models but they show that the bulk of the CI arises from PDRs. Furthermore, Pineau des Forêts *et al.* (1992) show that the chemistry reaches an equilibrium with abundances that are crucially depending upon the ionisation level. In the picture of Pineau des Forêts *et al.* (1992) the low density, interclump gas has a high ionisation level and a correspondingly high C/CO and the higher density clumps have a low ionisation level and a correspondingly low C/CO. Moreover, dynamical mixing between the clumps and interclump gas will also help to enhance the C/CO ratio within the dense gas (Chièze *et al.* 1991).

If the suggestion by Minchin *et al.* (1994), White (1994) and Hernichel *et al.* (1992) that the atomic carbon abundance is enhanced due to the passage of a shock is correct, then this will provide support to the proposal of Williams & Hartquist (1984) that shocks transfer carbon-rich grain mantles from the solid phase into the gas phase. The evidence for shock-enhanced carbon is controversial and further observations are required to confirm these claims, particularly towards S140. Even if carbon is enhanced in shocks, such shocks have a low volume filling factor and they will not dominate the emission from a molecular cloud.

Towards M82, carbon seems to be far more abundant than can be accounted for by PDR models. A possible solution for the over-abundant atomic carbon in M82 is its enhancement deep within molecular clouds, above the level found from Galactic studies, possibly due to the impact of a high cosmic ray flux on dark-cloud chemistry (Schilke *et al.* 1993).

5.3.3 The case for observing NGC 253

The proposal of Schilke *et al.* (1994) and White *et al.* (1994), that the models of Flower *et al.* (1994) in conjunction with a very high cosmic ray flux produces bright carbon emission, needs to be checked in other starbursts. The cosmic ray rates are presumed similar in NGC 253 and M82; since the far-IR luminosities of the two galaxies are similar (NGC 253: $1.5\times10^{10}\,L_{\odot}$ in $\sim$ 400 pc diameter; M82: $3\times10^{10}\,L_{\odot}$ in $\sim$ 400 pc diameter), and if they have similar IMFs, the star-formation, and hence supernova rates will be comparable. If the proposal of Schilke *et al.* (1994) and White *et al.* (1994) is correct then it is to be expected that atomic carbon will also be overabundant in NGC 253.

Alternatively, standard PDR models predict that carbon emission has a fairly constant brightness for a range of UV densities and gas densities (Hollenbach *et al.* 1991). If this is the case then CI emission is a direct measure of the area filling factor of PDRs towards the nucleus of NGC 253. Carral *et al.* (1994) claim, from observations of CII, OI and the far-IR emission from NGC 253, that the area filling factor of PDRs is close to unity. Thus, a measure of atomic carbon in NGC 253 can be used to test the validity of the conclusions of Schilke *et al.* (1993), White *et al.* (1994) and Carral *et al.* (1994).

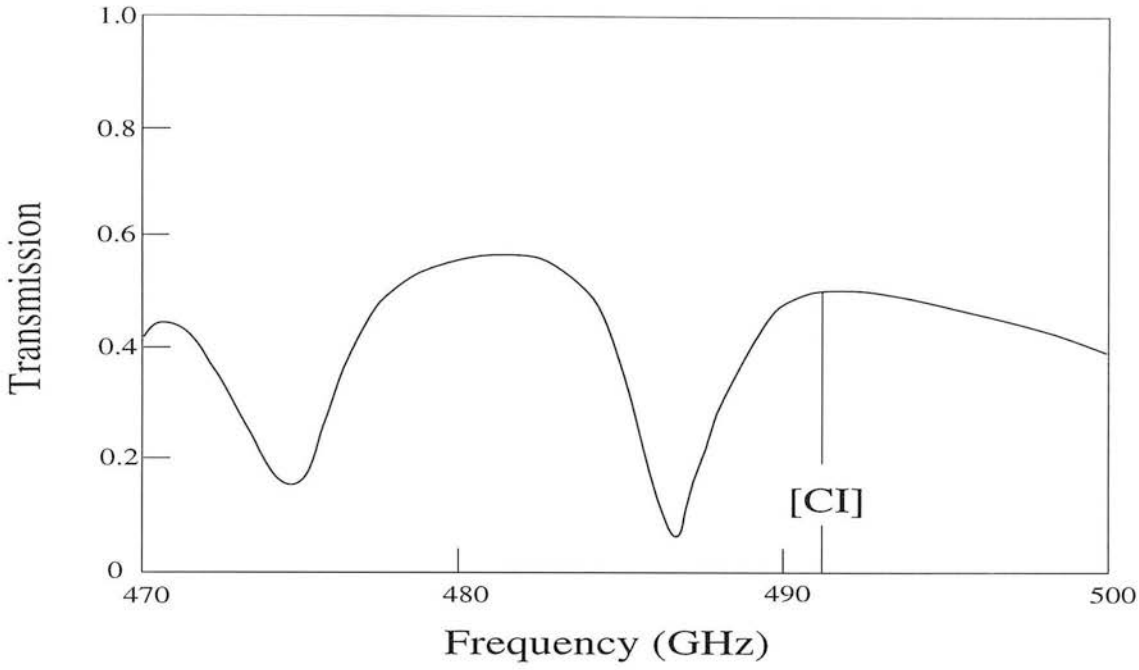

Figure 5.10: The variation of sky transmission above Mauna Kea for 0.5 mm of precipitable water vapour. The CI frequency is close to a large dip in transmission through the atmosphere. Thus, observations of CI are only feasible from a very dry site like Mauna Kea.

5.4 Observations and Results

The rest frequency of the $^3P_1 \rightarrow {}^3P_0$ transition is at 492 GHz which coincides with a transmission window in the atmosphere, Figure 5.10. The transmission at this frequency, is dependent upon the water content of the atmosphere and it is only in very dry sites, like the summit of Mauna Kea, that observations of atomic carbon are possible from the ground.

5.4.1 Observations

The observations were made with the 15 m James Clerk Maxwell Telescope (JCMT). The backend used was the Dutch Auto-correlation Spectrometer (DAS). The adopted map centre (0,0) was the nucleus of NGC 253, which was taken to be $\alpha(1950) = 0^h\ 45^m\ 05.8^s$, δ = -25° 33′ 38″. The observations were made by beam switching to a reference position 120″–150″ north of the source.

A grid of 17 CI spectra was observed towards NGC 253 on 10-11 November 1993, using the SIS receiver Rx C2 and with the DAS operated in 920 MHz bandwidth mode. The telescope efficiency was measured using Saturn and assuming a two component beam with 80% of the power in the 10″ diffraction beam and 20% of the power in a 30″ error beam.[2] This composite beam has a coupling efficiency of $\eta_{c(Sat)} = 0.71$ to Saturn (diameter of 16.3″). Correcting for this coupling, η_B (the fraction of power in the two component beam) measured from Saturn is 0.35.[3] This is effectively the coupling of the telescope to a source of roughly 60″ diameter. Saturn was used to check the pointing which was good to 2″ (rms).

[2] The parameters of the composite beam have been derived from numerous measurements of the JCMT surface and estimates of how the beam couples to calibration sources at different frequencies. The numbers I have used came from Adrian Russell (private communication) and were believed to be the best estimate of the beam working at 492 GHz in November 1993.

[3] Our estimate of the radiation temperature of Saturn should not be affected by emission from the rings as at the time of the observations the rings were nearly edge on.

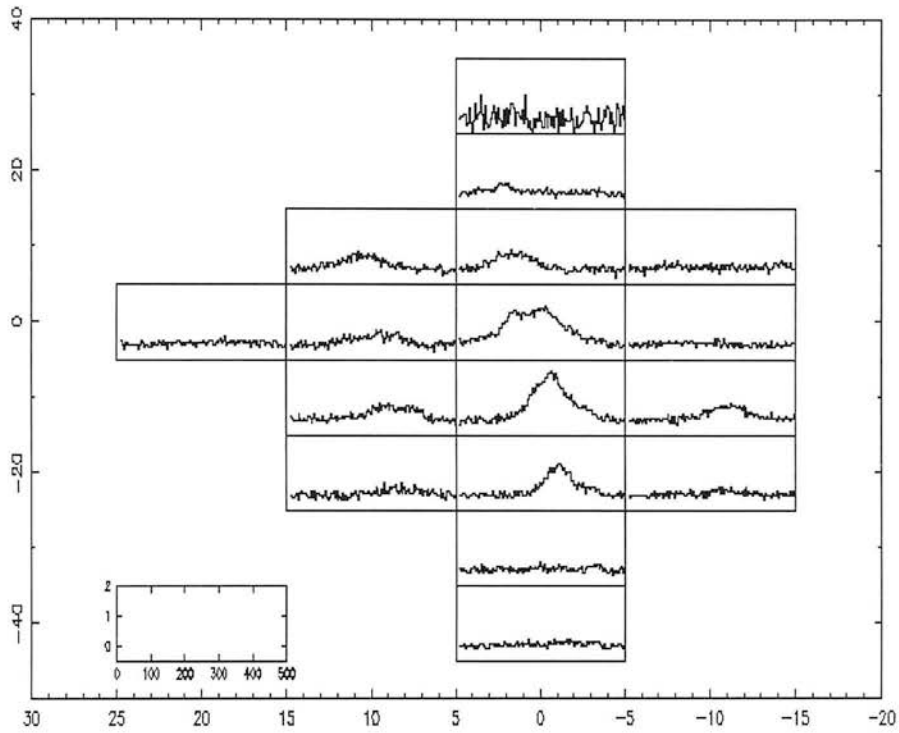

Figure 5.11: The grid map of the atomic carbon spectra observed towards NGC 253. This map is rotated by a P.A. -39^0 so that the major axis of NGC 253 is along the vertical.

5.4.2 Results

A grid of 17 CI spectra, spaced at 10″ intervals, was observed towards NGC 253 (10″ corresponds to 120 pc if NGC253 is at 2.5 Mpc). Figure 5.11 shows a rotated RA-dec map at P.A. -39° of the 16 spectra on a T_{Beam} scale ($T_{Beam}=T_A^*/\eta_B$).

CI shows a similar distribution to the CO bar (Canzian *et al.* 1988) and shows that CI and CO are tracing the same gas, *i.e.* the atomic gas is well mixed with the molecular gas, at least on a scale of 100 pc. The map of CI was convolved to a resolution of 23″ to match the ^{13}CO observations of Wall *et al.* (1991) and the C^{18}O observations (see Chapter 4 for further details on CO in NGC 253). From the central 23″ of NGC 253, the integrated intensity of CI is $\int T_{Beam} dV = 320$ K km s^{-1}. Under the assumption that the intensity of the line is directly proportional to the observed brightness temperature

$$I(CI) = 1.22 \times 10^{-7} \int T_b dV \ (erg\ cm^{-2}\, s^{-1}\, sr^{-1}) \tag{5.9}$$

492 GHz is no longer in the Rayleigh-Jeans regime and so a correction needs to be applied to the brightness temperature in order to estimate the true radiation temperature. The correction is given by

$$T_R(T_b, \nu) = \frac{h\nu}{k} \frac{1}{e^{h\nu/kT_b} - 1} = \frac{T_b}{1 + \frac{h\nu}{2kT_b} + ...} \tag{5.10}$$

which at 492 GHz becomes

$$T_R \approx \frac{T_b}{1 + \frac{11.8}{T_b}} \tag{5.11}$$

For brightness temperatures of $\sim$ 100 K the change in the intensity is of the order of 10%. With the assumption that the brightness temperature of the CI emission is about 53 K the intensity is

$$I(CI) \sim 1 \times 10^{-7} \int T_R dV \tag{5.12}$$

Equating $\int T_R dV$ with the integrated beam temperature, $\int T_{beam} dV$, and using the composite beam of the JCMT, towards the central 23″ of NGC 253, CI has an integrated intensity of $\sim 3{\times}10^{-5}$ erg cm^{-2} s^{-1} sr^{-1}. As CI has only three accessible energy states at temperatures common in the interstellar medium (T < 100 K), with energies $E_0 = 0$, $E_1/k = 23.6$ K and $E_2/k = 62.5$ K, the partition function is given by

$$Q = 1 + 3e^{-23.6/T_{ex}} + 5e^{-62.5/T_{ex}} \tag{5.13}$$

As discussed in Appendix B, the total number of atomic carbon atoms observed in an optically thin line is given by

$$N_T \approx \frac{Q}{g_J \, e^{E_J/kT_{ex}}} \frac{8\pi \, K\nu^2}{A_{J,J'}hc^3} \int T_R dV \tag{5.14}$$

The Einstein $A_{1,0}$ coefficient for CI is $A_{1,0} = 7.9{\times}10^{-8}$ s^{-1} (Nussbaumer 1971). Inserting the numerical constants for the $^3P_1 \rightarrow {}^3P_0$ line results in

$$N(CI) = 1.9 \times 10^{15} \frac{\tau_0}{1 - e^{-\tau_0}} \int T_R dV \; Q e^{23.6/T_{ex}} \; (cm^{-2}) \tag{5.15}$$

The integrated intensity ($\int T_R dV$) is in units of K km s^{-1}. The critical density for CI is 10^3 cm^{-3} (Schröder *et al.* 1991) and, given that ^{13}CO is thermalised ($n_{crit} = 3 \times 10^4$ cm^{-3} for the 3→2 transition), it is safe to assume that atomic carbon is thermalised in NGC 253. The derived column density of atomic carbon has a weak dependence on kinetic temperature—the derived column density only increases by $\sim$ 10% for gas at T = 100 K compared to gas at T = 24 K (24 K gives a lower limit to the column density).

As I discuss in chapter 4, most of the ^{13}CO emission arises from T $\sim$ 100 K gas in NGC 253 and so, under the assumption that ^{13}CO and CI are well mixed, $T_{ex} \sim 100$ K. The map of CI was convolved to a resolution of 23″, to match the ^{13}CO data. Across the central 23″, an integrated temperature of $\int T_{Beam} dV = 330$ K km s^{-1} is measured. Assuming $T_{ex} = 100$ K and the CI emission is optically thin, the column density is N(CI) = $4.8{\times}10^{18}$ cm^{-2}.

Therefore, assuming that carbon monoxide and atomic carbon are coextensive, averaged over the central 23″ of NGC 253, the abundance ratio of atomic carbon to carbon monoxide is C/CO = N(CI)/N(CO) = 4.8×10^{18} / $(2.4{\times}10^{17} \times 40)$ = 0.5.

5.5 The radiation expected from PDRs in galaxy nuclei

The bulk of atomic carbon emission in our Galaxy arises from PDRs. PDRs are where UV photons impinge upon molecular gas, producing a layer of dissociated atomic gas. The gas in the PDRs is heated through the photoelectric effect and is cooled through line emission from several gas-phase species. The balance between heating and cooling typically results in gas in the PDR reaching temperatures of several hundred K. With densities in the PDRs of typically 10^4 cm^{-3} the hot gas will collisionally excite the ions, atoms and molecules and these ions, atoms and molecules will then emit radiation, thus changing heat into radiation. Some of this

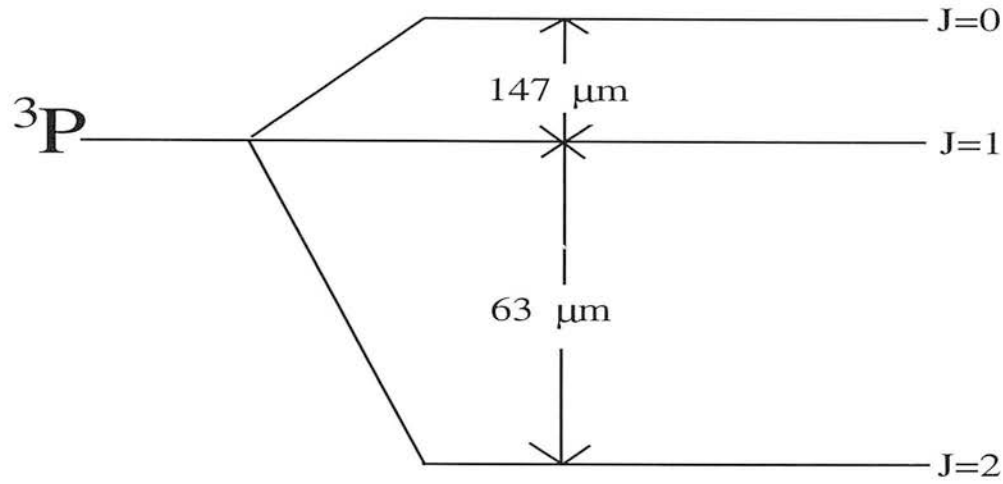

Figure 5.12: The fine-structure of the ground state of atomic oxygen. Spin-orbit interactions split the ^{3}P state into three levels: the ground state $^3P_2$; the first excited state, $^3P_1$, which is 228 K above ground; the second excited state, $^3P_0$, which is 326 K above ground. The critical density of the $^3P_1$ level is 4.7×10^5 cm^{-3} and the critical density of the $^3P_0$ state is 9.5×10^4 cm^{-3}. The degeneracy of 3 results in two fine-structure transitions—the $^3P_0 \rightarrow {}^3P_1$ line is at 147 μm and the $^3P_1 \rightarrow {}^3P_2$ line is at 63 μm. The transition $^3P_0 \rightarrow {}^3P_0$ line is a strongly forbidden magnetic quadrupole flip and is very weak.

line radiation escapes from the PDR resulting in a energy loss and thus cooling. The energy balance of the PDRs is thus controlled by how efficiently the gas is cooled through the radiation emitted from the collisionally excited species. Detailed theoretical models of the chemistry expected in PDRs have been constructed in order to show the radiation expected from PDRs for a range of UV field strengths and gas density.

An equilibrium between heating and cooling produces gas temperature in PDRs of the order of 100 K and so it is to be expected that species with energy levels above ground of about 10-1000 K will be the principal coolants. Ions and atoms have fine-structure transitions in which the levels are separated by this much and so it is these collisionally excited fine-structure transitions which are the dominant gas coolants. In particular, the high abundance of oxygen and carbon means that these two elements produce the strongest line emission.

Oxygen has an ionisation potential of 13.6 eV and so the bulk of oxygen is atomic in PDRs, where there are no photons with energy above 13.6 eV. Figure 5.12 shows how the ^{3}P state of O is split into three different levels.

Carbon has an ionisation potential of 11.26 eV and so photons with energy between 11.26 and 13.6 eV will readily ionise carbon. Thus, the bulk of the carbon expected in PDRs is singly ionised carbon. Figure 5.13 shows how the ^{2}P ground state of C^+ is split into two different levels.

The first excited state above ground for atomic oxygen, 228 K, is at a higher energy than the first excited state of ionised carbon, 92 K. Moreover, the first excited state of atomic oxygen needs a larger density to thermalise it, n = 4.7×10^5 cm^{-3}, than that of ionised carbon, n = 2.8×10^3 cm^{-3}. Therefore the ratio of atomic oxygen to ionised carbon emission is dependent upon the density and temperature in a PDR. It should be remembered that the temperature in PDRs is controlled by the density because the heating is controlled through the photoelectric effect—for denser gas, collisions will redistribute the energy stored by the species in excited

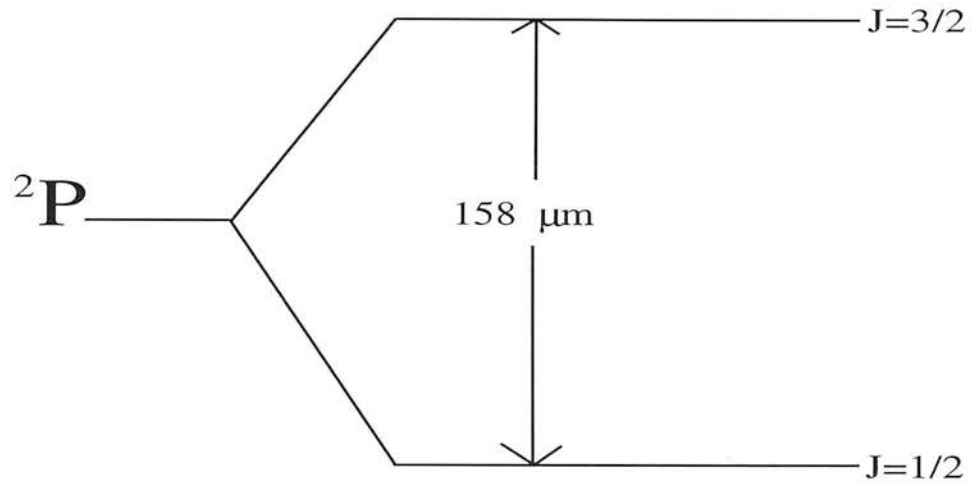

Figure 5.13: The fine-structure of the ground state of singly ionised carbon. Spin-orbit interactions split the ^{2}P state into two levels: the ground state $^2P_{1/2}$; the first excited state, $^2P_{3/2}$, which is 92 K above ground. The critical density of the $^2P_{3/2}$ level is 2.8×10^3 cm^{-3}. The degeneracy of 2 results in a fine-structure transition, $^2P_{3/2} \rightarrow {}^2P_{1/2}$, at 158 μm.

states whereas at lower densities some of this energy from the excited states will be radiated away. Therefore, the ratio of ionised carbon to atomic oxygen emission is particularly sensitive to the gas density in the PDR. Within PDRs dust grains absorb the bulk of the incident ultraviolet radiation and reradiate most of the energy in the infrared continuum. Typically $\sim$ 0.5% of the incident energy is converted to gas heating via photoelectric ejection of electrons from grains (see chapter 1 for further details). Since OI 63 μm, CII 158 μm and SiII 35 μm are the dominant cooling lines from the PDRs, the ratio of these line luminosities to that of the far-IR continuum luminosity measures the efficiency of photoelectric heating (the ratio of gas heating to grain heating by the UV flux). Lines of constant photoelectric heating efficiency should approximately follow the relation $G_o \approx n/T^{1/2}$ (Tielens & Hollenbach 1985). The temperature structure in PDRs is dependent on G_o and n and so it is possible to invert the problem in order to see what are values of G_o and n can produce the observed ratios of OI/CII and OI + CII + SiII / I_{FIR} (Wolfire *et al.* 1990, hereafter WTH). Figure 5.14 highlights how the two ratios can be used to estimate n and G_o.

Using this approach, Carral *et al.* (1994) took their observations of CII and OI, in conjunction with the FIR continuum measurements of Telesco & Harper (1980) to infer that, averaged over the central 40″ of NGC 253, a typical PDR had a density of 10^4 cm^{-3} and was exposed to a UV field $\sim 10^4$ times the intensity of the local value. Carral *et al.* (1994) argued that the observed brightness of C^+ was a factor of $\sim$ 1.5 larger than predicted by Hollenbach *et al.* (1991) for such a PDR (G = 10^4, n = 10^4) and so they suggested that the area filling factor of these PDRs is about 1.5.

As the predicted CI intensity is fairly independent of n and G, our measured intensity of the $^3P_1 \rightarrow {}^3P_0$ line should provide a measure of the number of PDRs along the line of sight, the area filling factor, if the neutral carbon emission arises solely from PDR gas (Hollenbach *et al.* 1991). Typically, the intensity of the $^3P_1 \rightarrow {}^3P_0$ line from a face-on PDR is 2×10^{-6} erg cm^{-2} s^{-1} sr^{-1} (Hollenbach *et al.* 1991). From the central 23″, $< I_{CI} > \sim 4\times10^{-5}$ erg cm^{-2} s^{-1} sr^{-1} indicating that the area filling factor is $\sim$ 20. This is clearly inconsistent with the value of 1.5 suggested by Carral *et al.* (1994).

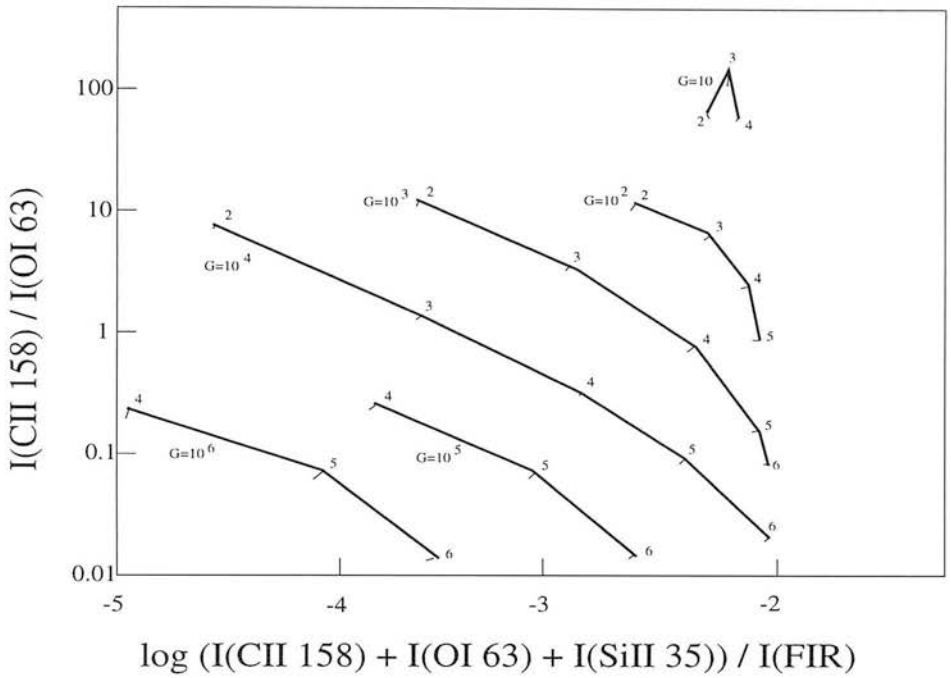

Figure 5.14: The ratio of CII 158 μm / OI 63 μm intensities vs. the ratio of (I(OI 63 μm) + I(CII 158 μm) + I(SiII 35 μm))/I(FIR) intensities, adapted from Wolfire *et al.* (1990). Tick marks are labelled with log n cm^{-3} and are spaced at one decade intervals along lines of constant G_0 .

5.5.1 Estimating PDR parameters using far-infrared radiation.

Carral *et al.* (1994) used the KAO to observe various fine-structure lines from NGC 253. They observed CII 158 μm with a 41″ beam and reported a flux of 4.8×10^{-18} W cm^{-2}, and OI 63 μm with a 42″ beam and reported a flux of 4.5×10^{-18} W cm^{-2}. If NGC 253 is assumed to be at 2.6 Mpc then the sum of the OI and CII line luminosities is 1.6×10^{7} L$_\odot$. Telesco & Harper (1980) reported a far-IR continuum luminosity of 1.6×10^{10} L$_\odot$.[4]

An initial expectation is that the CII, OI and FIR continuum emission from PDRs in NGC 253 arises from the same source area and so the luminosity values can be compared without knowledge of the source size. A problem is how much of the emission arises from outside PDRs. The ionisation balance in HII regions results in some O^0 and C^+ in the plasma. Oxygen has an ionisation potential similar to hydrogen, Table 5.1, and a rapid charge exchange reaction proceeds between the two species. This results in the O^+/O ratio being nearly identical to the H^+/H ratio in HII regions. Therefore, the O^0 abundance is extremely low, and the OI 63 μm contribution from HII regions is insignificant (Lord *et al.* 1996).

However, the contribution of CII emission from HII regions is not negligible. The contribution of CII from HII regions in NGC 253 is estimated to be about 30% by Carral *et al.* (1994). This fraction is dependent on the effective temperature of the stars, the electron density of the HII regions and the number of Lyman continuum photons generated by the central cluster of O and B stars at the centre of the HII region, Figure 5.14.

Hence, the observed PDR luminosity ratios from the nucleus of NGC 253 is I(OI)/I(CII) = 0.75 and (I(OII) + I(CII))/I(FIR) = 9×10^{-4}. The SiII line at 35 μm is the brightest far-IR line in

[4] Telesco & Harper claimed a luminosity of 2.8×10^{10}L$_\odot$ but this was derived assuming NGC 253 was 3.4 Mpc distant, not 2.6 Mpc

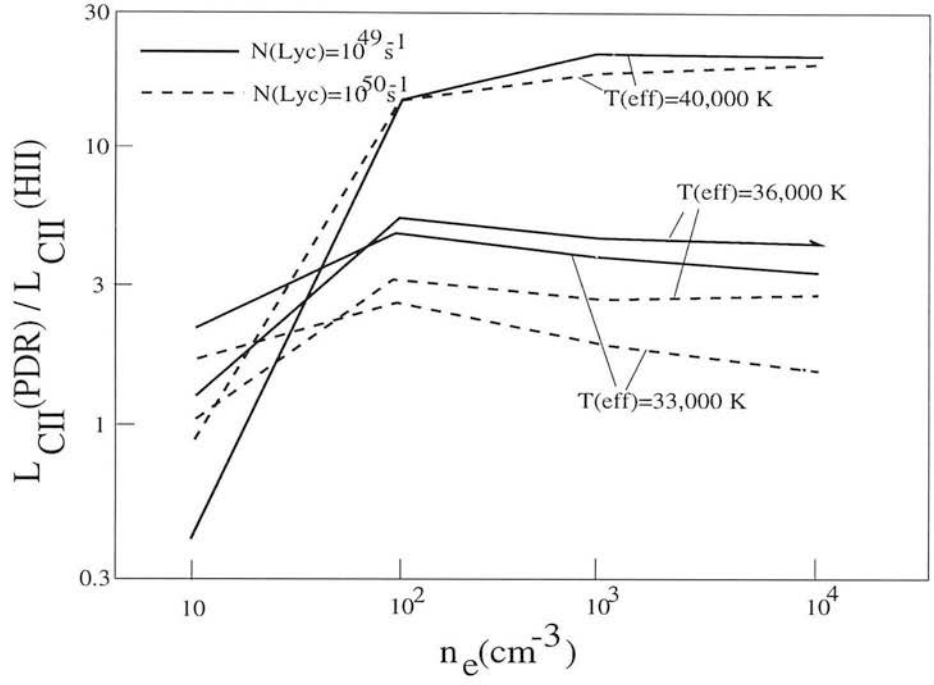

Figure 5.15: The ratio of CII(158 μm) PDR luminosity, L_{CII}(PDR), to CII HII region luminosity, L_{CII}(HII), as a function of electron density in the ionised gas, calculated for $N_{Lyc} = 10^{49}$ s^{-1} (solid line) and 10^{50} s^{-1} (broken line), with T_{eff} = 33,000, 36,000 and 40,000 K as indicated. The figure is adapted from Carral *et al.* (1994).

NGC 253 but Carral *et al.* (1994) have argued that this line is overabundant because there is a far higher gas phase abundance of silicon than expected because of grain destruction. Furthermore, Carral *et al.* (1994) suggest that the dominant contribution to the line flux in NGC 253 is from HII regions, rather than from PDRs. Therefore it may be hazardous to use the observed intensity in NGC 253 and compare it with the PDR models of WTH. The comparison of the above luminosity ratios with Figure 5.14 suggests that a PDR model with n $\sim 10^4$ cm^{-3} and $G_o \sim 10^4$. Inspection of Figure 5.14 suggests that even if the SiII flux is included in the overall cooling budget, estimates of n $\sim 10^4$ and $G_o \sim 10^4$ would still be obtained from this figure.

5.5.2 The size of the starburst in NGC 253

The molecular gas in NGC 253 will be contained in clouds that will fill the starburst in some manner. Without prior knowledge of the actual clouds positions there is a need to rely on information about an "average" cloud. I consider a mixture of clouds of comparable sizes spaced homogeneously throughout the region of interest. WTH defined λ as the mean cloud separation along a line of sight. Since the clouds are optically thick to far-UV radiation, the far-UV light leaving a star (or central engine) only travels on average a distance λ which is given by:

$$\lambda = \left(n_c \pi r_a^2\right)^{-1} \tag{5.16}$$

where n_c is the mean space density of clouds and r_a^2 is the typical radius of a cloud. The clouds have a mean space density of

$$n_c = \frac{N_{cloud}}{\frac{4}{3}\pi R^3} \tag{5.17}$$

where N_{cloud} is the total number of clouds distributed within a radius R. The radius of the clouds, r_a, can be estimated by knowing the area, Φ_A, and volume, Φ_V, filling factors of the clouds through

$$r_a = \frac{\Phi_V R}{\Phi_A}\xi \tag{5.18}$$

where ξ is a correction factor which depends on the geometry of the UV sources[5]. The number of clouds, N_{cloud}, is simply related to Φ_V, R and r_a through

$$N_{cloud} = \Phi_V \frac{R^3}{r_a^3} \tag{5.19}$$

It follows, from equations 5.16-5.19, that

$$\lambda = \frac{4\xi R}{3\Phi_A} \tag{5.20}$$

Towards the central 23″ of NGC 253, Mauersberger *et al.* (1996) measure the CO 1-0 brightness temperature to be $\sim$ 4 K. They suggest that most of the molecular gas has a kinetic temperature of $\sim$ 40 K, which suggests that the area filling factor of the molecular gas is around 0.2.[6] Hence, if the clouds are homogeneously mixed with the stars across the central 23″ of NGC 253 (R = 150 pc if NGC 253 is at a distance 2.6 Mpc, $\xi = 4$) then

$$\lambda = 4kpc \tag{5.22}$$

As λ is the mean distance the UV photons travel before being absorbed this highlights that the far-IR luminosity, which is reprocessed UV, would only trace a small fraction of the total bolometric luminosity emitted by NGC 253. More importantly, much of the nuclear radiation would be absorbed further away from the nucleus and so the far-IR radiation would not be centrally concentrated as is observed. A homogeneous mix of stars and gas is not, therefore, representative of the central 23″.

Telesco & Harper (1980) estimated a lower limit of 7″ for the source diameter at 60 μm by assuming optically thick thermal emission from dust grains with temperatures of $\sim$ 40 K. Telesco *et al.* (1993) observed NGC 253 at 30 μm and suggested that the bulk of the far-IR luminosity is coming from a small compact region of half-intensity size $\sim 7'' \times 3''$. These values appear to be in conflict with Telesco & Harper (1980) but they indicate that the starburst in NGC 253 is compact and has a size of about $\sim$ 8″. This is the size in which the bulk of the UV generated in the starburst has to be absorbed and reprocessed. Our observations of Brγ, discussed in chapter 3, suggest that the FWHM source size of the HII regions is also $\sim$ 8″.

Equation 5.20 indicates that for λ to be comparable to R, then Φ_A needs to be close to, or greater than, unity. This produces a further constraint because it is likely that much of the molecular gas towards the nucleus will be exposed to a high UV field. Wolfire *et al.* (1989) discussed the CO 1-0 emission expected from PDRs. Most of the emerging CO 1-0 emission is

[5] For clouds illuminated by a UV radiation field over 4π sr, as for clouds in an interstellar radiation field, $\xi = 4$ (this corresponds to the surface area $4\pi r^2$ of a cloud divided by its projected area πr^2). For the cases of an AGN or a very close association of stars and clouds, $\xi = 1$.

[6] As discussed in Appendix B, the area filling factor, Φ_A, can be derived from

$$T_{MB} = \eta_{coupling}\Phi_A T_B \tag{5.21}$$

where $\eta_{coupling}$ is the coupling of the telescope to the source. For the 23″ IRAM beam coupled to the 23″ gaussian source of NGC 253, $\eta_{coupling}$ would be 0.5 and so Φ_A is then twice the observed temperature divided by the radiation temperature of the optically thick CO. I have taken the radiation temperature of CO to be the kinetic temperature, 40 K.

produced close to the C^+/CO transition region and so the emission depends mainly on the gas temperature in this transition region. The gas temperature at this point depends on the local far-UV flux, and is therefore relatively constant, typically about 100 K. A region of source size R will therefore have an emitted radiation temperature of

$$T_R \approx \Phi_A * 100K \tag{5.23}$$

but saturating at $T_R \approx 100$ K when $\Phi_A \geq 1$. This assumes that there is no foreground gas at a lower temperature. Mauersberger *et al.* (1996) observed CO 1-0 towards the nucleus of NGC 253 with the IRAM telescope, which has a 23″ beam at the CO 1-0 frequency. They reported a main beam brightness temperature of $T_{MB} \approx 4$ K. The total CO emission from NGC 253 is from a bright nuclear region and a colder bar. There is almost certainly a change in the CO brightness and kinetic temperature along the bar. It is possible to set up an upper limit on the nuclear region by assuming that all the emission, reported by Mauersberger *et al.* (1996), is from the central source.

For example, the coupling between the 23″ IRAM dish and a 8″ face-on disk nucleus is 0.08. In this case, this would suggest that Φ_A is about 0.5 for the 8″ disk. If Φ_A is unity, and assuming that there is no foreground gas towards the nucleus, the CO disk size is ~ 5-6″. If there is cold foreground gas towards the nuclear disk, the estimated source size is greater than 6″. Alternatively, including the contribution of the bar to the overall CO emission budget results in an estimated nuclear disk size smaller than 5″.

Mauersberger *et al.* (1996) also reported observations of CO 2-1 towards the centre of NGC 253. At 230 GHz they quoted the IRAM beam as consisting of 2 components, the 12″ diffraction beam which contains 70% of the power and a 3′ error beam which contains 30% of the power. Mauersberger *et al.* (1996) reported a maximum T_{MB} of ~ 6 K. Under the assumption that PDRs produce CO 2-1 emission that goes optically thick at a temperature of ~ 100 K, a similar analysis to that discussed above indicates that a disk of about 5″, with an area-filling factor of unity, can explain the observations of Mauersberger *et al.* (1996). The same uncertainties, due to cold foreground gas and emission from the bar, still apply.

From the above discussion, it is clear that there is some uncertainty in the actual limits to the scale of the starburst but because the dust has to be reprocessed on a scale of about 8″, there has to be a small compact region of star formation of size ~ 8″ that has an area filling factor of molecular gas close to unity. The starburst cannot be too large otherwise this conflicts with observations of CO. Therefore, it is likely that the starburst in NGC 253 is within a region of 8″. If NGC 253 is at a distance of 2.6 Mpc, the starburst is within a diameter of about 100 pc and is generating a luminosity of over 10^{10} $L_\odot$.

5.5.3 The average UV field within the starburst

WTH discussed how the UV field is dependent on the spatial relationship between the stars/AGN producing the UV and the molecular clouds that absorb this UV field, Figure 5.16.

The first case that WTH discussed was if the stars are closely associated with molecular clouds—panel a) in Figure 5.16. In this case, the incident far-UV flux, in Habing units, is given by

$$< G_0 >^{OB} \simeq 1.0 \times 10^{-2} \left(\frac{L_*}{L_\odot} \right) r_{pc}^{-2} \tag{5.24}$$

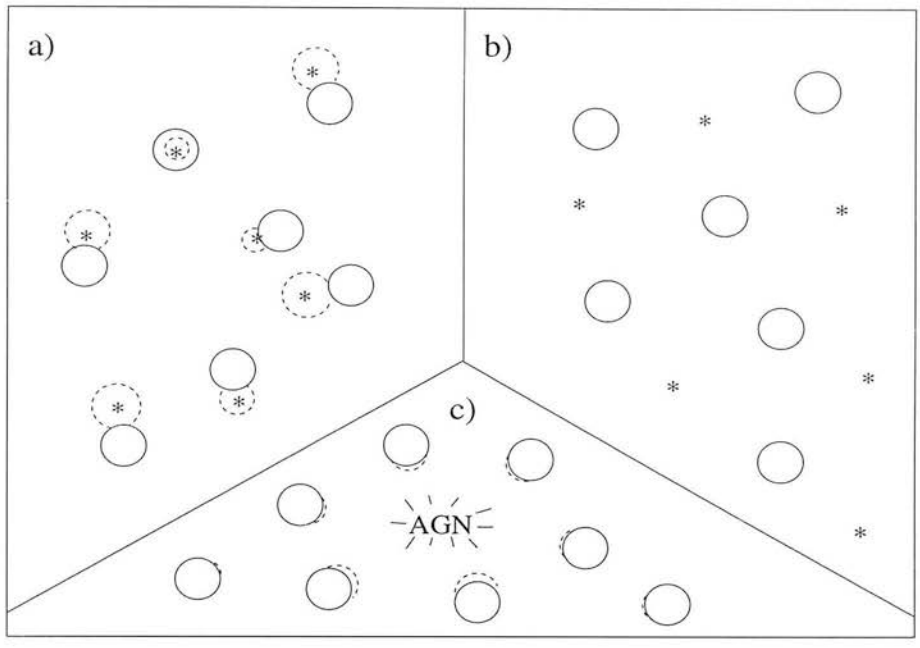

Figure 5.16: Panels a),b) and c) show three scenarios for the illumination of clouds in the nuclei of infrared galaxies such as NGC 253, adapted from Wolfire *et al.* (1990). In a) OB stars are closely associated with the clouds; in b) OB stars are randomly placed with respect to the clouds, and the far-UV field on the clouds is the average interstellar field; in c) an AGN dominates the excitation of the clouds. Dotted lines represent HII regions.

where L_* is the stellar or OB association luminosity and r_{pc} is the distance from the stars to the molecular gas.[7] For OB associations and their neighbouring clouds such as Orion, using equation 5.24, with estimates of L_* and r_{pc}, indicates that $< G_0 >$ is 10^{4-5}. Equation 5.24 can be used to estimate G_o at a radius of 50 pc in the limit that the nuclear region is a supercavity filled with O and B stars, in which there is no absorption of UV—in this case all the UV is absorbed and reprocessed in the PDR skin enveloping the cavity. The far-IR luminosity of 1.6×10^{10} $L_\odot$ results in a UV field estimate of $G_o \approx 6.4\times10^4$. This would also be the UV field if a central engine was responsible for the luminosity, although of course the situation would be complicated because the spectrum may have a smaller/larger contribution of power in the far-UV range. If a central engine is responsible and the clouds fill the region, as in panel c) in Figure 5.16, then the average UV flux upon on the clouds is given by

$$< G_0 >^{AGN} \simeq 3.0 \times 10^{-2} \left(\frac{L_*}{L_\odot}\right) r_{pc}^{-2} \tag{5.25}$$

which results in an estimate of $< G > \approx 1.9\times10^5$. If the total nuclear luminosity, L_{IR}, is produced by a random distribution of stars, then the mean distance between stars is given by

$$d_* \approx \left[\left(\frac{L_{IR}}{L_*}\right) / \left(\frac{4}{3}\pi R^3\right)\right]^{-1/3} \tag{5.26}$$

where L_* is the average stellar luminosity. In this case, the far-UV flux incident on clouds is dominated by the average interstellar radiation field, ISRF—panel b) in Figure 5.16. For this case, the Habing flux incident on the clouds is given by

[7] Equation 5.24 has taken into account the expected factor of 2, appropriate for B stars, in the ratio of the total luminosity to that of the luminosity between 6 and 13.6 eV, Wolfire *et al.* (1989). For O stars about equal amounts of energy are radiated above and below the Lyman limit, while the stellar flux below 6 eV is negligible. Thus, like B stars, O stars emit half their energy in the far-UV band of G_I.

$$< G_0 >^{ISRF} \simeq 3.0 \times 10^{-2} \left(\frac{L_{IR}}{L_\odot}\right) r_{pc}^{-3} \lambda_{pc} \left[1 - e^{-R/\lambda}\right] \quad (5.27)$$

As discussed above, there is a lot of uncertainty in λ. Under the assumption that $\lambda \approx R$, equation 5.27 leads to an estimate of $G^{ISRF} \sim 1.2 \times 10^5$. This estimate can be lowered if λ is greater than R but then there is the worry of keeping the far-IR emission in a small region.

Summarising the above, the small size of the starburst and the large luminosity coming from such a region lead to the conclusion that the average UV field, G, is high within the starburst. There is some uncertainty in the true value because of uncertainties about geometry, but it is clear that G_o has to be greater than 10^4, and is probably closer to 10^5. This is close to the strength of the UV field towards the PDR in the Orion bar but in NGC 253 this scale of star formation covers a region $\sim$ 100 pc across.

5.6 The CII emission from NGC 253 is too bright to be explained by PDR models

Summarising the previous few sections, Carral *et al.* (1994) suggested that the typical PDRs in NGC 253 have a density of 10^4 cm^{-3}, are exposed to a UV field of $\sim 10^4$ and cover the central 23″ of NGC 253 with an area-filling factor around unity. Observations of atomic carbon are too bright to be consistent with this description of PDRs in NGC 253. Considerations of the size and luminosity of the emission from NGC 253, using mid- and far- IR observations, lead to the conclusion that the starburst is on the scale of about 100 pc ($\sim$ 8″), rather than $\sim$ 300 pc ($\sim$ 23″) estimated by Carral *et al.* (1994), and the UV field strength is greater, by maybe an order of magnitude, than 10^4 times the local value. In this section I discuss the possibility of reconciling the observations reported by Carral *et al.* (1994) with other observational constraints of NGC 253. I conclude that the flux of CII emission reported by Carral *et al.* (1994) is about 10× higher than is predicted by theoretical models of PDRs in NGC 253.

5.6.1 Emission from PDRs exposed to a high UV field

Carral *et al.* (1994) reported line fluxes. To convert the line fluxes reported by Carral *et al.* (1994) into intensity units, a knowledge of the source size from which the lines are emitted is needed. Decreasing the source size results in an increased intensity. As discussed below, the fine-structure lines start to saturate at certain intensity levels, either caused by optical depths increasing to large numbers or because there is a limit to the column density of a given species that can be produced in a PDR.

For a given density, n_H, the CII intensity effectively saturates at large UV fields because for such high radiation fields the total column density of CII is determined by the dust penetration depth of the UV photons, which varies only logarithmically with the UV field (Stacey *et al.* 1991). For smaller UV field intensities, the CII intensity decreases rapidly with decreasing G_o because the CII column density is then determined by the CII formation rate, which is proportional to the UV field intensity. Moreover, as the UV field is reduced a decreasing fraction of the CII emitting gas is at a temperature which is above the transition (92 K) of the 158 μm line. If $n < n_{cr}$ then the first excited state is subthermally populated and the population in the excited level, N_2, falls as $N_2 \propto nN(C^+)$. Thus, for the same far-UV field the CII intensity scales with n for a low density PDR. Figure 5.17 shows graphically how the CII intensity is related to density and UV field.

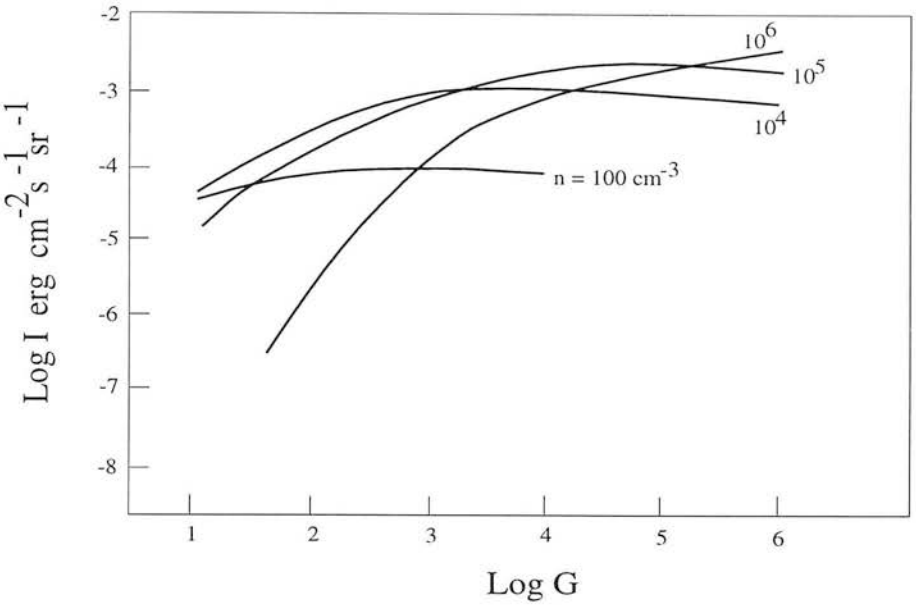

Figure 5.17: Calculated CII intensity emitted from a PDR vs. incident far-UV flux G_o, for different densities. At the highest UV fields the CII intensity saturates at few $\times$ 10^{-3} erg cm^{-2} s^{-1} sr^{-1}. The figure is adapted from Wolfire *et al.* (1989).

The emergent intensity of OI 63 μm, unlike CII, increases monotonically with the gas density and the UV field. The line reaches an optical depth of a few in the photoelectrically heated region. Figure 5.18 shows graphically how the OI intensity is related to density and UV field. In the previous section it was argued that the size of the starburst is close to 8″. If it is assumed that all the OI emission is generated in this region then the flux measurements of Carral *et al.* (1994) indicate that the OI intensity expected from the central 8″ is $\approx$ 0.04 erg s^{-1} cm^{-2} sr^{-1}. If the PDRs cover the 8″ with a filling factor of unity, this intensity is consistent with the theoretical models of PDRs, with $G_o = 10^{4-5}$ and n = 10^{4-5} cm^{-3} (Burton *et al.* 1990).

5.6.2 The CII emission from the PDRs in NGC 253

Carral *et al.* (1994) estimated the FWHM of the CII line to be $\approx$ 217 km s^{-1} and $V_{LSR} \approx$ 182 km s^{-1}. They noted that these values are very similar to the measurements of ^{13}CO 3-2 reported by Wall *et al.* (1991). As the ^{13}CO 3-2 is centrally concentrated this suggests that the CII emission is also centrally concentrated. Carral *et al.* (1994) argued that the line shift of the C^+ emission is only $\sim \frac{1}{4}$ of the line width and therefore it was likely that a significant contribution to the C^+ emission is coming away from the nucleus. In chapter 3 I discuss near-IR spectroscopy using a 3″ pixel size. Both the H_2 and Brγ emission show a velocity dispersion of about 200 km s^{-1}. Furthermore, the H_2 emission, which is tracing PDRs, shows quite a steep rotation curve towards the nucleus, which acts to broaden any line. Therefore, a FWHM of about 200 km s^{-1} for the C^+ line is not inconsistent with the emission being centrally concentrated in the nuclear starburst.

Crawford *et al.* (1985) reviewed how observed intensities of CII can be used to estimate the column density of the C^+ ions. The degeneracy of the ^{2}P ground state of the C^+ ion is only two and so the calculation of the partition function, and level filling, is straightforward. For collisional excitation, the integrated line intensity (ergs cm^{-2} s^{-1} sr^{-1}) in the optically thin limit is given by

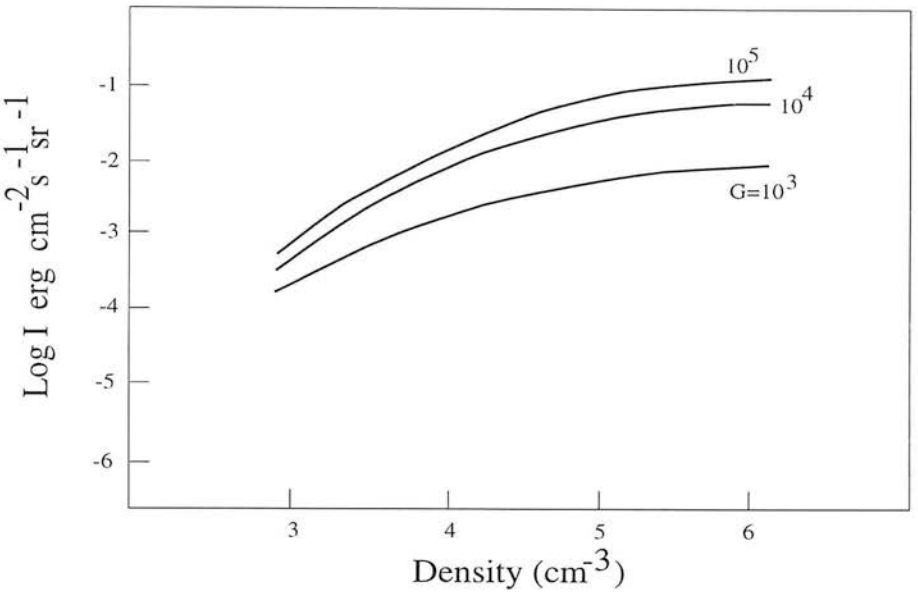

Figure 5.18: Calculated OI intensity emitted from a PDR vs. density n, for different UV field strengths. The OI intensity reaches values of few $\times$ 10^{-1} erg cm^{-2} s^{-1} sr^{-1}. Comparison with the predictions of CII indicates that in the G_o, high n the OI intensity will be the dominant coolant of the PDR gas. The figure is adapted from Burton *et al.* (1990).

$$I_{CII} = \frac{h\nu A}{4\pi}\left[\frac{g_u/g_l e^{-h\nu/kT}}{1+g_u/g_l e^{-h\nu/kT}+n_{crit}/n}\right] N_{C+}\Phi_b \tag{5.28}$$

where Φ_b is the beam filling factor, g_u/g_l is the ratio of statistical weights in the upper and lower levels, ($g_u/g_l = 2$), and N_{C+} is the column density of C^+. At high densities ($n \gg 4\times10^3$ cm^{-3}) and temperatures ($T \gg 91$ K), the intensity of the 158 μm line is proportional to the column density of C^+ ions through

$$I_{CII} = 5\times10^{-4} N_{C+}[17.5]\Phi_B \ \ ergs\ s^{-1}\ cm^{-2}\ sr^{-1} \tag{5.29}$$

where $N_{C+}[17.5]$ is the column density of C^+ in units of 3×10^{17} cm^{-2}. The optical depth of the CII line is given, after some algebra and use of the equations in Appendix B, by

$$\tau_{CII} = \frac{c^3 A}{8\pi\nu^3\Delta V}\left[\left(1+\frac{n_{crit}}{n}\right)e^{h\nu/kT}-1\right]\left(\frac{g_u/g_l e^{-h\nu/kT}}{1+g_u/g_l e^{-h\nu/kT}+n_{crit}/n}\right) \tag{5.30}$$

which in the high-density and high-temperature limit becomes

$$\tau_{CII} = 1.63\times10^{-1} N_{C+}[17.5]\Delta V_5^{-1}\left(\frac{91K}{T}\right) \tag{5.31}$$

where ΔV_5 is the equivalent velocity with of the line in units of 5 km s^{-1}. Assuming the CII flux comes from the 8″ starburst region, the PDRs fill the beam with a factor unity, and these PDRs have a temperature of 240 K, the average optical depth in the CII line is

$$\tau_{CII} \approx \frac{5}{\Delta V_5} \tag{5.32}$$

So, unless the PDRs in NGC 253 have a velocity dispersion greater than 25 km s^{-1}, the optical depth of the CII line will be greater than unity. This conclusion is for the case in which the PDRs fill the central 8″ with a factor unity. It is always possible that the central

8″ have a filling factor of PDRs which is greater than unity. It should be noted that under the assumption that the CII intensity arises solely from the central 8″, the intensity of the CII line is $\approx$ 0.04 erg s^{-1} cm^{-2} sr^{-1}. This is a factor of 10 greater than the saturated intensity expected from dense, high G_o, PDRs. This suggests that the minimum area filling factor of PDRs towards the central 8″ is around 10. If each PDR has a velocity dispersion of less than 20 km s^{-1} then it is possible to shield 10 PDRs along each line of sight with no shadowing in velocity phase space, and still keep within the total observed FWHM of the CII line.

An independent estimate of the area filling factor of the PDRs is through observations of atomic hydrogen. At the front of a PDR exposed to UV photons there is a layer in which the molecular hydrogen is dissociated and the dominant species, in terms of mass, is atomic hydrogen. The column density of HI in this layer is dependent on how far the UV travels as well as the density of the layer (Sternberg 1988)—the HI column density in a PDR depends on the ratio between the impinging UV field strength, G_o, and the molecular cloud density, n_o through

$$N_{HI} = 5 \times 10^{20} \; ln\left(90\frac{G_0}{n_0} + 1\right) \; cm^{-2} \tag{5.33}$$

For a UV field of 10^4 and density 10^4 cm^{-3}, each PDR produces a column density of atomic hydrogen of $N_{HI} \approx 2{\times}10^{21}$ cm^{-2}. This value is fairly insensitive to changes in the estimate of $G_o/n = 1$. Therefore the column density of atomic hydrogen produced towards the central 8″ of NGC 253 is

$$N_{HI} = 2 \times 10^{21} \Phi_B \tag{5.34}$$

Combes *et al.* (1977) made a map of HI in NGC 253 with a synthesised beam of 2′ × 3′. After correction for absorption from the nuclear region they derived a maximum HI column density towards the nucleus of $1.3{\times}10^{22}$ cm^{-2}. If this is the column density over the central 8″, it suggests, from equation 5.34, a beam filling factor of 6-7. This estimate would be lowered, if in fact higher resolution observations showed that much of the emission detected by Combes *et al.* (1977) came from outside the nucleus, or raised, if most of the emission came from the nucleus and the strength of the nuclear emission was diluted by the large beam of Combes *et al.* (1977). Unfortunately, there are currently no observations of HI at a high enough resolution to estimate the column density of HI produced only in the nuclear region.[8] Therefore, observations of atomic hydrogen do not, currently, constrain the beam filling factor of PDRs in the nuclear region of NGC 253.

An indirect approach to estimate the area filling factor of the PDRs is through estimates of the extinction in the region. Sams *et al.* (1994) observed near-IR images of the J and K emission from the nucleus of NGC 253. They suggested that the underlying IR emission from stars is relatively smooth but patchy extinction results in varying near-IR brightness across the starburst. Sams *et al.* (1994) estimated that the patchy emission was due to foreground extinction of $A_v \approx$ 1-5. Estimates of extinction are prone to uncertainties caused by the unknown spatial relationship between the sources of emission and the dust causing the extinction, with large differences in the estimated extinction resulting from the assumption that all the dust is foreground to the emission, compared to estimates obtained with the assumption that the emission is well mixed with the dust, Puxley (1991). Even with these uncertainties, the observations of Sams *et al.* (1994) indicate that the average extinction across the starburst in NGC 253 will

[8] It is noted that HI measurements are potentially powerful estimates of the area filling factor of PDRs in galaxy nuclei where there are strong UV fields impinging upon molecular gas.

be no more than 10. The C^+/CO transition in PDRs typically occurs at $A_v \approx 5$. Therefore it is not possible for the beam filling factor of PDRs to exceed ~ 2 before it becomes a conflict with the estimates of extinction obtained in the near-IR. Of course, a way out of this constraint would be for all the PDRs to be behind the IR emission sources but this is highly contrived. More realistically, the estimates of extinction by Sams *et al.* (1994) are consistent with a maximum PDR beam filling of around unity or less. Of course, the discussion in the previous paragraph shows that this filling factor can be checked by high resolution observations of HI which would show an average column density of HI around 2×10^{21} cm^{-2} across the central 8″ of NGC 253. If therefore, the area filling factors of PDRs towards NGC 253 is close to unity then CII 158 μm will almost certainly be optically thick.

5.6.3 The CII emission from HII regions in NGC 253

Carral *et al.* (1994) argued that maybe up to 30% of the observed CII emission arose from HII regions. Figure 5.15 shows the results of a model run by Carral *et al.* (1994), illustrating the relative contribution to the C^+ emission budget from PDRs and HII regions. Inspection of Figure 5.15 shows that one of the major factors controlling the relative contributions from the HII region and the surrounding PDR is the number of Lyman continuum photons emitted by the central source(s).[9] As I argue in chapter 3, it is likely that the nucleus of NGC 253 contains several giant clusters of O and B stars. In the case of giant O and B clusters, the ratio of HII CII to that of PDR CII approaches its maximum. A limit to the number of Lyman continuum photons produced by a cluster is that of the maximum number of Lyman continuum photons emitted by NGC 253, 2×10^{53} s^{-1} (Beck & Beckwith 1984). If I make a very conservative estimate, that the most copious O and B association produces 5×10^{51} s^{-1}, a rough extrapolation of Figure 5.15 leads to the conclusion that for this OB association the ionised plasma contributes almost as much as the PDR to the total CII emission. Increasing the number of Lyman photons generated in each O and B cluster, which is more realistic, strengthens the conclusion that the HII regions provide at least 40% of the total CII flux from NGC 253.

5.6.4 Summary

Summarising the above discussion, PDRs of $n \sim 10^{4-5}$ cm^{-3} exposed to UV fields of $G_o \sim 10^{4-5}$ fill the central 8″ of NGC 253 with a factor of order unity. These PDRs can only account for about 10% of the observed CII 158 μm emission. CII is so bright that it is almost certainly tracing optically thick gas. Some solution is needed that will put more ionised carbon into the theoretical PDR models so as to make their predictions consistent with the observations of NGC 253.

5.7 The CI emission is too bright to be explained by PDR models

Atomic carbon should be quite a robust diagnostic of PDR gas since the $^3P_1 \rightarrow ^3P_0$ intensity is predicted to be fairly insensitive to both the density, n_o, and the UV field, G_o (Hollenbach

[9] The CII flux expected from a HII region should be proportional to the number of Lyman continuum photons whereas the UV flux impinging upon PDRs is proportional to the number of Lyman continuum photons divided by the surface area of the Strömgren sphere. It should be remembered that the CII intensity saturates at the highest UV fluxes. The highest fluxes are obtained when there is a large cluster of O and B stars, with more modest fluxes obtained around compact HII regions containing only a few O and B stars.

et al. 1991), Figure 5.19. The total neutral carbon column density N(CI) within a PDR is expected to be about 10^{18} cm^{-2}. N(CI) changes by less than a factor of 2 as G_o is increased by five orders of magnitude—increasing G_o simply increases the depth into the cloud where the C^+/CO transition occurs, but the column density across this transition remains constant. The density dependence of N(C) is also weak, with an increase of N(CI) with decreasing density. This is caused by a drop in temperature with decreasing density, which tends to favour the formation of C rather than CO from C^+.

The excitation energies of the CI transitions are low, Figure 5.1, so that generally $T \geq \Delta E/k$ in the CI regions. Therefore, the CI emission is not very temperature-sensitive. There is a slow rise in I(CI) with G_l as the temperature rises in the CI zone (the gas temperature is only weakly dependent on G_l at the depths of the CI zone). There is also a slight increase of I(CI) with decreasing n, as N(CI) increases, but finally a decrease in I(CI) as n significantly drops below the critical density of CI.

As the predicted CI intensity is fairly independent of n and G_o, our measured intensity of the $^3P_1 \rightarrow {}^3P_0$ line should provide a measure of the number of PDRs along the line of sight ,the area filling factor, if the neutral carbon emission arises solely from PDR gas. Typically, the intensity of the $^3P_1 \rightarrow {}^3P_0$ line from a face-on PDR is 2×10^{-6} erg cm^{-2} s^{-1} sr^{-1} (Hollenbach *et al.* 1991). This would be the intensity observed along a line of sight, normal to the cloud surface. For a line of sight which intersected the cloud at an angle θ to the normal, the observed intensity of the optically thin line would be $\sim (\cos\theta)^{-1}$ times the "emergent intensity". For an optically thick line the angular dependence is complicated because of the temperature gradients into the cloud, but the observed intensity is approximately 2 times the "emergent intensity". Given that there is more than one PDR in NGC 253, there will be a number of different geometries between the PDRs and the local O and B stars producing the incident UV field. Summing these geometries and the resulting intensities is non-trivial, and so I make the simplifying assumption that the summed intensity would be twice the "emergent intensity" from an average PDR.

5.7.1 There are UV photons across the starburst in NGC 253

In previous sections it was discussed how the small compact size of the starburst, delineated by the 30 μm emission (Telesco *et al.* 1993), suggested that most of the UV photons from the starburst will be mopped up by the dust in this region. Even though the highest UV field occurs within the starburst, it is to be expected that there will be some UV photons outside the nucleus. There are observational results which support the idea of a low UV field outside the main compact starburst.

In chapter 3, there is a discussion about observations of the ortho to para ratio of H_2 outside the main starburst. The observed value is around $\sim$ 2, not 3, and so H_2 emission comes from PDRs and not from shocks. Furthermore, the rise in 1-0S(1) / Brγ outside the starburst indicates a rise in the efficiency of converting far-UV photons into near-IR H_2 emission. The highest conversion efficiency is obtained when the UV field creating the PDRs is relatively low (Black & van Dishoeck 1987). This would suggest that the rise in efficiency is tracing the low UV field away from the starburst. Other evidence comes from Telesco *et al.* (1993) who observed NGC 253 at 10.8 μm. As with the 30 μm map, the emission is compact, with a FWHM of $\sim 7'' \times 4''$, but the lowest contours of the 10.8 μm emission are more extended than the 30 μm contours. This was taken as evidence, by Telesco *et al.* (1993), for the destruction of the smallest grains within the starburst. Telesco *et al.* (1993) suggest that emission from the

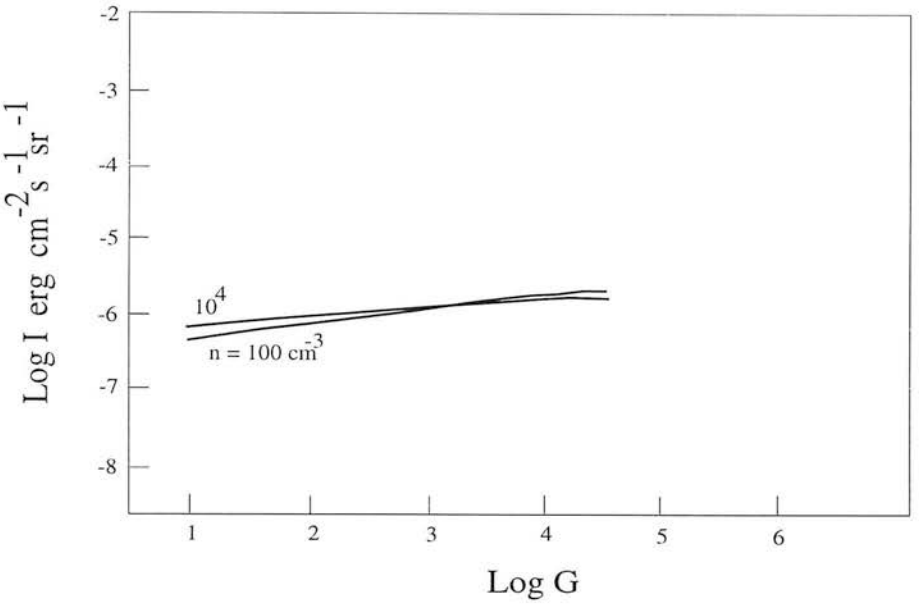

Figure 5.19: Calculated CI face-on intensity emitted from a PDR vs. incident far-UV flux G_o, for different densities. The predicted intensity is fairly independent of both density and UV field, typically 10^{-6} erg cm^{-2} s^{-1} sr^{-1}. The figure is adapted from Hollenbach *et al.* (1991). Geometrical and optical depth effects will act to increase the total intensity arising from the PDR and so care must be taken when comparing the observations with the models. I have assumed that the prediced intensity of CI arising from each individual PDR in NGC 253 is twice the intensity predicted by Hollenbach *et al.* (1991).

small, transiently heated grains becomes more important at the lower energy densities of the starburst periphery. The lowest contours of the 10.8 μm emission extend out to over 25″ and so this suggests that there are UV photons impinging upon molecular clouds across this region.

It seems reasonable to describe NGC 253 as having a compact starburst nucleus in which most of the UV is mopped up. NGC 253 also has an extended region outside this starburst, in which there are UV photons impinging upon molecular gas. It is not clear if the UV photons in the halo are produced locally or whether they escape from the main starburst.

5.7.2 Most of the atomic and molecular gas in NGC 253 is at relatively high densities

CI/CO is ~ 0.5 in NGC 253, which is an order of magnitude higher than Galactic GMCs. In the Galactic cold diffuse ISM the gas is mainly atomic and $C^0/CO > 1$ for $A_v < 1$ (Keene 1990). Thus, a possible explanation for our observed CI/CO value is to postulate a population of cold diffuse clouds in the starburst nucleus with most of the C^0 emission arising from these diffuse clouds. There are several problems, however, with the picture of a substantial component of diffuse low density gas in the nuclear region of NGC 253.

Firstly, this gas cannot be in the form of self-gravitating clouds because there is a limit to the minimum density of gravitationally bound clouds in galaxy nuclei. Stark *et al.* (1989) considered a roughly spherical cloud of radius r_o, at a distance R_o from the galaxy's centre. The gravitational forces on a parcel of gas at a distance r_o from the cloud centre along a line of sight can be used to see if the cloud is bound. If this parcel of gas is bound to the cloud, so that it follows a circular trajectory around the galaxy's centre at a slower-than-orbital velocity, the cloud must exert a gravitational acceleration on it equal to $T \times r_o$, where

$$T \equiv -\frac{d}{dR}\left(\frac{v_{circular}^2}{R}\right)_{R_o} + \frac{v_{circular0}^2}{R_o^2} \approx 2\frac{v_{circular}^2}{R_o^2} \tag{5.35}$$

in the limit that the rotation velocity is independent of R. This acceleration is caused by the gravitational pull of the cloud, so that

$$\frac{GM_{cloud}}{r_0^2} \geq Tr_o \tag{5.36}$$

Thus, the mean H_2 density in the cloud before it is unstable against tidal disruption, is

$$< \rho_{cloud} > \equiv \frac{M_{cloud}}{4/3\pi r_o^3} \geq \frac{3T}{4\pi G} \approx \frac{3}{2\pi G}\frac{v_{circular}^2}{R_o^2} \approx 10^4\left[\frac{75}{R_o}\right]^2 cm^{-3} \tag{5.37}$$

This analysis is approximate in that $v_{circular}(R)$ will depend upon the mass distribution of NGC 253, which may give a different relationship than the one that was used, *i.e.* $v_{circular}(R)$ is independent of R. However, for gas lower than a critical density, which is $\geq 10^3$ cm^{-3} across the central 23″ in NGC 253, rapid shearing takes place and the low density gas rapidly come into contact with other phases of the ISM in NGC 253. The ISM in NGC 253 is at high pressure ($\sim 5\times10^6$ K cm^{-3}, Carral *et al.* 1994) and, thus, if we have to postulate the existence of diffuse clouds of n $\sim$ 40 cm^{-3}, to allow C°/CO $\sim$ 0.5, these clouds must be unreasonably hot, $\sim 10^5$ K. Therefore it is unlikely that there will be a considerable level of low density gas within the starburst region and even if there is some diffuse gas its contribution to the carbon emission budget is small.

Moreover, even if there is low density gas in NGC 253, the critical density of the CI transition is $\sim 10^3$ cm^{-3} (Schröder *et al.* 1991) and so the low density gas would not be traced by the sub-mm emission. Furthermore, the observational evidence points towards most of the molecular gas in the nuclear region of NGC 253 being in a high density phase, with little evidence observationally for a substantial component of diffuse gas. ^{13}CO is tracing the bulk of the molecular component and given that the 3→2 line is thermalised, (see chapter 4), the majority of the molecular gas must be at densities greater than 3×10^4 cm^{-3}.

Finally, another problem with a large amount of diffuse gas is that we measure the column density of atomic carbon to be 5×10^{18} cm^{-2}, which should be a lower limit as we have assumed the CI emission is optically thin. Assuming an abundance ratio for carbon of x_c=3.3×10^{-4}, this results in the abundance of atomic hydrogen to be 1.5×10^{22} cm^{-2}. This is greater than the maximum of 1.3×10^{22} cm^{-2} claimed by Combes *et al.* (1977), although this is not a tight constraint as the beam of 3′ × 2′ used by Combes *et al.* (1977) does not provide detailed measurements of the HI column density in the central 23″.

5.7.3 The observed CI emission from NGC 253 is too bright to be explained by PDR models

The picture of the PDRs in NGC 253, outside the main starburst, is that of reasonably high density molecular clouds, n $\sim 10^{3-4}$ cm^{-3}, exposed to relatively low UV fields, G $\sim 10^{1-3}$. Theoretical models of the atomic carbon emission from such PDRs indicate that the face-on intensity from such PDRs is about 2×10^{-6} erg s^{-1} cm^{-2} sr^{-2}. This intensity can be increased by arbitrary amounts, dependent upon geometry but realistically the predicted intensities from a sum of PDRs filling the beam with unity is about 4×10^{-6} erg s^{-1} cm^{-2} sr^{-1}. Observations of NGC 253 give an observed intensity of about 10 times this prediction.

One way to make the predictions compatible with the observations is to make the area filling factor of PDRs in the central $23'' \sim 10$. This does not work in NGC 253 for the following reason. As discussed in section 5.5, when estimating the source size of PDRs, the observed brightness temperature of optically thick ^{12}CO $1 \rightarrow 0$ from the central $23''$ is about 4 K (Mauersberger *et al.* 1996). If the area filling factor of the ^{12}CO is close to unity then it is hard to explain such a low observed brightness temperature, unless the molecular gas is heated by the microwave background. More realistically, the area filling factor of the molecular gas is less than 50%. It is expected that 50% will be an upper limit to the area filling factor of PDRs.

Therefore, we are left with the conclusion that the CI emission from NGC 253 is far brighter (a factor of 10-20) than predicted by theoretical models of PDRs. Therefore, we either need some way of increasing the carbon intensity in PDRs or we have to argue that the bulk of atomic carbon does not arise from PDRs in NGC 253.

5.8 Non-PDR explanations for the observed C^0 in NGC 253

5.8.1 Enhanced cosmic ray fluxes?

Schilke *et al.* (1993) and White *et al.* (1994) observed CI towards the nucleus of M82 and argued that CI is brighter than predicted by PDR models by a factor of 5 or so. Both Schilke *et al.* (1993) and White *et al.* (1994) also claimed that N(CI)/N(CO) is high (0.1–0.5) in M82.

Whilst it is clear that in M82 CI is brighter than predicted by the PDR models of Hollenbach *et al.* (1991), it is not clear what true value of N(CI)/N(CO) is in M82. Both Schilke *et al.* (1993) and White *et al.* (1994) derived their CO column densities from the $C^{18}O$ 2→1 observations of Wild *et al.* (1992) and assumed $^{16}O/^{18}O = 500$. As discussed in chapter 4, $C^{18}O$ may not be a reliable tracer of the bulk of carbon monoxide within the environment of a starburst nucleus. If a much larger proportion of molecular gas is at larger depths in M82, *i.e.* cold and shielded from UV photons, then $C^{18}O$ will be a more realistic tracer of CO in M82 than in NGC 253. Wild *et al.* (1992) derived ^{13}CO 3→2 to be optically thick towards the nucleus of M82 and so, without detailed modelling, it is hazardous to use ^{13}CO to derive the CO column density in M82. Even if $C^{18}O$ is tracing the bulk of CO in M82, it is not clear what the $^{16}O/^{18}O$ ratio is and, thus, the true value of C/CO.

To explain the enhanced carbon in M82, with respect to both PDRs and CO, Schilke *et al.* (1993) proposed that a significant fraction of the CI emission was from carbon existing within molecular clouds. Recent chemical models, *e.g.* Flower *et al.* (1994), suggest that an enhanced ionisation fraction, deep within clouds, drives the chemistry to equilibrium with a high C/CO value. Schilke *et al.* (1993) proposed the enhanced cosmic ray flux supplied by frequently occurring supernovae remnants as the source of ionisation. Schilke *et al.* (1993) claimed that with a cosmic ray flux $\sim$ 300 times the local solar neighbourhood value, the models of Flower *et al.* (1994) produced significant carbon emission at large depths into the cloud and a large C/CO abundance ratio deep within the cloud. The summed emission from atomic carbon rises with depth into the cloud and the total emission is dependent on the maximum A_v of the cloud. The models of Flower *et al.* (1994) naturally explained the high C/CO value in M82 and also accounted for the fact that CI was brighter than predicted by the PDR models of Hollenbach *et al.* (1991)—atomic carbon is produced throughout the cloud whereas other PDR tracers such as CII and OI are only produced at low A_v—Figure 5.20.

Such a source of carbon emission would seem an attractive solution to the problem of bright carbon emission from the nucleus of NGC 253. The cosmic ray density in the starburst may be

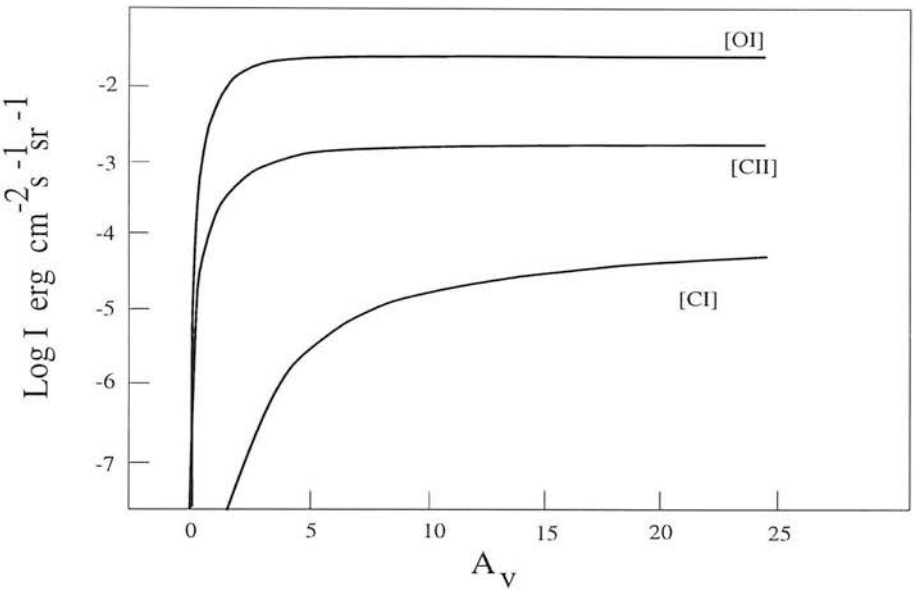

Figure 5.20: Intensity of fine-structure lines when the molecular cloud is in a region of a high cosmic-ray density, adapted from Schilke *et al.* (1993). Intensities of the OI and CII transitions are dominated by the PDR at only a few A_v, whereas the CI intensity continues to rise into the cloud because of the contribution from atomic carbon in the dark interior.

higher in NGC 253 than in M82; the SN rates are comparable but the starburst is more compact in NGC 253 (Paglione *et al.* 1996). However, the state of the bulk of molecular gas in NGC 253 rules out the Flower *et al.* (1994) model as a possible solution.

As we have previously argued in this chapter, and chapter 4, the bulk of molecular gas in NGC 253 in the nuclear region is at low A_v, hot and exposed to UV photons. In such an environment the chemistry is photon dominated and the small perturbation of an extra ionising source, such as cosmic rays, should have little bearing on the chemical abundances. The cosmic ray explanation also requires atomic carbon emission to steadily rise with depth into the cloud. In the nucleus of NGC 253 this rise with depth will be curtailed at a few A_v. Thus, there is not enough cold and shielded gas for a contribution to the CI emission to be significant from the nuclear region. Furthermore, as discussed previously, the area filling factor of molecular gas across the central 23″ is less than unity. In this case the predicted intensity from each of the molecular clouds needs to be $1/\Phi_A$ greater than for the case of an area filling factor of unity. Moreover, in M82 CI is perhaps a factor of 5 brighter than predicted by PDR models whereas in NGC 253, CI is a factor of $\sim$ 10 or more higher. So, with the low area filling factor of molecular gas, it appears from Figure 5.20 that each cloud would need to have a lot of gas, shielded to a visual extinction of $\sim$ 50-100. This is unlikely, given that the observed extinction across the starburst is of the order of $A_v \sim 5$ (Sams *et al.* 1994).

The proposal of Schilke *et al.* (1993) allowed a major contribution to the atomic carbon emission budget from a cloud's interior. This contribution was due to the dark cloud chemistry undergoing a phase transition in equilibrium abundances if the cosmic ray flux reached a certain threshold, which is quoted by Schilke *et al.* (1993) as being about 200 times the local value. The cosmic ray flux may be $\sim$ 1000 times greater in the nucleus of NGC 253 than the local value, well above the threshold level suggested by Schilke *et al.* (1993). Due to the phase nature of equilibrium abundances, it could always be possible that once a second threshold of cosmic ray flux is reached, probably somewhere between 200 and 1000 times the local value, another phase

transition results in which the equilibrium abundances produce even more free atomic carbon, which then dominate the emission budget. This can only be checked through running chemical models, which is beyond the scope of this work.

Therefore, unless the dark-cloud chemistry undergoes another "phase-transition" in its equilibrium abundances, it is concluded that because of the relatively low area filling factor of molecular gas and the low observed extinction towards NGC 253, the perturbation on dark cloud chemistry induced by the large cosmic ray flux is unlikely to be the principal cause of the bright atomic carbon emission from NGC 253.

5.8.2 Chemical and elemental explanations

The chemical abundances in a molecular cloud, as well as being sensitive to the physical conditions, change with time. Time-dependent chemical models reach equilibrium abundances after about 10^7 yrs, Leung *et al.* (1984). These models show that at early times, *i.e.* $< 10^6$ yrs, large amounts of CI exist yielding CI/CO abundance ratios greater than 0.5 and it is only at later times, when equilibrium is approached, that most of the C gets tied up in CO resulting in a decrease in the CI/CO ratio, Figure 5.6. The carbon chemistry in such models is still uncertain, however, as many of the chemical reactions at low temperatures involving carbon bearing molecules have been found to proceed at a much higher rate than was previously thought, Herbst *et al.* (1994). It would seem reasonable that in a starburst nucleus, where the molecular gas is frequently being perturbed, the chemistry never reaches steady state and the most realistic description of the chemistry might be that of early time. Mauersberger *et al.* (1991) claimed that the derived abundances of carbon-rich molecules in NGC 253 pointed towards non-equilibrium chemistry.

Another explanation for the observed CI in NGC 253 is that the elemental abundances are not identical in NGC 253 and the models to which we are comparing our observations. It is hard to distinguish observationally between early-time chemistry and a high C/O elemental ratio as both models produce similar chemical signatures, e.g. molecules that are carbon-rich. However, in order for the CI/CO ratio in NGC 253 to be explained by early-time chemistry, we must be seeing a snapshot of NGC 253 shortly after a major reconfiguration of the interstellar medium has occurred, within $\sim 10^6$ years, across a region of size $\sim$ 300pc. I feel that this is implausible. Moreover, the chemistry in the nucleus of NGC 253 is dominated by UV photons, which produces different chemical abundances compared to the chemistry of cold, dark clouds. As models of the chemistry in photon dominated regions predict only $\sim 5\%$ of the observed CI emission, the only plausible explanation left to explain the observed brightness of CI in NGC 253, is to invoke an enhanced C/O elemental ratio in NGC 253. Increasing the C/O ratio in the gas phase towards NGC 253 clears up the mystery of why CII emission from the nucleus of NGC 253 is far brighter than predicted by PDR models.

5.9 Possible explanations for a high C/O ratio in the gas-phase of NGC253

5.9.1 An increase in the C/O elemental ratio

Pantelaki & Clayton (1988) note that carbon is produced in SNII and intermediate-mass stars whereas oxygen is synthesised by high mass stars. If the C/O elemental ratio is enhanced in NGC 253 then this could be due to a large number of intermediate mass stars, around $8\,M_\odot$,

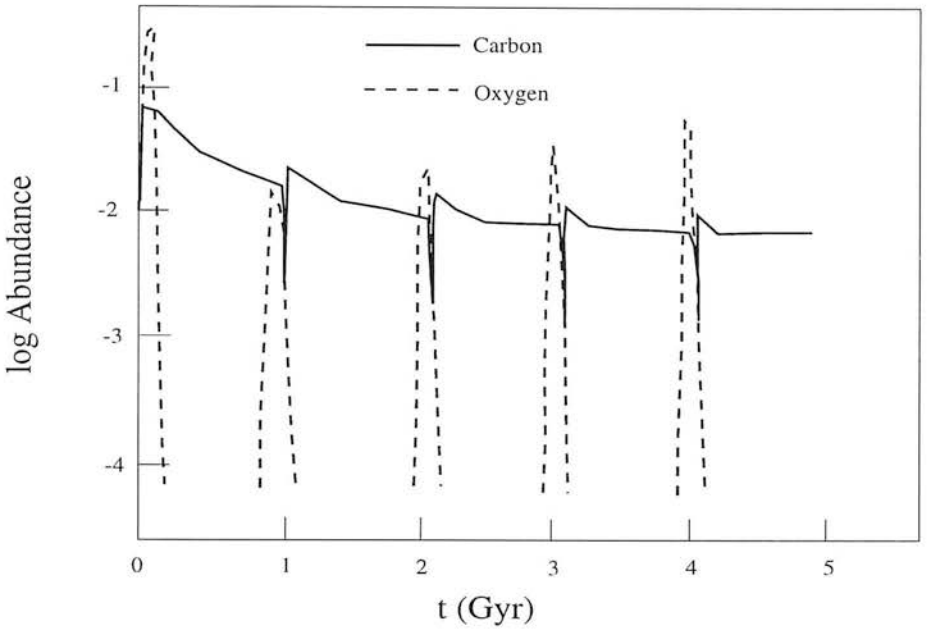

Figure 5.21: A model of the concentrations of O and C in the hot medium of a starburst galaxy as a function of time. The figure is adapted from Pantelaki & Clayton (1988)

existing in the nuclear region of NGC 253. It is also possible that the nuclear region of NGC 253 has a high C/O elemental ratio because the gas that is being driven into the nucleus (Canzian *et al.* 1988) has a high C/O ratio.

A different explanation is that suggested by the chemical evolution of starburst models of Pantelaki & Clayton (1988). In these models the elemental ratio of C/O is sensitive to time. The reason for this is that the superwind, driven by numerous SNII, causes the ejecta of high mass stars, which are oxygen rich, to be expelled from the nucleus. At later times intermediate stars eject large amounts of mass after termination of the SNII which is oxygen free but carbon rich. Thus, NGC 253 may be in the stage of producing the high C/O ejecta from intermediate mass stars. Figure 5.21 illustrates the chemical evolution in a cyclic starburst, adapted from Pantelaki & Clayton (1988) The picture of Pantelaki & Clayton (1988) may need fine tuning to explain why the C/O ratio is probably higher in NGC 253 than in M82. It is noted that the models of Pantelaki & Clayton (1988) suggest that there may be C/O elemental gradients along the major axis of superwinds.

It is not clear how applicable standard chemical evolutionary models are to the nuclear regions of starbursts. Maeder (1992) has argued that a crucial parameter in chemical evolutionary models is metallicity. An increase in metallicity changes the nuclear processing within stars and increases the opacity in the outer layers of stars. This increase in opacity changes the mass-loss rates of stars. Maeder (1992) claims that massive stars at high Z eject carbon back into the ISM before it is processed into heavier elements. Thus, at high Z, stars enrich the ISM with material that has a high C/O elemental ratio, Figure 5.22. If the nuclear region of NGC 253 has a high metallicity then the work of Maeder (1992) provides a natural explanation for the high C/O ratio. If this explanation is correct then it is noted that an interesting effect in the chemical evolution of starbursts might be that, once a threshold of metallicity is passed, stars that form from gas with a high C/O ratio will eject gas, with an even higher C/O, back into the ISM. This scenario, of a positive feedback loop steadily increasing C/O, suggests that starbursts with high metallicities will have high C/O ratios.

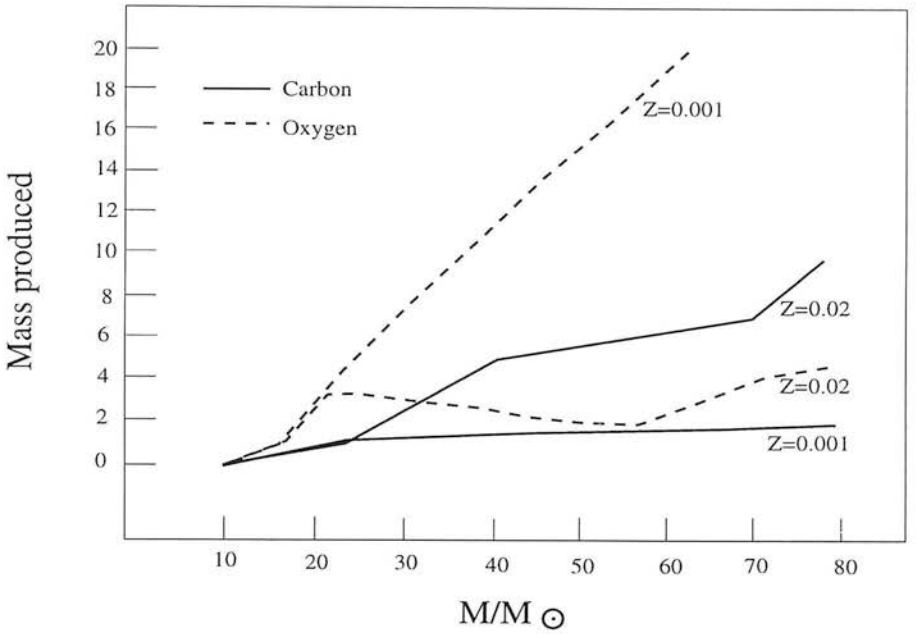

Figure 5.22: The amount of carbon and oxygen produced (in units of solar mass) as a function of the initial stellar mass and for two metallicities. The figure is adapted from Maeder (1992)

5.9.2 Tapping into the solid reservoir of carbon in the ISM of NGC 253

Evidence for grain destruction in NGC 253 has been proposed by Telesco *et al.* (1993). Mid-infrared colour gradients suggest that the dust is hottest in a ring around the active starburst—see Chapter 2 for further details. The hottest dust is expected to trace the population of the smallest grains and therefore such a ring of hot dust is suggestive of a scenario in which the smallest grains are destroyed within the harsh environment of the starburst but are able to survive in the periphery of the active star forming region.

It has been recognised that grain destruction will result in the gas phase being enhanced in the elements that are usually locked up in the grains, *e.g.* Telesco *et al.* (1993). The SiII emission is brighter than expected towards NGC 253 and this has been proposed as further evidence of grain destruction on the starburst (Carral *et al.* 1994). It is expected that destruction of polycyclic aromatic hydrocarbons (PAHs) and small grains will recycle carbon into the gas phase of the starbursts ISM.

It is not clear how much carbon is stored in the smallest grains and large molecules (Snow & Witt 1995) in our local environment and so we certainly cannot constrain the level of solid phase carbon in NGC 253. But if grains and molecules are being destroyed in the starburst of NGC 253 then the gas-phase carbon abundance will be increased. The question is, to what degree is the gas-phase carbon abundance enhanced? Such a study is beyond the scope of this work.

5.10 Conclusions

This chapter discusses observations of CI emission towards the nucleus of NGC 253. The starburst, traced by the mid- to far- IR continuum, in NGC 253 is compact, on a scale of about 8″ ($\sim$ 100 pc if NGC 253 is at 2.6 Mpc). The luminosity coming from such a small region indicates that the average UV field in this region is $\sim 10^5$ times the local value. PDR models of the far-IR emission expected from such a region can only account for about 10% of the observed luminosity

of CII. CI emission from a more extended region, $\sim$ 300 pc, is also overabundant by a factor of 10, both with respect to PDR models and to CO (CI/CO $\sim$ 0.5). It is unlikely that cosmic rays perturb the chemistry enough to explain the CI emission. The size ($\sim$ 300 pc) over which $C^0/CO \sim 0.5$, and the environment of the molecular gas, rules out non-equilibrium chemistry.

The only plausible explanation for the amount and distribution of C^0 in NGC 253 is an enhanced C/O elemental ratio in the gas phase of NGC 253. There is no obvious reason why this should be so, but possible mechanisms include chemical evolution in a high metallicity starburst, and the destruction of dust which will free carbon from the solid phase and put it into the gas phase.[10]

5.11 Acknowledgements

I thank Peter Brand, Henry Buckley, Patricia Carral, David Flower, Christian Henkel, David Hollenbach, Jocelyn Keene, Guillaume Pineau des Forêts, Peter Papadopoulos, Phil Puxley, Milagros Ruiz, Adrian Russel, Ewine van Dishoeck and Karen Willacy for very helpful and interesting discussions and an anonymous referee for a critical and insightful reading of a draft of some of this work when it was submitted for publication to MNRAS. I also thank Tom Millar and Glenn White for sending preprints, Rachael Padman and John Lightfoot for help with SPECX and Bill Dent, Jeff Cox, Kimberley Pisciotta and Jim Pomeroy for help with the observations.

[10] A recent paper by Israel *et al.* (1995) disagrees with my conclusions over why the emission of atomic carbon is brighter than predicted by PDR models. Israel *et al.* (1995) suggest that the ratio of the CII flux to that of the CI flux, averaged over the central $\sim 30''$ can be used to estimate the conditions in the PDRs. Moreover, Israel *et al.* (1995) suggest that the explanation for the higher than expected absolute brightness of carbon is that the area filling factor of PDRs is $\sim$ 30, along every line of sight. As outlined in this chapter, I disagree with Israel *et al.* (1995) on both these points. Firstly, I propose that the source size of the CII emission is smaller than that of CI—this makes a comparison of fluxes of CII and CI an unreliable diagnostic of PDR conditions. Secondly, I argue that because the observed brightness temperature of CO 1$\rightarrow$0 is $\sim$ 5 K, the area filling factor of PDRs in NGC 253 is $\leq$ 0.3, two orders of magnitude less than suggested by Israel *et al.* (1995).

Chapter 6

A summary of the thesis and suggestions for future research

6.1 Summary of the preceding chapters

This thesis contains several complementary sets of observations of the starburst in the circumnuclear region of NGC 253. The observations probe directly the interface between HII regions and molecular gas in NGC 253, where UV photons dominate the heating and chemistry of the gas. A summary of the various results follows.

6.1.1 Determination of how H_2 is excited in NGC 253

In chapter 3, I presented measurements of several near-IR emission lines from NGC 253. In particular, I have been able to measure 4 H_2 lines across the starburst which has allowed an estimate of the ortho to para ratio of H_2. The ratio is observed to be close to 2, and not 3, which indicates that the bulk of the H_2 emission arises in PDRs rather than shocks. This is the case across the entire starburst. As the H_2 emission arises from PDRs, it is likely that the ratio of Brγ to 1-0 S(1) is a measure of the geometry of O and B stars to PDRs. Towards the nucleus of NGC 253 the geometry is tightly clustered O and B stars in a few giant HII regions which are encompassed by PDRs. The UV flux impinging upon the nuclear PDRs is high, $> 10^4$ times the local value. Away from the nuclear region, the geometry becomes that of PDRs bathed in a relatively diffuse UV radiation field. The rotation curves of H_2 and Brγ suggest that the ionised gas is tracing a different kinematic system to that of the molecular gas, particularly away from the nucleus where it is likely that the PDRs are bathed in a relatively low UV field. This work has been submitted for publication to MNRAS.

The work I have carried out for my thesis, on the excitation of H_2 in NGC 253, is readily applicable to other galaxies. My work has shown that it is straightforward, in principle, to determine whether the H_2 emission results from shocks or fluorescence—measure the ortho to para ratio using the relative intensities of 1-0 S(2) 1-0 S(1) and 1-0S(0), and if the ratio is less than 3 then UV photons must play a part, probably dominant, in producing the H_2 emission.

6.1.2 The excitation of CO and its isotopomers

In chapter 4, I presented observations of $C^{18}O$ 3→2 and $C^{18}O$ 2→1 towards the nuclear region of the starburst galaxy NGC 253. The observed $C^{18}O$ 3-2/2-1 brightness temperature ratio, averaged over the central $\sim$ 300 pc, is $\sim$ 1.1. This is in contrast to the 3-2/2-1 temperature

ratio of ^{13}CO, $\sim$ 2, over the same region (Wall *et al.* 1991). The observations of ^{13}CO by Wall *et al.* (1991) indicate that most of the gas in the nuclear region is hot and so it appears that $C^{18}O$ is only tracing a minor fraction ($< 10\%$) of the total CO. The separation between $C^{18}O$ and ^{13}CO emitting gas needs to be confirmed but at the moment there is evidence for a mechanism that removes $C^{18}O$ from the warm gas associated with PDRs in NGC 253. A proposed process is selective photodissociation of CO and its isotopomers. This work has been published in Harrison *et al.* (1995).

6.1.3 The overabundance of carbon in NGC 253

In chapter 5, I presented observations of a fine-structure transition of atomic carbon. The emission shows a significant overabundance of atomic carbon, a factor of 10 or more, with theoretical models of PDRs. Considerations of the size of the compact starburst, traced by the mid to far IR radiation from dust, indicates that the starburst is concentrated within the central 100 pc of NGC 253. The luminosity coming from such a region indicates that the UV field is very high within the starburst, possibly greater than 10^5 times the local value. If all the C^+ flux is generated within this starburst, as is likely, then the ionised carbon emission is also a factor of 10 or more brighter than is predicted by PDR models. The most likely explanation for the discrepancy between the brightness of C^0 and C^+ and the models is that the elemental abundance of carbon is higher in the gas-phase of NGC 253 than it is in the PDR models to which the observations are compared. There is no obvious reason why this should be so, but possible mechanisms of increasing the gas-phase carbon abundance include nucleo-synthesis in a high metallicity starburst, or the destruction of dust which will free carbon from the solid phase and put it into the gas phase. This work has been published in Harrison *et al.* (1995).

6.1.4 Conclusions derived from the work in the thesis

The work in the thesis has involved a detailed case study of NGC 253 and the conclusions of each chapter add to the overall description of the physics of the starburst in NGC 253. Below is a brief discussion of what I have learnt, as an *observer*.

The physics of molecular absorption of UV photons has been at the core of the chapters on CO and H_2. Both CO and H_2 absorb UV photons at specific frequencies, rather than through broad-band absorption. This results in molecules towards the front of a molecular cloud "mopping up" all the UV, leaving molecules deeper in the cloud "safe" from photodissociation. Molecules which absorb UV in bands would not be safe from the UV in the regions in which CO and H_2 is safe. The chemistry resulting from the self-shielding of molecules in PDRs will control much of the isotopic chemistry in NGC 253 as well as in other starbursts. This chemistry needs to be understood before determinations of the isotopic ratios in NGC 253 are established. The ratios need to be secure, in order to allow molecular abundances to be determined, because the abundances underpin much of what can be learnt about the chemistry in NGC 253. Many of the observations needed, such as the confirmation of the selective photodissociation of CO in NGC 253 and a check for isotopic anomalies in other molecules such as CN, can be achieved with existing facilities on ground-based telescopes.

Observations of far-IR and sub-mm fine-structure lines from species of carbon and oxygen, in conjunction with observations of the IR emission from dust can be used to highlight not only elemental anomalies, such as an overabundance of carbon, but can also shed light on the physical conditions within PDRs. The most important characteristics of PDRs, for comparing

observations to theoretical models, are the density of the gas and the local UV field. The nuclei of galaxies contain dense molecular gas, resulting from the high gas pressure associated with the ISM in their circum-nuclear regions. Therefore, theoretical models of low-density PDRs will not be applicable to most starbursts and effort should be concentrated on comparing the high-density PDR models with observations. The strength of the UV field in starbursts has to be controlled, to some degree, by the level of clustering of O and B stars in the nuclei of galaxies. In practise, it is difficult to estimate the UV field impinging upon PDRs to within a factor of ~ 5 because of uncertainties over the spatial relationship between the O and B stars and their surrounding PDRs. Unless we have more understanding of how O and B stars cluster whilst forming, I cannot see this factor of 5 in uncertainty being reduced.

At the present time, the observations of far-IR emission from NGC 253, as well as other objects, is limited by the relatively small collecting area of the telescopes used, which results in large diffraction beams. Future planned observatories, such as FIRST and SOFIA, with their smaller diffraction beams will be able to map the OI and CII lines, as well as the far-IR continuum, at spatial resolutions close to what can be achieved from sub-mm telescopes. Until these new facilities come on-line I feel little new can be learnt about NGC 253 from observations of the far-IR emission, using observatories with a similar beam size to that of the KAO. When these new facilities do come on-line then it is important that the beams of the sub-mm telescopes, such as the JCMT and CSO, have as small an error beam as possible. This wish for small error beams comes from the experience of having to calibrate the atomic carbon emission from NGC 253, and then trying to understand its morphology.

The key to determining how H_2 is excited in NGC 253 was determining the ortho to para ratio. The largest uncertainty in the ratio resulted from the need to combine adjoining spectra to obtain complete wavelength coverage over 2.02-2.32μm with a resolving power of $\sim$ 1,350. At this resolution the lines become partially resolved and it is then possible to study the kinematics of the lines. Any future experiments designed to measure the ortho to para ratio of H_2 in a galaxy's circum-nuclear region should be able to cover 2.02—2.32μm with one spectrum at a resolution of $\geq$ 1350. This will remove the systematic errors incurred from combining adjoining spectra.

6.2 Future lines of research

6.2.1 Measuring the dominant excitation mechanism of H_2 in galaxies

The research discussed in chapter 3 indicates that there is a straightforward way, in principle, to determine how the hydrogen molecule is excited in galaxy nuclei—observe the 1-0 S(2),1-0 S(1) & 1-0 S(0) lines and use the ratios of these lines to derive the ortho to para ratio of the excited H_2. It is straightforward, in principle, to measure the ortho to para ratio of H_2 in other galaxies. This would be the first step in identifying whether the excitation of H_2 occurs predominantly in PDRs or whether shocks and/or X-rays play some role. The dominant excitation mechanism may well depend on whether the galaxy is undergoing a tidal interaction/merger or whether there is an active nucleus. Suitable candidates in which to start to identify the dominant excitation mechanisms in various galaxies are the merger system NGC 6240 and the nearby Seyfert galaxy NGC 1068.

6.2.2 The clustering of star formation in the nucleus of NGC 253

The typical UV field in the starburst of NGC 253 is greater than 10^4 times the local value. The high observed ratio of Brγ/1-0 S(1) in the circum-nuclear region of NGC 253 suggests that the O and B stars have to be clustered, so as to produce a large HII region enveloping many individual O and B stars. There is also other observational evidence for giant O and B clusters in the nucleus of NGC 253. Observations made in the radio show a population of luminous flat radio sources across the nucleus of NGC 253. If these are HII regions, then their brightness indicates that each one must contain many hundreds, possibly thousands, of O and B stars. Images of NGC 253 in the IR show one particular strong emitter that is located at a flat spectrum source. This particular source appears to have a bolometric luminosity of $\sim 2{\times}10^9$ $L_\odot$, generated by a cluster of stars with a half-light radius of ≤ 3 pc. HST images also show several other young clusters in the starburst, which are less luminous than the main cluster. The HST clusters spatially coincide with several of the near-IR peaks (Sams *et al.* 1994) although it appears that some of the "clusters" may be spatially offset from the flat radio sources. It is possible that source confusion in the radio images and pointing offsets in the optical and IR images may partially account for the apparent difference in positions between the radio and optical "counterparts".

Sams *et al.* (1994) suggested that the near-IR "hot-spots" were just holes in extinction. It was argued that these holes resulted in the relatively smooth background of near-IR light taking on a patchy appearance, with the low extinction patches appearing to be hot. As I discuss in chapter 3, the analysis of near-IR colours used by Sams *et al.* (1994) may be prone to uncertainties because the unreddened stellar colours of regions within NGC 253 may not be identical to that of a Sc galaxy. Puxley (1991) suggested that hydrogen recombination lines can be used to measure extinction. A future experiment which could shed light on whether the unreddened near-IR light in NGC 253 is clustered or not would be to take narrow-band images of several hydrogen recombination lines, with complementary images of the surrounding continuum around the lines, in order to produce an extinction map. This map can then be compared with an extinction map obtained from a comparison of near-IR broad-band colours. If the two maps resemble each other closely then this would support the conclusions of Sams *et al.* (1994). Contrarily, a clear difference in the two extinction maps would not support the conclusions of Sams *et al.* (1994) and may highlight the intrinsic clustering of much of the near-IR light.

With the probable discovery that much of the power of the starburst in NGC 253 is generated in compact clusters, each containing many O and B stars, this leads to several questions and lines of research that may shed insight into the physics of many, if not all, starbursts. In particular: why and how do the clusters form?; what controls their size and luminosity?; how will they evolve?; have they formed at a special location in the starburst? This final question may be answered, along with possible clues to the answers of the other questions, from detailed studies of the kinematics of the starburst in NGC 253.

6.2.3 Kinematics in the circum-nuclear region of NGC 253

Quoting Achtermann & Lacy (1995), the secret to understanding the causes and inner workings of starburst galaxies lies in understanding the kinematics of the gas—for it is the gas which forms the molecular clouds from whence the stars form. As I discussed in Chapter 3, there is a rich kinematic structure within the starburst although at the moment the nature of this structure is unclear. Outside the main starburst, it appears that a molecular bar is rotating as

a solid body, but close to and within the starburst there is evidence for spiral arms or maybe a region of much higher mass density than outside the active region. Furthermore, it appears that the ionised and molecular kinematics may be distinct identities. At this moment in time, the nature of the stellar kinematics in NGC 253 is not known.

Observations of kinematic tracers at high spatial resolution in NGC 253 should resolve the basic structure to the kinematics of the different components of gas and stars. A possible approach to tracing the kinematics would be observations of NGC 253 at 2 μm where observations of 1-0 S(1), Brγ and the CO band-head will trace the kinematics of PDRs, HII regions and stars directly. Alternatively, radio and mm interferometers can be used to trace the kinematics of the atomic gas, via the 21 cm line,[1] the molecular gas, via *e.g.* CO 1-0, and the ionised gas, via hydrogen recombination lines.

6.2.4 Is there too much carbon in NGC 253 and, if so, why?

In Chapter 5 I discussed the observed overabundance of carbon in the gas-phase of the ISM in NGC 253. Confirmation, or a dispute, of the high carbon abundance in NGC 253 from observations at other wavelengths may not be straightforward. At X-ray wavelengths, carbon emission lines lie well below the ASCA bandpass (0.5-10.0 keV) and determination of the C abundance with ROSAT PSPC data would be difficult, if not impossible, due to a prominent C edge in its response at $\sim$ 0.3 keV (Andy Ptak, private communication). In the UV, collisionally-excited lines become vanishingly weak at high metallicities, due to low electron temperatures, and the high interstellar dust obscuration presents observational difficulties (Don Garnett, private communication).

It is possible that tests of my description of the starburst in NGC 253, outlined in Chapter 5, may come with the next generation of far-IR telescopes, such as FIRST and SOFIA. The mid-IR radiation is centrally concentrated and so this should be the approximate size of the region containing PDRs exposed to large UV fields. Thus, I make the prediction that the source size for the OI 63 μm and CII 158 μm lines should be $\leq 10''$. Observations of these lines with the relatively large collecting area of FIRST and SOFIA can be used to test whether my estimate of the far-IR source size is correct. If my prediction is correct, and assuming the current reported observations of CO 1-0 towards the nucleus are secure, then PDR models struggle to explain not only the brightness of CI, but also that of CII, towards NGC 253, unless the C/O ratio is enhanced in these models.

It is a mystery why there should be a high C/O ratio in NGC 253—a starburst producing an IMF biased towards high mass stars would be expected to decrease the C/O elemental ratio rather than increase it. One plausible explanation is that NGC 253 has a normal C/O ratio but has had its gas-phase ratio increased through the tapping of a reservoir of carbon, namely the carbon that is usually stored in the solid-phase. Towards NGC 253 the mid-IR colours imply that the dust temperature is lower towards the starburst center than in the surrounding regions. It is widely accepted that very small dust grains (sizes less than 0.01 μm), which are transiently heated to high temperatures by single ultraviolet photons, contribute significantly to the mid-IR emission and, furthermore, these grains are expected to be rich in carbon. The colour gradients therefore appear to indicate that the starburst region is depleted in these small particles relative to the surroundings where the ultraviolet energy density is lower. In effect, the starburst region possesses a halo that is relatively rich in mid-infrared emitting small grains. The mid-IR has

[1] With existing observational facilities, the 21 cm observations will be at lower spatial resolution than the proposed observations of CO and the near-IR.

several 'unidentified emission features' usually attributed to polycyclic aromatic hydrocarbons (PAHs).

I predict that the starburst centre in NGC 253 will be relatively depleted in the PAHs, and hence the emission features, and so the line-to-continuum ratio of the features should be highest towards the 'mid-IR rich' ring around the starburst. This prediction can be tested through narrow-band images of the 11.3 μm feature, and the continuum around 11.3 μm, towards NGC 253. The signature of PAH destruction would be a "doughnut" structure, enveloping the starburst, in a map of the line-to-continuum ratio. Although speculative at this stage, the depletion of small grains in the starburst will provide a natural explanation for the high gas-phase C/O ratio in NGC 253. If such a connection can be made then it is critical to know how, why and in what environment the small grains are destroyed. Understanding the ecology of these small grains will infringe upon many areas of research into the interstellar medium.

Chapter 7

References

Achtermann J. & Lacy J. 1995, ApJ, 439, 163

André P., Ward-Thompson D. & Barsony M. 1993, ApJ, 406, 122

Antonucci R. & Ulvestad J. 1988, ApJ Lett., 330, L97

Bakes E. & Tielens A. 1994, ApJ, 427, 822

Bania T., Rood R. & Wilson T. 1987, ApJ, 323, 30

Beck S. & Beckwith S. 1984, MNRAS, 207, 671

Becklin E., Fomalont E. & Neugebauer G. 1973, ApJ Lett., 181, L27

Begelman M. 1989, in "The Interstellar Medium in Galaxies", ed. Thronson H. & Shull J., Kluwer Academic Publishers

Bhattacharya D., The L.-S., Kurfess J., Clayton D., Gehrels N., Leising M., Grabelsky D., Johnson W., Jung G., Kinzer R., Purcell W., Strickman M. & Ulmer M. 1994, ApJ, 437, 173

Black J. & Dalgarno A. 1976, ApJ, 203, 132

Black J. & van Dishoeck E. 1987, ApJ, 322, 412 (B&vD)

Blecha A. 1986, A&A, 154, 321

Boland W. & de Jong T. 1982, ApJ, 261, 110

Braine J., Combes F., Casoli F. *et al.* 1993, A&AS, 97, 887

Brand P., Moorhouse A., Burton M., Geballe T., Bird M. & Wade R. 1988, ApJ Lett., 334, L103

Burton M. 1992, Aust. J. Phys. 45, 463

Burton M., Hollenbach D. & Tielens A. 1990, ApJ, 365, 620

Büttgenbach T., Keene J., Phillips T. & Walker C. 1992, ApJ Lett., 397, L15

Canzian B., Mundy L. & Scoville N. 1988, ApJ, 333, 157

Carlstrom J., Jackson J., Ho P. & Turner J. 1989, in "The interstellar medium in external galaxies", ed. Hollenbach D. & Thronson H., NASA Conf Pub. 3084

Carral P., Hollenbach D., Lord S., Colgan S., Haas M., Rubin R. & Erickson E. 1994 ApJ, 423, 223

Chevalier R. & Clegg A. 1985, Nature, 317, vol. 5, 44

Chièze J.-P., Pineau des Forêts G. & Herbst E. 1991, ApJ, 374

Chrysostomou A. 1993, PhD Thesis, University of Edinburgh

Chrysostomou A., Brand P., Burton M. & Moorhouse A. 1993, MNRAS, 265, 329

Combes F. 1988, in "Galactic and Extragalactic Star Formation", ed. Pudritz R. & Fich M., Kluwer Academic Publishers

Combes F. 1991, Ann. Rev. Astr. & Ap. 29, 195

Combes F., Gottesman S. & Weliachew L. 1977, A&A, 59, 181

Crawford M., Genzel R., Townes C. & Watson D. 1985, ApJ, 291, 755

Davidge T. & Pritchet C. 1990, AJ, 100, 102

de Vaucouleurs G., de Vaucouleurs A., Corwin H. 1991, "Third Reference Catalogue of Bright Galaxies", Springer

Draine B. 1978, ApJ Supp., 36, 595

Draine B., Roberge W. & Dalgarno A. 1983, ApJ, 264, 485

Dyson J. & Williams D. 1980, "The physics of the interstellar medium", Manchester University Press

Fabbiano G. 1988 ApJ, 330, 672

Fabbiano G. & Trinchieri G. 1984, ApJ, 286, 491

Fernandes A., 1993, PhD Thesis, University of Edinburgh

Field G., Somerville W. & Dressler K. 1966, Ann. Rev. Astr. & Ap., 4, 207

Flower D., Le Bourlot J., Pineau des Forêts G. & Roueff E. 1994, A&A, 282, 225

Forbes D., Ward M., Rotaciuc V., Blietz M., Genzel R., Drapatz S., van Der Werf P. & Krabbe A. 1993, ApJ Lett., 406, L11

Frerking M., Keene J., Blake G. & Phillips T. 1989, ApJ, 344, 311

Frogel J. 1988, in Ann. Rev. Astr. & Ap., 51

Fuente A., Martin-Pintado J., Cernicharo J. & Bachiller R. 1993, A&A, 276, 473

Genzel R. 1991, in "The physics of star formation and early stellar evolution", ed. Lada C. & Kylafis N., Kluwer Academic Publishers

Genzel R., Harris A., Jaffe D. & Stutzki J. 1988, ApJ, 332, 1049

Glassgold A. & Langer W. 1975, ApJ, 197, 347

Goldschmidt O. & Rephaeli Y. 1995, ApJ, 444, 113

Goldschmidt O. & Sternberg A. 1995, ApJ, 439, 256

Graf U. 1991, PhD Thesis, Ludwig-Maximilians-Universität, Munich

Graham J. 1982, ApJ, 252, 474

Graham J., Wright G. & Longmore A. 1987, ApJ, 313, 847

Griffin M., Ade P., Orton G., Robson E., Gear W., Nolt I & Radostitz J. 1986, Icarus, 65, 244

Güsten R., Serabyn E., Kasemann C., Schinckel A., Schneider G., Schulz A. & Young, K. 1993, ApJ, 402, 537

Harris A., Hills R., Stutzki J., Graf U., Russell A. & Genzel R. 1991, ApJ Lett., 382, L75

Harrison A., Puxley P., Russell A. & Brand P. 1995, MNRAS, 277, 413

Heckman T. 1993, in "The Nearest Active Galaxies", ed. Beckman J., Colina L. & Netzer H., Consejo Superior de Investigaciones Cientificas

Heckman T., Armus L. & Miley G. 1990, ApJ Supp., 74, 833

Henkel C., Baan W. & Mauersberger R. 1991, Astr. & Ap. Rev., 3, 47

Henkel C. & Mauersberger R. 1993, A&A, 274, 730

Henkel C., Mauersberger R., Wiklind T., Hüttemeister S., Lemme C. & Millar T. 1993, A&A, 268, L17

Herbst E., Lee H., Howe D. & Millar T. 1994, MNRAS, 268, 335

Hernichel J., Krause D., Röhrig R., Stutzki J. & Winnewisser G. 1992, A&A, 259, L77

Hildebrand R., Lowenstein R., Harper D., Orton G., Keene J. & Whitcomb S. 1985, Icarus, 64, 64

Ho P., Turner J., Fazio G. & Willner S. 1989, ApJ, 344, 135

Hollenbach D. & McKee C. 1989, ApJ, 342, 306

Hollenbach, D. & Natta, A. 1995, ApJ, 455, 133

Hollenbach D., Takahashi T. & Tielens A. 1991, ApJ, 377, 192

Hollenbach D. & Thronson H. 1987, "Interstellar Processes", Kluwer Academic Publishers

Hummer D. & Storey P. 1987, MNRAS, 224, 801

Hüttemeister S., Henkel C., Mauersberger R., Brouillet N., Wiklind T. & Millar T. 1995, A&A, 295, 571

Israel F., White G. & Baas F. 1995, A&A, 302, 343

Jansen D. 1995, PhD Thesis, University of Leiden

Joseph R. & Wright G. 1985, MNRAS, 214, 87

Joy M. & Lester D. 1988, ApJ, 331, 145

Keene J. 1990, in "Carbon in the Galaxy: studies from earth & space", ed. Tarter J., Chang S. & Defrees D. (NASA CP-3061),181

Keene J. 1995, in "The Physics & Chemistry of Interstellar Molecular Clouds", ed. Winnewisser G. & Pelz G., Springer-Verlag

Keene J., Blake G., Phillips T., Huggins P. & Beichman C. 1985, ApJ, 299, 967

Keto E., Ball R., Arens J., Jernighan G., Meixner M., Skinner C. & Graham J. 1993, ApJ Lett., 413, L23

Kleinmann S. & Hall D. 1986, ApJ Supp., 62, 501 (KH)

Knapp G. 1989, in "The Interstellar Medium in Galaxies", ed. Thronson H. & Shull J., Kluwer Academic Publishers

Köster B., Störzer H., Stutzki J. and Sternberg A. 1994, A&A, 284, 545

Kutner M. & Ulich B. 1981, ApJ, 250, 341

Landini M., Natta A., Oliva E., Salinari P. & Moorwood A. 1984, A&A, 134, 284

Langer W. 1976, ApJ, 206, 699

Larson R. 1981, MNRAS, 194, 809

Larson R. 1987, in "Starbursts and Galaxy Evolution", ed. Xuan Thuan T., Montmerle T. & Tran Thanh Van J., Editions Frontieres

Lester D., Carr J., Joy M. & Gaffney N. 1990, ApJ, 352, 544

Letzelter C., Eidelsberg M., Rostas F., Breton J. and Thieblemont B. 1987, Chem. Phys., 114, 273

Leung C., Herbst E. & Heubner W. 1984, ApJ Supp., 56, 231

Lord S., Hollenbach D., Haas M., Rubin R., Colgan S. & Erickson E. 1996, ApJ, 465, 703

Maeder A. 1992, A&A, 264, 108

Marscher A. 1977, ApJ, 216, 244

Mauersberger R. & Henkel C. 1989, A&A, 223, 79

Mauersberger R. & Henkel C. 1991, A&A, 245, 457

Mauersberger R., Henkel C. & Chin Y-N. 1995, A&A, 294, 23

Mauersberger R., Henkel C. & Sage L. 1990, A&A, 236, 63

Mauersberger R., Henkel C., Walmsley C., Sage L. & Wilkind T. 1991, A&A, 247, 307

Mauersberger R., Henkel C., Wielebinski R., Wilkind T. & Reuter H. 1996, A&A, 305, 421

McCarthy P., Heckman T. & van Breugel W. 1987, AJ, 92, 264

McWilliam A. & Lambert D. 1984, Pub. Ast. Soc. Pacific., 96, 882

Meixner M. & Tielens A. 1993, ApJ, 405, 216
Minchin N., White G., Stutzki J. & Krause D. 1994, A&A, 291, 250
Minchin N., White G. & Ward-Thompson D. 1995, A&A, 301, 894
Morton D., Drake J., Jenkins E., Rogerson J., Spitzer L. & York D. 1973, ApJ Lett., 181, L103
Nguyen-Q-Rieu, Jackson J., Henkel C., Troung-Bach & Mauersberger R. 1992, ApJ, 399, 512
Nguyen-Q-Rieu, Nakai N. & Jackson J. 1989, A&A, 220, 57
Nussbaumer H. 1971, ApJ, 166, 411
Ohashi T., Makishima K, Tsuru T., Takano S., Koyama K. & Stewart G. 1990, ApJ, 365, 180
Origlia L., Moorwood A. & Oliva E. 1993, A&A, 280, 536
Outred M. 1978, J. Phys. Chem. Ref. Data, 7, 81
Paglione T., Marscher A., Jackson J. & Bertsch D. 1996, ApJ, 460, 295
Paglione T., Tosaki T. & Jackson J. 1995, ApJ Lett., 454, L117
Pantelaki I. & Clayton D. 1988, in "Starbursts and Galaxy Evolution", ed. Thuan T., Montmerle T. & Tran Thanh Van J., Editions Frontières
Pence W. 1981, ApJ, 247, 473
Petre R. 1993, in "The Nearest Active Galaxies", ed. Beckman J., Colina L. & Netzer H., Consejo Superior de Investigaciones Cientificas
Petuchowski S. & Bennet C. 1992, ApJ, 391, 137
Phillips T. & Huggins P. 1981, ApJ, 251, 533
Piña R., Jones B., Puetter R. & Stein W. 1992, ApJ Lett., 401, L75
Pineau des Forêts G., Roueff E. & Flower D. 1992, MNRAS, 258, 45P
Plume R., Jaffe D. & Keene J. 1994, ApJ Lett., 425, L49
Prada F., Manchado A., Canzian B., Peletier R., McKeith C. & Beckman J. 1996, ApJ, 458, 537
Puxley P. 1991, MNRAS, 249, 11P
Puxley P. & Brand P. 1995, MNRAS, 274, L77
Puxley P., Hawarden T. & Mountain M. 1990, ApJ, 364, 77 (PHM)
Ramsay S., Chrysostomou A., Geballe T., Brand P. & Mountain M. 1993, MNRAS, 263, 695
Ramsay S., Moutain C. & Geballe T. 1992, MNRAS, 259, 751
Raymond J., Cox D. & Smith B. 1976, ApJ, 204, 290
Renzini A. & Buzzoni A. 1986, in "Spectral Evolution of Galaxies", ed. Chiosi C. & Renzini A.
Rieke G., Lebofsky M., Thompson R., Low F. & Tokunga T. 1980, ApJ, 233, 24
Rieke G., Lebofsky M. & Walker C. 1988, ApJ, 325, 679
Roberge W., Dalgarno A. & Flannery B. 1981, ApJ, 243, 817
Ruze J. 1966, Proc. IEEE, Vol. 54, No. 4, p.633
Sage L., Mauersberger R. & Henkel C. 1991, A&A, 249, 31
Sams III B., Genzel R., Eckart A., Tacconi-Garman L. & Hofmann R. 1994, ApJ Lett., 430, L33
Sandage A. & Bedke J. 1995, The Carnegie Atlas Of Galaxies
Sandage A. & Tammann G. 1975, ApJ, 196, 313
Sanders D., Soifer B., Elias J., Madore B., Mathews K., Neugebauer G. & Scoville N. 1988, ApJ, 325, 74
Savage B. & Mathis J. 1979, Ann. Rev. Astr. & Ap., 17, 73
Schilke P., Carlstrom J., Keene J. and Phillips T. 1993, ApJ Lett., 417, L67
Schröder K., Staemmler V., Smith M., Flower D. & Jaquet R. 1991, J.Phys.B: At. Mol. Opt. Phys, 24, 287
Schulz H. & Wegner G. 1992, A&A, 266, 167

Scoville N., Soifer B., Neugebauer G., Young J., Mathews K. & Yerka K. 1985, ApJ, 289, 129
Scoville N., Yun M., Clemens D., Sanders D. & Waller W. 1987, ApJ Suppl. 63, 821
Shu F. 1993, "Radiation", University Science Books
Shu F., Adams F. & Lizano S. 1987, Ann. Rev. Astr. & Ap., 25, 23
Shull M. 1987, in "Interstellar Processes", Kluwer Academic Publishers
Smith P. 1992, PhD Thesis, University of Edinburgh
Snow T. & Witt A. 1995, Science, 270, 1455
Solomon P. 1966, cited in Field *et al.* (1966)
Solomon P., Rivolo A., Mooney T., Barrett J. & Sage L. 1987, in "Star Formation in Galaxies", ed. Persson C., U.S. Government Printing Office, Washington
Spaans M., Tielens A., van Dishoeck E. & Bakes E. 1994, ApJ, 437, 270
Stacey G., Geis N., Genzel R., Lugten J., Poglitsch A., Sternberg A., Townes C. 1991, ApJ, 373, 423
Stark A., Bally J., Wilson R. & Pound M. 1989, in "The Center of the Galaxy", ed. Morris M., 1AU Symp. 136
Stecher T. & Williams, D. 1967, ApJ Lett., 149, L29
Sternberg A. 1988, ApJ, 332, 400
Sternberg A. & Dalgarno A. 1989, ApJ, 338, 197
Takayanagi K., Sakimoto K. & Onda K. 1987, ApJ Lett., 318, L81
Tauber J., Lis D., Keene J., Schilke P. & Büttgenbach T. 1995, A&A, 297, 567
Telesco C. 1988, Ann. Rev. Astr. & Ap., 26, 343
Telesco C. 1993, in "Infrared Astronomy", ed. Mampaso A., Prieto M. & Sánchez F., Cambridge University Press
Telesco C., Dressel L. & Wolstencroft R. 1993, ApJ, 414, 120
Telesco C. & Harper D. 1980, ApJ, 235, 392
Tielens A. & Hollenbach D. 1985, ApJ, 291, 722
Tomisaka K. & Ikeuchi S. 1988, ApJ, 330, 695
Turner B. 1985, ApJ, 299, 312
Turner J. & Ho P. 1983, ApJ Lett., 268, L79
Turner J. & Ho P. 1985, ApJ Lett., 299, L77
Ulrich M-H. 1978, ApJ, 219, 424
Ulvestad J. & Antonucci R. 1991, AJ, 102, 875
Ulvestad J. & Antonucci R. 1994, ApJ Lett., 424, L29
van den Bergh S. 1992, PASP 104, 861
van Dishoeck E. 1988, in "Rate Coefficients in Astrochemistry", ed. Millar T. & Williams D., Kluwer Academic Publishers
van Dishoeck E. & Black J. 1988, ApJ, 334, 771
Völk H., Klein U. & Wielbinski R. 1989, A&A, 213, L12
Walker C., Narayanan G., Büttgenbach T., Carlstrom J., Keene J. & Phillips T. 1993, ApJ, 415, 672
Wall W., Jaffe D., Bash F., Israel F., Maloney P. & Baas F. 1993, ApJ, 414, 98
Wall W., Jaffe D., Israel F. & Bash F. 1991, ApJ, 380, 384
Watson A., Gallagher III J., Holtzmann J., Hester J., Mould J., Ballester G., Burrows C., Casertano S., Clarke J., Crisp D., Evans R., Griffiths R., Hoessel J., Scowen P., Stapelfeldt K., Trauger J. & Westphal J. 1996, AJ, 112, 534
Werner M. 1970, Ap. Lett., 6, 81

White G. 1994, A&A, 283, L25
White G., Ellison B., Claude S., Dent W. & Matheson D. 1994, A&A, 284, L23
White G. & Padman R. 1991, Nature, 354, 511
Whitworth A. 1979, MNRAS, 186, 59
Wild W. 1990, PhD Thesis, Ludwig-Maximilians-Universität, Munich
Wild W., Harris A., Eckart A., Genzel R., Graf U., Jackson J., Russell, A. & Stutzki J. 1992, A&A, 265, 447
Willacy K. & Brand P. 1996, in prep.
Williams D. & Hartquist T. 1984, MNRAS, 210, 141
Wright E. 1976, ApJ, 210, 250
Wolfire M., Hollenbach D. & Tielens A. 1989, ApJ, 344, 770
Wolfire M., Tielens A. & Hollenbach D. 1990, ApJ, 358, 116
Wynn-Williams G., Becklin E., Mathews K. & Neugebauer G. 1979, MNRAS, 189, 163
Zmuidzinas J., Betz A., Boreiko R. & Goldhaber D. 1988, ApJ, 335, 774

Appendix A

The K spectra observed across the starburst in NGC 253

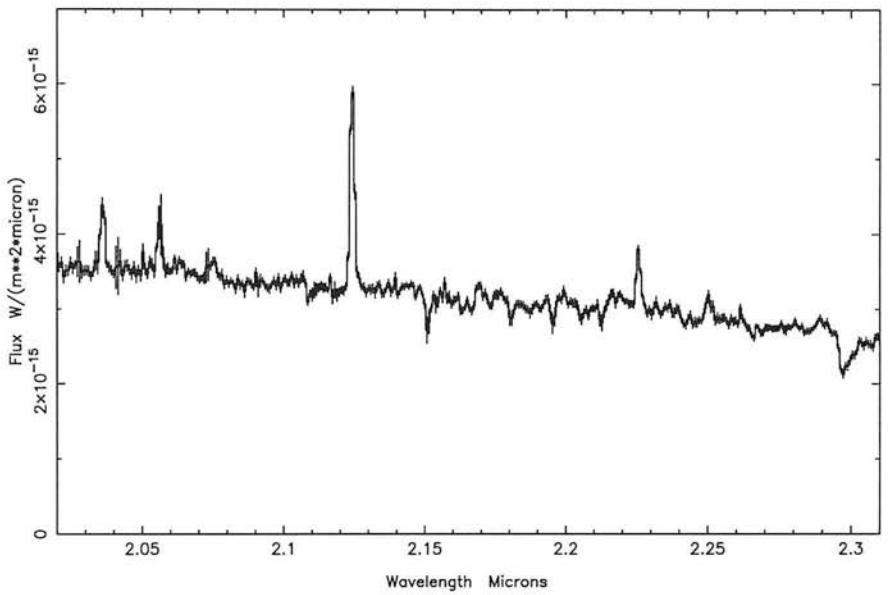

Figure A.1: The spectrum from +280 pc away the nucleus.

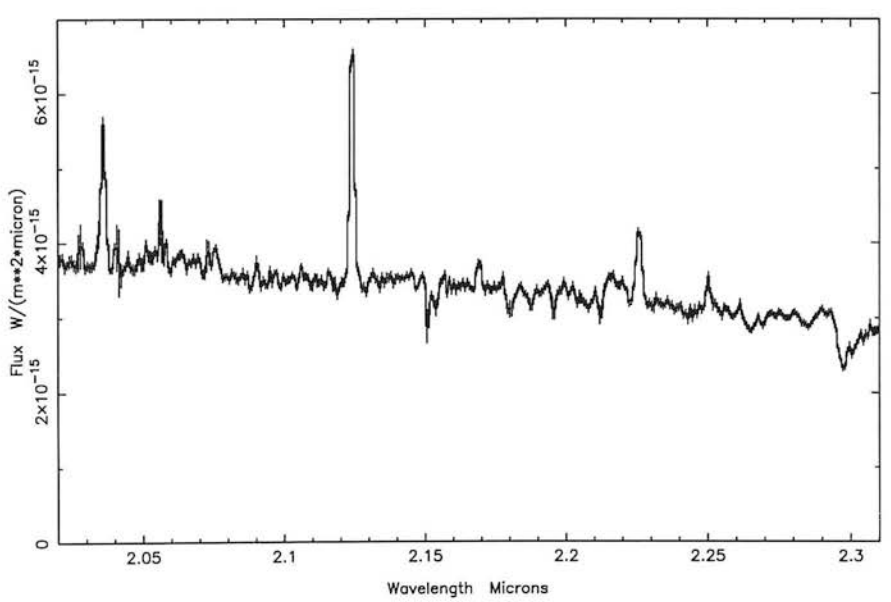

Figure A.2: The spectrum from +240 pc away the nucleus.

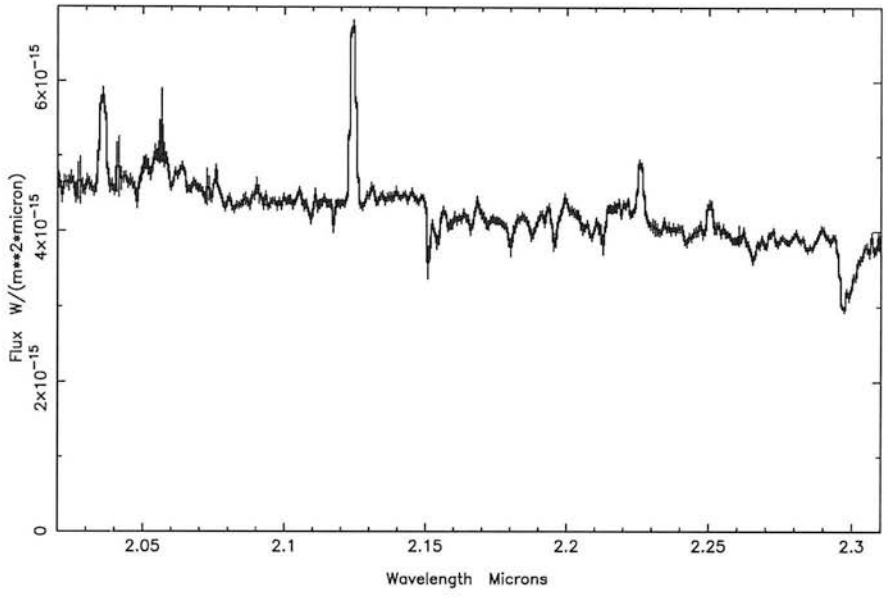

Figure A.3: The spectrum from +200 pc away the nucleus.

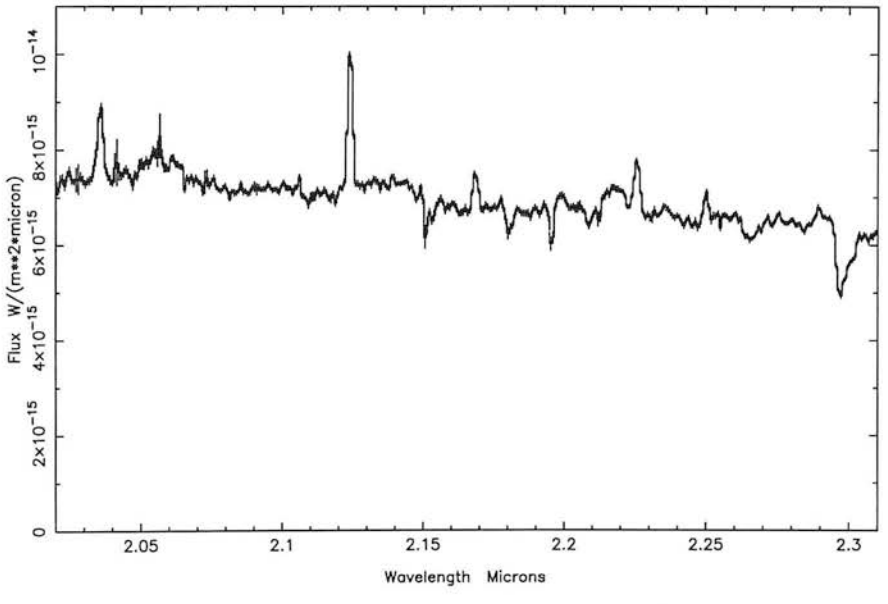

Figure A.4: The spectrum from +160 pc away the nucleus.

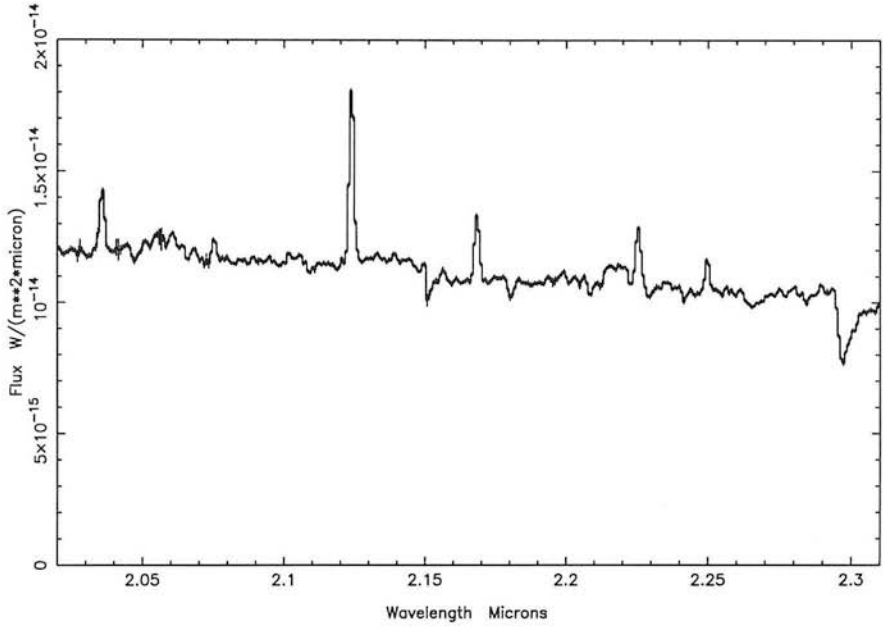

Figure A.5: The spectrum from +120 pc away the nucleus.

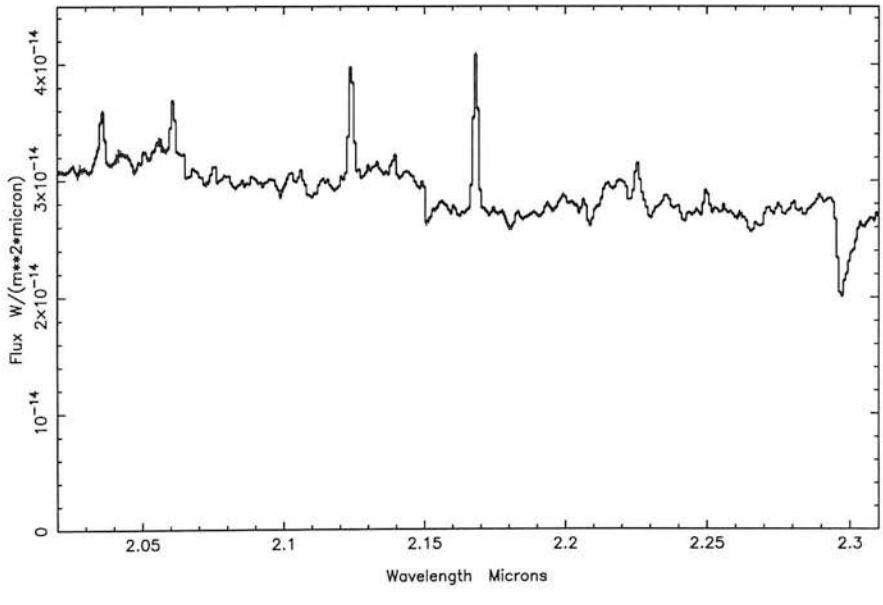

Figure A.6: The spectrum from +80 pc away the nucleus.

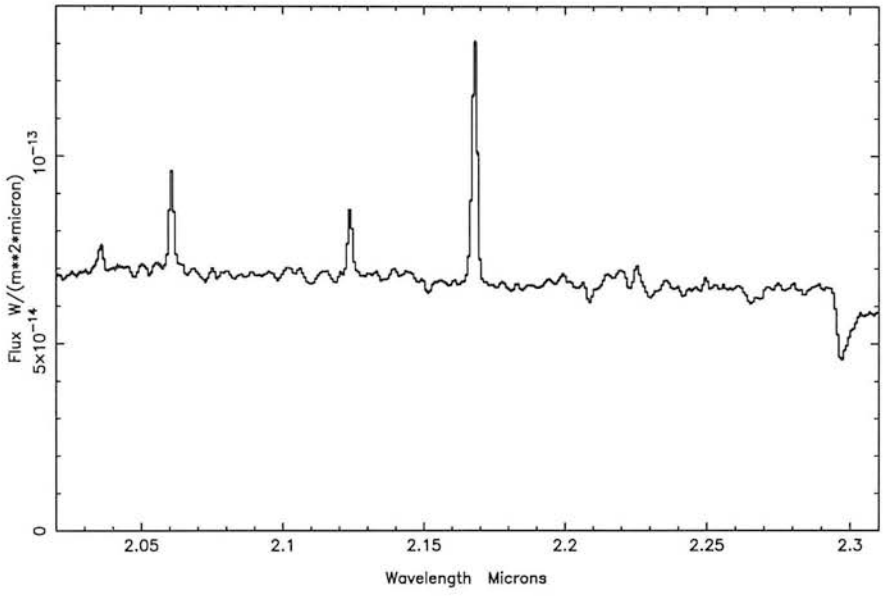

Figure A.7: The spectrum from +40 pc away the nucleus.

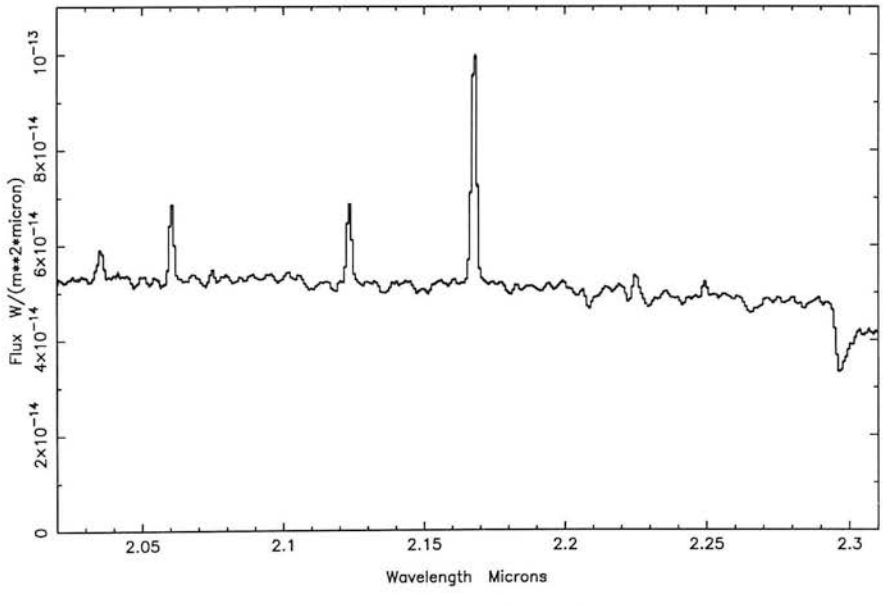

Figure A.8: The spectrum from the nucleus.

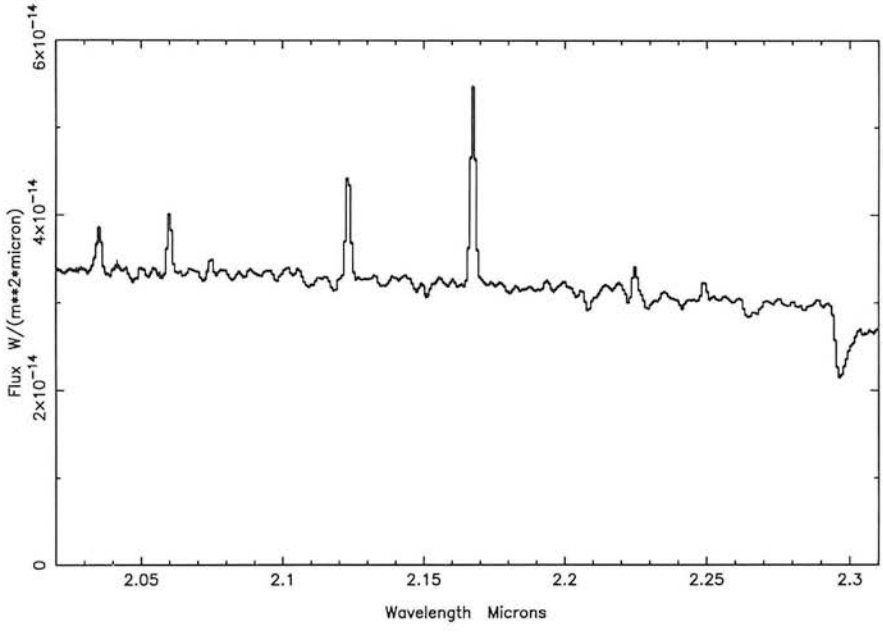

Figure A.9: The spectrum -40 pc away from the nucleus.

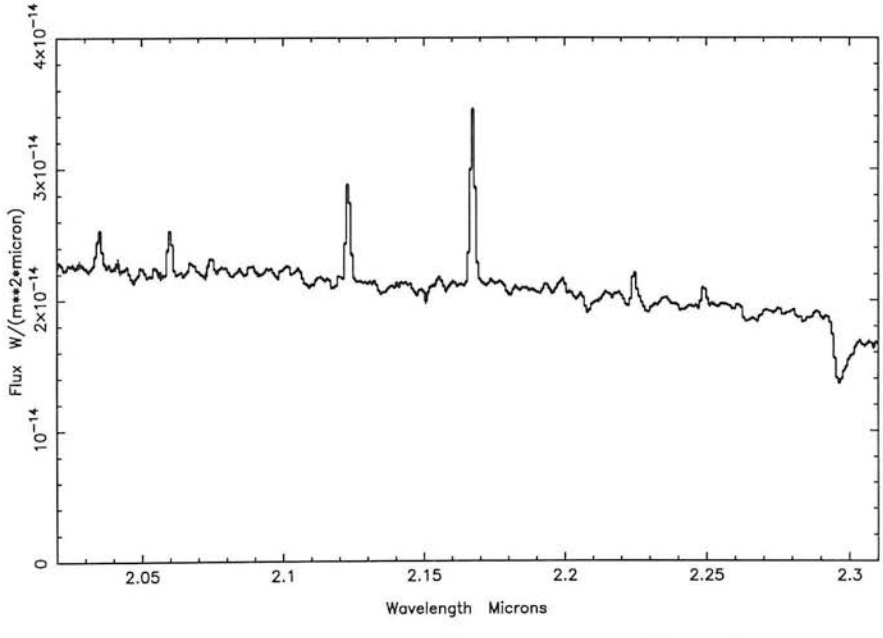

Figure A.10: The spectrum -80 pc away from the nucleus.

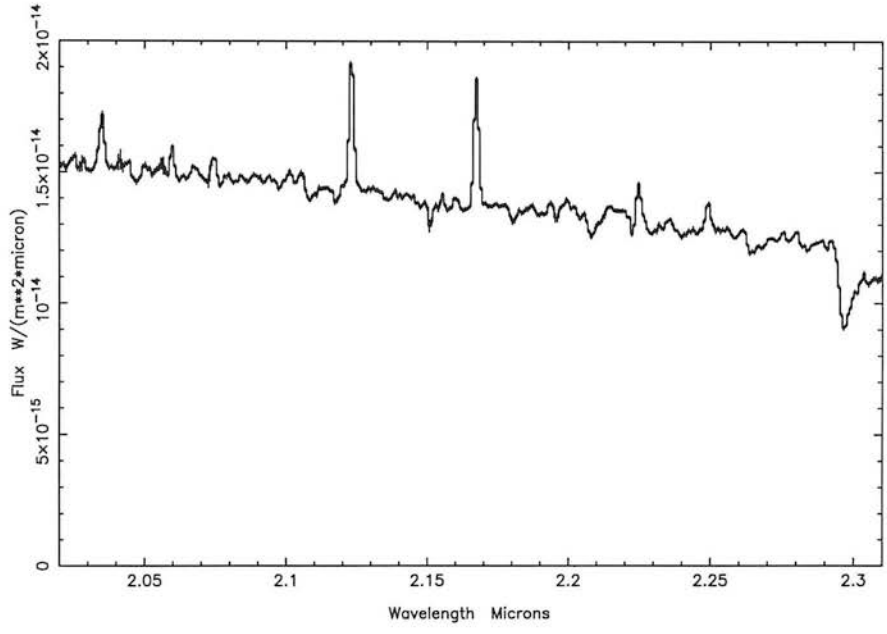

Figure A.11: The spectrum -120 pc away from the nucleus.

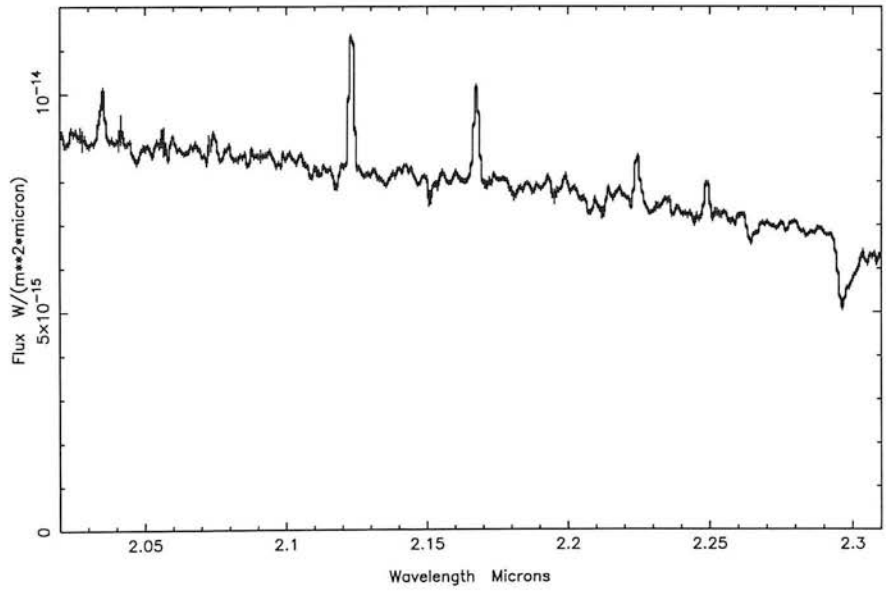

Figure A.12: The spectrum -160 pc away from the nucleus.

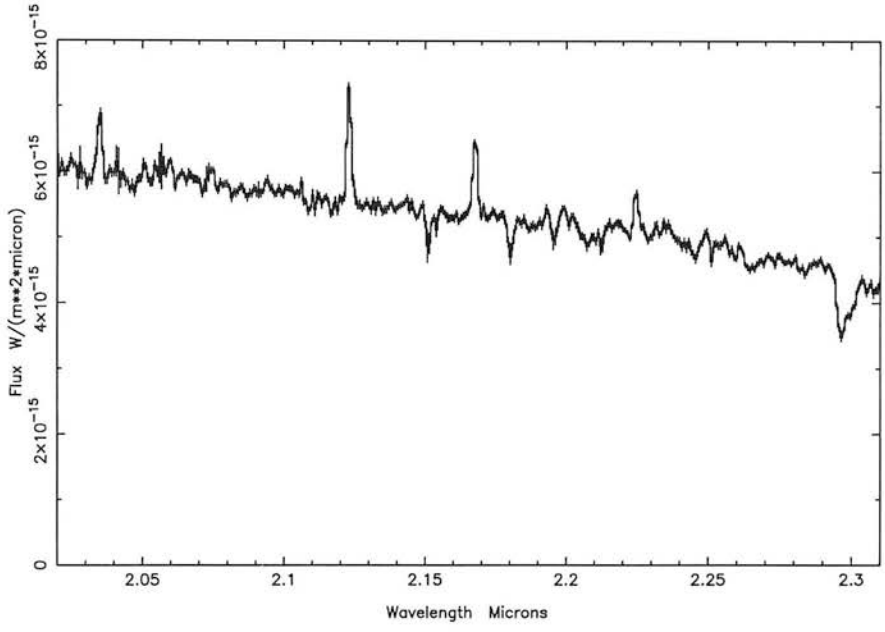

Figure A.13: The spectrum -200 pc away from the nucleus.

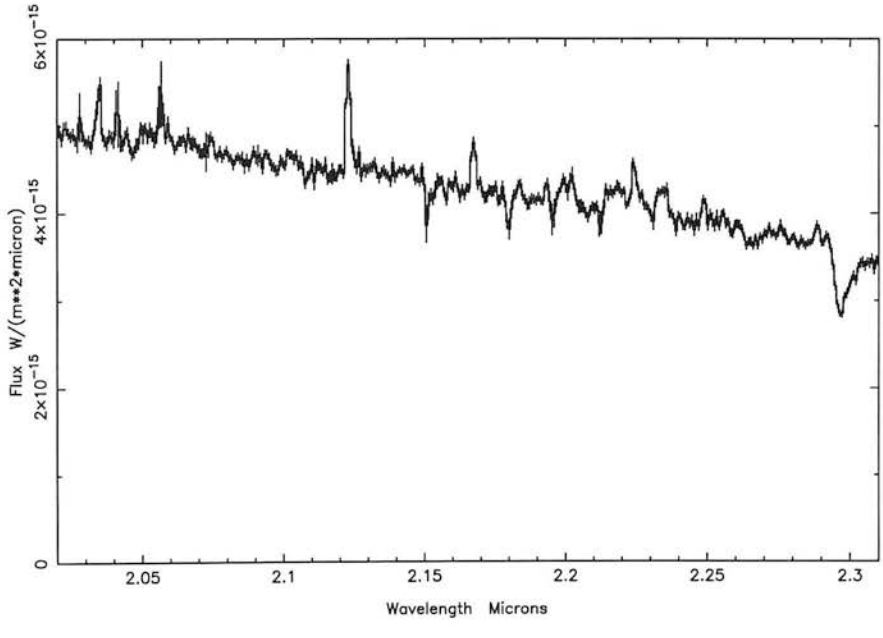

Figure A.14: The spectrum -240 pc away from the nucleus.

Appendix B

The use of sub-mm/mm lines as diagnostics of physical conditions

The only way we have to study CO, and indeed any component of the ISM, in a galaxy's nucleus is to observe the radiation it emits. It is therefore of importance to understand how the radiation is emitted and absorbed and what we can learn from this radiation. Below is a review of the physics of CO rotational emission.

B.1 Radiative Transfer in the Interstellar Medium

The change in specific radiation intensity dI_ν (units ergs s^{-1} cm^{-2} Hz^{-1} $ster^{-1}$) per path element ds is[1]

$$\frac{dI_\nu}{ds} = -\kappa_\nu I_\nu + \epsilon_\nu \tag{B.1}$$

where κ_ν and ϵ_ν are the absorption and emission coefficients respectively. Defining the optical depth as

$$\tau_\nu = \int_0^r \kappa_\nu \, ds \tag{B.2}$$

yields the transfer equation

$$\frac{dI_\nu}{d\tau_\nu} = -I_\nu + \frac{\epsilon_\nu}{\kappa_\nu} \tag{B.3}$$

which is linear and may be integrated, using an integrating factor e^{τ_ν}, to give

$$I_\nu = I_{\nu_0} e^{-\tau_\nu} + \int_0^{\tau_\nu} \frac{\epsilon_\nu}{\kappa_\nu} \, exp\left[-(\tau_\nu - \tau_\nu^{'})\right] d\tau_\nu^{'} \tag{B.4}$$

where I_ν is defined in Figure B.1 and ϵ_ν/κ_ν may vary throughout the absorbing region. If the emission is controlled solely by the temperature of the material, T, as it is when in thermal equilibrium with its surroundings, then Kirchoff's law states that

$$\epsilon_\nu = \kappa_\nu \, B_\nu(T) \tag{B.5}$$

where $B_\nu(T)$ is the Planck function,

$$B_\nu(T) = \frac{2h\nu^3}{c^2} \frac{1}{e^{h\nu/kT} - 1} \tag{B.6}$$

[1] Much of this section has been taken from Dyson & Williams (1980).

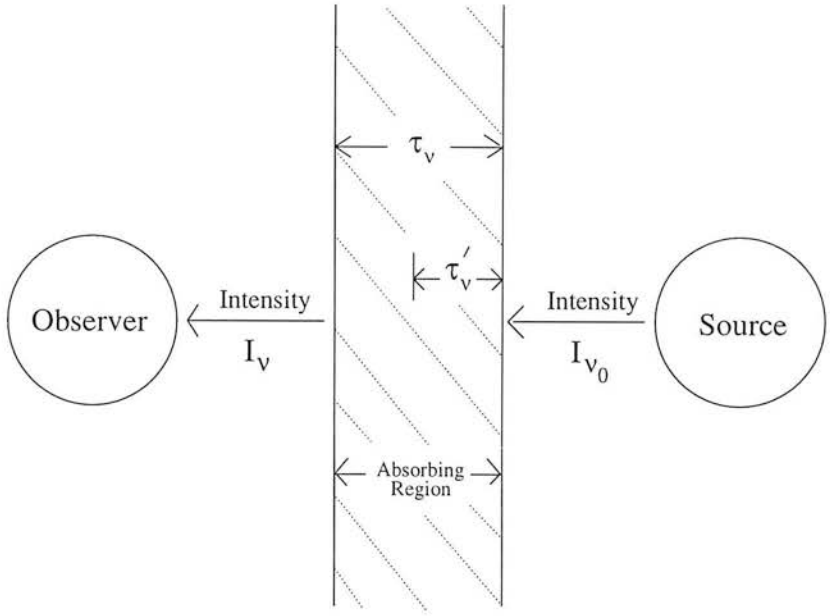

Figure B.1: A schematic diagram defining intensities after absorption

With equation B.5, equation B.4 becomes

$$I_\nu = I_{\nu_0} e^{-\tau_\nu} + B_\nu(T)\left(1 - e^{-\tau_\nu}\right) \tag{B.7}$$

B.2 Line emission and absorption

For a radiative transition between two energy levels, i and j, the emission and absorption coefficients are given by[2]

$$\epsilon_\nu^{Line} = \frac{h\nu_{ij}\Phi(\nu)}{4\pi} A_{ij} n_i \tag{B.8}$$

$$\kappa_\nu^{Line} = \frac{h\nu_{ij}\Phi(\nu)}{c}\left(B_{ji} n_j - B_{ij} n_i\right) \tag{B.9}$$

$\Phi(\nu)$ is the line profile (normalised to $\int \Phi_\nu d\nu = 1$), A_{ij}, B_{ij} and B_{ji} are the Einstein coefficients for spontaneous and stimulated emission and absorption, n_i is the number density of particles (*i.e.* ions, atoms, molecules) in a given energy state i. Statistical equilibrium requires that the rate of absorption exactly balances the rate of spontaneous and induced emission which means that the Einstein coefficients are related by

$$A_{ij} = \frac{8\pi h\nu^3}{c^3} B_{ij} = \frac{8\pi h\nu^3}{c^3}\frac{g_j}{g_i} B_{ji} \tag{B.10}$$

where g denotes the statistical weight of the energy levels.
With Eqs. B.2, B.9 and B.10 the optical depth in a transition $i \rightarrow j$ can be expressed as

$$\tau_\nu = \frac{c^2}{8\,\pi\,\nu^2} A_{ij}\Phi(\nu)\left(\frac{g_i}{g_j}\frac{N_j}{N_i} - 1\right) N_i \tag{B.11}$$

[2] Much of this section has been taken from Shu (1993).

where N_i denotes the column density in the level i. The level populations are determined by the balance between excitation and de-excitation and can be described by an excitation temperature, T_{ex}, defined by

$$\frac{N_i}{N_j} = \frac{g_i}{g_j} e^{-h\nu_{ij}/kT_{ex}} \tag{B.12}$$

The gas is said to be in *local thermodynamic equilibrium* (LTE) if the excitation temperature is the same for all levels.

CO is an example of the most common type of diatomic molecule because in its ground electronic state it has no net electronic angular momentum, *i.e.* the ground electronic state is $^1\Sigma$. This greatly decreases the number of available energy levels and facilitates the calculation of their energies and transition probabilities. The rotational states in the ground vibrational state of CO, and any linear molecule, have energies above the J = 0 ground state which are given to first order by

$$E_J = hB.J(J+1) \tag{B.13}$$

where J = 0,1,2... is the rotational quantum number (actually the total angular momentum quantum number) and B is the rotational constant of the molecule. For CO, hB/k = 2.77 K, for ^{13}CO, 2.64 K and, for C^{18}O, 2.63 K. The statistical weights of the levels are given by $g_J = 2J + 1$.

The Einstein A-coefficient for any transition is related to the dipole matrix element, $|\mu_{J',J}|$, by (Shu 1993)

$$A_{J,J'} = \frac{64\pi^4\nu^3}{3hc^3} \frac{g_{J'}}{g_J} |\mu_{J',J}|^2 \tag{B.14}$$

For a molecule such as CO, with a $^1\Sigma$ electronic ground state, the dipole matrix element is given by

$$|\mu_{J-1,J}|^2 = \mu_{rot}^2 \frac{J}{2J-1} \tag{B.15}$$

where μ_{rot} is the molecule's permanent electric dipole moment. Radiative transitions other than $\Delta J = \pm 1$ are forbidden. Thus, the Einstein A-coefficient for rotational transitions of CO from levels $J \rightarrow J$-1 is

$$A_{J\rightarrow J-1} = \frac{64\pi^4\nu^3}{3hc^3} \mu_{rot}^2 \frac{J}{2J+1} \tag{B.16}$$

μ_{rot} for CO (as well as its isotopes) is 0.11 Debyes (0.11×10^{-18} cgs).

B.3 Deriving the column density of carbon monoxide

B.3.1 When the molecular gas is in local thermodynamic equilibrium and optically thin

If the emission lines under consideration are optically thin, *i.e.* $\tau_\nu \ll 1$, then the calculation of column density is relatively straightforward.[3] The average column density of molecules in the telescope beam in the upper level J, N_J, is simply related to the energy intensity averaged over a telescope beam, I_ν, as

[3] Much of this section has been taken from Wild (1990) and Graf(1991).

$$N_J = \frac{4\pi}{A_{J',J} h\nu} \int I_\nu \, d\nu \tag{B.17}$$

In radio astronomy the energy intensity is usually expressed as a *brightness temperature* T_b defined as the temperature at which $B_\nu(T_b)$ equals the observed intensity I_ν. Under the condition that $h\nu \ll kT$ (the Rayleigh-Jeans limit), T_b is strictly proportional to I_ν:

$$I_\nu \stackrel{\text{def}}{=} B_\nu(T_b) = \frac{2\nu^2 k}{c^2} T_b \quad for \quad h\nu << kT \tag{B.18}$$

At sub-millimetre wavelengths the Rayleigh-Jeans condition is generally not satisfied. One therefore defines the *radiation temperature* T_R, which maintains the proportionality to I_ν at higher frequencies, by

$$I_\nu = \frac{2\nu^2 k}{c^2} T_R \tag{B.19}$$

and T_R is then related to T_b by (Rayleigh-Jeans correction):

$$T_R(T_b, \nu) = \frac{h\nu}{k} \frac{1}{e^{h\nu/kT_b} - 1} = T_b - \frac{h\nu}{2k} + ... \tag{B.20}$$

In terms of the radiation temperature, the average column density of molecules in state J observed in the optically thin $J \rightarrow J$-1 emission line is

$$N_J = \frac{8\pi k \nu^2}{A_{J,J-1} \, hc^3} \int T_R \, dV \tag{B.21}$$

where the integral is taken over all velocities in the line.

To calculate the total abundance of molecules we must correct for those in levels other than the observed one. Under the conditions of LTE the column density in the level J, N_J, relative to the total column density N_{tot} is given by

$$\frac{N_J}{N_{tot}} = \frac{g_J \; exp^{(-E_J/kT_{ex})}}{\sum_{J'=0}^{\infty} g_{J'} \; exp^{(-E_{J'}/kT_{ex})}} \tag{B.22}$$

which is usually referred to as the *Boltzmann equation*. For small B_{rot}/kT_{ex} the sum, called the *partition function*, may be replaced by an integral. Evaluation of the integral yields hB_{rot}/kT_{ex}. Using the statistical weights $g_J = 2J + 1$ we get

$$\frac{N_J}{N_{tot}} = \frac{hB_{rot}}{kT_{ex}} (2J + 1) \; exp^{(-E_J/kT_{ex})} \tag{B.23}$$

The total number of molecules (assuming LTE) is then related to the integrated radiation temperature of an optically thin line by

$$N_{tot} \approx \frac{1}{2J+1} \frac{8\pi k^2 \, \nu^2 \, T_{ex}}{A_{J,J-1} \, h^2 B_{rot} \, c^3} \; e^{E_J/kT_{ex}} \int T_R \, dV \tag{B.24}$$

B.3.2 Correcting for the optical depth of a line

From Eqs. B.11, B.12 and B.16 we have

$$\tau_\nu = \frac{8\pi^3}{3h} \frac{J}{2J+1} \mu_{rot}^2 \left[exp\left(\frac{2hBJ}{kT_{ex}} \right) - 1 \right] \frac{\nu}{c} N_J \Phi(\nu) \tag{B.25}$$

As $\Phi(\nu)d\nu$ is normalised to unity, it follows that the mean optical depth over the molecular rotational line $J \rightarrow J - 1$:

$$\tau_0 = \frac{8\pi^3}{3h}\frac{J}{2J+1}\mu_{rot}^2\left[exp\left(\frac{2hBJ}{kT_{ex}}\right)-1\right]\frac{N_J}{\Delta V} \tag{B.26}$$

where ΔV is the equivalent linewidth (defined in kms^{-1}). Substituting equation B.23 into B.26 we get

$$\tau_0 = \frac{8\pi^3}{3}\frac{\mu_{rot}^2 B_{rot}}{kT_{ex}}\frac{N_{tot}}{\Delta V}J\ f(J,T_{ex}) \tag{B.27}$$

where

$$f(J,T_{ex}) = \left[exp\left(\frac{-E_J}{kT_{ex}}\right)\right]\left[exp\left(\frac{h\nu}{kT_{ex}}\right)-1\right] \tag{B.28}$$

As $h\nu = 2hB_{rot}J$ and $E_J = hB_{rot}J(J+1)$, in the limit that $h\nu \ll kT_{ex}$ and $E_J \ll kT_{ex}$, it follows that

$$\tau_0 = \frac{16\pi^3}{3k^2}\frac{N_{tot}}{\Delta V}\frac{\mu_{rot}^2}{T_{ex}^2}J^2B_{rot}^2 \tag{B.29}$$

In the case where the line has a modest optical depth, *i.e.* $\tau \leq 1$, we can multiply the column density by $\tau_0/(1-e^{-\tau_0})$, where τ_0 is the optical depth at the center of the line, as an approximate correction.

B.3.3 Deriving the column density in non-equilibrium situations

In a very dense medium collisions, normally between the CO we are interested in and the more abundant H_2, are frequent enough to maintain a thermalised population, *i.e.* a population where $T_{ex} = T_{kin}$ (T_{kin} is the kinetic temperature of the gas) for all energy levels. In interstellar space, however, where collisions are relatively rare, de-excitation by spontaneous emission (described by the Einstein A-coefficient) can be much faster than de-excitation by collisions, leading to a decrease in population of the upper levels compared to a thermalised population. For these levels the excitation temperature is lower than the kinetic temperature and they are *subthermally excited*. The population of a given level j under non-LTE conditions is determined by the rate equation:

$$N_j\left[\sum_{k\neq j}(n_{H_2}\gamma_{jk} + R_{jk}) + \sum_{k<j}A_{jk}\right] = \sum_{k\neq j}N_k(n_{H_2}\gamma_{kj} + R_{kj}) + \sum_{k>j}N_kA_{kj} \tag{B.30}$$

where $R_{ij} = \int \mathrm{d}\Omega\ .\ B_{ij}/c$ is the induced radiative transition rate from level i to level j, which is proportional to the radiant energy density per frequency interval integrated over all solid angles. The left hand side describes all possible transitions going out from level j and the right hand side is the sum over all transitions leading into level j. γ_{jk} and γ_{kj} are collision rate coefficients. A simple indicator for the balance between spontaneous emission and collisional excitation is the *critical density*, defined as the ratio of the A-coefficient to the collision rate coefficient for a given transition: $\mathrm{n}_{crit} = A_{ij}/\gamma_{ij}$. If the gas density is substantially lower than n_{crit}, the transition i $\rightarrow$ j is subthermally excited.. This definition for n_{crit} is only useful in optically thin gas, *i.e.* when R_{jk} and R_{kj} are small. In optically thick gas the relative populations can be considerably altered by absorption of line photons emitted in a neighbouring part of the cloud (*trapping*). Trapping has the same effect as an A coefficient lower by a factor of $1/\tau$.

In very optically thick gas ($\tau > 10$) trapping ties the level populations to the brightness temperature of the radiation field, since the rate equation becomes dominated by the induced radiative transitions. Thus, a high optical depth can thermalise the level populations in the same way as a high gas density and effectively lowers the critical density.

B.4 Diagnosing the physical conditions within the emitting gas

The radiation temperature emitted in a spectral line is

$$T_R = (1 - e^{-\tau_\nu}) T_{ex}^{R-J} + e^{-\tau_\nu} T_{R,bg} \tag{B.31}$$

where T_{ex}^{R-J} is the *Rayleigh − Jeans corrected* excitation temperature and depends on T_{ex} in the same way as T_R depends on T_b. The observed brightness T_{obs} (corrected for telescope and atmospheric losses and source coupling) is given by

$$T_{obs} = \Phi \, f \, T_R \tag{B.32}$$

where the beam filling factor Φ is the fraction of the beam area that is filled by emitting gas. The beam dilution factor f (≤ 1) corrects for the coupling of the beam to a small source (see below). It is one for a source much larger than the beam and < 1 if the source is smaller than, or on the order of, the beam.

For high excitation temperatures we can neglect the 2.7 K cosmic microwave background, and the observed brightness temperature in the two limits of optically thick and optically thin emission is given by

$$T_b = \Phi \, f \, T_{ex} \quad (\tau_\nu \gg 1) \tag{B.33}$$

$$T_b = \Phi \, f \, T_{ex} \, \tau_\nu \quad (\tau_\nu \ll 1) \tag{B.34}$$

The brightness temperature ratio of different transitions of a molecule is used as a diagnostic in multi-line studies. It follows that, in the limit of excitation temperatures larger than 2.7 K

$$\frac{T_J}{T_{J'}} = \frac{\Phi_J \, f_J \, (1 - e^{-\tau_J})(T_J^{ex})}{\Phi_{J'} \, f_{J'} \, (1 - e^{-\tau_{J'}})(T_{J'}^{ex})} \tag{B.35}$$

where the indices J and J' refer to transitions $J \rightarrow J - 1$ and $J' \rightarrow J' - 1$, respectively. In the optically thick limit the ratio, for equal beam filling factors, becomes

$$\frac{T(J \rightarrow J-1)}{T(J' \rightarrow J'-1)} = \frac{f_J}{f_{J'}} \tag{B.36}$$

i.e. the ratio of the beam dilution factors for the two transitions. Thus, for a source large compared to both beam sizes (*i.e.* $f_J = f_{J'} = 1$) or equal beams the brightness temperature ratio for two optically thick transitions of the same molecule is unity.

For the optically thin case and equal beam filling factors and excitation temperatures the brightness temperature ratio is

$$\frac{T(J \rightarrow J-1)}{T(J' \rightarrow J'-1)} = \frac{f_J \, \tau_J}{f_{J'} \, \tau_{J'}} \tag{B.37}$$

Equation B.29 highlights that $\tau \propto J^2$. Including the weak temperature dependence, that equation B.26 ignores, optically thin gas from a source large compared to both beam sizes (*i.e.* $f_J = f_{J'} \approx 1$), with excitation temperature T_{ex}, has a brightness temperature ratio in the $J \rightarrow J-1$ to $J-1 \rightarrow J-2$ transitions of

$$\frac{T_J}{T_{J-1}} = \left(\frac{J}{J-1}\right)^2 e^{-2hBJ/kT_{ex}} \tag{B.38}$$

Thus, the brightness temperature ratio is larger than one in the optically thin case under the conditions mentioned above.

The situation becomes more complicated for non-LTE situations. Since the higher rotational levels depopulate radiatively faster than the lower levels (the Einstein A coefficient increases as ν^3, see Equation B.16) a higher density is required to maintain a given population. If the gas density is below the critical density of a level then this will be depopulated with respect to the level expected in LTE. Only levels with critical densities below the ambient particle density will have significant populations. An increase in temperature will tend to redistribute the population only among the thermalised states.

B.5 Fine-structure lines

The analysis of the radiation from species such as CI and CII is similar to CO, making use of the same definitions for excitation temperature and partition function.

The carbon atom has a ^{3}P ground term, split by spin-orbit coupling into three levels. The total electronic angular momentum quantum number, called J, has the values 0, 1 and 2 resulting in ground term levels $^3P_0$, $^3P_1$ and $^3P_2$. The statistical weights, g_J, of these lowest three energy levels are again equal to 2J + 1. Because CI has only three accessible energy states at temperatures common in molecular clouds (T < 100 K), with energies $E_0 = 0$, $E_1/k = 23.6$ K and $E_2/k = 62.5$ K, the partition function is given by

$$f = 1 + 3exp\left(-\frac{23.6}{T_{ex}}\right) + 5exp\left(-\frac{62.5}{T_{ex}}\right) \tag{B.39}$$

Similar to the case for CO, equation B.24, the total number of atoms is related to the integrated temperature of an optically thin line through

$$N_T \approx \frac{1}{g_J} exp\left(\frac{E_J}{kT_{ex}}\right) f \frac{8\pi k\nu^2}{A_{J,J'}hc^3} \int TdV \tag{B.40}$$

Singly ionised carbon, CII, has a ^{2}P ground state term, split by spin-orbit coupling into levels $^2P_{1/2}$ and $^2P_{3/2}$. Again, the statistical weight of each level is 2J + 1 where J has the values 1/2 and 3/2. Assuming LTE, the partition function for CII is

$$f = 2 + 4exp\left(-\frac{91.2}{T_{ex}}\right) \tag{B.41}$$

The total number of CII ions can be found from equation B.40.

B.6 Absolute calibration of data

The absolute calibration of mm and sub-mm line intensities is done by calibrating the receiver system with blackbody loads of known temperature and correcting for telescope and atmospheric

losses. The detected signal is then conveniently expressed in terms of an equivalent Rayleigh-Jeans antenna temperature, T_A^*, which is related to the Rayleigh-Jeans radiation temperature, T_R, of the source through the relationship (see Kutner & Ulich 1981)

$$T_A^* = \eta_{tot} \left(\frac{\int\int_{source} P_n(\Omega) B_n(\Omega) d\Omega}{\int\int_{4\pi} P_n(\Omega) d\Omega} \right) T_R \tag{B.42}$$

P_n is the normalised power pattern of the antenna ($P_n(0) = 1$) and B_n is the normalised brightness distribution of the source.

For the source-antenna coupling η_c, given by the term in parentheses in equation B.42, it is convenient to distinguish three different regimes depending on the source size relative to the power pattern of the telescope.

First, if the source solid angle Ω_s is much larger than Ω_0, the combined solid angle of diffraction main beam, side-lobes and error beam, the resulting coupling efficiency η_{fss} is a measure of the power lost due to (forward) scattering and spill-over

$$\eta_c(\Omega_s > \Omega_0(side-lobes, errorbeam)) = \eta_{fss} = \frac{\int\int_{\Omega_0} P_n(\Omega) d\Omega}{\int\int_{2\pi} P_n(\Omega) d\Omega} \tag{B.43}$$

The source coupling efficiency for sources larger than the main diffraction beam (solid angle Ω_{mb}), but smaller than the side-lobes/error beam is often referred to as *main beam efficiency*, η_{mb}

$$\eta_c(\Omega_{mb} < \Omega_s \ll \Omega_0(side-lobes, errorbeam)) = \eta_{mb} = \frac{\int\int_{\Omega_{mb}} P_n(\Omega) d\Omega}{\int\int_{2\pi} P_n(\Omega) d\Omega} \tag{B.44}$$

The antenna temperature corrected for telescope and atmospheric losses, side band imbalance and main beam efficiency is referred to as *main beam brightness temperature*.

Finally, if the source size is comparable to, or smaller than, the main diffraction beam, the coupling efficiency is further reduced by the beam dilution factor $f(\leq 1)$, and is given by

$$\eta_c(\Omega_s < \Omega_{mb}(side-lobes, errorbeam)) = \eta_{mb} f(\Omega_s, \Omega_{mb}) = \frac{\int\int_{\Omega_s} P_n(\Omega) B_n(\Omega) d\Omega}{\int\int_{2\pi} P_n(\Omega) d\Omega} \tag{B.45}$$

B.7 Correcting for an error beam

The beam of the JCMT dish has been studied for several years.[4] "*Holography*" is employed to obtain a beam as close to a perfect paraboloid as possible. The beam pattern is recorded at two focus settings using a 94 GHz source located in the UKIRT dome, *i.e.* within the near field. Measurements with the holography technique show that the rms fluctuations of the antenna surface are about 25-30 μm; this is the result of small-scale (fractions of a panel in size) errors having an rms of 15 μm, and large-scale (typically about 5 m) structure with deviations of about 20 μm.

Random surface errors decrease the antenna gain in a way described by the Ruze (1966) equation:

$$G = G_0 e^{-(4\pi\epsilon/\lambda)^2} \tag{B.46}$$

where G_0 is the gain of an identical antenna without surface errors and ϵ is the effective reflector tolerance, usually defined by the RMS of the surface deviations. If the surface errors are random,

[4] Much of this section has been taken from Graf (1991).

i.e. no spherical aberration or astigmatism, the power missing in the telescope main beam gets distributed smoothly in a wider *error beam*, a pedestral underlying the main beam. The size of the error beam is inversely proportional to the correlation length of the surface errors. In general the individual panels of a telescope are accurate enough that their contribution to the error pattern is negligible. The main inaccuracies result from errors in the relative setting of the panels, causing phase jumps between panels. Thus the correlation length of the errors is usually on the order of the panel dimensions or larger. On large sub-millimeter telescopes, such as the JCMT, the panel size is typically on the order of a tenth of the telescope diameter and the error beam width is therefore not larger than approximately 10 times the width of the diffraction limited beam.

A strong error beam pattern leads to difficulties in the calibration of astronomical data, since the coupling efficiency to a given source (including calibration sources) can only be calculated if the detailed beam shape is well enough known. The definition of a beam size, which is usually given as the FWHM of the main beam, does not make sense if the beam is composed of several components of vastly different widths and if these components pick up comparable amounts of the source flux. In an extended source, even an error beam with relatively low on-axis power can obtain a large fraction of the total power, because it integrates over a larger area than the main beam.

Coupling of a multi-component beam to a source is given by (Graf 1991):

$$\frac{T_A^*}{T_R} = \eta'_{mb} \frac{\sum_i a_i \theta_i^2 f_i}{\sum_i a_i \theta_i^2} \tag{B.47}$$

where η'_{mb} is an equivalent main beam efficiency for the composite beam, a_i is the peak *power* amplitude of the i'th Gaussian beam, θ_i is the *power* FWHM of the i'th Gaussian beam and f_i is the geometrical filling factor in the i'th beam.

For a gaussian beam of FWHM θ_b centered on a Gaussian source (FWHM = θ_s), the filling factor is

$$f = \frac{1}{(\theta_{mb}/\theta_s)^2 + 1} \tag{B.48}$$

and on a uniform temperature disk of diameter D:

$$f = 1 - exp[-ln2(D/\theta_b)^2] \tag{B.49}$$

B.8 Calibration using standards

In the mm and sub-mm wavelength regime the Moon and the planets are used as standard flux calibrators. Absolute broad band fluxes for the planets have been given by Hildebrand *et al.* (1985) and Griffin *et al.* (1986) based on the model of infrared emission of Mars by Wright (1976). By observing a planet of known angular size, D, the filling factor of the planet can be obtained using equation B.47 for a beam of size θ_b.

Mon. Not. R. Astron. Soc. 277, 413–422 (1995)

Atomic carbon and carbon monoxide in the nuclear region of NGC 253

Andrew Harrison,[1] Phil Puxley,[2] Adrian Russell[2] and Peter Brand[1]
[1]Institute for Astronomy, University of Edinburgh, Blackford Hill, Edinburgh EH9 3HJ
[2]Royal Observatory, Blackford Hill, Edinburgh EH9 3HJ

Accepted 1995 May 12. Received 1995 May 12; in original form 1994 July 1

ABSTRACT

We have observed neutral carbon, [C I], and isotopic carbon monoxide ($C^{18}O$ 3→2 and $C^{18}O$ 2→1) towards the nucleus of the starburst galaxy NGC 253. [C I] is bright and we derive a mean abundance ratio $C^0/CO \sim 0.5$ across the central ~300 pc of the starburst. Observations of ^{13}CO, by Wall et al., indicate that the bulk of the molecular gas in the starburst region is hot ($T \sim 100$ K) and dense ($n > 10^4$ cm^{-3}). Our observations show that $C^{18}O$ traces the smaller fraction of cold molecular gas and, thus, is a poor tracer of the column density of molecular gas in NGC 253. The effects of selective photodissociation on CO and its isotopomers means that it is unwise to use CO to derive reliable estimates of the intrinsic $^{16}O/^{18}O$ ratio in starburst nuclei.

Standard models of photon-dominated regions (PDRs) can only account for about 5 per cent of the observed C^0 emission. As most of the molecular gas is at low visual extinction and is hot, the enhanced cosmic ray flux expected in the nucleus of NGC 253 should play little or no part in enhancing the carbon emission with respect to other PDR tracers and CO. The nature of the bulk of the molecular gas in NGC 253, and the size of the region (~300 pc), rules out time-dependent chemistry across the nucleus as the explanation for the large abundance of atomic carbon. The most plausible explanation for the brightness of [C I] emission is that the C/O elemental ratio is higher in NGC 253 than in the models with which we compare our observations.

NGC 253 shows evidence for a dense torus of gas around the nucleus ($R \sim 50$ pc) but does not have any inner Lindblad resonances. The most likely explanation for the existence of the torus is pressure confinement of the gas by a superwind.

Key words: ISM: molecules – galaxies: abundances – galaxies: individual: NGC 253 – galaxies: ISM – galaxies: nuclei – galaxies: starburst.

1 INTRODUCTION

The neutral carbon (C^0) ground-state fine-structure line ($^3P_1 \rightarrow {}^3P_0$) has been observed within our Galaxy and is found to be bright and widespread, and to bear a strong resemblance in antenna temperature, line shape and spatial distribution to the low-J rotational lines of ^{13}CO. This resemblance has been attributed to the similar opacities and excitation requirements of C^0 and ^{13}CO and shows that, to some degree, the species are co-existent. The initial chemical equilibrium models of molecular clouds, e.g. Langer (1976), predicted a C^0 abundance in a relatively thin layer near the cloud surface. Models of photon-dominated regions (PDRs), where high UV fields impinge on the surfaces of molecular clouds, showed that a layer of C^0 would be produced with a fairly constant column density of $N(C^0) \sim 5 \times 10^{17}$ cm^{-2} (Hollenbach, Takahashi & Tielens 1991), over a large range of UV field strengths and cloud densities.

Such homogeneous PDR models fail to account for C^0 observed at depths with A_V greater than ~10. However, molecular clouds are extremely clumpy and this clumpiness allows UV radiation to penetrate to greater depths than would be possible if the clouds were composed of a uniform medium. It is still uncertain theoretically whether the C^0 is produced in PDRs on the surfaces of the clumps (Stutzki et al. 1988), or arises predominantly from an interclump medium (Meixner & Tielens 1993).

Walker et al. (1993) argue that molecular outflows associated with young stellar objects show no evidence for shock enhancement of C^0, but White (1994) argues that, in the C-shocked region of IC 443C, C^0 is overabundant, by an order of magnitude, compared with quiescent molecular

cloud cores. This enhancement of C^0 in the supernova (SN) remnant could be caused by either the shock(s) or an enhanced cosmic ray flux density.

Only two extragalactic sources, IC 342 and M82, have been observed, to date, in [C I]. Büttgenbach et al. (1992), from a single spectrum of the nucleus, model the [C I] emission from IC 342 in terms of PDRs that have higher gas densities than those typically found in the Milky Way.

In M82, Schilke et al. (1993) observed five spectra at selected positions in the nuclear region. White et al. (1994) have complemented the work of Schilke et al. by making a map of the whole region. Both groups find that the C^0 emission from M82 is about an order of magnitude brighter than predicted by PDR models (Wolfire, Tielens & Hollenbach 1990). They also find that C^0/CO is ~0.6 (throughout this paper C^0/CO represents the ratio of total column densities of C^0 and CO). Both groups find that they can explain the enhanced carbon emission by invoking recent chemical models, outlined by Flower et al. (1994), which predict a high abundance of C^0 deep in the interiors of clouds even in the absence of UV radiation. The equilibrium value of C^0/CO depends on the fractional ionization of the gas and allows C^0 production in the presence of a strong cosmic ray flux. Both groups argue that there is a high cosmic ray rate (300 times the local solar neighbourhood value) in the centre of M82 and that the high carbon abundance can be explained by these chemical models.

Nearby (distance ~2.5 Mpc; de Vaucouleurs 1978), and luminous at all wavelengths, NGC 253 is a dusty highly inclined spiral and, along with M82, is an archetypal starburst galaxy. High-resolution millimetre-wave observations show that a 40×10 arcsec^2 FWHM bar-like feature dominates the ^{12}CO $J = 1 \rightarrow 0$ emission (Canzian, Mundy & Scoville 1988). Harris et al. (1991) detected ^{12}CO $J = 6 \rightarrow 5$ which shows that NGC 253 contains large amounts of molecular gas that is both warm and dense. Wall et al. (1991) have shown that a hot compact central source (diameter <15 arcsec) causes the higher lines of CO to be excited.

The existence of a starburst in NGC 253 is supported by the high far-infrared luminosity $L_{\rm FIR} = 1.6 \times 10^{10}\ {\rm L}_\odot$, most of which originates within the central 30 arcsec (Telesco & Harper 1980), IR hydrogen recombination Brackett line fluxes (Beck & Beckwith 1984), and ionic and atomic fine-structure lines (Carral et al. 1994). Mauersberger & Henkel (1991) noted that, because SiO was found over a large volume in the nuclear region of NGC 253, a heating mechanism was required that acted efficiently on a large volume of gas without destroying the molecules. They suggested dissipation of tidal energy as a suitable heating mechanism. An alternative heating agent would be large fluxes of cosmic rays as proposed by Suchkov, Allen & Heckman (1993).

Carral et al. (1994) suggested a scenario for the interstellar medium (ISM) of NGC 253 in which molecular clouds and H^+ gas are in pressure balance with a supernova-shocked, hot, low-density, all-pervasive medium. Pressure balance implies that the density scales inversely with temperature. The ISM in NGC 253 may be more complicated than the picture of Carral et al. (1994), as Wall et al. (1991) argue that the hot dense, and hence high-pressure CO is centred on the nucleus and that both density and temperature drop off with distance from the nucleus. Also, Mauersberger, Henkel & Sage (1990) argue that the HC_3N-emitting gas consists of two components, with the bulk of the HC_3N emission arising from gas with densities of about 10^4 cm^{-3} and a minor contribution arising from hotter and denser gas. It would seem that not all of the molecular gas around the nucleus of NGC 253 is in dynamic equilibrium, but all of the gas in NGC 253 is at high pressure ($P/k > 10^5$ K cm^{-3}). Carral et al. (1994) suggested that the high pressure is maintained by frequent supernovae. Although it may be not strictly true that all the ISM in NGC 253 is in pressure equilibrium, the majority of the mass of the ISM is close enough to equilibrium to allow a reasonable estimate of the temperature of a given component of the ISM at a certain density.

Given the robustness of [C I] emission, with a fairly constant brightness predicted for a range of UV fields and gas densities, it was hoped, when we made our observations, that we would have a direct measure of the number of PDRs towards the nucleus of NGC 253. $C^{18}O$ emission is expected to be optically thin and, as Henkel et al. (1993) derived $^{16}O/^{18}O \sim 200$, we hoped that observations of $C^{18}O$ would allow a direct comparison between atomic carbon and carbon monoxide.

2 OBSERVATIONS

All the observations were made with the 15-m James Clerk Maxwell Telescope (JCMT). The back-end used was the digital autocorrelation spectrometer (DAS). The adopted map centre (0, 0) was the nucleus of NGC 253, which was taken to be $\alpha(1950) = 0^{\rm h}45^{\rm m}5\overset{\rm s}{.}8$ $\delta = -25°33'38''$. The observations were made by beam switching to a reference position 120–150 arcsec north of the source.

A grid of 16 [C I] spectra was observed towards NGC 253 on 1993 November 10 and 11, using the SIS receiver Rx C2 and with the DAS operated in 920-MHz bandwidth mode. The telescope efficiency was measured using Saturn and assuming a two-component beam with 80 per cent of the power in the 10-arcsec diffraction beam and 20 per cent of the power in a 30-arcsec error beam. We calculate that this composite beam has a coupling efficiency of $\eta_{\rm c(Sat)} = 0.71$ to Saturn (diameter of 16.3 arcsec). Correcting for this coupling we find $\eta_{\rm B}$ (the fraction of power in the two-component beam) measured from Saturn to be $\eta_{\rm B} = 0.35$. This is effectively the coupling of the telescope to a source of roughly 60-arcsec diameter. Saturn was used to check the pointing, which was good to 2 arcsec (rms).

A single spectrum was taken of $C^{18}O$ $2 \rightarrow 1$ towards the (0, 0) position in NGC 253 on 1994 December 2, using the receiver Rx A2 and with the DAS operated in 500-MHz bandwidth mode. The telescope efficiency was measured using Saturn and assuming a single-component 22.9-arcsec diffraction beam. $\eta_{\rm MB}$ was found to be consistent with the values obtained from numerous observations of Jupiter and Mars as part of the JCMT maintenance programme (Russell, private communication) and so we take the standard value of $\eta_{\rm MB} = 0.68$. Saturn was used to check the pointing, which was good to 3 arcsec (rms).

A grid of seven $C^{18}O$ $3 \rightarrow 2$ spectra was observed towards NGC 253 on 1994 December 1–4, using the receiver Rx B3i and with the DAS operated in 760-MHz bandwidth mode. The telescope efficiency was measured using Uranus and Saturn and assuming a single-component 15.3-arcsec diffraction beam. $\eta_{\rm MB}$ was found to be consistent with the values

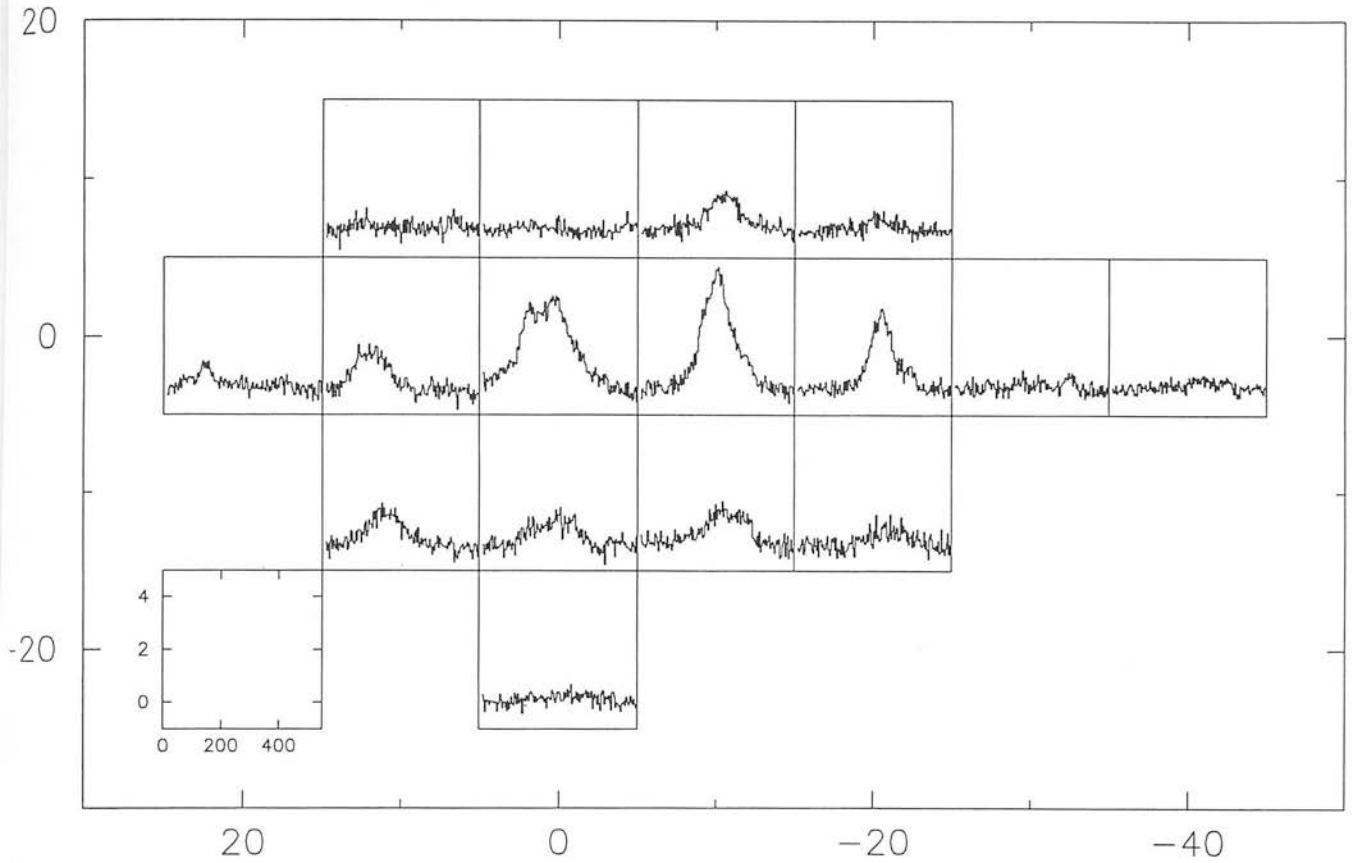

Figure 1. A rotated RA–Dec. map at a PA of 53° of the 16 [C I] spectra observed towards the nuclear region of NGC 253, shown on a T_B scale. The map centre (0, 0) is at $\alpha(1950) = 0^h45^m05\overset{s}{.}8$, $\delta(1950) = -25°33'38''$ and the spectra are spaced at 10-arcsec intervals.

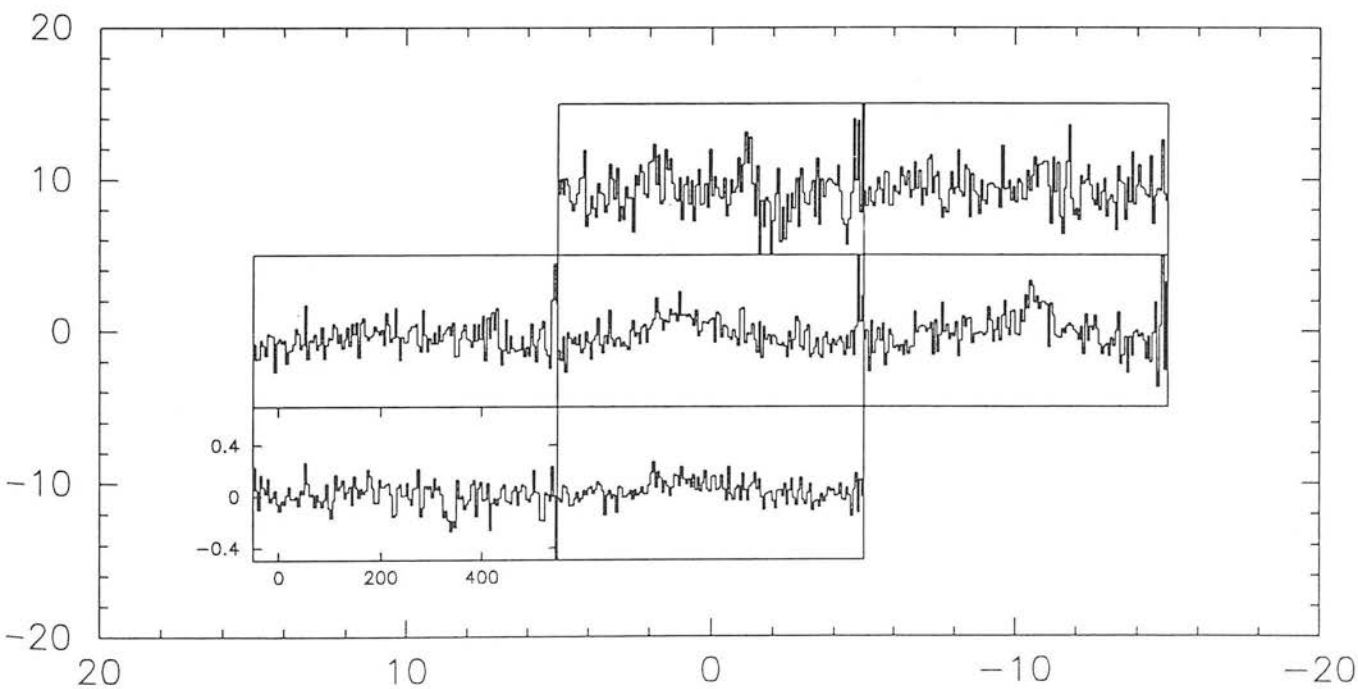

Figure 2. Rotated RA–Dec. map at a PA of 53° of the seven $C^{18}O$ 3→2 spectra, shown on a T_{MB} scale. The map is centred at the (0, 0) position and the spectra are spaced at 10-arcsec intervals. Map centre RA $0^h45^m6\overset{s}{.}0$, Dec. $-25°33'35\overset{''}{.}98$.

obtained from numerous observations of Jupiter and Mars as part of the JCMT maintenance programme (Russell, private communication) and so we take the standard value of $\eta_{MB} = 0.59$. Saturn was used to check the pointing, which was good to 3 arcsec (rms).

3 RESULTS

A grid of 16 [C I] spectra, spaced at 10-arcsec intervals, was observed towards NGC 253 (10 arcsec corresponds to 120 pc if NGC 253 is at 2.5 Mpc). Fig. 1 shows a rotated RA–Dec. map at PA 53° of the 16 spectra on a T_B scale ($T_B = T_A^*/\eta_B$).

C^0 shows a similar distribution to the CO bar (Canzian et al. 1988) and shows that the C^0 and CO are tracing the same gas, i.e. the atomic gas is well-mixed with the molecular gas, at least on a scale of 100 pc. We convolved our map of [C I] to a resolution of 23 arcsec to match the ^{13}CO observations of Wall et al. (1991) and our own $C^{18}O$ observations. From the central 23 arcsec we derive an integrated intensity $\int T_B dV = 320$ K km s^{-1}. Philips & Huggins (1981) show that the relation between the integrated temperature and intensity is

$$I(C\,I) = 1.22 \times 10^{-7} \int T_B \, dV \ (\mathrm{erg\ cm^{-2}\ s^{-1}\ sr^{-1}}).$$

Hence, we find that towards the central 23 arcsec of NGC 253, [C I] has an integrated intensity of 3.9×10^{-5} erg cm^{-2} s^{-1} sr^{-1}.

Seven spectra of $C^{18}O$ 3→2, spaced at 10-arcsec intervals, were observed towards NGC 253. Fig. 2 shows a rotated RA–Dec. map at PA 53° of the seven spectra on a T_{MB} scale. We convolved our map of $C^{18}O$ 3→2 to a resolution of 23 arcsec. From the central 23 arcsec we derive an integrated intensity $\int T_{MB} dV = 30$ K km s^{-1}.

Fig. 3 shows the single spectrum we observed of $C^{18}O$ 2→1 (at a resolution of 23 arcsec) towards NGC 253. We derive an integrated intensity of $\int T_{MB} dV = 27$ K km s^{-1}. Hence, we derive a $C^{18}O$ 3→2/2→1 intensity ratio of 1.1 which is clearly different from ^{13}CO where Wall et al. (1991) found the ^{13}CO 3→2/2→1 intensity ratio to be between 2.0 and 2.8.

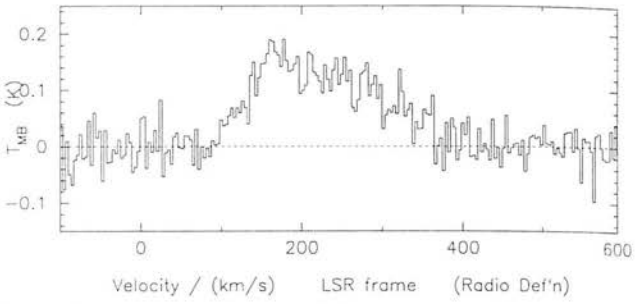

Figure 3. The spectrum of C^{18} 2→1 taken towards the (0, 0) position.

4 DISCUSSION

4.1 Evidence for a torus in NGC 253

Figs 4(a) and (b) are maps of the integrated intensity of [C I] towards NGC 253 over the blue and redshifted intervals (100–250 km s^{-1} and 250–400 km s^{-1}) which reveal that the position of maximum emission varies with the velocity. The peaks in blue and redshifted emission are separated by ~9 arcsec.

An interferometer map in HCO^+ emission shows two peaks in intensity separated by about ~9 arcsec (Carlstrom et al. 1990). Mauersberger & Henkel (1989, 1991) showed velocity-averaged contour maps of CS 2→1 and N_2H^+ 1→0 that both had two peaks which were separated by ~9 arcsec and were spatially coincident with the peaks in [C I] emission. Hence, the peaks in [C I] are not solely associated with [C I] emission, but are highlighting enhancements in the column density of atomic and molecular gas. Near-IR (Forbes et al. 1993) and mid-IR images (Keto et al. 1993; Piña et al. 1992) also show two peaks, or hotspots, but the IR peaks are separated by about 3.5 arcsec. The near-IR hotspots may be an artefact of holes in the extinction (Sams et al. 1994). The rotation curve in NGC 253 (Canzian et al. 1988), along with our own unpublished spectra of H_2 in the nuclear region, shows that it is hard to reconcile an angular separation of ~3.5 arcsec with a velocity separation of ~90 km s^{-1}. This gives us further confidence that the [C I] peaks are associated with two hotspots that are separated by about ~9 arcsec.

NGC 253 is seen at high inclination, and so a plausible explanation for the two peaks is that they are limb-brightened emission from a ring of gas. Telesco et al. (1993) argue that NGC 253 does not have any inner Lindblad resonances and so it is unlikely that such a ring in NGC 253 could be caused by gas accumulating at a stable orbit. However, the evolutionary scenario of starbursts outlined by Rieke, Lebofsky & Walker (1988) predicts the formation of such a circumnuclear ring of gas. In this scenario, superbubbles of the thermalized ejecta of numerous supernovae have broken out of one of the poles of NGC 253, disrupting the molecular clouds. Within the plane of the galaxy a portion of the kinetic energy has compressed and pushed the molecular clouds out of the centre, forming a dense molecular torus. McCarthy, Heckman & van Breugel (1987) have shown evidence for a superwind blowing off from the nuclear region of NGC 253, and Carlstrom et al. (1990) have noted that the HCO^+ centroid is coincident with the base of the X-ray emission which comes from shocked gas (Fabbiano & Trinchieri 1984). If the two peaks show the ends of a torus, then the torus is perpendicular to the superwind as expected.

4.2 Comparing atomic carbon and carbon monoxide in the nuclear region of NGC 253

4.2.1 Is ^{13}CO or $C^{18}O$ a more reliable tracer of CO column density towards the central 300 pc of NGC 253?

Wall et al. (1991) argue that there are two components to the CO-emitting gas in NGC 253: a hot dense core of size <15 arcsec, which dominates the emission towards the nucleus, and a 40×10 arcsec^2 bar, of colder and more tenuous gas, which dominates the emission away from the nucleus. This picture is supported by the observations of ^{13}CO and ^{12}CO made by Wall et al. (1991). The intensity ratio of ^{12}CO and ^{13}CO indicates that $\tau^{13}CO$ 3→2 ~ 0.2. Wall et al. (1991) observed the ^{13}CO 3→2/2→1 intensity ratio to be between 2.0 and 2.8 from the central 23 arcsec (~300 pc). Given the

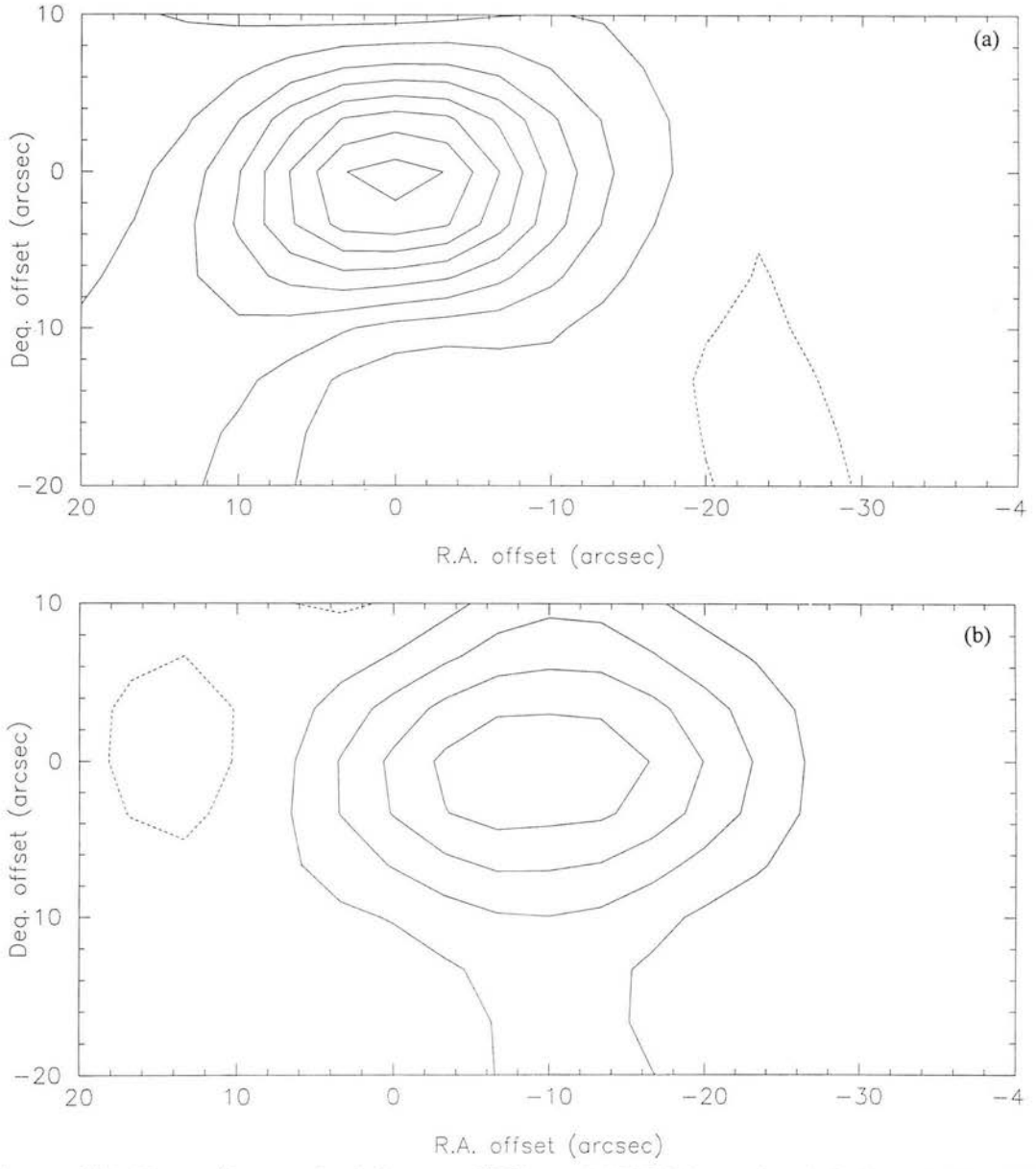

Figure 4. (a) A rotated (PA 53 arcsec) integrated emission map of [C I] towards NGC 253 over the velocity interval 100 to 250 km s^{-1}. (b) A rotated (PA 53 arcsec) integrated emission map of [C I] towards NGC 253 over the velocity interval 250 to 400 km s^{-1}.

uncertainties in the observations (the data were taken from different telescopes) this ratio is close enough to the limiting value of 2.25 to indicate that most, if not all, of the ^{13}CO-emitting gas is hot ($T \sim 100$ K), optically thin and thermalized. An intensity ratio at the lower end of the observed range (^{13}CO $3\rightarrow 2/2\rightarrow 1 = 2.0$) can be explained by having a two-component model of the ^{13}CO-emitting gas with 90 per cent of the emission from hot gas and 10 per cent of the emission coming from cold ($T \sim 20$ K) gas. Modification, due to a subthermal population of ^{13}CO or an increased optical depth (if the ^{13}CO- and ^{12}CO-emitting gas is not well-mixed), must be small because otherwise the observed $3\rightarrow 2/2\rightarrow 1$ intensity ratio of ^{13}CO would be much closer to unity.

C^{18}O paints a different picture of CO excitation towards the nucleus of NGC 253. Convolving our C^{18}O $3\rightarrow 2$ spectra to the same resolution as our C^{18}O $2\rightarrow 1$ spectrum, 23 arcsec, we find that the intensity ratio of C^{18}O $3\rightarrow 2/2\rightarrow 1$ is ~ 1.1, clearly different from ^{13}CO. C^{18}O is almost certainly optically thin, given that ^{13}CO is optically thin, and, furthermore, the critical densities of the energy levels of ^{13}CO and C^{18}O are close enough that, if ^{13}CO is thermalized, C^{18}O is thermalized. Hence, it would seem from the $3\rightarrow 2/2\rightarrow 1$ ratio that the bulk of the C^{18}O-emitting gas is cold ($T \sim 20$ K) towards the nucleus of NGC 253; an intensity ratio of 1.1 can be explained with a two-component model of C^{18}O-emitting gas, but with only 10 per cent of the emission arising from hot gas and 90 per cent of the emission arising from cold gas. It appears that C^{18}O and ^{13}CO may be tracing different components of the ISM towards the nucleus of NGC 253. This conclusion is supported by the morphology of the $3\rightarrow 2$ line from both isotopomers, with the ^{13}CO centrally peaked (Wall et al. 1991) whereas C^{18}O is more widespread, particularly to the south-west of the nucleus (Fig. 2).

The effect of selective photodissociation of isotopic CO has been observed by several authors, e.g. Fuente et al. (1993), who find that ^{12}CO and ^{13}CO become self-shielding to an external UV field at smaller depths into a cloud than C^{18}O. This results in the column density ratio of ^{13}CO/C^{18}O being enhanced towards the edge of the cloud. It is to be expected that the temperature of the gas will be higher towards the edge of the cloud, where UV heating is more efficient, thus, ^{13}CO $3\rightarrow2/2\rightarrow1 > $ C^{18}O $3\rightarrow2/2\rightarrow1$. The ^{13}CO intensity ratio indicates that, towards the nucleus of NGC 253, most of the gas is hot and, thus, at low visual extinction ($A_V < 5$). Such a low visual extinction indicates that most of the molecular gas in NGC 253 is either filamentary or clumpy in nature.

The only observations of an ^{18}O-bearing molecule in NGC 253 are those of the three lowest energy transitions of C^{18}O. Converting these observations into measures of ^{12}CO may be hazardous because C^{18}O appears to trace only a small fraction of the total CO column density, i.e. that which is in a cold state. This uncertainty in calculating ^{16}O/^{18}O is highlighted by the values derived for different lines. Henkel et al. (1993), using observations of several carbon-bearing molecules towards the nucleus of NGC 253, derived ^{12}C/^{13}C ~ 40. Henkel et al. (1993) derived ^{16}O/^{18}O ~ 200 because the observed intensity ratio of ^{13}CO/C^{18}O in the $1\rightarrow0$ line was ~ 5. The observation of C^{18}O $1\rightarrow0$ was made by Sage, Mauersberger & Henkel (1991) with the National Radio Astronomy Observatory (NRAO) 12-m telescope. A similar observation of C^{18}O $1\rightarrow0$, made with the 12-m by Wall et al. (1993), indicates that observations of C^{18}O $1\rightarrow1$ are prone to uncertainties associated with subtracting baselines and spectral features. Using the beam-matched (23-arcsec) $2\rightarrow1$ observations of ^{13}CO (Wall et al. 1991) and C^{18}O (this work) we derive ^{16}O/^{18}O ~ 110–150 (the uncertainty is due to the brightness uncertainty reported by Wall et al. 1991). If we use the beam-matched (23-arcsec) $3\rightarrow2$ observations of ^{13}CO (Wall et al. 1991) and C^{18}O, this work, we derive ^{16}O/^{18}O ~ 280. The fact that the highest ^{16}O/^{18}O ratio is obtained for the $3\rightarrow2$ line is no surprise given that ^{13}CO is tracing hot gas whereas C^{18}O appears to be tracing cold gas.

We highlight the fact that in NGC 253 C^{18}O is tracing cold gas whereas most of the gas is hot. It appears that C^{18}O is not a good tracer of column density in NGC 253. The environment of the bulk of the molecular gas in NGC 253, which is hot (~ 100 K) and at low visual extinction, is different from the darker and colder environment that is typically found in Galactic giant molecular clouds. Selective photodissociation of C^{18}O in NGC 253 means that it is not possible to use isotopomers of CO to give reliable estimates of the *intrinsic* ^{16}O/^{18}O ratio in the starburst region – we do measure the C^{18}O/^{13}CO ratio but this cannot be used to infer the ^{16}O/^{18}O ratio.

4.2.2 The C^0/CO ratio in NGC 253

We have assumed that C^0 is optically thin in NGC 253. The column density is derived from (Philips & Huggins 1981):

$$N(\mathrm{C\,I}) = 1.9\times10^{15} \int T_B \,\mathrm{d}V \exp(23.6/T_{ex})\, Q(\mathrm{cm}^{-2}),$$

where the partition function is given by

$$Q = 1 + 3\exp(-23.6/T_{ex}) + 5\exp(-6.25/T_{ex}).$$

The integrated intensity ($\int T_B \mathrm{d}V$) is in units of K km s^{-1}. The critical density for [C I] is 10^3 cm^{-3} (Schröder et al. 1991) and, given that ^{13}CO is thermalized ($n_{crit} = 3\times10^4$ cm^{-3} for the $3\rightarrow2$ transition), it is safe to assume that atomic carbon is thermalized. The derived intensities and column densities of atomic carbon have a weak dependence on temperature – the derived column density only increases by ~ 10 per cent for gas at $T = 100$ K compared with gas at $T = 24$ K (24 K gives a lower limit to the column density). Most of the ^{13}CO emission arises from $T \sim 100$ K gas and so, if we assume that ^{13}CO and [C I] are well-mixed, $T_{ex} \sim 100$ K. We have convolved our spectra of [C I] in NGC 253 to a resolution of 23 arcsec to match the ^{13}CO data. Across the central 23 arcsec we find that, for [C I], $\int T_B \mathrm{d}V = 330$ K km s^{-1}. Assuming $T_{ex} = 100$ K, we find that $N(\mathrm{C\,I}) = 4.8\times10^{18}$ cm^{-2}.

The ratio of ^{13}CO $3\rightarrow2/2\rightarrow1$ may be as low as 2.0. Thus there is some uncertainty in the nature of the ^{13}CO-emitting gas. One hot component ($T \sim 100$ K) provides a good fit as does a two-component model, with ~ 90 per cent of the emission from very hot ($T = 200$ K) gas and ~ 10 per cent of the emission from cold ($T = 20$ K) gas. If τ^{13}CO $(3\rightarrow2) \sim 0.5$ then this can also explain the observations, but it indicates that ^{12}CO and ^{13}CO are not co-extensive and would require the partially optically thick gas to have a large column density [$N(\mathrm{H_2}) > 10^{23}$ cm^{-2}] and to be very hot ($T > 250$ K). This latter possibility seems unrealistic. The derived ^{13}CO column densities are obviously dependent upon the chosen description of the gas that is emitting ^{13}CO. Fortunately, in NGC 253 it is clear that > 90 per cent of ^{13}CO is at $T \geq 100$ K. There is less than 20 per cent uncertainty in the derived ^{13}CO column density between the models of 100 per cent at $T = 100$ K ($N_{^{13}CO} = 2.1\times10^{17}$ cm^{-2}), and 90 per cent at 200 K and 10 per cent at 20 K ($N_{^{13}CO} = 2.4\times10^{17}$ cm^{-2}). Given that C^{18}O is tracing a cold component, the second option, of a mixture of hot and cold CO, should be a reasonable description of the molecular gas in NGC 253.

There is little C^{18}O in the hot gas towards NGC 253, which indicates that photodissociation plays an important role in the chemistry of the bulk of CO. The effects of photodissociation on the chemistry of CO have been studied in detail by Van Dishoeck & Black (1988) for low-density gas (10^3 cm^{-3}) and more recently by Köster et al. (1994), for denser gas ($\geq 10^4$ cm^{-3}). It appears, from these studies, that the effect of selective photodissociation on CO/^{13}CO is a slight increase at intermediate depths due to the differences in self-shielding. The ^{13}CO/C^{18}O ratio appears more sensitive to self-shielding (Van Dishoeck & Black 1988) and shows a much larger increase than the CO/^{13}CO ratio. Hence, if the bulk of the molecular gas in NGC 253 is in an environment where self-shielding and photodissociation play a crucial role in determining the molecular abundances, particularly isotopic CO, the chemical models indicate that ^{13}CO will be a more reliable tracer of CO column density than C^{18}O.

Henkel et al. (1993) argue that because H^{13}CN emission arises from dense UV-shielded cores, and $\tau(^{12}\mathrm{CO}\ 1\rightarrow0) \sim \tau(\mathrm{H^{12}CN}\ 1\rightarrow0) \sim 3$–4, if isotopic selective photodissociation is an important effect in NGC 253 then the ratio $I(^{12}\mathrm{CO})/I(^{13}\mathrm{CO})$ will be much greater than $I(\mathrm{H^{12}CN})/I(\mathrm{H^{13}CN})$. We do not feel that this is the case. Selective photodissociation does not have a dramatic effect on $I(^{12}\mathrm{CO})/I(^{13}\mathrm{CO})$. Even if

selective photodissociation is important in NGC 253, this will not be highlighted by a comparison of ^{12}CO and ^{13}CO.

If the bulk of molecular gas in NGC 253 exists in a region where the chemistry is dominated by a high UV field then selective photodissociation may affect the derived isotopic ratios from many molecules. No theoretical work, to our knowledge, has studied the effects of a strong UV field on the chemistry of molecules and their isotopomers apart from the work on CO (Van Dishoeck & Black 1988; Köster et al. 1994). Henkel et al. (1993) derived $^{12}C/^{13}C \sim 40$ from observations of three carbon-bearing molecules (CS, HNC and CN) and their respective ^{13}C isotopomer. In NGC 253 most of the gas is not shielded from UV photons and it is likely that CO and molecules such as CS are co-extensive. The $^{12}CO/^{13}CO$ ratio does not have large variations for gas that is bathed in UV but it is unclear whether this is also the case for $^{12}CS/^{13}CS$. We have calculated our ^{12}CO column densities from $^{13}CO \times 40$ but we note that if selective photodissociation is important for the chemistry of CS then ^{13}CS might be underabundant and the intrinsic value of $^{12}C/^{13}C$ will be <40 in NGC 253.

So, assuming that carbon monoxide and atomic carbon are co-extensive, we find that, averaged over the central 23 arcsec of NGC 253, the abundance ratio of atomic carbon to carbon monoxide is $C/CO = N(C\,\textsc{i})/N(CO) = 4.8 \times 10^{18}/(2.4 \times 10^{17} \times 40) = 0.5$. This is a lower limit because $^{12}C/^{13}C$ may be <40.

4.3 Can existing PDR models explain the observed C^0?

Atomic carbon is quite a robust diagnostic of PDR gas since the $^3P_1 \rightarrow {}^3P_0$ intensity is fairly insensitive to both the density, n_0, and the UV field, G_0 (Hollenbach et al. 1991). Our measured intensity of the $^3P_1 \rightarrow {}^3P_0$ line should provide a measure of the number of PDRs along the line of sight – the area filling factor – if the neutral carbon emission arises solely from PDR gas. Typically, the intensity of the $^3P_1 \rightarrow {}^3P_0$ line from a face-on PDR is 2×10^{-6} erg cm^{-2} s^{-1} sr^{-1} (Hollenbach et al. 1991). From the central 23 arcsec we find that $\langle I_{C\,\textsc{i}} \rangle \sim 4 \times 10^{-5}$ erg cm^{-2} s^{-1} sr^{-1}, indicating that the area filling factor is ~ 20.

Carral et al. (1994) explain their observations of [O I] and [C II] in NGC 253 in terms of PDRs with an area filling factor of ~ 1. They derived their area filling factor by comparing the observed intensity ratios of $I_{O\,\textsc{i}}/I_{C\,\textsc{ii}}$ and $I_{O\,\textsc{i}}/I_{C\,\textsc{ii}}/I_{FIR}$ with the theoretical predictions of Wolfire et al. (1990). Clearly, our area filling factor is inconsistent with the one found by Carral et al.

If the area filling factor is ~ 20 then each PDR provides a fraction ~ 0.05 of the observed intensity. The PDR models of Hollenbach et al. (1991) showed that, by increasing G_0 to 10, $I_{C\,\textsc{ii}}$ dropped by a factor of ~ 20 and $I_{C\,\textsc{ii}}/I_{C\,\textsc{i}}$ became consistent with what was observed. However, this decreased the [O I] intensity by a factor of about 10^5, making $I_{O\,\textsc{i}}$ negligible from each PDR. Shocks produce large $I_{O\,\textsc{i}}/I_{C\,\textsc{ii}}$ and negligible $I_{C\,\textsc{i}}$ (Hollenbach & McKee 1989) and so, by having an ensemble of shocks and PDRs, we can make the O^0, C^+ and C^0 emissions consistent with each other. Unfortunately, this will not be consistent with emission from the dust. If L_{FIR} is tracing the stellar luminosity then $G_0 \sim 10^4$ (Carral et al. 1994) and not ~ 10. Thus, either we require the O^0, C^+ and the FIR emissions to be consistent with each other and PDRs to produce 5 per cent of the observed neutral carbon in NGC 253, or we require that O^0, C^+ and C^0 are consistent with each other but that the hot dust is not heated solely by UV photons from hot young stars (i.e. there is an average UV field in the nucleus of NGC 253 of $G_0 \sim 10$).

The Lyman continuum photon flux from the central 15 arcsec is $\sim 5 \times 10^{53}$ s^{-1} (Beck & Beckwith 1984; Carlstrom et al. 1990) and so, with an effective temperature of $\sim 35\,000$ K for the ionizing stars (Carral et al. 1994), the FUV energy density G_0 is $\sim 10^4$. There is some uncertainty in deriving the average UV field in this way because of the unknown spatial relationship between the FUV-emitting stars and the molecular clouds. Even with these uncertainties it is clear that the UV field is high ($G_0 \gg 10$) towards the nucleus of NGC 253.

Another argument for a high UV field is that the models of Hollenbach et al. (1991), in the scenario of a large area filling factor and low UV field, predict too much CO ($1 \rightarrow 0$) emission, an order of magnitude larger than is observed (Canzian et al. 1988). Furthermore, the models of Wolfire et al. (1990) indicate that the temperature, and hence pressure, at low G_0 would be low. Hence, invoking low UV fields would mean that the PDR gas would be far from being in dynamic equilibrium with the H^+ gas (Carral et al. 1994).

We have found that C^0/CO is ~ 0.5 in NGC 253, which is an order of magnitude higher than Galactic GMCs. In the Galactic cold diffuse ISM the gas is mainly atomic and $C^0/CO > 1$ for $A_V < 1$ (Keene 1990). Thus a possible explanation for our observed C^0/CO value is to postulate a population of cold diffuse clouds in the starburst nucleus with most of the C^0 emission arising from these diffuse clouds. Reducing the PDR density from $n_0 = 10^4$ to $n_0 = 10^2$ cm^{-3} reduces the [O I] and [C II] intensities but has little effect on the [C II] emission.

There are several problems, however, with the picture of a substantial component of diffuse gas in the nuclear region of NGC 253. Carral et al. (1994) argue that the contribution of a diffuse gas component to the observed [C II] brightness is insignificant and that the [C II] emission must come from dense gas. Stacey et al. (1991) argue that PDRs, in addition to producing the C^+ emission, can produce significant amounts of H^0. The H^0 column density, in a given PDR, depends on the ratio between the impinging UV field strength, G_0, and the molecular cloud density, n_0 (Sternberg 1988):

$$N_{H\,\textsc{i}} = 5 \times 10^{20} \ln(90 G_0/n_0 + 1)\ \mathrm{cm}^{-2}.$$

From interferometric H^0 (21-cm) observations, with a 2×1 arcmin^2 beam, Combes, Gottesman & Weliachew (1977) derive a maximum H^0 column density $N_{H^0} = 1.3 \times 10^{22}$ cm^{-2}. Therefore, with the area filling factor of 20 that is required by the C^0, such PDRs produce too much H^0 by an order of magnitude. Furthermore, Wolfire et al. (1990) note that a low-density, $n_0 = 10^2$ cm^{-3}, PDR exposed to a $G_0 = 10^4$ UV field has a temperature below 200 K, therefore such PDRs will be far from dynamic equilibrium with the rest of the ISM in NGC 253.

Another difficulty with this picture of a large population of diffuse clouds is that the ISM in NGC 253 is at high pressure ($\sim 5 \times 10^6$ K cm^{-3}, Carral et al. 1994) and thus, if we have to postulate the existence of diffuse clouds of $n \sim 40$ cm^{-3}, to allow $C^0/CO \sim 0.5$, these clouds must be unreasonably hot ($\sim 10^5$ K where both hydrogen and carbon will be

readily ionized). Even if we abandoned the assumption that the ISM in NGC 253 was in pressure equilibrium, most of the carbon in the diffuse gas would still be ionized. The observed Lyman continuum photon luminosity of 5×10^{53} s^{-1} (Beck & Beckwith 1984) and an effective temperature of the ionizing stars of ~ 35 000 K (Carral et al. 1994) mean that the carbon ionizing photon luminosity (photons with energy between C^0's ionization potential of ~ 11 eV and the Lyman limit, 13.6 eV) is ~ 1×10^{53} s^{-1}. If we postulate that the central 300 pc contains diffuse gas ($n = 10^2$ cm^{-3}) at $T \sim 5000$ K and we make the conservative estimate that only 10 per cent of the photons actually ionize carbon, due to absorption by dust and other species, then we derive $n_{C^0}/n_{C^+} < 0.1$. Assuming a C/H abundance ratio of 3.3×10^{-4} (Keene 1990), $N_{H^0} = 1.3 \times 10^{22}$ cm^{-2} (Combes et al. 1977), and $n_{C^0}/n_{C^+} \sim 0.1$, $N(C^0) = 4.3 \times 10^{17}$ cm^{-2}, which is a factor of ~ 10 smaller than the [C I] observation.

Furthermore, the observational evidence points towards most of the molecular gas in the nuclear region of NGC 253 being in a high-density phase, with little evidence observationally for a substantial component of diffuse gas. ^{13}CO traces the bulk of the molecular component and, given that the 3→2 line is thermalized, most of the molecular gas must be at densities greater than 3×10^4 cm^{-3}.

In summary, Carral et al. (1994) modelled the nucleus of NGC 253 in terms of a population of $n = 10^4$ cm^{-3}, $G_0 = 10^4$ PDRs filling the beam with a filling factor of order unity. These values are constrained by the hot dust, recombination lines of hydrogen, CO and H^0 (21 cm) and have the important benefit that they also explain the O^0 and C^+ emission. It is possible to make O^0, C^+ and C^0 consistent with each other in two ways, either by reducing the density of the PDR gas or by lowering the UV field, but both ways result in conflicts with observations. Reduction in the density of the PDRs would result in the production of more H^0 than is observed and there would be large pressure differentials between different components of the ISM. There is also little observational evidence for such a major component of diffuse gas. Because most of the carbon would be in an ionic rather than atomic form, observations of H^0 indicate that, at the most, < 10 per cent of the C^0 emission could possibly arise from diffuse gas. A reduction in the UV field also results in large pressure differentials in the gas, too much CO (1→0) emission, requires that the UV flux from OB stars plays only a minor role in heating the dust and would also be inconsistent with the observed Lyman continuum flux. It is only at low densities or at low UV fields that I[O I] and I[C II] are low enough to make the O^0, C^+ and C^0 consistent with each other. Hence intermediate densities and UV fields are also ruled out. The C^0 emission we have detected is inconsistent with the picture presented by Carral et al. and the models of Hollenbach et al. (1991), so we have to look for a non-PDR origin for the C^0 emission in NGC 253.

4.4 Non-PDR explanations for the observed C^0

4.4.1 Enhanced cosmic ray fluxes?

Schilke et al. (1993) and White et al. (1994) observed [C I] towards the nucleus of M82 and argued that [C I] is brighter than predicted by PDR models by a factor of 5 or so. Both Schilke et al. and White et al. also claimed that C/CO is high (0.1–0.5) in M82.

Whilst it is clear that in M82 [C I] is brighter than predicted by the PDR models of Hollenbach et al. (1991), the value of C/CO towards M82 is not clear. Both Schilke et al. and White et al. derived their CO column densities from the $C^{18}O$ 2→1 observations of Wild et al. (1992) and assumed that $^{16}O/^{18}O = 500$. As we argue in Section 4.2, $C^{18}O$ may not be a reliable tracer of the bulk of carbon monoxide within the environment of a starburst nucleus. If a much larger proportion of molecular gas is at larger depths in M82, i.e. cold and shielded from UV photons, then $C^{18}O$ will be a more realistic tracer of CO in M82 than in NGC 253. Wild et al. (1992) derived ^{13}CO 3→2 to be optically thick towards the nucleus of M82 and so, without detailed modelling, it is hazardous to use ^{13}CO to derive the CO column density in M82. Even if $C^{18}O$ is tracing the bulk of CO in M82, the value of the $^{16}O/^{18}O$ ratio is not clear and, thus, neither is the true value of C/CO.

To explain the enhanced carbon in M82, with respect to both PDRs and CO, Schilke et al. (1993) proposed that a significant fraction of the [C I] emission was from carbon existing within molecular clouds. Recent chemical models, e.g. Flower et al. (1994), suggest that an enhanced ionization fraction, deep within clouds, drives the chemistry to equilibrium with a high C/CO value. Schilke et al. proposed the enhanced cosmic ray flux supplied by the remnants of frequently occurring supernovae as the source of ionization. Schilke et al. claimed that, with a cosmic ray flux ~ 300 times the local solar neighbourhood value, the models of Flower et al. produced significant carbon emission at large depths into the cloud and a large C/CO abundance ratio deep within the cloud. The summed emission from atomic carbon rises with depth into the cloud and the total emission is dependent on the maximum A_V of the cloud. The models of Flower et al. naturally explained the high C/CO value in M82 and also accounted for the fact that [C I] was brighter than predicted by the PDR models of Hollenbach et al. (1991) – atomic carbon is produced throughout the cloud whereas other PDR tracers such as [C II] and [O I] are produced only at low A_V.

Such a source of carbon emission would seem an attractive solution to the problem of bright carbon emission from the nucleus of NGC 253. The cosmic ray rates are presumed similar in NGC 253 and M82; since the far-IR luminosities of the two galaxies are similar (NGC 253: 1.5×10^{10} $L_\odot$ in ~ 400-pc diameter; M82: 3×10^{10} $L_\odot$ in ~ 400-pc diameter) if they have similar initial mass functions, the star formation, and hence supernova, rates will be comparable. We believe, however, that the state of the bulk of molecular gas in NGC 253 rules out the Flower et al. model as a possible solution.

As we have argued in Section 4.2, the bulk of molecular gas in NGC 253 is at low A_V, hot and exposed to UV photons. In such an environment the chemistry is photon-dominated and the small perturbation of an extra ionizing source, such as cosmic rays, should have little bearing on the chemical abundances. The cosmic ray explanation also requires atomic carbon emission to rise steadily with depth into the cloud. In NGC 253 this rise with depth is curtailed at a few A_V. Thus, there is not enough cold and shielded gas for a contribution to the [C I] emission to be significant. Furthermore, in M82 [C I] is perhaps a factor of 5 brighter than predicted by PDR models whereas, in NGC 253, [C I] is a

factor of ~ 20 too high. Hence, although the perturbation on dark cloud chemistry induced by large cosmic ray fluxes may well be the explanation for why [C I] is so bright from M82, it is unlikely to be the principal cause in NGC 253.

4.4.2 *Chemical and elemental explanations?*

The chemical abundances in a molecular cloud, as well as being sensitive to the physical conditions, also changes with time. Time-dependent chemical models reach equilibrium abundances after about 10^7 yr (Leung, Herbst & Heubner 1984). These models show that at early time, i.e. $< 10^6$ yr, large amounts of C^0 exist, yielding C^0/CO abundance ratios greater than 0.5, and it is only at later times, when equilibrium is approached, that most of the C gets tied up in CO, resulting in a decrease of the C^0/CO ratio. The carbon chemistry in such models is still uncertain, however, as many of the chemical reactions at low temperatures involving carbon-bearing molecules have been found to proceed at a much higher rate than was previously thought (Herbst et al. 1994). It would seem reasonable that in a starburst nucleus, where the molecular gas is frequently being perturbed, the chemistry will never reach steady state and the most realistic description of the chemistry might be that of 'early time'. Mauersberger et al. (1991) claimed that the derived abundances of carbon-rich molecules in NGC 253 pointed towards non-equilibrium chemistry. Another explanation for the observed C^0 in NGC 253 is that the elemental abundances in NGC 253 are not identical to those of the models with which we are comparing our observations, with C/O enhanced in NGC 253. It is hard to distinguish observationally between early-time chemistry and a high C/O elemental ratio as both models produce similar chemical abundances, e.g. molecules that are carbon-rich. However, in order for the C^0/CO ratio in NGC 253 to be explained by early-time chemistry we must be seeing a snapshot of NGC 253 shortly after a major reconfiguration of the interstellar medium has occurred, within ~ 10^6 yr, across a region of size ~ 300 pc. We feel that this is implausible. Also, as we discuss in Sections 4.2 and 4.4.1, the chemistry in NGC 253 is dominated by UV photons, which will produce different chemical abundances from those produced by the chemistry of cold, dark clouds. As models of the chemistry in photon-dominated regions predict only ~ 5 per cent of the observed [C I] emission, we feel that the only plausible explanation with which we are left to explain our observations of [C I] in NGC 253 is to invoke an enhanced C/O elemental ratio in NGC 253.

4.5 Possible explanations for a high C/O elemental ratio in NGC 253

Pantelaki & Clayton (1988) note that carbon is produced in Type II supernovae (SNe II) and intermediate-mass stars whereas oxygen is synthesized by high-mass stars. If the C/O elemental ratio is enhanced in NGC 253, then this could be due to a large number of intermediate-mass stars (of about $8\,M_\odot$) existing in the nuclear region of NGC 253. It is also possible that the nuclear region of NGC 253 has a high C/O elemental ratio because the gas that is being driven into the nucleus (Canzian et al. 1988) has a high C/O ratio.

A different explanation is that suggested by the chemical evolution of starburst models of Pantelaki & Clayton (1988). In these models the elemental ratio of C/O is sensitive to time. The reason for this is that the superwind, driven by numerous SNe II, causes the ejecta of high-mass stars, which are oxygen-rich, to be expelled from the nucleus. At later times, intermediate-mass stars eject large amounts of mass after termination of the SNe II which is oxygen-free but carbon-rich. Thus, NGC 253 may be in the stage of producing the high-C/O ejecta from intermediate-mass stars. The lobes of the hypothesized ring in M82 are separated by about 400 pc, a factor of 3 higher than the lobes in NGC 253. If the rings were pressure-confined gas induced by star formation in the nuclear region of the galaxies, this would suggest that the starburst in M82 is more evolved than it is in NGC 253. The picture of Pantelaki & Clayton (1988) may need fine-tuning to explain why the C/O ratio is probably higher in NGC 253 than in M82. We note that the models of Pantelaki & Clayton (1988) suggest that there may be C/O elemental gradients along the major axes of superwinds.

It is not clear how applicable standard chemical evolutionary models are to the nuclear regions of starbursts. Maeder (1992) has argued that a crucial parameter in chemical evolutionary models is metallicity. An increase in metallicity changes the nuclear processing within stars and increases the opacity in the outer layers of stars. This increase in opacity changes the mass-loss rates of stars. Maeder claims that massive stars, at high Z, eject carbon back into the ISM before it is processed into heavier elements. Thus, at high Z, stars enrich the ISM with material that has a high C/O elemental ratio. If the nuclear region of NGC 253 has a high metallicity, the work of Maeder provides a natural explanation for the high C/O ratio. If this explanation is correct, we note that an interesting effect in the chemical evolution of starbursts might be that, when a threshold of metallicity is passed, stars that form from gas with a high C/O ratio will eject gas, with an even higher C/O, back into the ISM. This scenario, of a positive feedback loop steadily increasing C/O, suggests that starbursts with high metallicities will have high C/O ratios.

5 CONCLUSIONS

We have observed [C I], $C^{18}O$ 3→2 and $C^{18}O$ 2→1 in the nuclear region of the starburst galaxy NGC 253. NGC 253 shows evidence for a ring ($R \sim 50$ pc) around the nucleus which was predicted by Rieke et al. (1988). $C^{18}O$ appears to trace cold gas in NGC 253. Observations of ^{13}CO by Wall et al. (1991) indicate that most of the gas in the nuclear region is hot, such that it appears that $C^{18}O$ is only tracing a minor fraction (< 10 per cent) of the total CO. The separation between $C^{18}O$ and ^{13}CO highlights the fact that selective photodissociation is efficient in NGC 253. C^0 is overabundant both with respect to PDR models (~ 20× greater than predicted) and with respect to CO (C^0/CO ~ 0.5). Possible PDR ensembles are restricted by observations of dust, CO, H^0 and the derived Lyman continuum photon flux to such an extent that standard PDRs can provide only a minor contribution to [C I] emission in NGC 253. The bulk of the molecular gas in NGC 253 is dense ($n > 3 \times 10^4$ cm^{-3}), hot and at low A_V. Therefore, it is unlikely that cosmic rays perturb the chemistry enough to explain the [C I] emission. The size of the region (~ 300 pc) over which C^0/CO ~ 0.5, and the

environment of the molecular gas, rules out non-equilibrium chemistry. We feel that the only plausible explanation for the amount and distribution of C^0 in NGC 253 is an enhanced C/O elemental ratio in NGC 253. There is no obvious reason why this should be so, but, if it is the case that the elemental ratio of C/O is different in NGC 253, then this will affect chemical abundances. We predict that NGC 253 should be brighter than M82 in large carbon-bearing molecules such as HC_5N.

ACKNOWLEDGMENTS

We thank Patricia Carral, David Flower, Christian Henkel, Jocelyn Keene and Guillaume Pineau des Forêts for very helpful and interesting discussions, and an anonymous referee for a critical and insightful reading of an earlier draft of the manuscript. We also thank Tom Millar and Glenn White for sending preprints, Rachael Padman and John Lightfoot for help with SPECX, and Bill Dent, Jeff Cox, Kimberley Pisciotta and Jim Pomeroy for help with the observations. The JCMT is operated by the Royal Observatories on behalf of the UK Particle Physics and Astronomy Research Council (PPARC), the Netherlands Organization for Scientific Research and the Canadian National Research Council. AH acknowledges a studentship award from PPARC.

REFERENCES

Beck S. C., Beckwith S. V., 1984, MNRAS, 207, 671
Büttgenbach T. H., Keene J., Philips T. G., Walker C. K., 1992, ApJ, 397, L15
Canzian B., Mundy L. G., Scoville N. Z., 1988, ApJ, 333, 157
Carlstrom J. E., Jackson J., Ho P. T. P., Turner J. L., 1990, in Hollenbach D. J., Thronson H. A., Jr, eds, The Interstellar Medium in External Galaxies. NASA CP-3084, p. 337
Carral P., Hollenbach D. J., Lord S. D., Colgan S. W. J., Haas M. R., Rubin R. H., Erikson E. F., 1994, ApJ, 423, 223
de Vaucouleurs G., 1978, ApJ, 224, 79
Combes F., Gottesman S. T., Weliachew L., 1977, A&A, 59, 181
Fabbiano G., Trinchieri G., 1984, ApJ, 286, 491
Flower D. R., Le Bourlot J., Pineau des Forêts G., Roueff E., 1994, A&A, 282, 225
Forbes D. A., Ward M. J., Rotaciuc V., Blietz M., Genzel R., Drapatz S., Van Der Werf P. P., Krabbe A., 1993, ApJ, 406, L11
Fuente A., Martin-Pintado J., Cernicharo J., Bachiller R., 1993, A&A, 276, 473
Harris A. I., Hills R. E., Stutzki J., Graf U. U., Russell A. P. G., Genzel R., 1991, ApJ, 382, L75
Henkel C., Mauersberger R., Wiklind T., Hüttemeister S., Lemme C., Millar T. J., 1993, A&A, 268, L17
Herbst E., Lee H., Howe D. A., Millar T. J., 1994, MNRAS, 268, 335
Hollenbach D. J., McKee C. F., 1989, ApJ, 342, 306
Hollenbach D. J., Takahashi T., Tielens A. G. G. M., 1991, ApJ, 377, 192
Keene J., 1990, in Tarter J. C., Chang S., Defrees D. J., eds, Carbon in the Galaxy: Studies From Earth & Space. NASA CP-3061, p. 181
Keto E., Ball R., Arens J., Jerigan G., Meixner M., Skinner C., Graham J., 1993, ApJ, 413, L23
Köster B., Störzer H., Stutzki J., Sternberg A., 1994, A&A, 284, 545
Langer W. D., 1976, ApJ, 206, 699
Leung C. M., Herbst E., Heubner W. F., 1984, ApJ, 56, 231
Maeder A., 1992, A&A, 264, 108
Mauersberger R., Henkel C., 1989, A&A, 223, 79
Mauersberger R., Henkel C., 1991, A&A, 245, 457
Mauersberger R., Henkel C., Sage L. J., 1990, A&A, 236, 63
Mauersberger R., Henkel C., Walmsley C. M., Sage L. J., Wiklind T., 1991, A&A, 247, 307
McCarthy P. J., Heckman T., van Breugel W., 1987, AJ, 92, 264
Meixner M., Tielens A. G. G. M., 1993, ApJ, 405, 216
Pantelaki I., Clayton D., 1988, in Thuan T. X., Montmerle T., Tran Thanh Van J., eds, Starbursts and Galaxy Evolution. Editions Frontières, Gif-sur-Yvette
Philips T. G., Huggins P. J., 1981, ApJ, 251, 533
Piña R. K., Jones B., Puetter R. C., Stein W. A., 1992, ApJ, 401, L75
Rieke G. H., Lebofsky M. J., Walker C. E., 1988, ApJ, 325, 679
Sage L. J., Mauersberger R., Henkel C., 1991, A&A, 249, 31
Sams B. J., III, Genzel R., Eckart A., Tacconi-Garman L., Hofmann R., 1994, ApJ, 430, L33
Schilke P., Carlstrom J. E., Keene J., Philips T. G., 1993, ApJ, 417, L67
Scoville N. Z., Soifer B. T., Neugebauer G., Young J. S., Mathews K., Yerka J., 1985, ApJ, 289, 129
Schröder K., Staemmler V., Smith M. D., Flower D. R., Jaquet R., 1991, J. Phys. B (At. Mol. Opt. Phys.), 24, 287
Stacey G. J., Geis N., Genzel R., Lugten J. B., Poglitsch A., Sternberg A., Townes C. H., 1991, ApJ, 373, 423
Sternberg A., 1988, ApJ, 332, 400
Stutzki J., Stacey G. J., Genzel R., Harris A. I., Jaffe D. T., Lugten J. B., 1988, ApJ, 332, 379
Suchkov A., Allen R. J., Heckman T. M., 1993, ApJ, 413, 542
Telesco C. M., Harper D. A., 1980, ApJ, 235, 392
Telesco C. M., Dressel L. L., Wolstencroft R. D., 1993, ApJ, 414, 120
Ulvestad J. S., Antonucci R. R., 1994, ApJ, 424, L29
Van Dishoeck E. F., Black J. H., 1988, ApJ, 334, 771
Wall W. F., Jaffe D. T., Israel F. P., Bash F. N., 1991, ApJ, 380, 384
Wall W. F., Jaffe D. T., Bash F. N., Israel F. P., Maloney P. R., Baas F., 1993, ApJ, 414, 98
Walker C. K., Narayanan G., Büttgenbach T. H., Carlstrom J. E., Keene J., Philips T. G., 1993, ApJ, 415, 672
White G. J., 1994, A&A, 283, L25
White G. J., Ellison B., Claude S., Dent W. R. F., Matheson D. N., 1994, A&A, 284, L23
Wild W., Harris A. I., Eckart A., Genzel R., Graf U. U., Jackson J. M., Russell A. P. G., Stutzki J., 1992, A&A, 265, 447
Wolfire M. G., Tielens A. G. G. M., Hollenbach D. J., 1990, ApJ, 358, 116